Modelling of the Indonesian Throughflow on glacial-interglacial time-scales

Dissertation
zur Erlangung des Doktorgrades
der Mathematisch-Naturwissenschaftlichen Fakultät
der Christian-Albrechts-Universität zu Kiel

Vorgelegt von
Maja Žuvela-Aloise

Kiel, December 2005

Referent:	**Prof. Dr. Rolf Käse**
Korreferent:	**Prof. Dr. Martin Visbeck**
Tag der mündlichen Prüfung:	**16.12.2005**
Zum Druck genehmigt:	**06.06.2006**

Abstract

The Indonesian Throughflow transports warm and fresh Pacific waters into the Indian Ocean and is a major tropical pathway of the global thermohaline circulation. An important paleoclimatic question is to what extent lowered sea level at the Last Glacial Maximum effected the Indonesian Throughflow by restricting the gateways aperture. In this study, a regional dynamics of the Indonesian Throughflow are analysed for present-day and Last Glacial Maximum conditions. The focus of the study is on the impact of changes in Indonesian Gateways configuration on ocean circulation and distribution of marine organisms.

A high resolution regional ocean model with seasonal forcing is used to simulate mean climatic circulation through the Indonesian Gateways. During the Last Glacial Maximum, both bathymetry and climate conditions were different. Relative importance of individual effects is investigated by separately testing the sensitivity of the ITF volume and heat transport to the sea level lowering and to the glacial climate conditions.

The closure of the main passages is expected to reduce mean ITF transport during the glacial period. However, model results show that reduction in the glacial sea level of 120 m does not seem to be sufficient to severely block the flow within the Makassar Strait as the main passage of the Throughflow. An important impact of topographic changes is found in the vertical profile of the flow. Reduction in sill depth and absence of low buoyancy surface waters due to the exposure of shelf area lead to intensification of surface flow within Makassar Strait. Moreover, the seasonality of the surface flow is changed compared to the present-day. Both effects might have significant impact on the heat transport towards the Indian Ocean.

A strong impact of individual passages on ITF profile and seasonal variability emphasis the role of Indonesian Gateways on modulating the water masses exchange between the Pacific and the Indian Ocean. However, the intensity of the Throughflow seems to be highly dependant on the boundary conditions. Glacial climate conditions lead to reduction in ITF transport which might be related to several factors out of scope of regional dynamics. Such factors could include glacial changes in wind stress over Pacific, changes in density gradient between Pacific and Indian Ocean or overall El-Niño conditions over the tropical Pacific.

In addition, by calculating Lagrangian trajectories, main pathways, velocities of propagation and probabilities of exchange of marine biota between the Pacific and the Indian Ocean can be assessed. The developed patterns of distribution can be in the future compared with sedimentological evidence from the region.

Acknowledgements

This work was supported by the Deutsche Forschungsgemeinschaft (DFG) and was developed within Research Unit *Ocean Gateways* at the Institute for Geosciences at the Christian-Albrechts University of Kiel.

I wish to express my sincere and profound gratitude to Prof. Dr. Rolf Käse and Prof. Dr. Michael Schulz for the continuous supervision of this study, fundamental scientific input, their patient explanations and advice. I am greatly indebted to Prof. Dr. Michael Sarnthein for stimulating leadership of the *Ocean Gateways* research group who kindly supported me and also provided contact with climate modelling group of Prof. Dr. Mark Cane at LDEO (USA). I owe my gratitude to Dr. Andreas Schmittner for important contribution to this study, valuable suggestions and scientific input on paleoclimate modelling. Furthermore, I am thankful to Prof. Dr. Wolfgang Kuhnt and Dr. Ann Holbourn for supporting me with their expertise in micropaleontology and paleoceanography as well as for providing an opportunity for publishing part of the modelling results. I am particularly thankful to my colleague Dr. Frank Kösters for numerous discussions and unselfish help throughout this work as well as to Dr. Birgit Schneider for discussions and practical help in the last phase of the project. I wish to thank Claudia Sieler for her technical assistance and all of my colleagues from the Research Unit *Ocean Gateways* for stimulating and pleasant atmosphere at the Institute for Geosciences in Kiel.

A special thank to Dr. Andre Paul and Dr. Christian Schäfer-Neth for providing me with their LGM model results and the modelling group in Bremen for allowing usage of their computer resources. I thank Dr. Gerrit Lohmann for providing me with their atmospheric model simulations.

I am very thankful to Prof. Dr. Arnold Gordon and Dr. Dwi Susanto for most fruitful exchange of ideas and for putting on disposal their oceanographic data. I thank Dr. Myriam Khodri who provided me with the data of the NCAR CSM model and Dr. Qian Song for valuable discussion and usage of his ITF model experiments.

I especially wish to thank my family in Croatia and my husband Giulliano-Rocco for their patience and enormous support throughout this work.

Table of Contents

List of Figures

List of Tables

1. Introduction

1.1 The Indonesian Throughflow and the global climate system

The returning surface branch of the global thermohaline circulation (THC), that carries the warm and fresh Pacific water through the Indonesian Gateways into the Indian Ocean, is known as the Indonesian Throughflow (ITF). The Indonesian Gateways form one of the major pathways in the global conveyor belt and the only tropical ocean connection between the major ocean basins. Through its role in the mass, heat and salt exchange between the Pacific and the Indian Ocean, the ITF is believed to have a significant impact on the ocean circulation and climate.

The bulk of mass transport is confined in the top 500 m [*Meyers et al.*, 1995; *Gordon et al.*, 1999; *Wajsowicz et al.*, 2003]. The ITF effects the mass balance of the Pacific Ocean by exporting the North Pacific thermocline waters into the Indian Ocean which would be otherwise returned into the West Pacific equatorial current system [*Gordon*, 1986; *Gordon et al.*, 2003]. The equatorial upwelling in the Pacific is further intensified with the strong Throughflow [*Hirst and Godfrey*, 1993; 1994]. In the Indian Ocean, the ITF water proceeds westward enhancing the South Equatorial Current (SEC). The main flow crosses the Indian Ocean, while the remaining part flows southward and south eastward where it sinks near the West Australian coast. The downwelled flow further reverses into the undercurrent that returns back towards Madagascar. The Agulhas Current is strengthened both by the direct flow across the Indian Ocean and by the return flow below 500m from the downwelling off western Australia. Therefore, the ITF influences both horizontal and vertical circulation in the Indian Ocean.

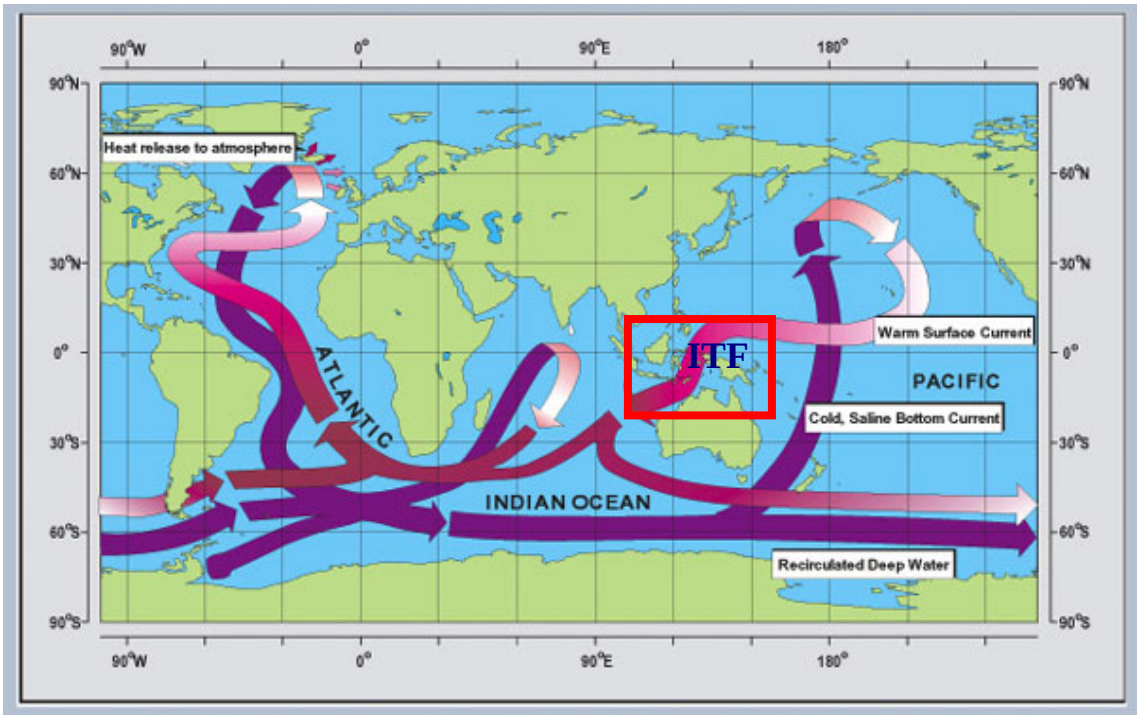

Figure 1-1 Schematic diagram of the global ocean conveyer belt (after W. Broecker, modified by E. Maier-Reimer).

The magnitude of the heat transported by the ITF into the Indian Ocean is approximately 0.5 PW which makes a substantial loss for the equatorial Pacific Ocean heat budget. The main thermal response to enhanced ITF is warming of the upper Indian Ocean and cooling of the upper Pacific Ocean. Model experiments with blocked Indonesian Passages [*Hirst and Godfrey*, 1993; *Godfrey*, 1996; *Schneider and Barnett*, 1997; *Schneider*, 1998, *Wajsowicz and Schneider*, 2002] show largest temperature differences in the main thermocline, while the sea surface temperature (SST) signal is small in both oceans except for the regions with strong upwelling or convective mixing such as the Agulhas Current, the downwelling region off western Australia, the Tasman Sea and the equatorial upwelling zones in the Pacific Ocean. The enhanced ITF heat transport leads to strengthening of the Leeuwin Current system by increasing the steric height off northwestern Australian coast [*Godfrey*, 1996; *Tomczak and Godfrey*, 1994].

Due to its geographical positioning the ITF is an integral part of the tropical climate system. Specifically, the ITF plays an important role in the tropical ocean-atmosphere coupling by influencing the position and extent of the West Pacific Warm Pool (WPWP). Results from the coupled ocean-atmosphere general circulation model (AOGCM) [*Schneider and Barnett*, 1997; *Schneider*, 1998] show that the intensified Throughflow shifts the warm pool and the centres of deep convection in the atmosphere further west. As a result, the atmospheric pressure in the entire tropics and the related surface wind stress is changed. Blocking of the ITF results in an ENSO-like signal in the Pacific and pattern similar to the Indian Dipole Mode over the Indian Ocean [*Wajsowicz and Schneider*, 2002]. In the Indian Ocean, blocking of the ITF is associated with colder SSTs in the eastern Indian Ocean and warmer temperatures in the western basin. The resulting wind signal is an increase in southeast trades over the Indian Ocean. Accompanying precipitation anomalies show a northward shift in rainfall from Indonesia and small increase of rainfall over East Africa. The response of the Pacific Ocean is an enhanced warming in the eastern equatorial Pacific associated with increased westerly anomalies in wind stress and rise in precipitation along the equator.

1.2 Present-day circulation

The Indonesian Gateways topography consist of numerous islands with narrow passages in between them, shallow seas (Java Sea, Arafura Sea) and deep ocean basins (Celebes Sea, Banda Sea). A system of both shallow (Lombok Strait (250 – 300 m), intermediate (Makassar Strait (680 m), Ombai Strait (~1000 m) and deep ocean passages (Lifamotola Passage (1940 m), Timor Passage (1200 – 1500 m)) separates the major seas (Figure 1-2). The ITF is formed in the complex equatorial current system in the Western Pacific. The southward flowing Mindanao Current (MC) carries subtropical North Pacific water towards the equator. At the entrance of the Indonesian Seas, the MC splits into the ITF and the eastward flowing North Equatorial Countercurrent (NECC) forming the Mindanao Eddy (ME). South Pacific waters are carried by the South Equatorial Current (SEC) that partly enters the Indonesian Gateways near the Halmahera Island forming the Halmahera Eddy (HE) and partly turns eastward joining the NECC [*Godfrey*, 1996; *Gordon*, 2001]. The observations based on hydrography [*Wyrtki*, 1987; *Gordon*, 1986; *Ffield and Gordon*, 1992; *Bingham and Lukas*, 1994; Ilahude and *Gordon*, 1996; *Gordon and Fine*, 1996], drifters [*Lukas et al.*, 1991] and tritium content [*Fine*, 1985] from the West Pacific and Indian Ocean indicate that in the upper 500 m, the ITF source water originates mainly from the North Pacific thermocline and intermediate waters. In the deep channels at the eastern entrance to the

Indonesian archipelago, South Pacific water infiltrates the lower thermocline and deep layers [*van Aken et al*., 1988; *Ilahude and Gordon*, 1996; *Gordon and Fine*, 1996; *Hautala et al.*, 1996; *Gordon and McClean*, 1999]. Inside the Indonesian Seas, the main path of the ITF is through the westernmost Celebes Sea and Makassar Strait [*Ffield and Gordon*, 1992]. While part of the flow enters the Indian Ocean through Lombok Strait [*Murray and Arief*, 1998; *Murray et al*., 1989; *Meyers et al*., 1995; *Arief and Murray*, 1996], the bulk of the flow turns eastward via the Flores Sea towards the Banda Sea. Finally, the flow exits into the Indian Ocean through the Ombai Strait and Timor Passage to join the SEC [*Fieux et al.*, 1994; *Hautala et al.*, 1996; *Gordon and Fine*; 1996, *Hautala et al*., 2001; *Potemra et al.*, 2003]. Additional South Pacific waters enter the Gateways near Halmahera flowing into the Banda Sea [*Illahude and Gordon*, 1996].

Estimating the ITF transport magnitude and variability has been a challenging task for both observational and modelling oceanography in recent years due to the complex equatorial ocean dynamics and the complicated topography of the Indonesian Gateways. Considering that all of the equatorial Western Pacific currents are of the similar order of magnitude as the ITF and show strong variability, the balance between the given currents and related intensity of the ITF is still not well understood. Estimates of the ITF volume transport range from almost 0 to 20 Sv depending on the method and data used in calculation [*Wyrtki*, 1961; *Murray and Arief*, 1988; *Fieux et al*., 1994; *Meyers et al*., 1995; *Gordon et al.*, 1999; *Hautala et al*., 2001; *Molcard et al.*, 2001; *Susanto and Gordon*, 2004]. Several observational programs monitoring the Throughflow exist (ARLINDO, JADE, TOGA-WOCE; see *Siedler et al.* [2001] for review). However, long-term simultaneous measurements within both inflow and outflow passages to unambiguously determine the mean magnitude of the ITF are still lacking. Based on the recent mooring measurements in Makassar Strait [*Gordon et al.*, 1999; *Wajsowicz et al*., 2003; *Susanto and Gordon*, 2004], as the main passage of the Throughflow and estimates of the transport in the outflow passages [*Murray and Arief*, 1988; *Creswell et al.*, 1993; *Molcard et al.*, 1994; 1996; 2001; *Hautala et al.*, 2001] a general agreement is found where the ITF carries approximately 10 Sv of Pacific waters towards the Indian Ocean [*Gordon*, 2001].

The ITF transport shows high variability on both inter and intra-annual time-scales. The seasonal cycle is characterized by the monsoonal wind change. The transport within Makassar Strait is strongest in boreal summer during the southeastern (SE) monsoon with its maximum in June. The flow is weakest in boreal winter during the northwestern (NW) monsoon with its maximum in December [*Gordon et al.*, 1999, *Gordon et al.*, 2003]. The transport time series based on the shallow pressure gauge and ADCP data in the main outflow passages (Lombok Strait, Sumba Strait, Ombai Strait, Savu/Dao Strait and Timor Passage) show similar mean annual cycle as in Makassar Strait [*Hautala et al.*, 2001]. However, possible differences in timing of the outflow transport relative to the transport from the inflow passages point to the convergence in the Indonesian Seas [*Gordon and Susanto*, 2001; *Potemra et al.*, 2003].

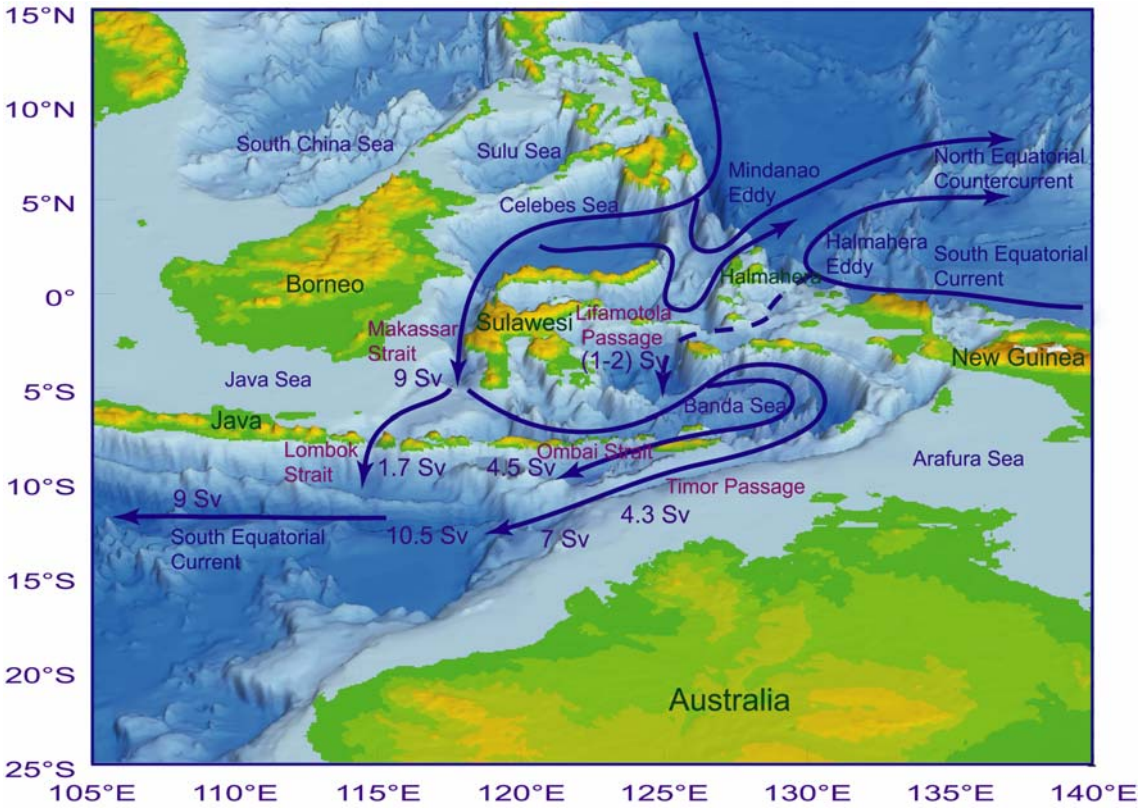

Figure 1-2 Main current system of the Indonesian Gateways with annual mean volume transport values within the main passages modified from *Gordon* [2001] and *Gordon et al.* [2003] and drawn on a topographic map derived from the ETOPO5 bathymetric data set [*NOAA*, 1988].

The relationship between inter-annual fluctuations of the ITF and the El-Niño Southern Oscillation (ENSO) has been widely discussed. The variations associated with ENSO show a maximum during the La Niña and minimum during the El Niño events, with the peak to peak amplitude of 5 Sv [*Meyers*, 1996]. The modelling experiments of *Murtugudde et al.* [1998] confirmed that the Pacific Ocean wind stress exerts control over the ENSO related inter-annual variability of the ITF and showed that downstream and local winds in the Indian Ocean might play a significant role. Even though, the correlation between the ITF and the ENSO signal is well established, the feedback mechanisms and the ITF control an ENSO are still not well known.

1.3 What drives the Indonesian Throughflow?

In his early work, *Wyrtki* [1961; 1987] suggested that the ITF is driven by a pressure head between the Pacific and Indian Ocean. *Wyrtki* based his hypothesis on hydrographic observations, sea level records, ship drifts and climatological wind patterns and provided a first estimate of the ITF magnitude. His assumption was that the ITF magnitude can be correlated with the sea-level difference between Davao (Philippines, West Pacific) and Darwin (Australia, East Indian Ocean). However, the Davao record was found to be a poor indicator of sea-level variability in the western Pacific, as the signal was influenced by the high-frequency fluctuations of the unstable Mindanao Current and other off-equatorial signals [*Clarke and Liu*, 1993]. These studies left open questions as what controls the pressure head between the Pacific and

Indian Ocean on the long-term mean and how to asses the variability of the Throughflow.

Godfrey [1989] formulated an *island rule* based on a Sverdrup model to estimate the mean ITF magnitude. The *island rule* is derived by integrating the depth-averaged, linear, horizontal momentum equations for the stratified ocean, subjected to a wind forcing. In the simplest formulation, the *island rule* states that the long-term (inter-annual or longer time-scales) depth-integrated transport of the ITF can be obtained by the wind stress line integral across the Pacific and around Australia and New Guinea (Figure 1-3). The prevailing winds cause an increase in sea level on the western side of the oceans and a lowering on the eastern side. Additional components to the *island rule* include topographic and frictional effects as well as the pressure difference between the northern and southern entrances to the Indonesian Seas that balances the alongshore wind stress. Godfrey's *island rule* gives an estimate of the net mean depth-integrated transport of 16 ± 4 Sv (Sv = 10^6 m^3s^{-1}) using annual mean wind stress. The value is considered too large compared to the observational estimates of the mean ITF transport of approximately 10 – 12 Sv [*Godfrey and Golding*, 1981; *Fu*, 1986; *Murray and Arief*, 1988; *Meyers et al*., 1995; *Gordon et al*., 1999; *Wajsowicz et al.*, 2003]. This implies that frictional and topographic effects might play a significant role in reducing the net Pacific to Indian Ocean transport.

Wajsowicz [1993a, b; 1994] further modified Godfrey's *island rule* to account for the complex geometry of the Indonesian Gateways by including the bottom topography, frictional effects and multiple straits. The resulting analytical model shows that the narrow channels in the Indonesian archipelago could indeed reduce the net transport due to the frictional effects. However, estimates of frictional contribution are dependent on the parameterization and boundary conditions adopted in the model. The transport reduction ranged from 5% to 20%. Including multiple straits, specifically Halmahera Island, in the analytical derivation of the *island rule*, leads to the redistribution of the ITF source water between the North and South Pacific. In this case, preference is given to the North Pacific source which is in consistence with the observations [*Gordon*, 1986; *Lukas et al.*, 1991]. *Wajsowicz* [1993a] further suggested that the topographic effects can be described by the Joint Effect of Baroclinicity and Relief (JEBAR effect) [*Huthnance*, 1984] taking the simple sill representation of the Indonesian archipelago. The shallow Indonesian sills intersect the level of no motion at which the horizontal pressure gradients in the ocean are approximately zero. Due to the density difference between the Pacific (warm, fresh) and Indian Ocean waters (cold, salty), a bottom pressure gradient over the sill is induced. The net transport is, therefore, enhanced. In this way, topography of the Indonesian archipelago can exert control over the mass and heat balance between the Pacific and Indian Ocean.

In agreement with the modified *island rule*, ocean general circulation model (OGCM) experiments [*Wajsowicz*, 1995; 1996] confirm that inter-annual variability in the depth-integrated Throughflow is generated by wind stress variations over the Pacific. However, a simple estimate of the magnitude and variability of the ITF using the analytical model still seems to be problematic when topographic effects and density driven flow are considered. Moreover, comparison of the inter-annual variations in depth-integrated transport predicted by the theory and simulated by the coupled AOGCM shows disagreement in both magnitude and phasing of the Throughflow [*Wajsowicz and Schneider*, 2002].

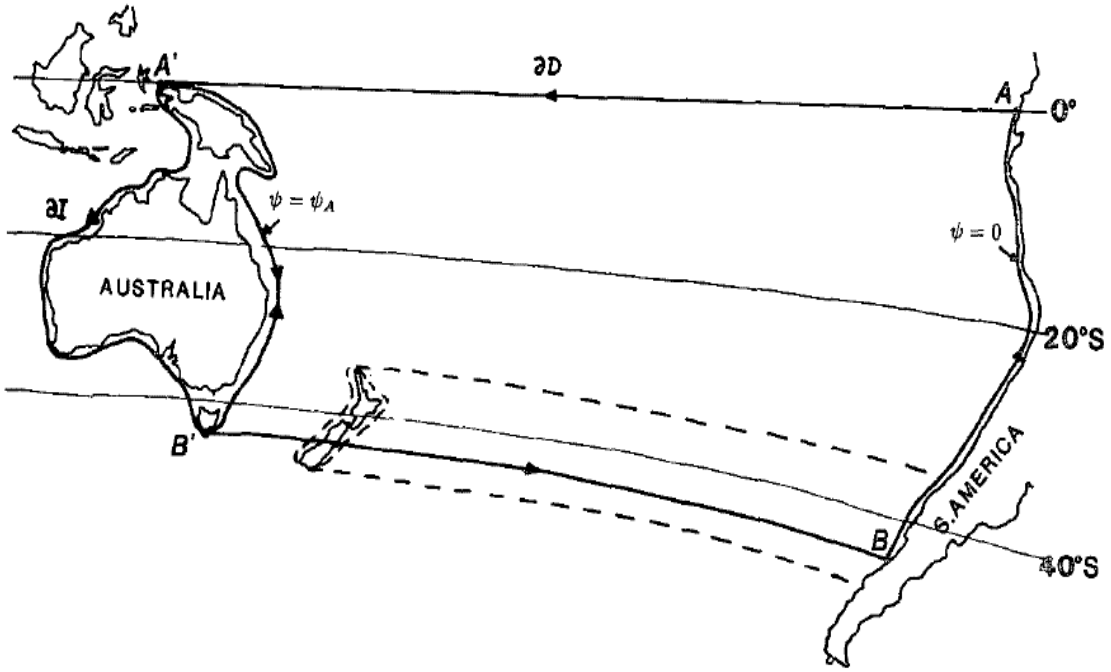

Figure 1-3 The geometry used in deriving Godfrey's *island rule*. The depth-integrated transport of the ITF can be obtained by calculating the wind stress line integral across the Pacific and around Australia and New Guinea. Taken from *Wajsowicz* [1994].

A different approach was suggested by *Andersson and Stigebrandt* [2004] where only density gradient between the Pacific and the Indian Ocean is considered to drive the Throughflow. The Indonesian Seas are taken as part of the North Pacific water masses assuming that the hydrographic properties do not change significantly within the Gateways. A downstream buoyant pool is formed in the North Australian Basin, which drives the upper flow from the Pacific towards the Indian Ocean due to the difference in sea level. The ITF is then predicted from the simple geostrophic transport taking into account the density difference and depth of the pool. Estimates of the ITF from the hydrographic data of steric sea level gradient between the North Pacific and the North Australian Basin compare well with the observed Throughflow (~10 Sv). However, these estimates crucially depend on the width and depth of the pool as well as on the reference temperature and salinity used in calculation.

The given theory of the Throughflow forcing still leaves unanswered the question how to approach the Throughflow dynamics in order to predict the transport magnitude and variability. A possible simplified description of the ITF that would also incorporate accurate estimates of the transport would be an useful tool in studying long-term climate changes.

1.4 Paleoclimatic changes during the Last Glacial Maximum

The most prominent impact of glacial climate conditions on the Indonesian Gateways is the sea level lowering associated with the global ice-sheet growth. Reconstructions of sea level change on the Sunda Shelf [*Hanebuth et al*., 2000] and the North-Australian Bonaparte Gulf [*Yokoyama et al.*, 2000] show that the sea level lowering during the Last Glacial Maximum (LGM) (23–19 ky ago) reached between 120 and 136 m of ice volume equivalent. The estimate of 120 m sea level change corresponds to the worldwide observational records and model calculations

[*Peltier*, 2002; *Lambeck et al.*, 2002] of sea level fluctuations on the glacial-interglacial time-scales. Land-sea distribution in the Indonesian Gateways changed significantly with the lowering of the sea level (Figure 1-4). Java Sea was exposed and the communication with the South China Sea was blocked. The North Australian Shelf was dry and the overall exposed land area almost doubled [*De Deckker et al*., 2002]. The sea level lowering closed most of the small and narrow Indonesian passages and significantly changed the aperture of the main straits by reducing the width of the channels and depth of the sills.

The Climate Long Range Investigation, Mapping and Prediction (CLIMAP) [1981] reconstruction for the LGM climate shows no significant change in SSTs in the Indo-Pacific Warm Pool (IPWP) compared to present-day (PD) values. However, recent reconstructions of paleotemperatures based on oxygen isotopes and Mg/Ca ratios of foraminiferal shells from the region suggest substantial cooling, ranging from 2°C to 5°C [*Lea et al.*, 2000; *Stott et al.*, 2002; *Rosenthal et al.*, 2003; *Visser et al.*, 2003]. New estimates of SSTs based on multiproxy approach for the reconstruction of the glacial ocean (MARGO) show not only cooling, but also a reduction of the extent of the warm pool [*Kucera et al.*, 2005; *Barrows et al.*, 2000; *Barrows and Juggins*, 2005].

The sea surface salinity (SSS) reconstruction in the region is more ambiguous. There are few observational sites where both Mg/Ca and oxygen isotope records are used to estimate salinity changes. Based on $\delta^{18}O$ measurements of planktonic foraminifers, *Martinez et al.* [1997; 1999; 2002] and *De Deckker et al.* [2002] proposed drier conditions in the IPWP region while SST changed minimally (2°C at most). De *Deckker et al.* [2002] considered that the increase in land area would favour a drop in precipitation and related increase in salinity throughout the region. Increases in salinity were confirmed by both Mg/Ca and $\delta^{18}O$ measurements in the Mindanao Sea [*Stott et al.*, 2002] and Makassar Strait [*Visser et al.*, 2003]. This is, however, in contrast with the salinity anomalies derived from the Sulu Sea [*Rosenthal et al.*, 2003; *Dannemann et al.*, 2003; *Oppo et al.*, 2003] and Ontong Java Plateau [*Lea et al.*, 2000] where the data indicate fresher conditions at the LGM.

Vegetation reconstructions based on the organic carbon records from the sediment core recovered from Makassar Strait [*Visser et al.*, 2004] suggest no significant change in vegetation in the region indicating similar hydrological conditions possibly achieved by strengthening the monsoon during the winter period. Changes in vegetation and monsoonal activity have been also inferred from the pollen records from the Indonesian region [*van der Kaars et al.*, 2000; *van der Kaars et al*., 2001]. These findings point out that regional wind forcing might be an important climatological factor.

Considering glacial to interglacial changes in the paleoproductivity and nutrient utilization in the Timor Strait, *Müller and Opdyke* [2000] suggested that the ITF was reduced in strength during the glacial periods. The observed glacial increase in productivity appears to be related to the weaker ITF transport. Today, spreading of the ITF low salinity surface waters inhibits vertical mixing and reduces productivity in Timor Strait. Weaker Throughflow and the sea level lowering during the LGM would, therefore, enhance the possibility of upwelling and higher productivity.

Further indications for the reduction in the ITF strength has been deduced from the clay mineral distribution in surface sediments between Indonesia and northwestern Australia [*Gingele et al.*, 2001a,b]. The distribution of clay minerals is closely related to the surface and subsurface ocean currents. Characteristic assemblages of clay minerals can be used as tracers for the Throughflow. Evidence from Timor Passage shows a reduction in the current speed as indicated by the accumulation of finer material during glacial periods. Decrease of kaolinite and chlorite originating from the Java Sea during

the LGM could be related to overall reduced advection by the ITF. However, clay mineral distribution is not only related to changes in the current system, but displays changes in the geological setting and weathering conditions as well. Assumptions on the changes in the land-sea distribution, hydrological cycle and related river runoff are, therefore, necessary for the interpretation of the clay mineral patterns and are prerequisite to determine the changes in the Throufghlow strength.

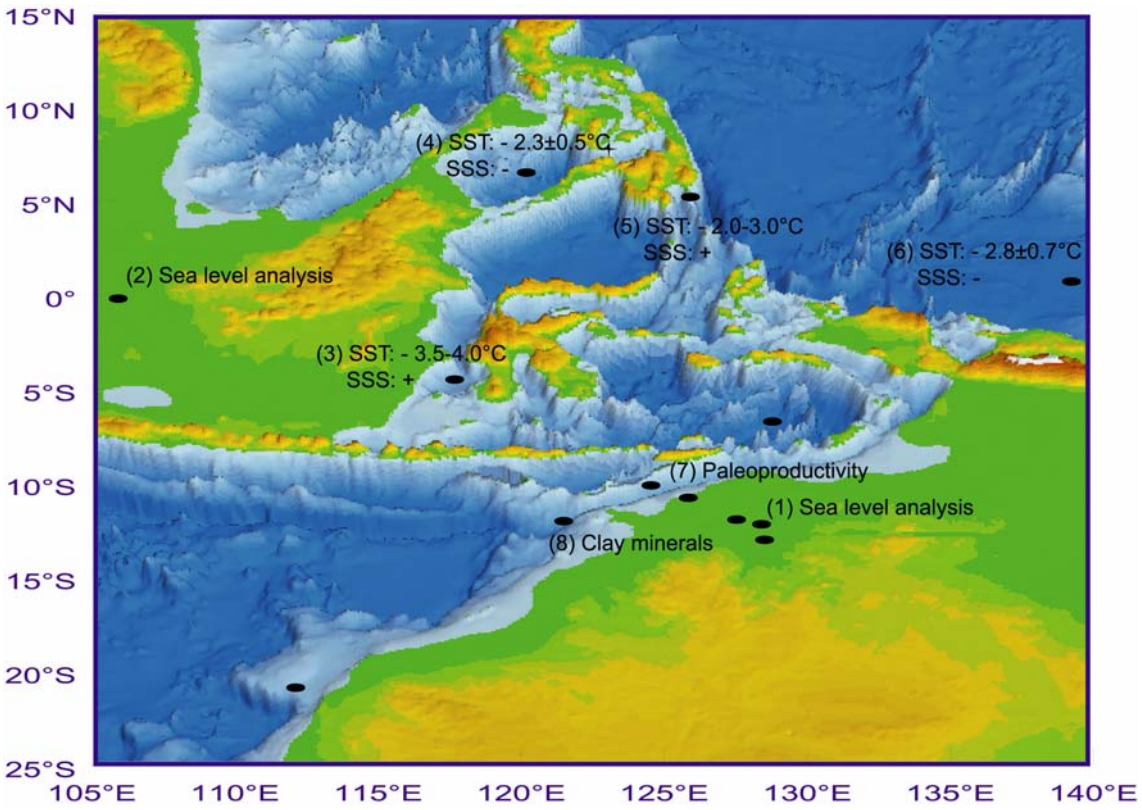

Figure 1-4 Topography of the Indonesian Gateways with lowered sea level by 120 m. Indicated are locations of sampling sites used in sea level reconstruction (1) *Hanebuth et al* [2000] and (2) *Yokoyama et al* [2000], paleoproductivity (7) *Müller and Opdyke* [2000] and clay minerals analysis (8) *Gingele et al.* [2001a,b]. Depicted are the coring sites of the LGM SST anomaly and SSS tendency based on $\delta^{18}O$ records and Mg/Ca paleothermometry from (3) *Visser et al.* [2003], (4) *Rosenthal et al.* [2003], (5) *Stott et al.* [2002] and (6) *Lea et al.* [2000].

Even though there has been a large interest in the past years to determine the role of low-latitude dynamics in global climate variations on glacial-interglacial time-scales, the number of paleoceanographic data from the tropical regions, especially from the Indonesian Gateways, is still insufficient to clarify observed changes.

1.5 Scientific questions and objectives

The study of the low-latitude Indonesian Gateways is part of the DFG funded project "Research Unit Ocean Gateways" investigating impacts of gateways on ocean circulation, climate and evolution. The Indonesian Gateways are one of the key regions in the global THC controlling heat and freshwater flux from the Pacific to the Indian Ocean. Taking into account that the shutting off of the ITF has significant impact on the tropical climate the question arises whether the partial closing of the Indonesian passages such as during the LGM changes the ITF magnitude. Coarse resolution

climate models do not properly resolve the Indonesian passages and dynamical aspects of the circulation inside the Indonesian Seas. The aim of this study is to determine the impact of topographic changes on glacial-interglacial time-scales on the ITF by using a regional high-resolution ocean model. The main questions addressed are:

- to what extent the glacial sea level lowering effects the ITF volume and heat transport?
- in which way ocean dynamics within the main passages influence vertical structure and variations of the ITF?
- what controls the ITF magnitude under glacial conditions?

Additional particle tracing experiments are designed to investigate the exchange of marine biota and distribution of sedimentological/geochemical tracers through the Indonesian passages under present-day and glacial conditions. The focus of the experiments is on main pathways of the particles within the Indonesian Seas, possible changes in particle exchange within main passages under glacial climate conditions and how are the particle distribution and velocity of propagation related to particles origin, depth and seasonal variations of the flow. The resulting patterns of glacial-interglacial particle dispersal can be, in the future, compared with micropaleontological and sedimentological evidence from the region or used as help in selection of future sampling sites.

2. Modelling the Indonesian Throughflow

The Indonesian Throughflow has been a subject of investigation in numerous analytical and numerical studies. In an early study of *Hirst and Godfrey* [1994] a depth-integrated numerical ocean model, has been used to test the hypothesis of the Godfrey's *island rule* as to show that it is indeed the wind stress governing the Throughflow. The relationship between the wind stress and the ITF on inter-annual time-scales has been further investigated in the numerical model of *Wajsowicz* [1995; 1996]. The study of *Wajsowicz* [1995; 1996] has shown that the variability in the ITF largely correlates with wind variations. However, topographic effects might be the reason for the disagreement between the ITF estimates from the *island rule* and the observations. *Schiller et al.* [1996; 1998; 2004] investigated mixing of the water masses inside the Indonesian Seas using a global OGCM. The results pointed out to the strong mixing occurring in the Indonesian Seas possibly due to tidally induced vertical mixing.

The complexity of topography of the Indonesian Gateways has so far been difficult to assess in global model simulations. The regional study of the ITF with realistic topography has been investigated with a barotropic numerical model [*Burnett et al.*, 2003; *Kamenkovich et al.*, 2003]. An analysis of the momentum and energy balance in the model showed that the total transport of the ITF correlates with the pressure gradient between the Davao (North Pacific) and Darwin (Indian Ocean) on seasonal time-scale. Other factors, including local wind stress, bottom form stress and the resultant forces acting on the internal sides have a large impact on the ITF. The model formulation, however, did not include density driven flow.

Here, a regional OGCM is applied to simulate ITF dynamics. The model incorporates high resolution of the bottom topography and coastline and small-scale processes and is therefore suitable to simulate the interactions between the flow and the complex topography of the Indonesian Gateways. The model experiments are designed to test sensitivity of the ITF circulation to topographic changes. Special attention is given to the representation of the boundary forcing in the regional model and its role in controlling the Throughflow.

2.1 MIT general circulation model

Experiments are performed with the MIT General Circulation Model [*Marshall et al.,* 1997a, b], a primitive equations numerical model with z-coordinates in the vertical. The MITgcm is designed for both process and general circulation studies of the atmosphere, ocean and climate. In the ocean, the MITgcm has been successfully used in study of whole range of phenomena from small-scale process, such as convection and mixing over topography and boundary forced internal waves to large-scale processes such as study of gyres in the ocean [*Herbaut et al.*, 2001] and global state estimation [*Stammer et al.*, 2001; 2003] as well as estimating atmospheric fluxes [*Huang and Mehta*, 2004].

The state of the ocean is described by a set of primitive equations that include equations of motion, continuity, state and thermodynamics (Appendix B). The general circulation model is based on numerical solutions of the incompressible Navier Stokes equations supporting both hydrostatic and non-hydrostatic formulations. The model grid uses curvilinear orthogonal horizontal coordinates and z-coordinate in vertical. Numerical discretization algorithms employed in the model are based on the finite volume approach compared to the finite difference techniques used generally in

ocean models [*Marshall et al.*, 1997b]. The finite volume technique is equivalent to the flux-form finite difference technique in the interior of the ocean, but on the boundaries it allows irregular representation of the topography and coastline by using shaved cells to fit the topography [*Adcroft et al.*, 1997]. In this way, the model performance compares to the terrain following coordinates models in simulating interactions between the flow and topography, but at the same time avoids the common problems of the terrain following models such as the pressure-gradient error. The model uses a staggered grid analogous to the Arakawa C grid. Formulation of model can support Cartesian, spherical-polar or curvilinear coordinate system. The time stepping follows quasi second-order Adams-Bashforth method for explicit terms in both the momentum and tracer equations. Vertical diffusion and viscosity is treated implicitly in time using the backward method. The time stepping in the model is synchronous with possibility of staggering in time the thermodynamic variables with flow variables. The surface pressure or height can be described either by prognostic or diagnostic equation with hydrostatic or non-hydrostatic formulation giving several options for the basic formulation of the model.

Momentum equations use Laplacian and biharmonic lateral viscosity and Laplacian vertical dissipation with no-slip or free slip lateral boundary conditions. The bottom drag represents additional friction to the no-slip conditions as a linear or quadratic function of the mean flow above the topography. The tracer equations use optional linear or non-linear advection schemes and Laplacian or biharmonic formulation for diffusivity. The linear advection schemes include centred second-order, centred fourth order, first order upwind and upwind biased third order. Subgrid scale processes are treated with numerous physical parameterizations such as the Gent-McWilliams eddy parameterization, KPP mixing scheme and PV flux parameterization. Two forms of the equation of state are available: linear with the specified thermal and haline expansion coefficients and polynomial. Polynomial coefficients are generated by the Knudsen algorithm or optional higher polynomial formulations of the equations of state such as UNESCO [*Fofonoff and Millard*, 1983] and modified UNESCO formulas can be used.

2.2 Model configuration

The model domain covers the Indonesian Seas from 105°E - 140°E and 20°S - 10°N (Figure 2-1). The horizontal resolution of the model is 1/6° in both zonal and meridional direction and it has 25 vertical levels with resolution ranging from 10 m near the surface to 500 m close to 4500 m depth. The model bathymetry is derived from the 5-min ETOPO5 topography database [*NOAA*, 1988]. The topography is represented by the shaved cells approach with defined minimum fraction of the layer thickness (hFac). Representation of the topography in the main passages is illustrated in Figure 2-2. The basic formulation of the numerical algorithms used in experiments is the semi-implicit pressure method for hydrostatic equations with an implicit linear free-surface and variables co-located in time and with Adams-Bashfort time stepping.

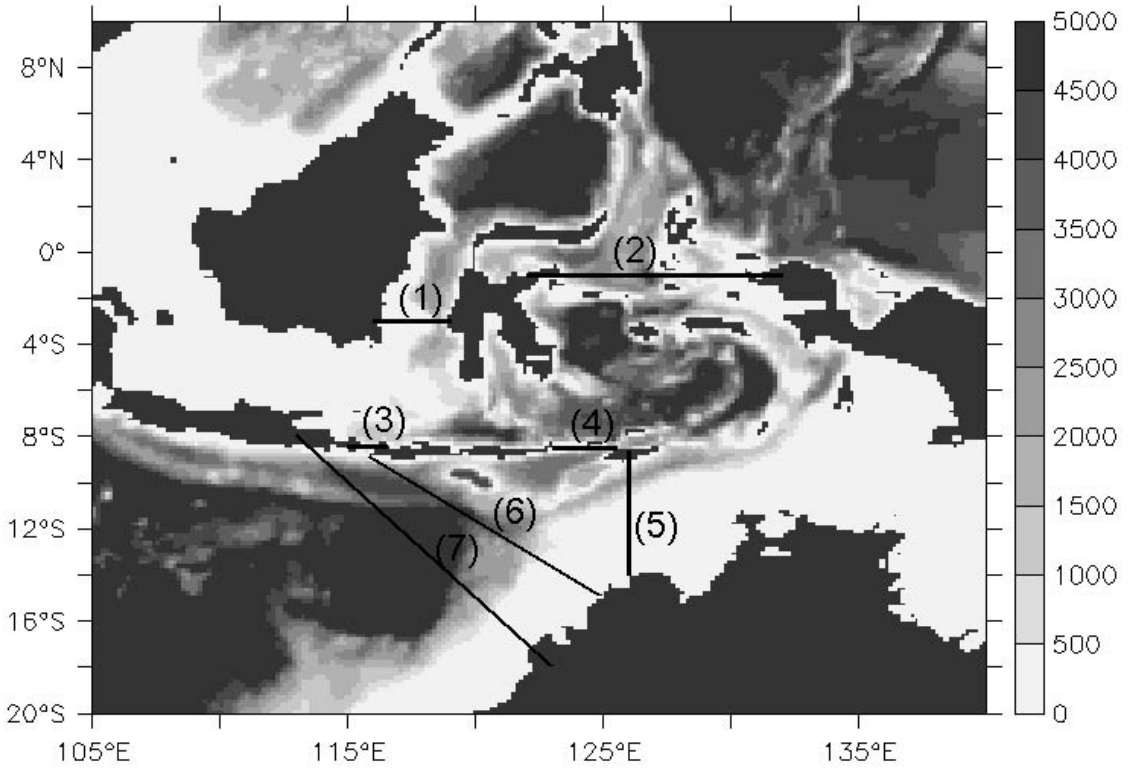

Figure 2-1 Model domain and bathymetry (m) of the Indonesian Gateways with indicated cross-sections through the main passages used in calculation: (1) Makassar Strait, (2) Sulawesi – New Guinea, (3) Lombok Strait, (4) Ombai Strait, (5) Timor Passage, (6) Timor and Ombai Strait (TOS), (7) ITF total.

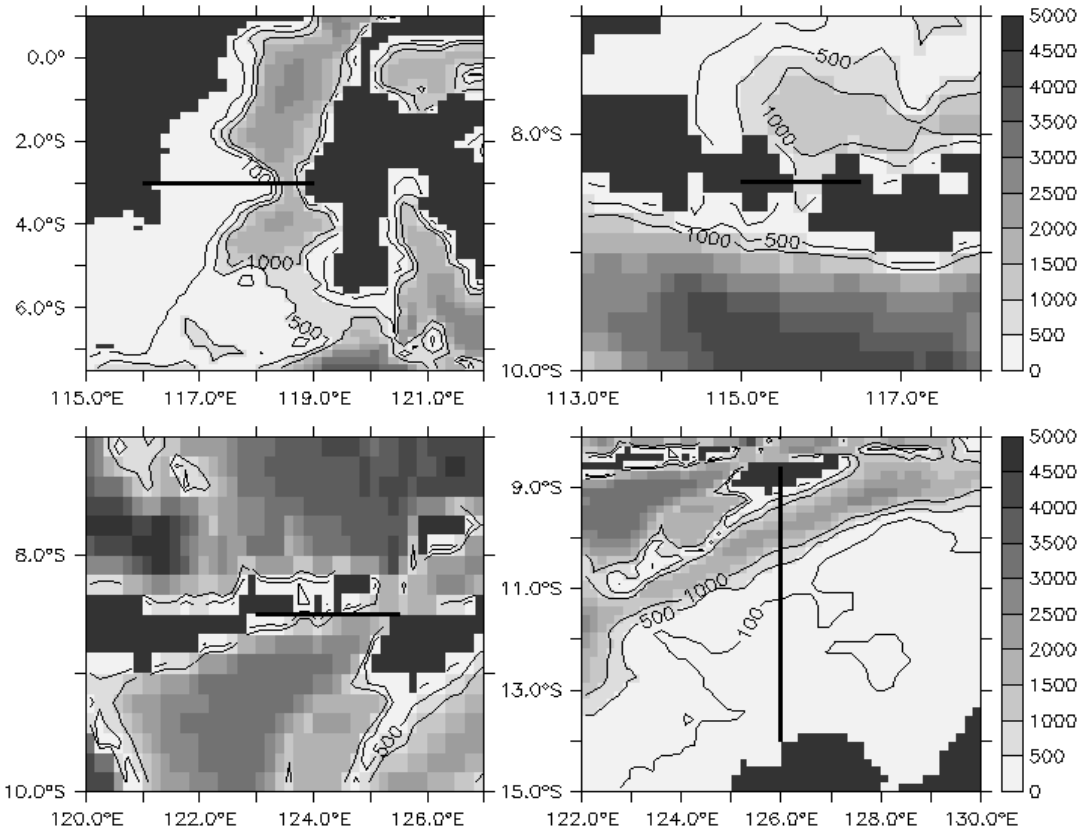

Figure 2-2 Representation of the topography in the main passages: Makassar Strait (upper left), Lombok Strait (upper right), Ombai Strait (lower left) and Timor Strait (lower right).

The equation of state is formulated by polynomial approximation with Knudsen algorithm using grid specific polynomial coefficients. Overview of the model parameters is given in Table 2-1. Duration of model integration is at least 5 years with the time stepping of 10 min, which follows stability criteria for the given spatial resolution. The first 2 months of the initial adjustment are excluded from the analysis. The model approaches energy equilibrium after approximately 3 years of integration. Tidal mixing is not implemented in the MITgcm formulation and possible effects of different mixing parameterizations could be in future investigated in the model.

The model is initialized with potential temperature and salinity for the month January taken from the monthly climatological data. For the experiments of the present-day climate, initial hydrography is taken from the World Ocean Atlas 1998 [*Conkright et al.*, 1998]. In the glacial experiments, the initial field is interpolated from the global OGCM MOM experiment for the LGM conditions [*Paul and Schäfer-Neth*, 2003]. Initial velocity field is set to zero.

Table 2-1 MITgcm configuration

Model parameter	Value
Horizontal grid	1/6° x 1/6°
Vertical grid	25 levels
Time-stepping	600 s
Boundary conditions	free slip
Lateral boundary	OBC
Viscosity horizontal	biharmonic: 10^{11} m^4s^{-1}
vertical	Laplacian: 10^{-3} m^2s^{-1}
Diffusion horizontal	Laplacian: 10^{3} m^2s^{-1}
vertical	Laplacian: 10^{-5} m^2s^{-1}
Equation of state	polynomial
hFac minimum	0.2
Mixing	implicit viscosity implicit diffusion
Advection scheme	centred 2nd order
Surface forcing	monthly climatology

2.3 Boundary forcing and source data

The forcing in the model is applied through surface and lateral boundary conditions. The forcing by atmosphere includes wind stress forcing and surface heat and freshwater fluxes represented in the model by restoring the SST and SSS to climatological values. For the purpose of this study, only seasonal variations are included in the boundary forcing. The forcing fields are varied on a monthly time-scale with annual periodicity. The main focus of the experiments is to establish and compare mean climatological dynamics for the present-day and LGM climate. High uncertainty in the glacial boundary conditions presents additional limitation when including more realistic forcing to simulate the Throughflow. For this reason, inter-annual variability in the boundary conditions related to internal modes of the Pacific and Indian Ocean such as ENSO events or Indian Ocean dipole is not considered. High-frequency variability in forcing such as Kelvin waves or variations in the local wind stress has been also neglected. The climatological data sets are available at IRI/LDEO Climate Data Library (http://ingrid.ldgo.columbia.edu). The overview of source data is given in Table 2-2.

Table 2-2 Source data

Experiment	Present-day	Last Glacial Maximum
Wind stress	Atlas of Surface Marine Data, *Da Silva* [1994]	NCEP + glacial anomaly, *Paul and Schäfer-Neth* [2003] ECHAM3 AOGCM, *Lohmann and Lorenz.* [2000] NCAR AOGCM, *Shin et al.* [2003]
SST/SSS	WOA 98, *Conkright et al.*[1998]	MOM OGCM, *Paul and Schäfer-Neth* [2003]
Heat fluxes	NCEP, *Kalnay et al.* [1996]	NCAR AOGCM, *Shin et al.* [2003]
OBC	PD MOM OGCM, *Paul and Schäfer-Neth* [2003] ECCO, *Stammer et al.* [2003]	LGM MOM OGCM, *Paul and Schäfer-Neth* [2003] NCAR AOGCM, *Shin et al.* [2003]

2.3.1 Wind stress

For the present-day conditions the model is forced with monthly wind stress data derived from the Atlas of Surface Marine Data [*da Silva et al*., 1994] (Figure 2-3).

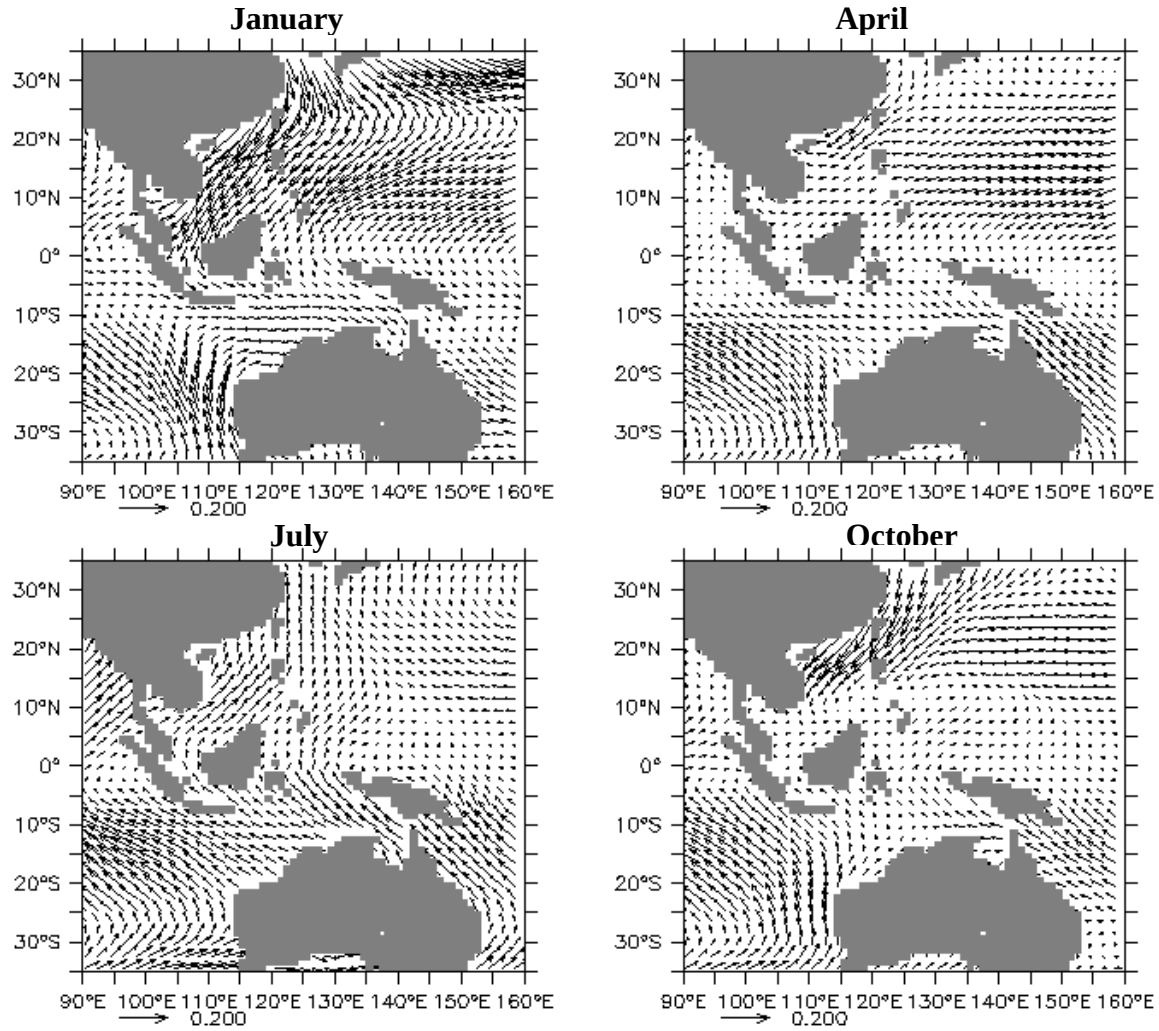

Figure 2-3 Present-day monthly wind stress forcing (Nm^{-2}) [*da Silva et al*., 1994].

The glacial wind stress data are based on the model simulations for the LGM climate (Figure 2-4). Glacial wind forcing is derived from the atmospheric general circulation model (AGCM) ECHAM3 [*Lohmann and Lorenz*, 2000] experiments

for the LGM conditions. The wind field is calculated by taking the difference between the control and the LGM simulation of the AGCM experiment and adding the anomaly to the NCEP monthly climatology [*Paul and Schäfer-Neth*, 2003]. Additional glacial wind stress data are used to test the sensitivity of the circulation to the wind forcing: the sensitivity LGM experiment of the AGCM ECHAM3 [*Lohmann and Lorenz*, 2000] forced with the CLIMAP [1981] surface boundary conditions with cooled tropics and glacial wind stress from the coupled ocean-atmosphere model output of the NCAR Climate System Model (CSM) [*Shin et al.*, 2003] (Figure 2-4).

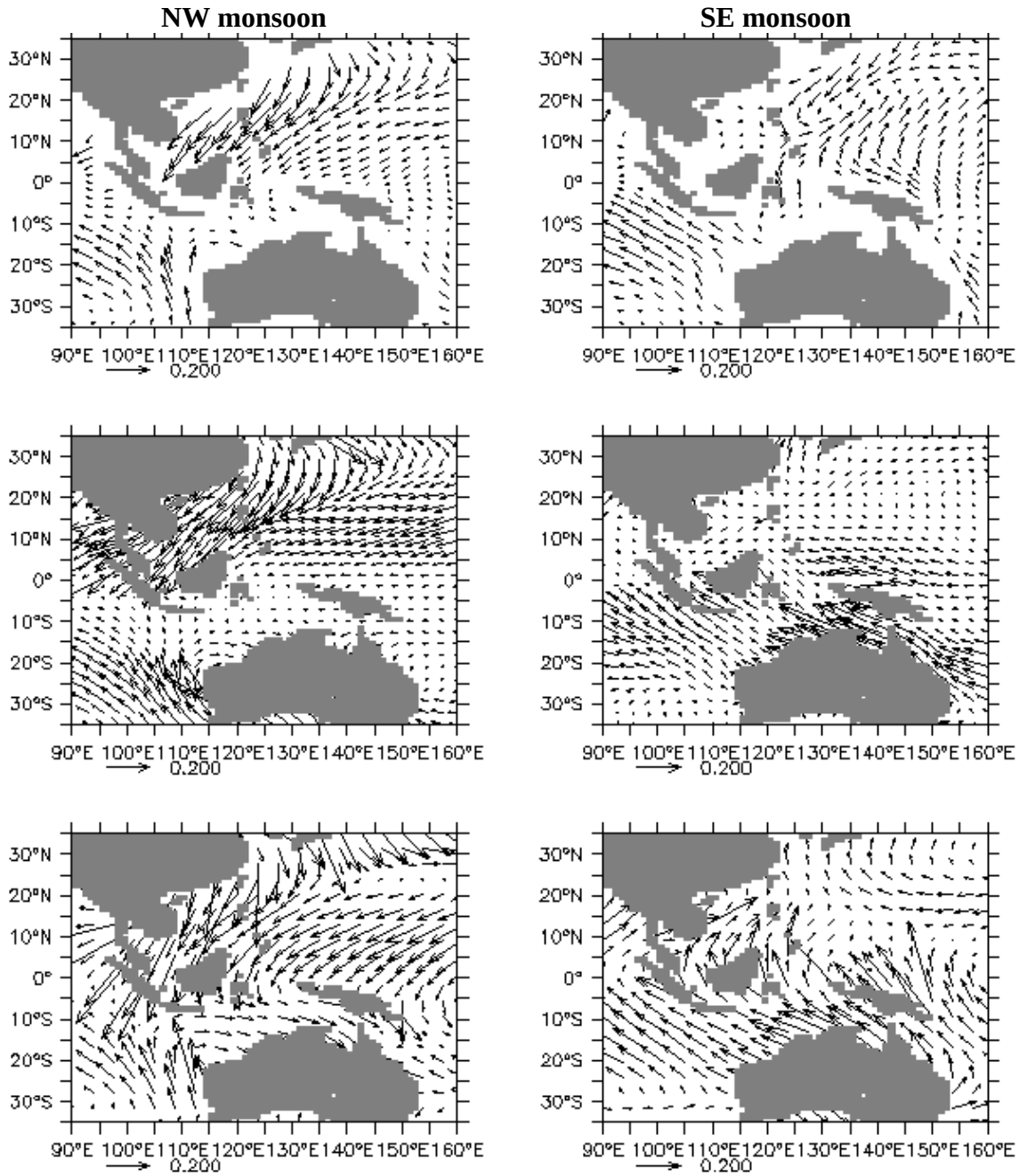

Figure 2-4 Glacial wind stress (Nm^{-2}) for January – NW monsoon (left) and July – SE monsoon (right) taken from model simulations of *Paul and Schäfer-Neth* [2003] (top), *Lohmann and Lorenz* [2000] (middle) and *Shin et al.* [2003] (bottom).

2.3.2 Surface heat and fresh water fluxes

Due to the poor constraints of the heat and salt surface fluxes for the glacial climate, restoration of sea surface temperature and salinity is used instead. The SST and SSS are relaxed to the climatological values on a time-scale of 30 days. The sensitivity of the circulation to surface heat fluxes and their impact on the ocean heat balance is additionally tested for the present-day conditions (see 3.6.2).

Sea surface temperature and salinity for present-day conditions are taken from the monthly climatology of the 1998 World Ocean Atlas [*Conkright et al.*, 1998] (Figure 2-4; Figure 2-6). The surface heat fluxes in the sensitivity experiment are derived from the monthly NOAA NCEP/NCAR Reanalysis Project surface data [*Kalnay et al.*, 1996]. The glacial boundary conditions for temperature and salinity are adopted from the global OGCM MOM experiment of *Paul and Schäfer-Neth* [2003] for the LGM climate. The SSTs in the global ocean model are based on compilation of reconstructed temperature data for the LGM. However, the Pacific and Indian Ocean SSTs have been restored to the CLIMAP [1981] temperature [*Paul and Schäfer-Neth,* 2003]. The glacial SSS data are based on the $\delta^{18}O$ measurements where available. Otherwise global salinity anomaly of 1.02 psu is added to the climatological values.

The glacial SSTs taken from the OGCM MOM experiment (Figure 2-5 right) are in average lower by approximately 2°C compared to the PD values. Strong cooling (3–5°C) is found off western Australian coast and in the South China Sea, while within Indonesian Gateways and equatorial West Pacific the temperature anomaly is small (1–2°C). Glacial SSS values in the OGCM MOM simulation (Figure 2-6 right) are higher by approximately 1 psu and show similar regional pattern as for the PD conditions.

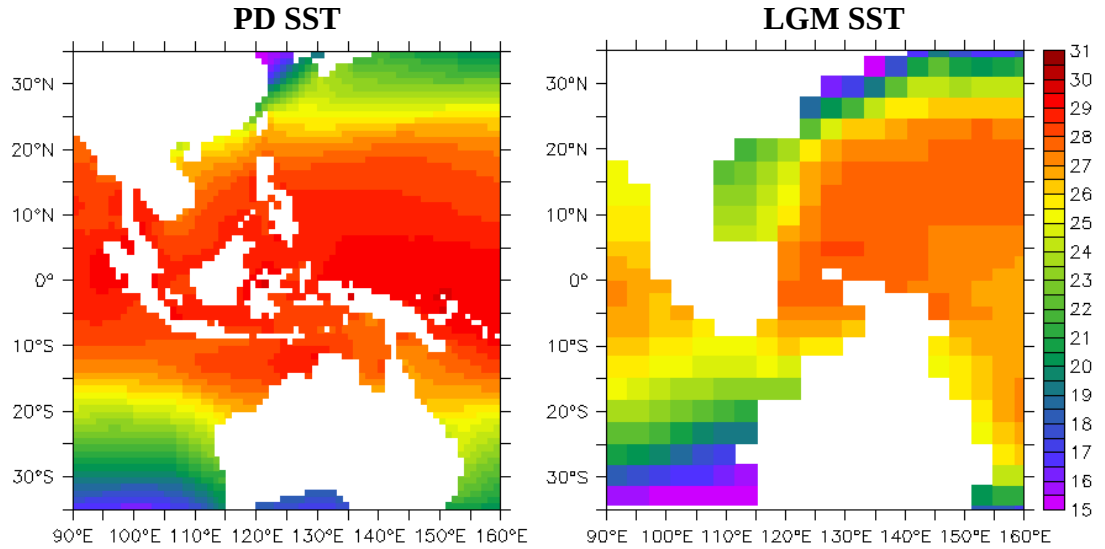

Figure 2-5 Mean annual sea surface temperature for present day [WOA 98] (left) and glacial conditions [*Paul and Schäfer-Neth,* 2003] (right).

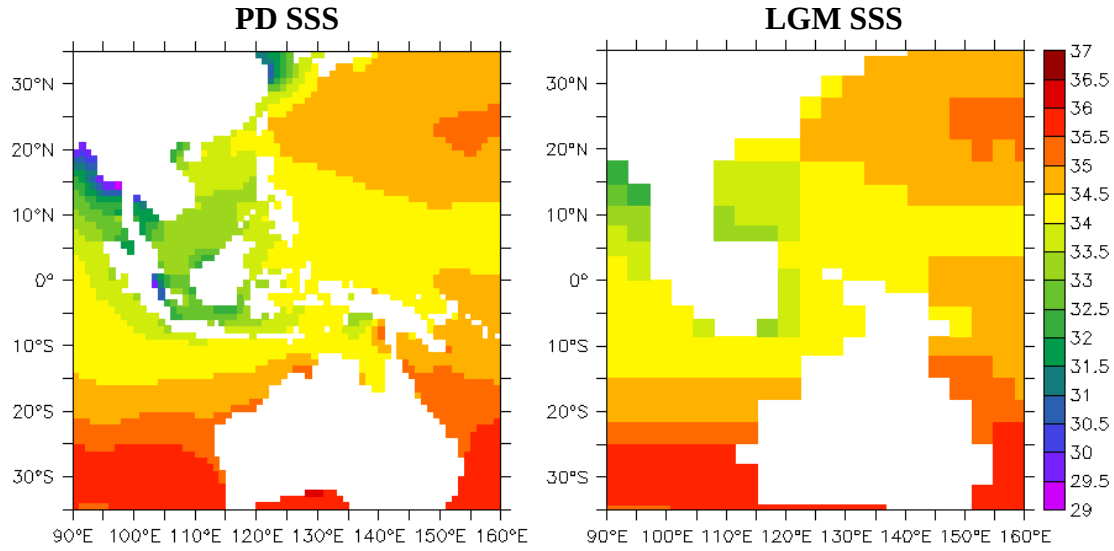

Figure 2-6 Mean annual sea surface salinity for present day [WOA 98] (left) and glacial conditions [*Paul and Schäfer-Neth,* 2003] (right).

The glacial temperature and salinity field is compared with the coupled ocean-atmosphere simulation from the NCAR CSM [*Shin et al.,* 2003] for the LGM climate (Figure 2-7). Both models show mean decrease in glacial SST by approximately 2°C, while the glacial SSS have been raised by approximately 1 psu compared to the control simulation (Table 2-3). However, models show different regional patterns in glacial SST and SSS anomalies. The salinity values in the ITF region in the control NCAR CSM simulation are significantly lower than observed so difference between the control and LGM experiment is considered for comparison (Figure 2-8). The LGM NCAR CSM model shows colder temperatures (2 – 3°C) in equatorial West Pacific compared to observations and area of WPWP is decreased. Strong cooling can be also found off West coast of Australia compared to the control simulation. Surface temperatures in Indonesian Gateways, South China Sea and East Indian Ocean are colder by about 2°C. Glacial SSS in the NCAR CSM experiment show higher values in the Indonesian Gateways and near the coast of Australia by more than 1.4 psu compared to the control simulation. Low salinity anomalies (0 – 1 psu) are found south of Java, in the equatorial West Pacific and South China Sea.

Table 2-3 Comparison of global model estimates of the glacial anomaly for the SST and SSS in the Indonesian Gateways (105°E – 140°E, 20°S – 10°N).

	MOM [*Paul and Schäfer-Neth,* 2003]	NCAR [*Shin et al.,* 2003]
ΔSST (°C)	-1.9 ± 0.1	-2.0 ± 0.3
	max: -2.1; min: -1.7	max: -3.3; min: -0.9
ΔSSS (psu)	1.18 ± 0.02	0.8 ± 0.5
	max: 1.22; min: 1.15	max: 2.9; min: -0.4

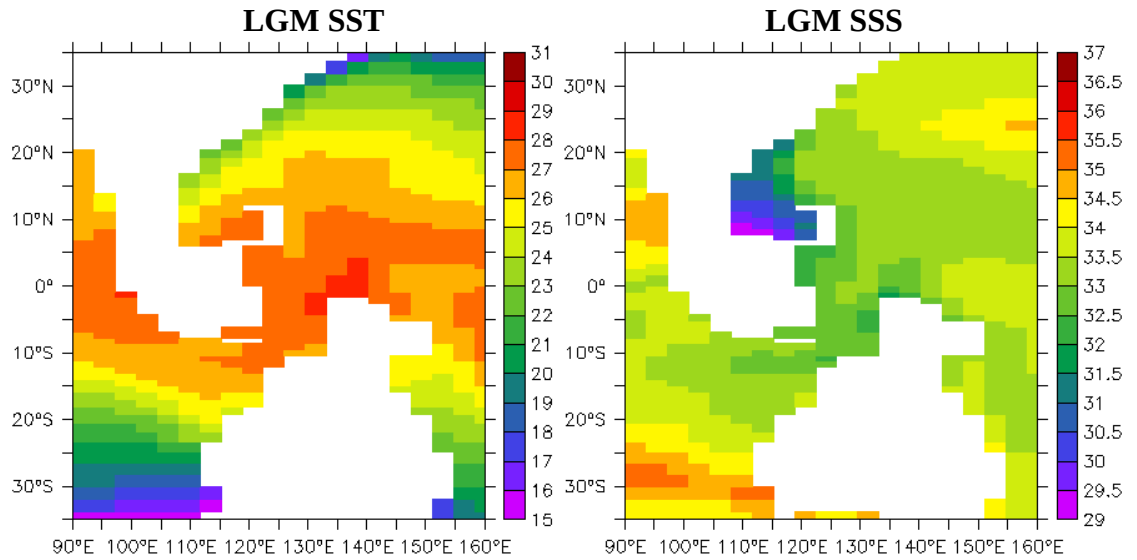

Figure 2-7 Glacial sea surface temperature (left) and salinity (right) from global NCAR CSM [*Shin et al.,* 2003].

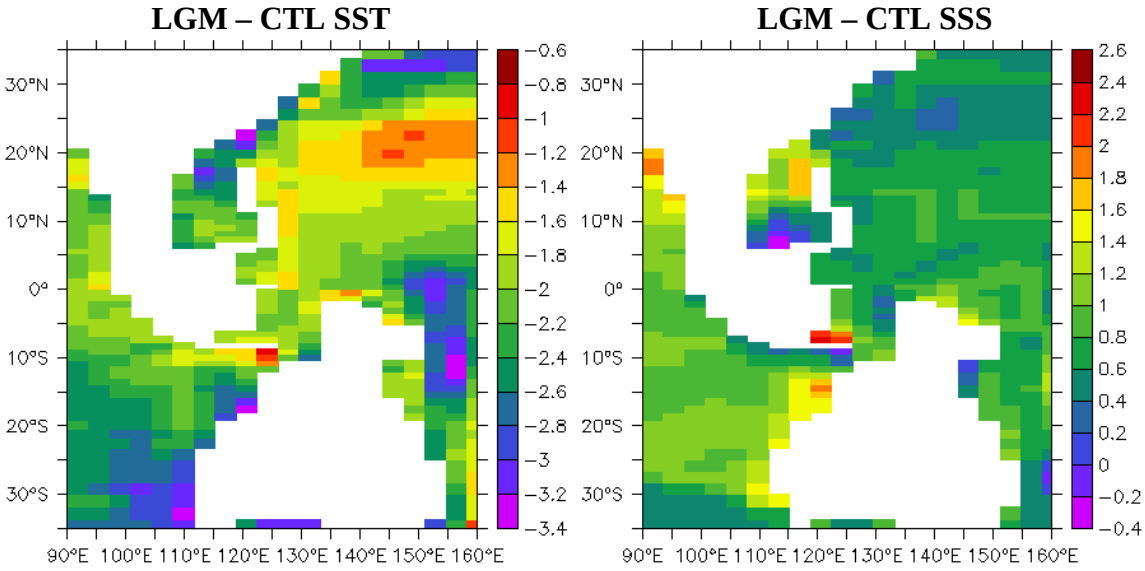

Figure 2-8 Sea surface temperature (left) and salinity (right) anomaly from LGM and control simulation of NCAR CSM [*Shin et al.,* 2003].

2.3.3 Open boundary conditions

The regional model configuration implies specification of the dynamical variables at the lateral boundaries. The simplest formulation of the lateral boundary conditions is the closed domain where the velocities at the boundary walls are set to zero. The MITgcm open boundary conditions (OBC) are formulated by setting the Orlanski radiation that allows propagation of the waves through the domain or prescribing the values of the dynamical variables at the boundary grid points. The dynamical variables include zonal (u) and meridional (v) velocity, potential temperature (θ) and salinity (S). The values for the sea surface height (SSH) and vertical velocity (w) are used dependent on the formulation of the free surface (non-linear free surface, non-hydrostatic formulation). In order to maintain mass conservation in the model, the transport balance between the inflow and outflow boundaries needs to be carefully set. The prescribed variables at the lateral boundaries do not allow ocean dynamics to develop freely near the boundary and possible discrepancies between the interior points and the boundary may occur due to the ocean dynamics developed in the model that are not included or differ from the boundary conditions. For this reason, the boundary and the nearby grid points are generally disregarded when analysing the ocean dynamics and possible additional damping near the boundary can be applied.

The model is setup with the four open lateral boundaries. Monthly climatologies of potential temperature and salinity fields are prescribed at the lateral boundaries at the inflow points. At the outflow points the temperature and salinity are taken from the nearby point inside the domain. The climatological data are taken from the same sources as for the surface values.

The velocity field at the lateral boundaries is taken from the global OGCM simulation for present-day conditions [*Paul and Schäfer-Neth*, 2003] and interpolated on the 1/6° horizontal resolution grid. The velocity at the western boundary at the Sunda shelf (105°E, 2°S – 10°N) and northern boundary in the South China Sea (105°E - 125° E, 10° N) is set to zero (Figure 2-9). The total volume transport is set to the annual mean value of ~12 Sv which is close to the observations [*Gordon*, 2001] and held constant throughout the simulation. In the glacial simulation, the total volume transport was reduced by 1/3 in accordance with global model prediction for the ITF transport during the LGM [MOM LGM experiment; *Paul and Schäfer-Neth*, 2003]. Values of the inflow and outflow transport at the lateral boundaries are given in Table 2-4.

Table 2-4 Prescribed volume transport (Sv) at the boundaries. Negative values indicate southward or westward velocities.

	PD	LGM
North 105°E – 140°E, 10°N	-9.2	-6.1
East 140°E, 20°S – 10°N	-3.0	-2
South 105°E - 140°E, 20°S	0.7	0.5
West 105°E, 20°S – 10°N	-12.9	-8.6
Total	**-12.2**	**-8.1**

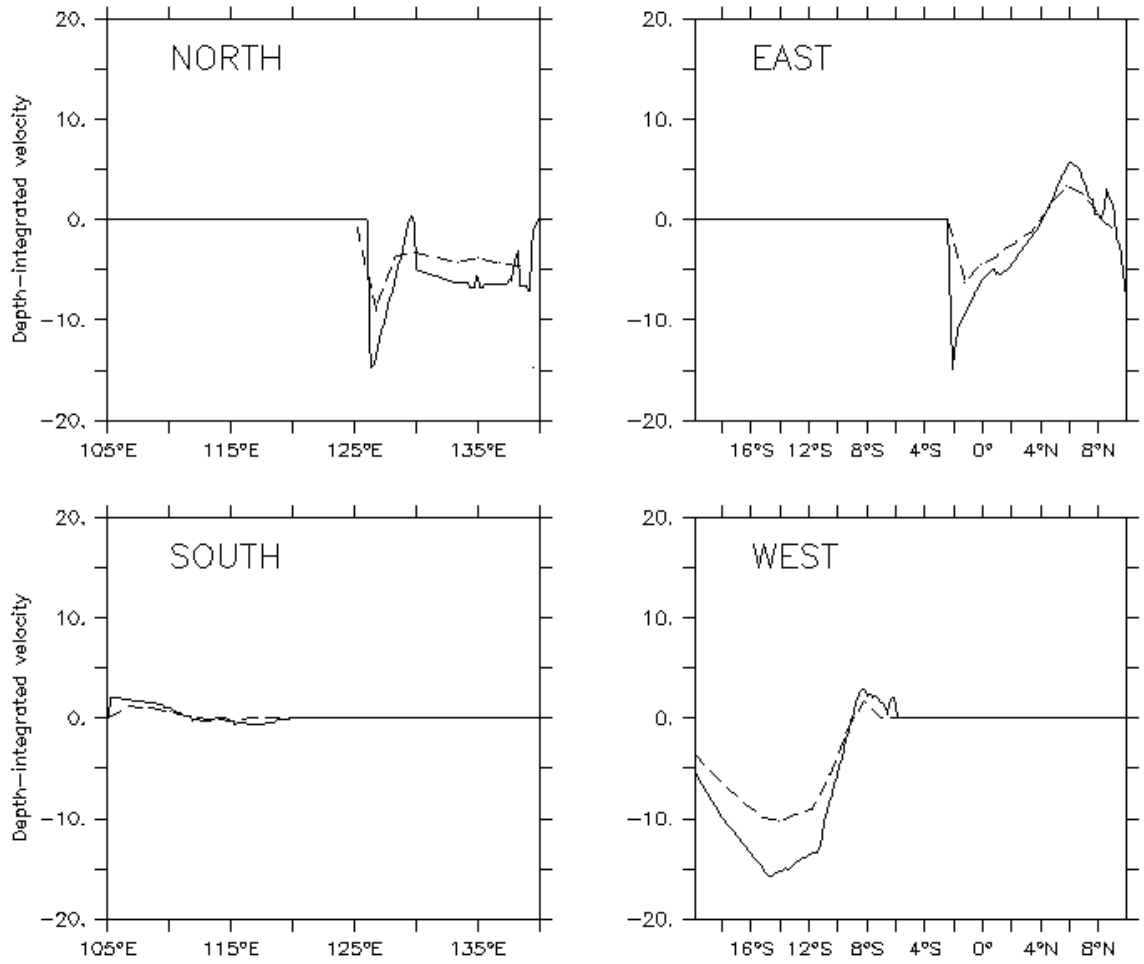

Figure 2-9 Depth integrated velocity (m^2s^{-1}) at the boundary walls for PD (solid line) and LGM conditions (dash line). The velocity field is derived from global MOM OGCM [*Paul and Schäfer-Neth*, 2003].

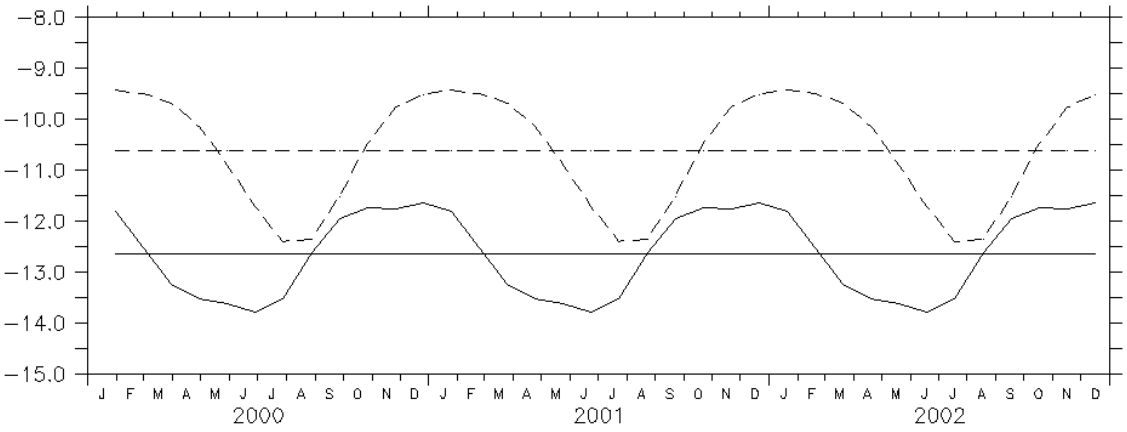

Figure 2-10 Seasonal cycle of the boundary transport (Sv) prescribed at the inflow boundaries for the PD (solid line) and LGM conditions (dash line). Negative values indicate transport towards Indian Ocean.

Sensitivity experiments are performed in which the boundary transport is varied on a monthly time-scale with velocity fields interpolated from the OGCM MOM experiments [*Paul and Schäfer-Neth*, 2003] for both PD and LGM conditions (Figure 2-10). The transport values show strong inflow for PD experiment during the SE monsoon from April to August. In the LGM experiment maximum transport occurs from July to September. For the sensitivity experiments configuration see also experimental setup in the following chapters.

2.4 Particle-trajectory module

The Lagrangian particle-tracing module is implemented in the MITgcm model. The stepping of the float advection is done using a second order Runge-Kutta scheme [*Press et al.*, 1992], whereby velocities and positions are bilaterally interpolated between the grid points. The original formulation of the float experiments is to simulate the floats that drift in depth and to the surface at a defined time. However, the drifters can be used as non-advective profiling floats for sampling dynamic variables at the mooring position or as non-profiling drifters on a fixed level including the surface. The implementation of the three-dimensional advection of the floats has not yet been sufficiently tested in the model. For the purpose of this study the drifters are considered weightless. A pre-defined vertical level of motion is used, therefore no vertical motion of the floats is allowed (dz/dt=0). The drifters are flagged out when reaching the outflow points at the lateral boundary or the coastline. In this way, the floats are allowed to leave the domain via open boundaries. At each time-step velocity, potential temperature, salinity and sea surface height at the float position is calculated. The experiments are designed to investigate patterns of distribution of the floats from the specific regions. The floats, therefore, represent potential marine organism or a tracer being transported through the Indonesian Gateways via ocean circulation. To incorporate temporal changes in the distribution patterns, the floats are released in the region of interest in repetitive time intervals.

3. Present-day Throughflow dynamics

3.1 Introduction

This chapter presents results of the experiments simulating the circulation in the Indonesian Gateways under present-day climate conditions. The main characteristics of the ITF are discussed and compared with the observations where possible. The focus of the analysis is on the volume and heat transport of the ITF, considered separately in inflow and outflow passages. The impact of topography on the vertical structure and seasonal variability of the transport inside the main passages is investigated. For the purpose of this study, only seasonal changes in ITF forcing are taken into account with the objective to establish the mean climatological circulation inside the Indonesian archipelago. For validation of the mean climatic characteristics of the ITF developed in the model it is compared to model results with a global OGCM experiments of similar resolution [ECCO project, *Menemenlis*, 2004] that include high-frequency surface forcing (6-hour) and inter-annual variability as well. Additional sensitivity experiments are performed to test the influence of the boundary conditions on the model developed circulation. Influence of the wind forcing, surface heat fluxes and temporal and spatial variations of the boundary currents are discussed.

Of the inflow passages, the main focus is on the dynamics in Makassar Strait as the major passage for the ITF. The second entrance to the Indonesian Gateways, through the eastern passages is between Sulawesi and Halmahera with the most important deep Lifamotola Passage. The eastern inflow passages have, so far, been poorly investigated and there are few data available to give reliable estimates of the transport. The recent 2-year long mooring measurements in Makassar Strait (ARLINDO project 1996-1998) provided a good description of the Throughflow dynamics within the passage. Makassar Strait topography is characterized by the deep and narrow Labani Channel (2000 m) and the broad and shallow Dewakang sill (~ 670 m) in the southern Makassar Strait. The flow below the sill depth is zero or even reversed towards north [*Gordon et al.*, 1999]. There is no significant discontinuity in the density stratification over the sill to indicate overflow processes [*Gordon*, 2003]. However, the sill appears to be a barrier for deep North Pacific waters to propagate towards south. The hydrographic measurements in the Flores Sea south of the sill show higher salinity and oxygen concentrations characteristic for the Indian Ocean. The available data are insufficient to investigate the long-term variability of the Throughflow within Makassar Strait. The mean annual cycle appears to be governed by local wind changes related to the monsoonal cycle. Regarding the heat transport variability associated with the monsoonal wind pattern *Gordon* [2003] proposed a mechanism on the basis of recent current and temperature measurements in Makassar Strait. During boreal winter monsoon low salinity Java Sea water enters the southern Makassar Strait and inhibits surface warm water transport from the Pacific to the Indian Ocean. During boreal summer, the wind reversal pushes the low salinity surface waters back into the Java Sea and allows intensified southward surface transport through Makassar Strait.

The exit passages investigated in the model include Lombok Strait, Ombai Strait and Timor Strait. The Lombok Strait is a narrow and shallow (250 – 300 m) westernmost exit passage. The surface flow from Makassar Strait is considered to be flowing directly through the Lombok Strait [*Sprintall et al.*, 2000]. The seasonal variability in the Lombok Strait derived form the CTD and pressure gauge measurement shows strongest outflow during the SE monsoon [*Murray and Arief*,

1988]. During the NW monsoon, the weak flow or reversal of the currents is observed [*Murray and Arief*, 1988; *Hautala et al.,* 2001]. Transport estimates based on January 1985 to March 1986 current meter mooring data [*Murray and Arief*, 1988] indicate that Lombok Strait carries only a small part of the total transport (~1.7 Sv) compared to the inflow from Makassar Strait.

A significant part of the Throughflow is considered to be flowing into the Indian Ocean through Ombai Strait (4.5 – 5.0 Sv) [*Hautala et al.*, 2001; *Molcard et al.* 2001]. The flow through Ombai Strait is restricted by sills of ~ 1000 m depth. Vertical profiles of the flow shows two distinct modes with upper layer flow displaying episodic reversals [*Sprintall et al.*, 2000; *Hautala et al.* 2001]. The reversal of the surface flow has been monitored during December and is most likely associated with the passage of costal Kelvin waves [*Chong et al.*, 2000; *Molcard et al.*, 2001]. The mean flow is strongest during the SE monsoon as observed in other exit passages. Although the mean current is strongest in the upper 200 m, the deeper flow carries significant part of the transport [*Molcard et al.*, 2001].

The easternmost exit passage is the Timor Strait. Bathymetry of the Timor Strait has two specific topographic structures: a shallow broad shelf and a deep passage (1300 – 1500 m) which allows deep water exchange with the Indian Ocean. Along the shelf a shallow coastal current is formed. Based on ADCP measurements and complementary historical data monitored in the strait in the period from 1976 to 1988, a total transport estimate of about 7 Sv is suggested with half of the transport in the upper 350 m [*Creswell et al.*, 1993]. Data from moored current meters on the shelf show a southward flowing coastal current transporting roughly 1 Sv towards the Indian Ocean with the shelf transport exceeding 3 Sv during the autumn transitions of the monsoon [*Creswell et al.*, 1993]. More recent current meter moorings give estimates of the transport of 3.4 to 5.3 Sv for the layer 0-1250 m in period March 1992 to April 1993 [*Molcard et al.*, 1996]. Hydrological characteristics indicate presence of upper Indian Ocean Deep Water near the bottom and opposite direction of the bottom flow is therefore expected. The upper 500 m flow are under influence of monsoon regime variability and show maximum of 3-4 Sv during the boreal spring and minimum of 1-2 Sv in boreal winter. The deeper transport (500 – 1250 m) has minimum in August [*Molcard et al.*, 1996].

The topographic barriers in the Indonesian Gateways redistribute the flow originating from the Pacific and reshape the profile of the ITF. The long pathway through the Indonesian Seas allows mixing of the waters by interactions with the atmosphere and topography thus changing its original properties. Observations show that individual passages have different variability in the transport associated with both large-scale and local forcing and therefore control the magnitude and timing of the flow. The aim of these experiments is to investigate the dynamics of the main passages and their role in modulating the ITF.

3.2 Experimental setup

The model configuration and data sources used in the control experiment for the PD conditions are described in sections 2.2 and 2.3. Overview of the sensitivity experiments designed to test the impact of lateral and surface boundary conditions on the model developed circulation is given in Table 3-1.

Sensitivity to surface forcing is considered in the PD - *no wind* and PD – *fluxes* experiments. In the PD – *no wind* simulation, the wind stress was switched off compared to the PD – *control* experiment to test the influence of the local seasonal wind forcing on the circulation.

Additional set of experiments were performed where total transport through the lateral boundaries is not varied in time, but its magnitude was scaled by factors: 0.25, 0.5, 0.75, 1 and 1.5. Absence of wind stress forcing was additionally tested in experiments with 0.5, 1 and 1.5 scaling. Seasonal variations are prescribed only for surface and lateral temperature and salinity fields. The intention of these experiments is to find response of the Makassar Strait volume transport to the prescribed total transport at the boundaries which is not governed by regional dynamics, but larger scale balance between Pacific and Indian Ocean.

Influence of surface heat fluxes on ocean circulation and heat transport is tested in PD – *fluxes* experiments. Difference between applied monthly climatological heat fluxes and surface restoring of temperatures is investigated.

Special attention is given to the representation of the lateral boundary currents. Finding the correct representation of the inflow and outflow currents particularly in the equatorial West Pacific is a difficult task since there are no reliable estimates of the relative strength and temporal variability of the main currents.

In experiment PD – *cyclic*, temporal variability in the boundary transport is considered by varying the velocity field with a repeating annual cycle. The monthly averages of the velocity field are interpolated from the PD OGCM MOM experiment [*Paul and Schäfer-Neth*, 2003].

Table 3-1 Overview of sensitivity experiments for the present-day (PD) climate conditions.

Experiment	Wind stress	Surface fluxes	Lateral boundary velocity
PD - *control*	monthly	monthly restoring	annual - MOM
PD - *no wind*	no wind	monthly restoring	annual - MOM
PD - *fluxes*	monthly/no wind	monthly restoring/heat fluxes	annual - MOM
PD - *cyclic*	monthly	monthly restoring	monthly - MOM
PD - *ecco*	monthly	monthly restoring	annual - ECCO

An additional experiment is designed to test the sensitivity of the circulation to the spatial representation of the boundary currents where the velocity field is taken form the global MITgcm output of ECCO project [*Stammer et al., 2003*]. In experiment PD – *ecco* the boundary currents are interpolated from the 10-year average (1992-2002) ECCO global run with 1° zonal and 0.3° meridional resolution (near the equator). Experiment description and model configuration can be found at: http://www.ecco-group.org, http://ecco.jpl.nasa.gov/datasets/ecco2.html. The transport is held constant at long term mean annual values throughout the simulation. The high-resolution velocity field gives a significantly different representation of boundary currents even though the mean volume transport is similar (10.9 Sv compared to 12.2 Sv taken from the OGCM MOM). The time mean, depth-integrated circulation developed in the OGCM MOM and ECCO MITgcm is shown in Figure 3-1. Volume transports of the inflow and

outflow currents are given in Table 3-2. The main difference appears in the West Pacific equatorial currents. The representation of the north and east inflow boundary is illustrated in Figure 3-2. The inflowing Mindanao Current has stronger amplitude in the higher resolution model (ECCO) and the flow is more surface intensified. The eastern boundary shows strong outflow with the NECC in the ECCO experiment, which is not well distinguished in the low-resolution model.

Assuming that the ECCO model has more realistic representation of the West Pacific boundary currents than the OGCM MOM, the purpose of this experiment is to find to what extent representation of the boundary currents influences the ITF volume and heat transport. If the ITF characteristics do not change significantly with the more detailed spatial representation of the boundaries, the low-resolution model can be further used as forcing for the ITF. Considering that high resolution model for LGM climate is not available this would be a great advantage.

Table 3-2 Mean volume transport (Sv) of the main equatorial currents in the global model estimates. Negative values indicate southward/westward velocities.

	MOM	ECCO
Mindanao Current (120°E – 135°E, 10°N)	-9.4	-20.7
New Guinea Current (140°E, 4°S – 1°N)	-2.4	-6.7
NECC (140°E, 2°N – 8°N)	-2.0	19.6
SEC (105°E, 18°S – 6°S)	-14.5	-11.8

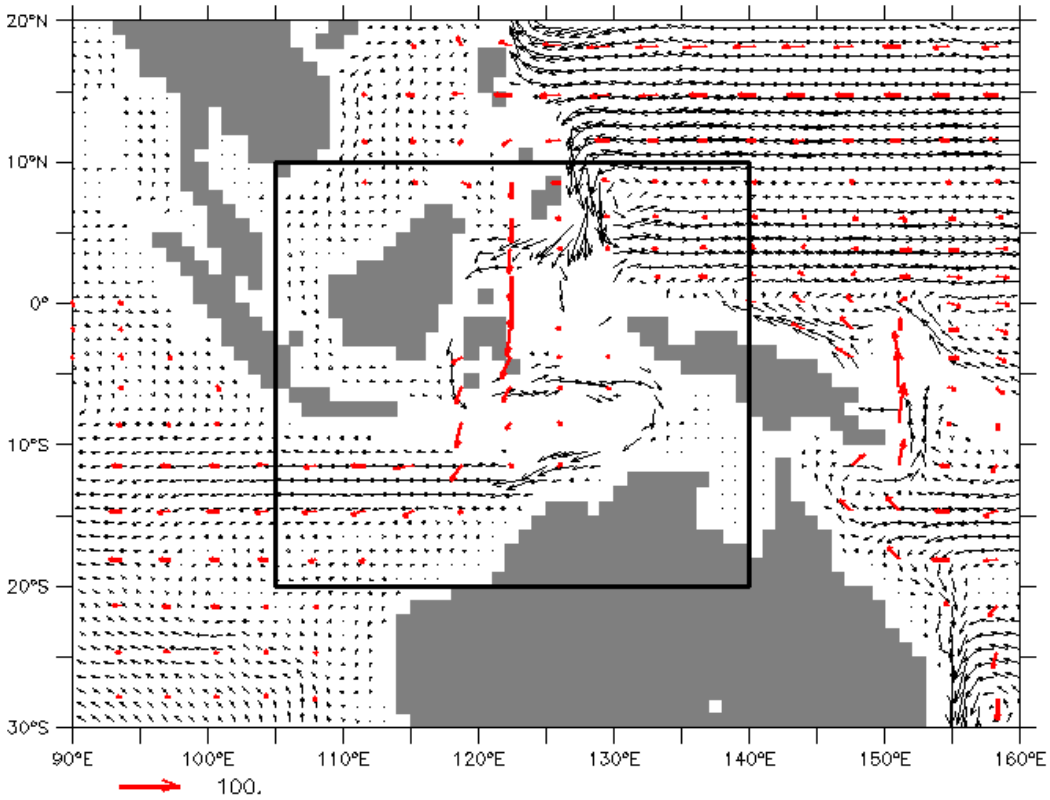

Figure 3-1 Depth-integrated velocity (m^2s^{-1}) taken from the global MOM (red) and MIT ECCO (black) OGCM. The thick black square shows the model domain.

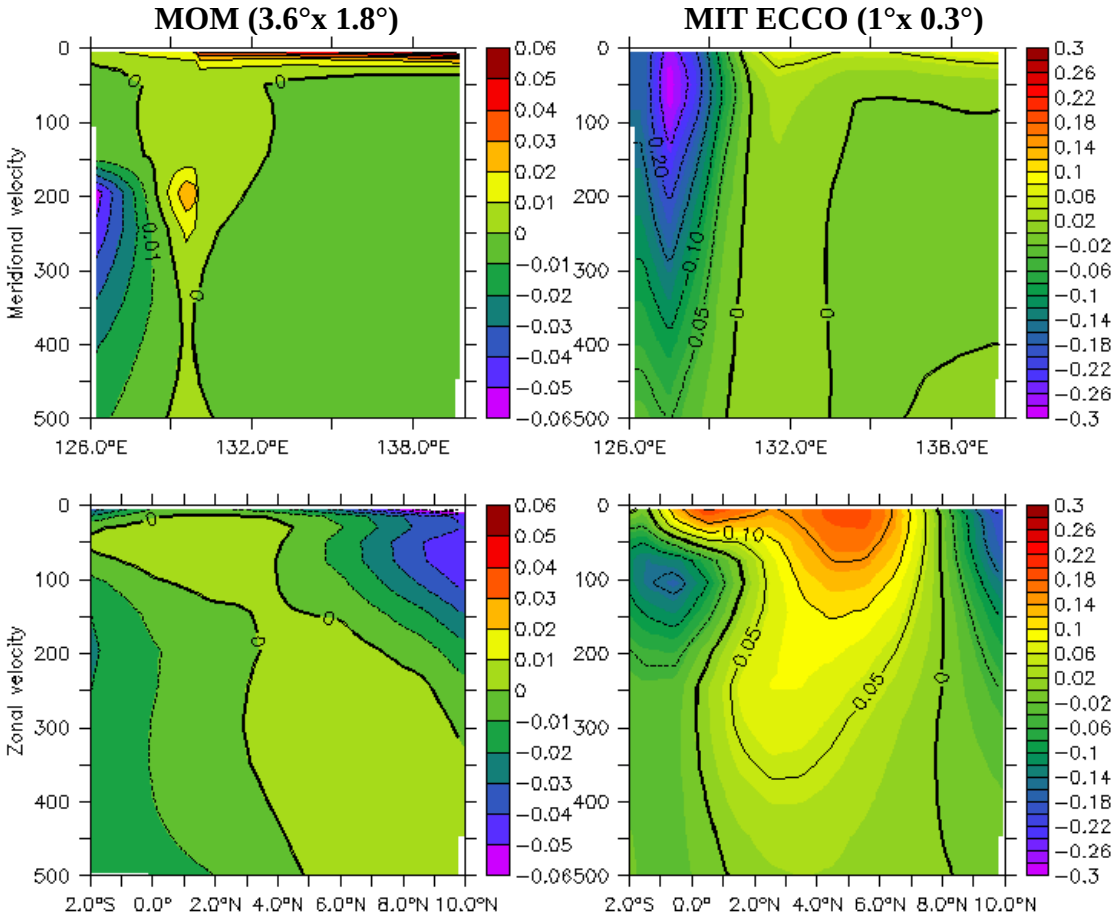

Figure 3-2 North boundary at 10°N (up) and east boundary at 140°E (down) velocity field (ms^{-1}) as derived from global model MOM (left) and MIT ECCO (right).

3.3 Mean circulation

The bulk of the ITF takes route through Makassar Strait. Deep water flow enters the Indonesian region through the Lifamatola Passage between the Celebes and Halmahera. Part of the surface flow exits through the Lombok Strait into the Indian Ocean. The major part of the ITF waters turns eastward and exits the Indonesian Gateways through the Ombai and Timor Passages (Figure 3-3).

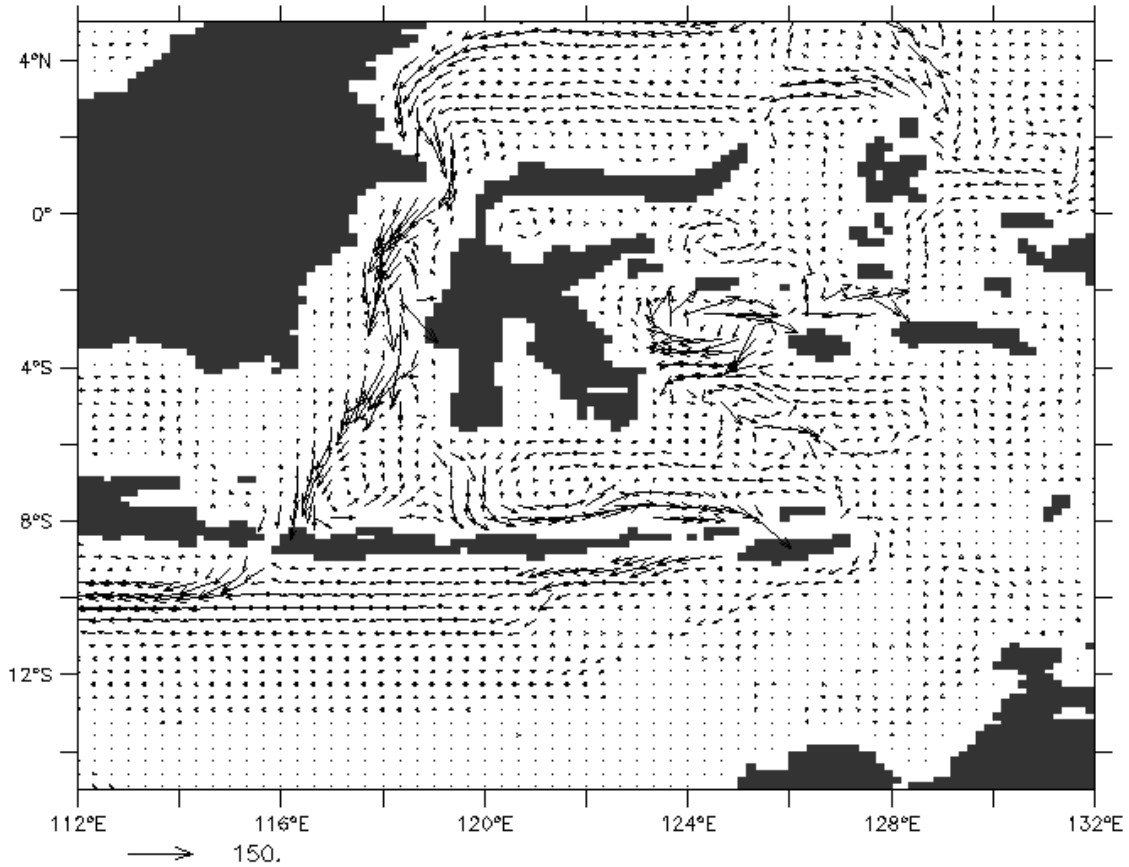

Figure 3-3 Mean annual depth-integrated flow (m^2s^{-1}) through the Indonesian Gateways.

3.3.1 Volume transport

Horizontal volume transport (Q_v) through the passage of width L and depth $h(x)$ is defined conventionally as integral of the velocity component (v) normal to a cross section of the passage:

$$Q_v(t) = \int_0^L \int_{-h(x)}^0 v(x,z,t)dzdx \qquad 3\text{-}1$$

The volume transport values through the main passages are given in Table 3-3. The flow through Lombok Strait in the model is higher then observed (3.7 Sv compared to 1.7 Sv [*Murray and Arief*, 1988]). The narrow Lombok Strait (~18 km width) had to be widened in the model to 36.7 km due to the horizontal resolution of the model. This might be one reason for the overestimated transport. Overall, the model produces mean circulation patterns through the passages in reasonable agreement with the observations.

Table 3-3 Volume transport (Sv) through the main Indonesian passages (for the location of transects see Figure 2-1). Model results compared to the observations. Given are annual mean values and standard deviations of the transports. The numbers in brackets show minimum and maximum value of the transport. Positive values indicate southward transport towards the Indian Ocean.

	Model transport	Observations
Makassar Strait	9.3 ± 1.3	9.3 ± 2.5 *Gordon et al.* [1999]
	(7.0 – 11.7)	8.1 ± 1.5 *Susanto and Gordon* [2004]
Sulawesi – New	2.4 ± 2.2	~ 1-2 *Gordon et al.* [2000]
Guinea	(-1.5 – 6.0)	
Lombok Strait	3.7 ± 0.5	1.7 ± 1.2 *Murray and Arief* [1988]
	(3.0 – 4.9)	2.6 ± 0.8 *Hautala et al.* [2001]
Ombai Strait	5.9 ± 1.5	5.0 ± 1.0 *Molcard et al.* [2001]
	(3.4 – 7.8)	
Timor Passage	2.5 ± 1.2	7.0 *Creswell et al.* [1993]
	(0.8 – 4.6)	4.5 ± 1.5 *Molcard et al.* [1994]
		4.3 ± 1.0 *Molcard et al.* [1996]

3.3.2 Heat transport

The ocean heat content (Q) is given by:

$$Q = \rho_0 c_p \iiint_V \theta dz dx dy \qquad 3\text{-}2$$

where V is the volume of the basin, c_p is the specific heat capacity (~ 4000 $Jkg^{-1}K^{-1}$) and ρ_0 is the water density (~ 1025 kgm^{-3}) (adopted from *Stammer et al.* [2003]). The rate of heat change is then given by the sum of the divergence of heat transported by the ocean (Q_h) and net surface heat flux (H_Q):

$$\frac{\partial Q}{\partial t} = -\nabla \cdot Q_h + H_Q \qquad 3\text{-}3$$

The meridional ocean heat transport is defined as the zonally integrated meridional temperature transport relative to the reference temperature (θ_r):

$$Q_v = \rho_0 c_p \int_0^L \int_{-h(x)}^0 v(\theta - \theta_r) dz dx \qquad 3\text{-}4$$

The diffusion term in the heat transport formulation is usually small and is therefore generally excluded from the calculation. The heat fluxes at the surface in the model are given by relaxation on a monthly time-scale towards the climatological values. The average difference between the top layer (5 m) temperature developed in the model and the restoring temperature is ~ 1°C and does not exceed 2°C. In this case, the surface heat fluxes are order of magnitude smaller (~ 0.01 PW) compared to the meridional ocean heat transport and can be neglected. The absolute values of the heat transport (relative to 0°C) and the heat transport relative to 3.4 °C are given in Table 3-4. The 3.4°C is the spatially averaged temperature of the return flow into the Pacific between Australia and Antarctica [*Schneider and Barnett,* 1997]. The estimates of the meridional heat transport through Makassar Strait agree well with the observational estimate of 0.58 PW or 0.45 PW relative to the 0°C or 3.4°C, respectively, for the volume transport of 9.4 Sv [*Vranes et al.*, 2002].

Gordon and McClean, [1999] investigated relative importance of the ITF heat input for the Indian Ocean heat budget using model and observational data. The ITF heat transport valued 0.66 PW which accounted for 65% of the southern Indian Ocean heat input. The remaining 35% where provided by solar radiation north of the

Throughflow. However, mean volume transport in the model was underestimated (3.9 Sv) compared to the observations (9.3 Sv) [*Gordon et al.*, 1999]. More recent global ocean circulation estimates of volume, heat and freshwater fluxes using GCM constrained by World Ocean Circulation Experiment (WOCE) data [*Stammer et al.*, 2003] give value of the ITF heat transport of 1.12 ± 0.5 PW relative to 0°C, while mean volume transport values 11.5 ± 5 Sv for the period 1993 – 2000. The model value of 0.83 ± 0.14 PW for the total ITF heat transport relative to 0°C is in the range of expected observational values. However, the term "heat transport" is only applicable when mass balance is closed [*Bohren and Albrecht*, 1998].

Table 3-4 Heat transport Q (PW) through the main passages (for the location of transects see Figure 2-1). The heat transport is given relative to the reference temperature. Positive values indicate transport towards the Indian Ocean.

	relative to 0°C	relative to 3.4°C
Makassar Strait	0.61 ± 0.10	0.48 ± 0.09
Sulawesi – New Guinea	0.08 ± 0.23	0.05 ± 0.20
Lombok Strait	0.34 ± 0.05	0.29 ± 0.04
Ombai Strait	0.31 ± 0.19	0.23 ± 0.17
Timor Passage	0.12 ± 0.11	0.09 ± 0.09
TOS	0.43 ± 0.11	0.31 ± 0.11
ITF	0.83 ± 0.14	0.65 ± 0.14

The heat balance in the regional model with open boundaries is analysed by calculating individual components of the heat transport in the ocean interior and at the boundaries (Figure 3-4). Integrating the heat equation (Equation 3-3) in the model domain between west (x_W) and east (x_E) boundary starting from the north (y_N), the net heat divergence Q_{net} at the latitude y is given as:

$$Q_{net}(y) = \rho_0 c_p \int_{y_N}^{y}\int_{x_W}^{x_E}\int_{h}^{0} v(\theta-\theta_r)dxdydz + \rho_0 c_p \int_{y_N}^{y}\int_{h}^{0} u(\theta-\theta_r)dydz\Big|_{x_W}^{x_E} + \int_{y_N}^{y}\int_{x_W}^{x_E}\int_{h}^{0}\frac{\partial Q}{\partial t}dxdydz \quad 3\text{-}5$$

where first term is zonally integrated meridional temperature transport across the model domain $Q(y)$ minus component at the northern boundary Q_N. Second term can be separated into zonal heat transport at the eastern (Q_E) and western (Q_W) open boundaries given as following:

$$Q_E(y) = \rho_0 c_p \int_{y_N}^{y}\int_{h}^{0} u(\theta-\theta_r)dydz\Big|_{x_E} \quad 3\text{-}6$$

$$Q_W(y) = \rho_0 c_p \int_{y_N}^{y}\int_{h}^{0} u(\theta-\theta_r)dydz\Big|_{x_W} \quad 3\text{-}7$$

The third term is temporal heat storage change:

$$Q_{storage} = \int_{y_N}^{y}\int_{x_W}^{x_E}\int_{h}^{0}\frac{\partial Q}{\partial t}dxdydz \quad 3\text{-}8$$

The heat equation in the model can now be simply written as:

$$Q_{net}(y) = Q(y) - Q_N(y) + Q_E(y) - Q_W + Q_{storage} \quad 3\text{-}9$$

The resulting integrals are illustrated in Figure 3-4. The net heat transport shows cooling of the ocean interior from 0.2 PW at the northern part reaching approximately

0.35 PW at the southern boundary. The corresponding integrated NCEP climatological surface flux [*Kalnay et al.*, 1996] gives net heating of 0.35 PW over the model domain.

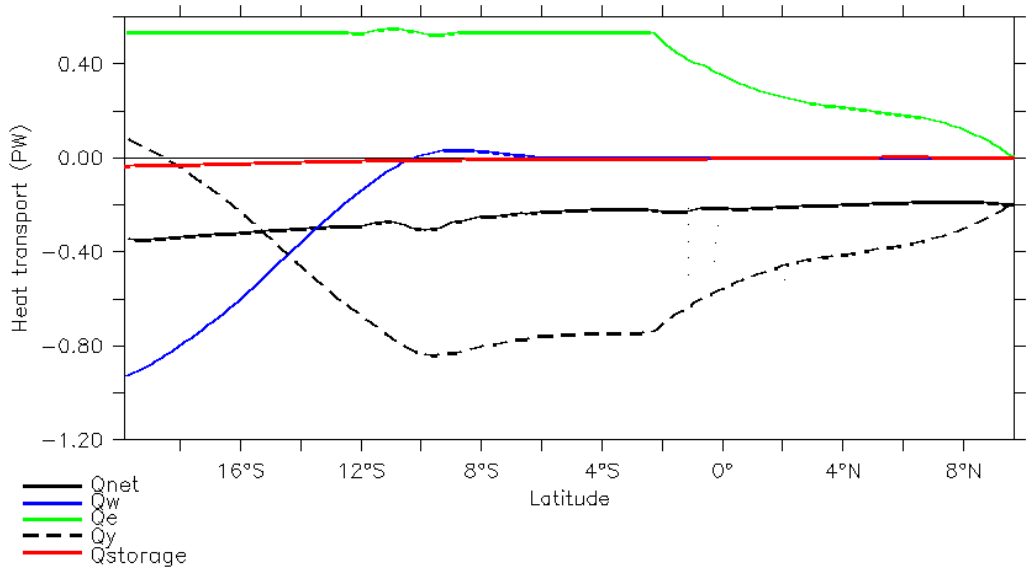

Figure 3-4 Net heat flux (Q_{net}) in the model is calculated using zonally integrated meridional heat transport relative to 0°C (Qy), east (Q_E) and west (Q_W) zonal transport components and heat storage ($Q_{storage}$).

3.3.3 Freshwater transport

Mean zonally integrated meridional freshwater transport (from *Stammer et al.* [2003]) is estimated as:

$$F_W = \int_0^L \int_{-h(x)}^0 \rho v (1 - \frac{S}{S_0}) dz dx \qquad 3\text{-}10$$

where S_0 is the mean salinity. In the ocean interior, zonally averaged meridional freshwater transport at 4°S values 0.036 ± 0.044·10^9 kgs^{-1} with reference average salinity in the model S_0=34.64 psu. If the reference salinity S_0=32.5 is taken as average salinity in the Bering Strait used for estimating Pacific and Indian Ocean freshwater transports [*Wijffels et al.*, 1992], the mean freshwater transport through the model domain at 4°S including boundary contribution is 0.775 ± 0.043·10^9 kgs^{-1}. Since the value of freshwater transport is dependant on the average salinity in a closed system, the salt budget could not be compared with climatological data and only relative values referenced to average salinity in the model (S_0=34.64 psu) are analysed.
The additional freshwater input at the surface is given by:

$$F = P - E + R \qquad 3\text{-}11$$

where P – E is difference between precipitation and evaporation and R is the river runoff. The total ocean-atmosphere freshwater exchange in the tropical Pacific (8°S – 24°N) and Indian Ocean (North – 8°S) are small (0.1 ± 0.3·10^9 kgs^{-1}) and uncertainties in estimates of freshwater transports are very large [*Ganachaud and Wunsch*, 2003]. A large source of uncertainty is estimate of river runoff [*Wijffels et al.*, 2001]. In the model, the freshwater air-sea fluxes are included only by restoring of sea surface salinities to monthly climatology [*Conkright et al.*, 1998] as:

$$F_{res} = \int_{o}^{L}\int_{o}^{M} \rho \frac{S - S_{res}}{S_0} \frac{\Delta z}{\tau} dxdy \qquad 3\text{-}12$$

where S_{res} is the restoring SSS and τ is the relaxation time. The difference between the model surface salinities and restoring values is in average 0.04 psu. For comparison, this gives surface freshwater flux between 4°S and 6°S of $0.011 \pm 0.007 \cdot 10^9$ kgs^{-1}. The surface freshwater fluxes in the Indonesian Seas could be important for the salt budget. However, the values are not well constraint, especially when glacial climate conditions are considered and are therefore not analysed in detail.

3.3.4 Transport of Pacific water masses

Hydrographic data from the Pacific Ocean show different water masses characteristics in the North and South Pacific (Figure 3-5). Analysis of relative contribution of different water masses in the Indonesian Seas shows that the ITF mainly contains North Pacific water masses [*Fine*, 1985; *Gordon*, 1986; *Ffiled and Gordon*, 1992]. Five major Pacific water masses are defined according to the hydrographic data [*Wyrtki*, 1961; *Gordon*, 1995; *Hautala et al.*, 1996] and their exchange through the Indonesian Seas is analysed in the model. Temperature, salinity, density class and approximate depth range of main water masses analysed in the model are given in Table 3-5.

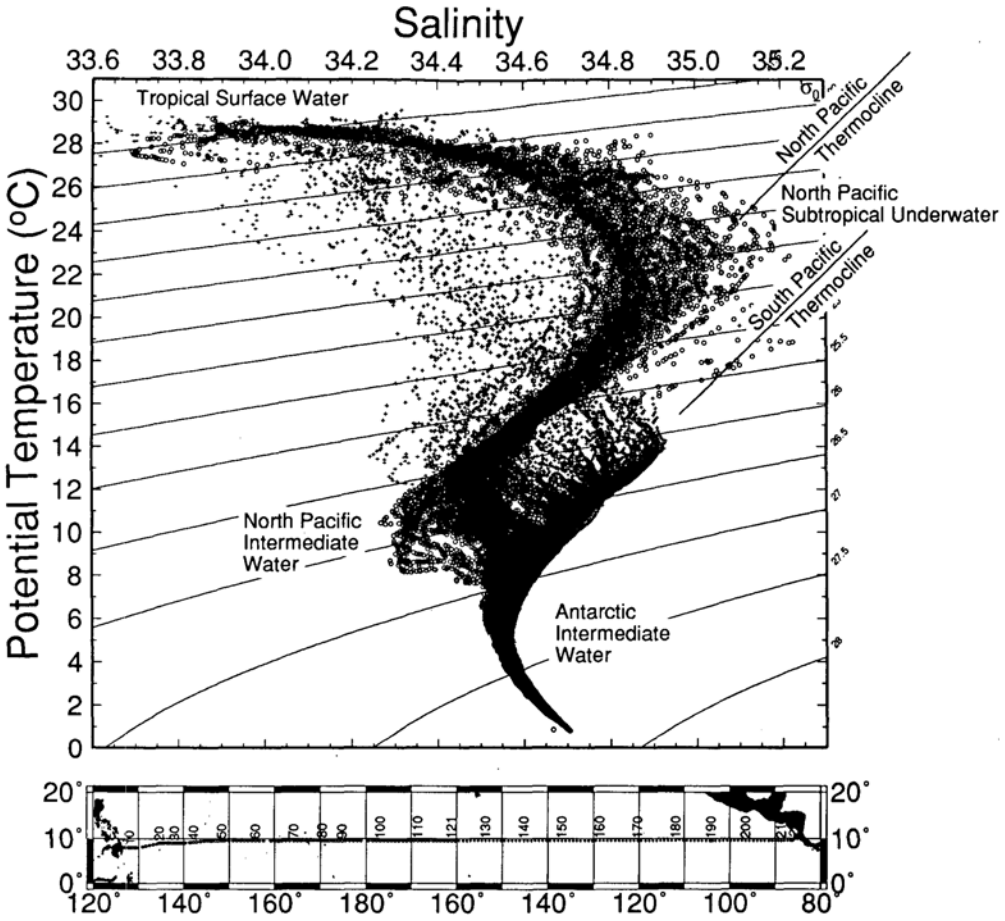

Figure 3-5 Potential temperature and salinity along 10°N in the Pacific Ocean from CTD stations from the R. V. *Moana Wave* in January – May 1989 [*Gordon*, 1995].

Table 3-5 Pacific water masses characteristics.

	Depth (m)	Potential density (σ_θ)	Temperature (°C)	Salinity (psu)
Tropical Surface Water	0 – 100	21 – 23	24 – 28	33.6 – 34.6
North Pacific Thermocline	100 – 220	23 – 25.5	15 – 24	34.6 – 35.1
South Pacific Thermocline	220 – 300	25.5 – 26.5	13 – 24	34.6 – 35.3
North Pacific Intermediate Water	300 – 550	26.5 – 27	7 – 11	34.1 – 34.5
Antarctic Intermediate Water	750 – 1200	27.25 – 27.5	3 – 7	34.45 – 34.6

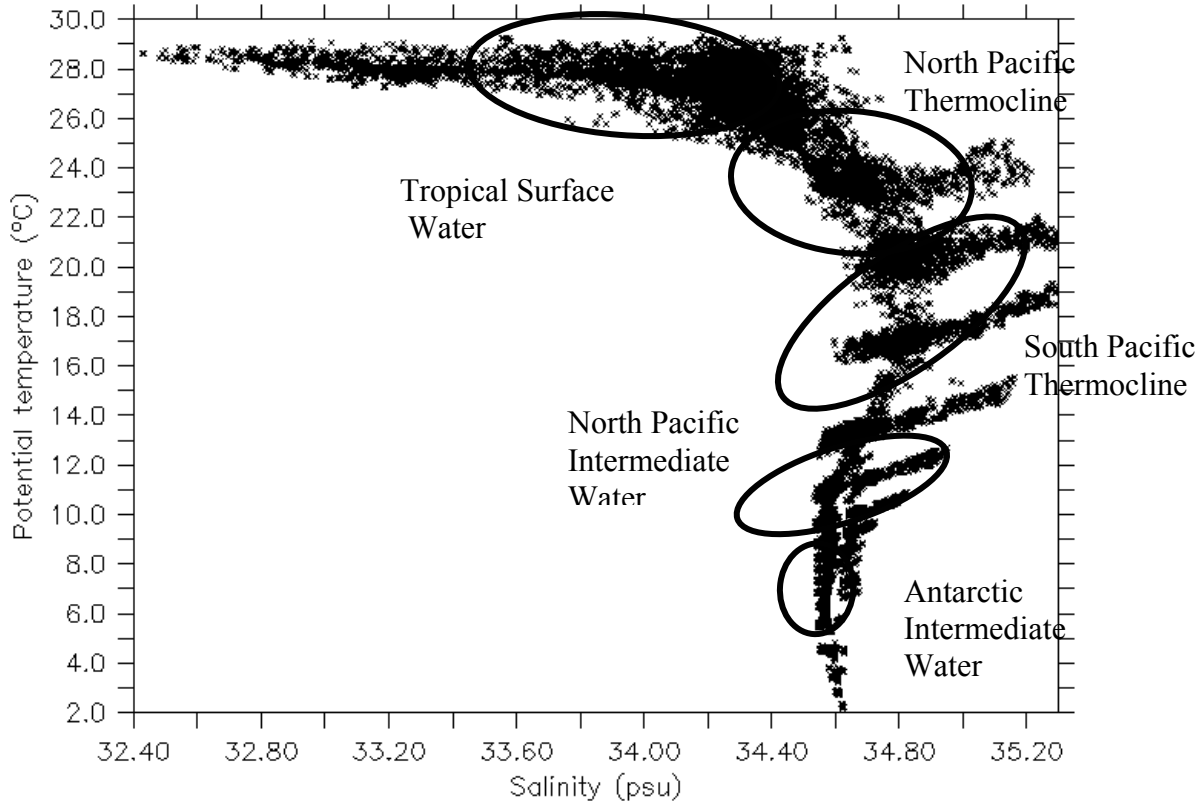

Figure 3-6 Regional model potential temperature and salinity in the Indonesian Seas between 110°E – 135°E and 8°S – 0°.

The temperature and salinity values in the model (Figure 3-6) show presence of different Pacific water masses in the Indonesian Seas. The mean volume, heat and freshwater transport of each water mass at 4°S are given in Table 3-6. The values of the volume transport confirm that the main contribution to the ITF is from the North Pacific (7.1 Sv compared to 2.8 Sv from South Pacific). The low salinity values (32.4 – 33.6 psu) characteristic for the surface water in the Indonesian Seas are not included in the Pacific water masses characteristics (see Figure 3-5). Their contribution would further enhance the freshwater transport towards the Indian Ocean. The North Pacific Thermocline characterized by the salinity maximum shows freshwater transport in opposite direction, indicating increase in salt input into the Indian Ocean. The South Pacific Thermocline transport is also indicating increase in salt into the Indian Ocean, however its contribution is small.

Table 3-6 Volume (Sv), heat transport (PW) relative to 0°C and freshwater transport referenced to mean salinity (S_0=34.64 psu) for individual water masses at 4°S. Positive values indicate transport towards the Indian Ocean.

	Volume transport (Sv)	Heat transport (PW) relative to 0°C	Freshwater transport (10^9 kgs^{-1}) reference to 34.64 psu
Tropical Surface Water	2.5 ± 1.4	0.27 ± 0.17	0.034 ± 0.030
North Pacific Thermocline	2.3 ± 0.5	0.19 ± 0.05	-0.013 ± 0.002
South Pacific Thermocline	1.8 ± 0.2	0.09 ± 0.01	-0.004 ± 0.002
North Pacific Intermediate Water	2.3 ± 0.5	0.08 ± 0.02	0.003 ± 0.001
Antarctic Intermediate Water	1.0 ± 0.2	0.02 ± 0.003	0.002 ± 0.0003

3.4 Makassar Strait

3.4.1 Geostrophic balance

Makassar Strait carries the bulk of the Throughflow and ocean dynamics within the Strait are analysed in more detail. The flow within Makassar Strait can be described as geostrophic except for the region near the equator. Using Boussinesq approximation, therefore retaining full accuracy for density (ρ) only when calculating pressure, geostrophic balance for the meridional flow (taken from *Stewart* [2002]) is given by:

$$v_g = \frac{g}{f\rho_0}\frac{\partial}{\partial x}\int_{-h}^{0}\rho(z)dz + \frac{g}{f}\frac{\partial\zeta}{\partial x} \qquad 3\text{-}13$$

where g is the gravity constant (g = 9.81 ms^{-2}), $f = 2\Omega sin(\varphi)$ is Coriolis parameter at latitude φ, ρ_0 is mean ocean density and ξ is the sea surface height. First term in the Equation 3-13 gives relative velocity due to horizontal pressure gradient induced by variations in density and is depth dependant, while second term gives surface geostrophic current due to the slope of the sea surface. The vertical profile of geostrophic current is calculated referenced to the surface, therefore adding the surface geostrophic velocity to the relative velocity at the depth h.

In Figure 3-7 is illustrated geostrophic balance at the surface. A zonal sea surface gradient of $0.3\cdot10^{-6}$ at 6.4°S, where Coriolis parameter is approximately $-1.6\cdot10^{-5}$ s^{-1}, gives rise to a southward meridional velocity of approximately 0.2 ms^{-1}. The sea surface gradient does only reflect the flow in surface level and not the total barotropic flow. The vertical profile of the flow derived from the geostrophic approximation seems to be in good agreement with the mean model profile (Figure 3-8). The slope of the internal density surfaces forces baroclinic shear in the northward direction at intermediate levels (Figure 3-9). Maximum of the flow is between 50 and 150 m. The flow below the sill depth (~ 670 m) in the southern Makassar Strait is almost zero. The model developed vertical profile of the flow with subsurface maximum agrees well with the observations [*Gordon et al.*, 2003].

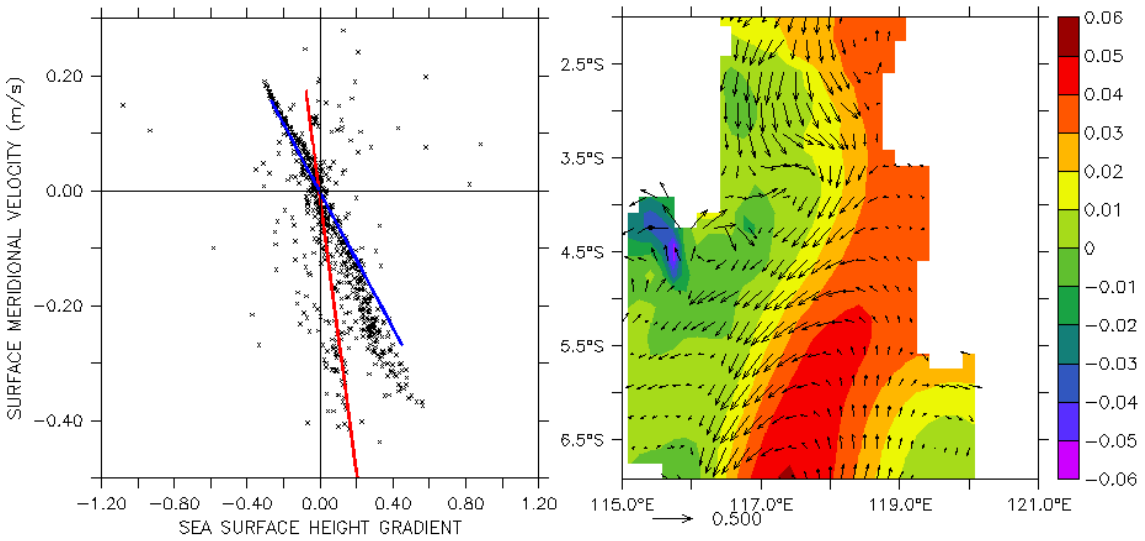

Figure 3-7 Geostrophic balance within Makassar Strait with contours of sea surface height (m) and mean surface velocity field (ms^{-1}) (right) and average surface meridional velocity (ms^{-1}) plotted against zonal sea surface gradient (10^{-6}) (left) for all grid points shown in the right panel. The linear regression is plotted for values at 4°S (red) and 6.4°S (blue).

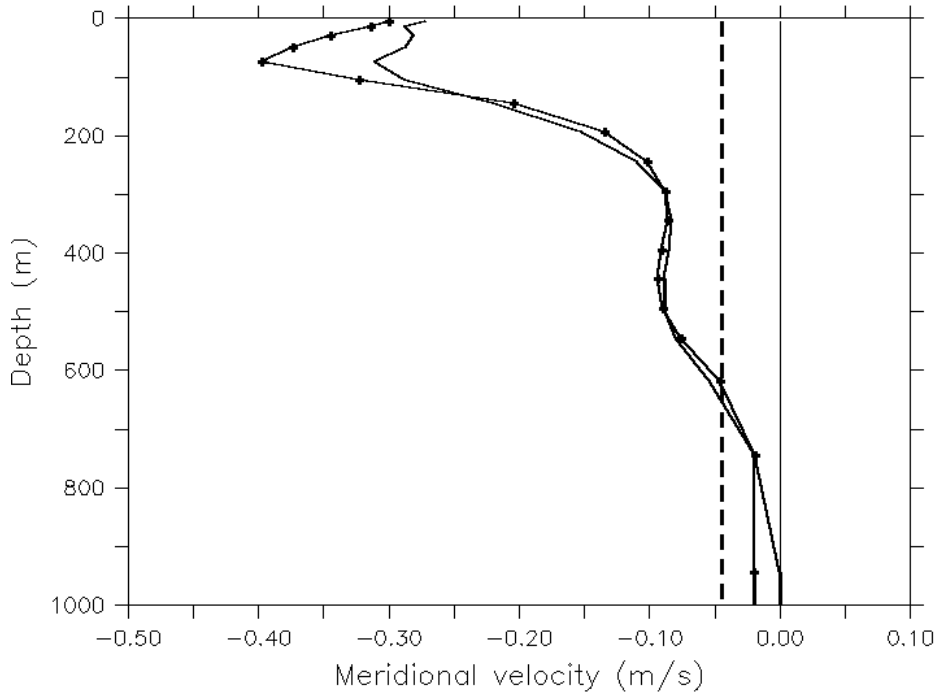

Figure 3-8 Makassar Strait velocity profile (ms^{-1}) with mean meridional velocity (thick line) at 118.1°E, 4°S, its barotropic component (dash line) and geostrophic approximation (dot thick line). Negative values indicate southward velocities.

Along-channel gradients in the density field seem to be very small and possible hydraulic control of the flow at the sill is therefore, hard to validate. A similar finding was reported by *Gordon* [2003] when investigating topographic barriers in the Indonesian Seas. However, hydraulic control cannot be completely excluded since small density gradients in the equatorial regions, where the Coriolis parameter ($f = 0 - 10^{-5}\ s^{-1}$) is very small, could be sufficient to drive the flow. Along-channel data to monitor difference in pressure along the strait are not available. However, combined measurements of the surface height, integrated thermal structure and bottom pressure in Makassar Strait [*Waworuntu et al.*, 2001] show that the flow has

highly baroclinic structure. The vertical structure of the flow requires at least a three-layer description consistent with the water mass structure observed.

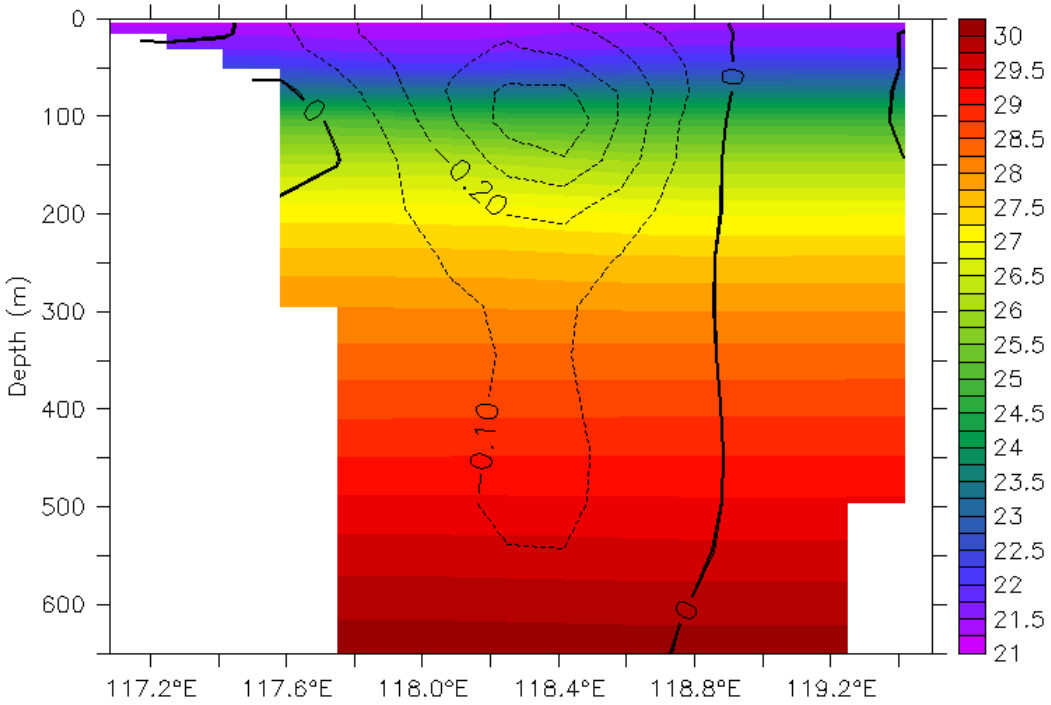

Figure 3-9 Potential density σ_θ (kgm^{-3}) and mean meridional velocity contours (ms^{-1}) in Makassar Strait at 4°S.

The geostrophic balance seems to be a good description of the mean flow within Makassar Strait excluding the regions near the equator. It is possible to capture baroclinic structures of the flow in the model, which is in good agreement with observations, using simple geostrophic approximation. Derived vertical velocity profiles from the density field can be used to estimate the volume transport of the ITF. This is particularly important when paleoclimatic reconstructions are considered where direct velocity measurements are not possible. However, large errors in transport estimates could occur when the surface layer flow is considered because changes in wind forcing and sea surface gradients are difficult to reconstruct.

3.4.2 Topographic effects

The topographic control of the ITF within Makassar Strait is analysed in terms of JEBAR effect [*Huthnance*, 1984]. Assuming that the wind stress and bottom-torque variations are on time scales much greater than the barotropic – topographic Rossby adjustment time scale, *Wajsowicz* [1993a] derived the topographic island rule that gives estimate of the ITF magnitude (Ψ_0) including arbitrarily bottom topography H and variable Pacific wind stress $\tau(x,y,t)$:

$$\left(\frac{f_N}{H_N}-\frac{f_S}{H_S}\right)\Psi_0(t)=-\oint_{\partial D+\partial I}\left\{P(x,y,t)\nabla_h H+\frac{\tau(x,y,t)}{\rho_0 H}\right\}\cdot dl \qquad 3\text{-}14$$

The path integral is taken over the South Pacific (∂D) and around coast of Australia (∂I) as shown in Figure 1-3. The variables f_N and f_S are Coriolis parameters and H_N and H_S are depths of the ocean at y_N and y_S the northernmost and southernmost latitudes of the island, P(x,y,t) is the depth averaged pressure field and ρ_0 is the mean water density. The bottom topography is assumed to be zonally constant at the

northernmost (A`A) and southernmost tips (B`B) of the island (Figure 1-3), while allowing variations along the meridional pathway. The JEBAR effect introduced in the estimate of the total ITF is:

$$T_{JEBAR} = -\oint_{\partial D+\partial I} P(l)(\partial H/\partial l)dl/(f_N/H_N - f_S/H_S) \qquad 3\text{-}15$$

where depth-averaged pressure P is given by:

$$P(x,y) = \frac{g}{\rho_0 H^2}\int_{-H}^{0}(H\rho - \int_{z}^{0}\rho dz')dz \qquad 3\text{-}16$$

Assuming constant bottom topography on the eastern side of the basin, the Indonesian sills represent the only contribution to the topographic effects in the island rule calculation. In first approximation, Indonesian Gateways can be represented as a simple sill intersecting the level of no motion (Figure 3-10). Density difference between Pacific and Indian side of the sill exerts pressure gradient over the topography. In general, if the western Pacific is warmer than Indian side, P will be less positive over the up slope, that is, where $\nabla_h H \cdot dl < 0$, then over the down slope of the sill. Supposing that $\rho_1(Pac) < \rho_1(Ind)$ ρ_1 and other quantities being equal, leads to $P(Pac) < P(Ind)$. Therefore, the integral $P\nabla_h H \cdot dl$ over the sill is positive and there is an increase in the Throughflow magnitude.

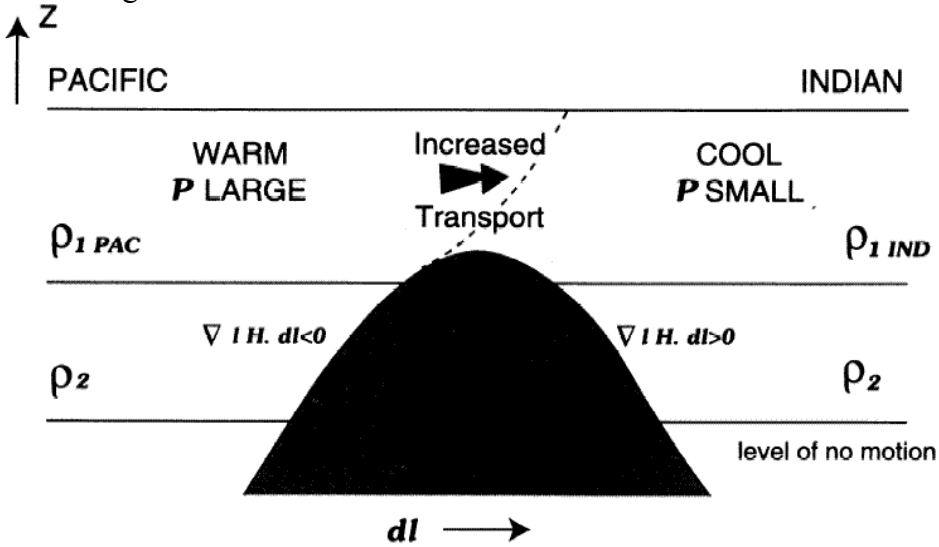

Figure 3-10 Schematic of the topographic effects in the Indonesian Gateways, represented by a simple sill, on the Pacific to Indian Ocean transport. A bottom pressure (P) gradient is induced over the sill due to the density difference between the Pacific (ρ_{1PAC}) and Indian Ocean (ρ_{1IND}). Taken from *Wajsowicz* [1993a].

The major sill blocking the flow between the Pacific and Indian Ocean is Dewakang Sill (~670 m) in southern Makassar Strait. The given theory of topographic effect in the Indonesian Gateways is tested on a meridional transect through Makassar Strait assuming that the northern part of the strait belongs to Pacific water masses, while hydrography south of the strait has Indian Ocean characteristics. The maximum depth of the ocean is taken to be *H*=4000 m at both sides of the sill and no other topographic barriers are considered. Time mean density field, vertical integral of density and depth-averaged pressure (Equation 3-10) are calculated along the path of strongest flow (Figure 3-11). The plotted vertical integral of density field is defined as:

$$h_s(z) = \frac{1}{\rho_0}(H\rho(z) - \int_z^0 \rho(z)dz') \qquad 3\text{-}17$$

The illustration of depth-integrated velocity magnitude:

$$V_{\max} = \int_H^0 \sqrt{u^2 + v^2}\, dz \qquad 3\text{-}18$$

shows mean pathway of the flow through Makassar Strait (Figure 3-11 top left). The strongest flow in southern Makassar Strait does not only take the deepest path on the eastern side of the strait, but it is spread over the broad sill. Even though the density gradients across the sill are small (Figure 3-11 top right), mean depth averaged pressure does seem to decrease up the slope and reaches minimum at the sill at 5.5°S (Figure 3-11 bottom left). The flow increases down the southern part of the slope. The maximum pressure difference between the northern and southern part of the sill is 0.009 Pa/m/kgm^{-3}. The calculations of the JEBAR term (Equation 3-9) in the model, using the step topography, do not seem to give good estimates so the topography and pressure field needed to be smoothen. The approximated value of JEBAR term gives estimate of 2.1±0.5 Sv of topographic effect in the Makassar Strait on the ITF transport. However, estimate of the transport is highly dependant on the parameters used in calculation.

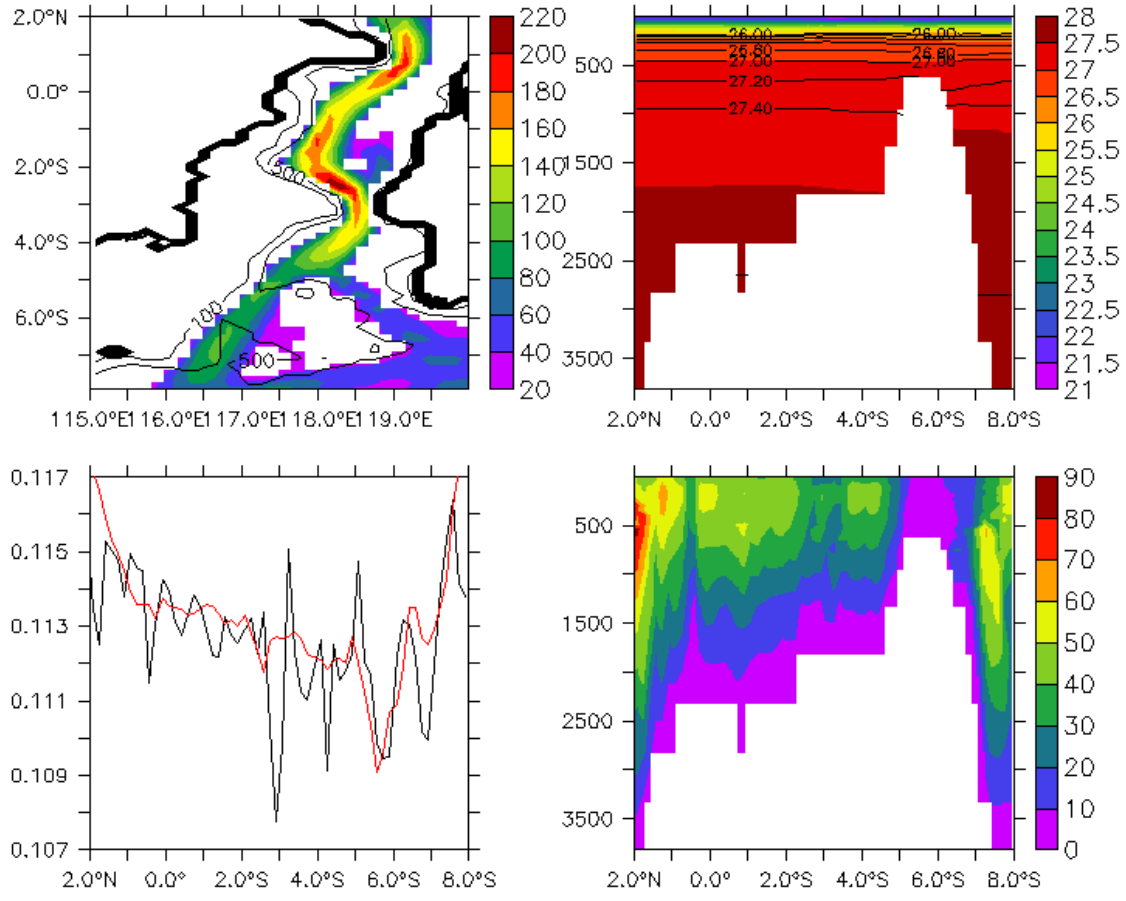

Figure 3-11 Topographic effects within Makassar Strait. Depth integrated velocity magnitude (m^{2}s^{-1}) shows path of the strongest flow in the channel (top left). Potential density stratification σ_0 (kgm^{-3}) (top right) and depth-integrated density (m) (bottom right) are zonally averaged along the path of the strongest flow. Depth-averaged pressure P (Pa/m/kgm^{-3}) (bottom left) is calculated along the Strait (black line). Red line indicates smoothed pressure values.

3.4.3 Seasonal variability

The seasonal cycle of the flow within Makassar Strait is characterized by monsoonal wind changes. The maximum of the flow appears in March during the wind reversal from the NW to the SE monsoon. Throughflow remains strong during the boreal summer (May – August) (Figure 3-12). Minimum flow appears during the boreal winter in the NW monsoon period (November - February). The volume transport in Makassar Strait is compared with the high-resolution global cube-sphere (CS) experiment of ECCO MITgcm project [*Menemenlis,* 2004]. Horizontal resolution in the tropics of the CS-ECCO experiment is approximately ¼° while the forcing in the model is similar to the global ECCO run described in the section 3.2. The global CS-ECCO model predicts 9.6 Sv average transport with high variability on seasonal and inter-annual time-scales. Note that the regional model exhibits neither intraseasonal nor interannual variability as it is forced with a repeating annual cycle of boundary conditions (see section 3.2). Excluding the high frequency variability, the global model and the regional model have similar seasonal variations in the volume transport. The amplitude of the seasonal cycle is slightly smaller (4-5 Sv) than that of the global model (6-7 Sv). Also, the intensification of the Throughflow in boreal winter is earlier in the regional model. However, disagreements between the models exist at certain time intervals. The largest discrepancy appears in the period between January 1997 and March 1998 when the CS-ECCO model predicts low values of the transport and the seasonal phase of the regional model is shifted compared to the global predictions. For this time interval, the CS-ECCO model estimates are in good agreement with the measurements of volume transport in Makassar Strait [*Susanto and Gordon*, 2004]. However, the 1997/98 was described as the year of a strong El-Nino event, which might be the reason for severe changes in the ITF transport compared to the normal state.

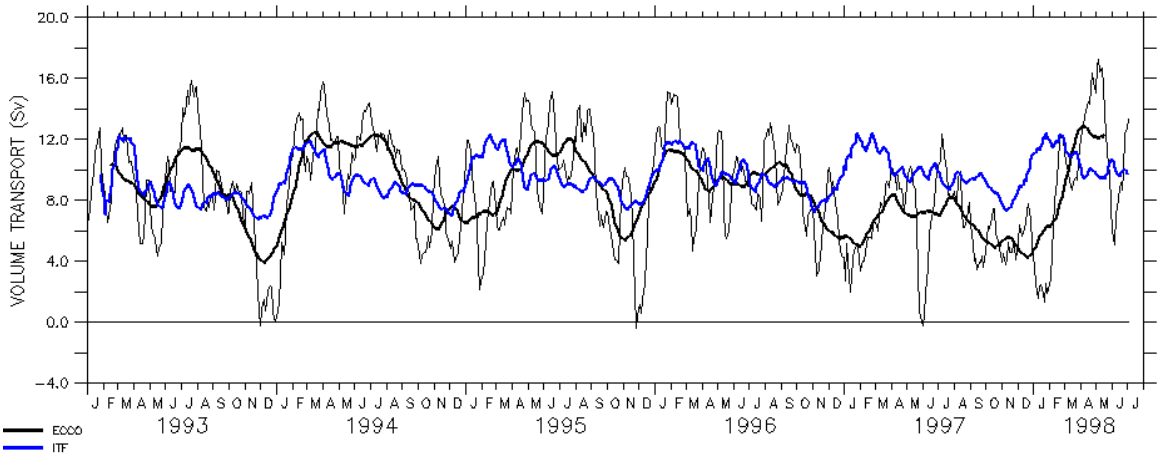

Figure 3-12 Time-series of the volume transport (Sv) within Makassar Strait as predicted by the regional model (blue line) and the global MIT ECCO model (thin black line) together with the 90-days running mean (thick black line).

Most authors report strong ITF transport during the SE monsoon with maximum appearing from April [*Gordon et al.*, 1999] until September [*Hautala et al.*, 1996]. Regarding the high variability of the ITF and lack of long-term measurements, accurate timing of the maximum transport is hard to constrain. The regional model, however, shows strongest transport within Makassar Strait in March. Possible explanation for the disagreement in timing can be found in the climatological wind stress and

constant boundary transport applied in the regional model, which do not reflect complete realistic forcing for the ITF.

The seasonal changes of surface circulation in Makassar Strait agree well with observed monsoonal patterns [*Gordon*, 2003]. From November to February the eastward wind in the Java Sea pushes low salinity water into the southern Makassar Strait (Figure 3-13 left). The surface flow is reduced despite southward blowing, along-channel winds because increase in sea surface height in southern Makassar Strait blocks southward flow. Reversal of the wind during the northern hemisphere summer pushes the low-salinity waters back into the Java Sea and allows southward surface layer transport (Figure 3-13 right).

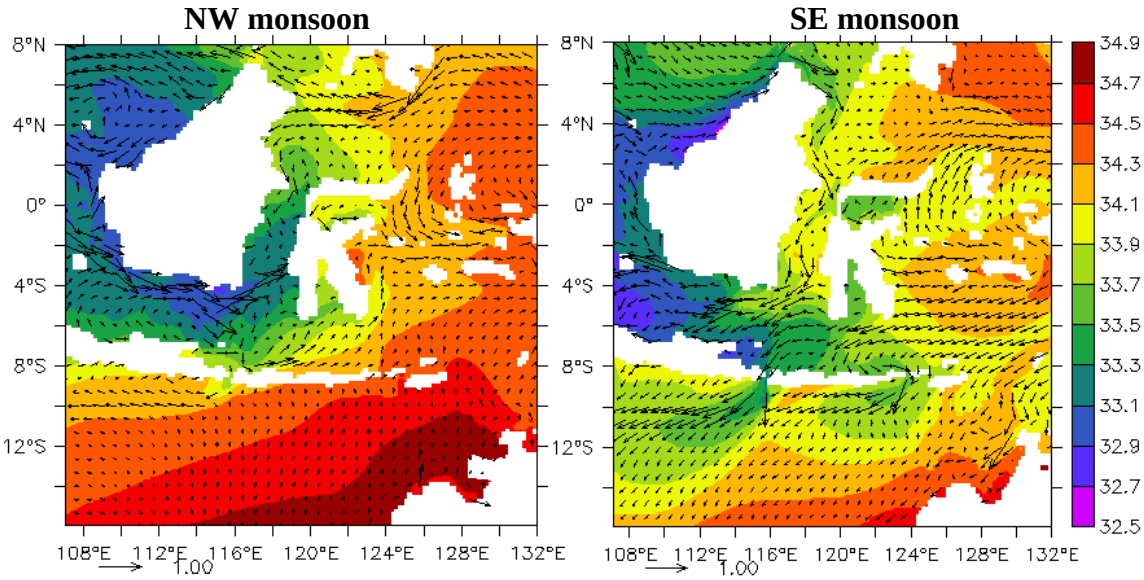

Figure 3-13 Monsoonal changes in surface circulation. Surface salinity (psu) and currents (ms^{-1}) for the November – February (left) and May – August (right).

Seasonal changes in the hydrographic profile are monitored on several CTD stations within Makassar Strait. Temperature and salinity data are available for August 1993 and February 1994 (http://www.ldeo.columbia.edu/~arlindo). The TS diagram for both monsoonal phases are shown in Figure 3-14 for southern Makassar Strait. The upper 200 m layer is characterized with the salinity maximum of North Pacific Subtropical Water while the intermediate layer is characterized by a North Pacific Intermediate Water salinity minimum [*Hautala et al.*, 1996; *Waworuntu et al.*, 2000]. The temperature/salinity stratification developed in the model generally agrees with the observations showing presence of the low salinity waters during the NW monsoon.

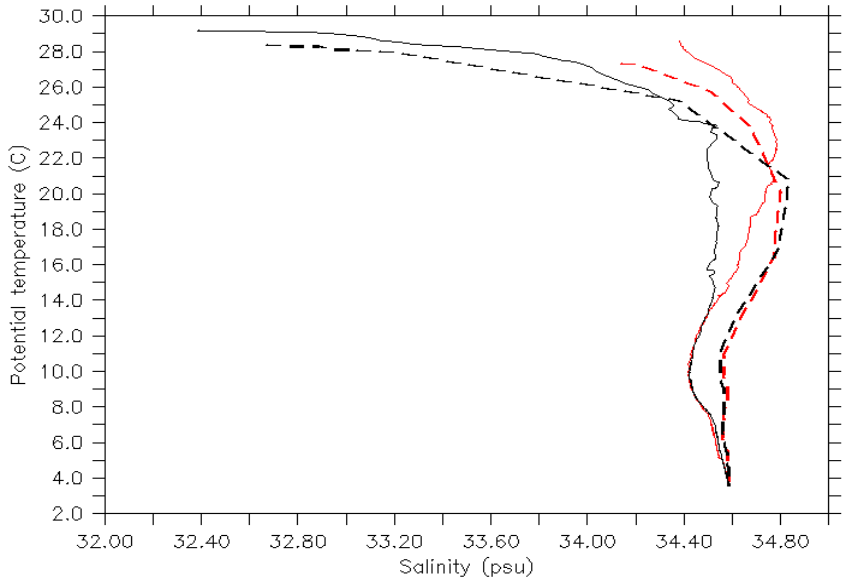

Figure 3-14 Seasonal variations in the temperature (°C) and salinity (psu) in the southern Makassar Strait (115°E–120°, 6°S–3°S). Model TS profile (dash line) is compared to observations (solid line) for February (black) and August (red).

Difference in density and dynamic height within the upper 100 m between the northern and southern Makassar Strait are calculated from the stratification data for two monsoon phases [*Gordon*, 2003]. During the NW monsoon (February 1994) the density difference is negative ($\Delta\sigma \approx -1$ kgm^{-3}) and isobaric surfaces are higher ($\Delta D \approx 0.5$ m^{3}kg^{-1}Pa) in the southern Makassar Strait. This indicates a northward pressure gradient induced by buoyant water in the southern Makassar Strait. During August 1993 the density difference is small ($\Delta\sigma \approx 0.5$ kgm^{-3}), but positive and the pressure gradient is essentially zero. In the model (), the integrated potential density gradient in the upper 100 m during the NW monsoon is negative and equals approximately -0.7 kgm^{-3} while the dynamic height difference is positive ($\Delta D \approx 0.4$ m^{3}kg^{-1}Pa). During the SE monsoon the density difference in the model is positive ($\Delta\sigma \approx 0.7$ kgm^{-3}) and dynamic height difference is small and negative ($\Delta D \approx -0.2$ m^{3}kg^{-1}Pa) which corresponds well with the observations. An additional effect of the buoyant surface water piling up in southern Makassar Strait is the shift of the main flow from the surface into thermocline levels (Figure 3-15)

The volume transport variations within Makassar Strait are compared to seasonal variations of transport in the outflow passages. In Figure 3-16 are given correlation diagrams showing lagged correlation between different time series of transport. A maximum positive correlation between Makassar and Lombok transport indicates lag of 1 month of the Lombok Strait transport compared to the Makassar Strait. The flow through Ombai Strait lags the flow in Makassar Strait by 4 – 5 months, while flow through Timor Strait leads the flow in Makassar Strait by 1 – 2 months. These results suggest significantly different seasonal variations in inflow and outflow passages that might modulate the resulting flow towards the Indian Ocean. The net outflow through eastern passages (TOS transect) shows lag similar to Ombai Strait transport, while the total Throughflow calculated in Indian Ocean (ITF transect) seems to be in phase with Makassar Strait transport

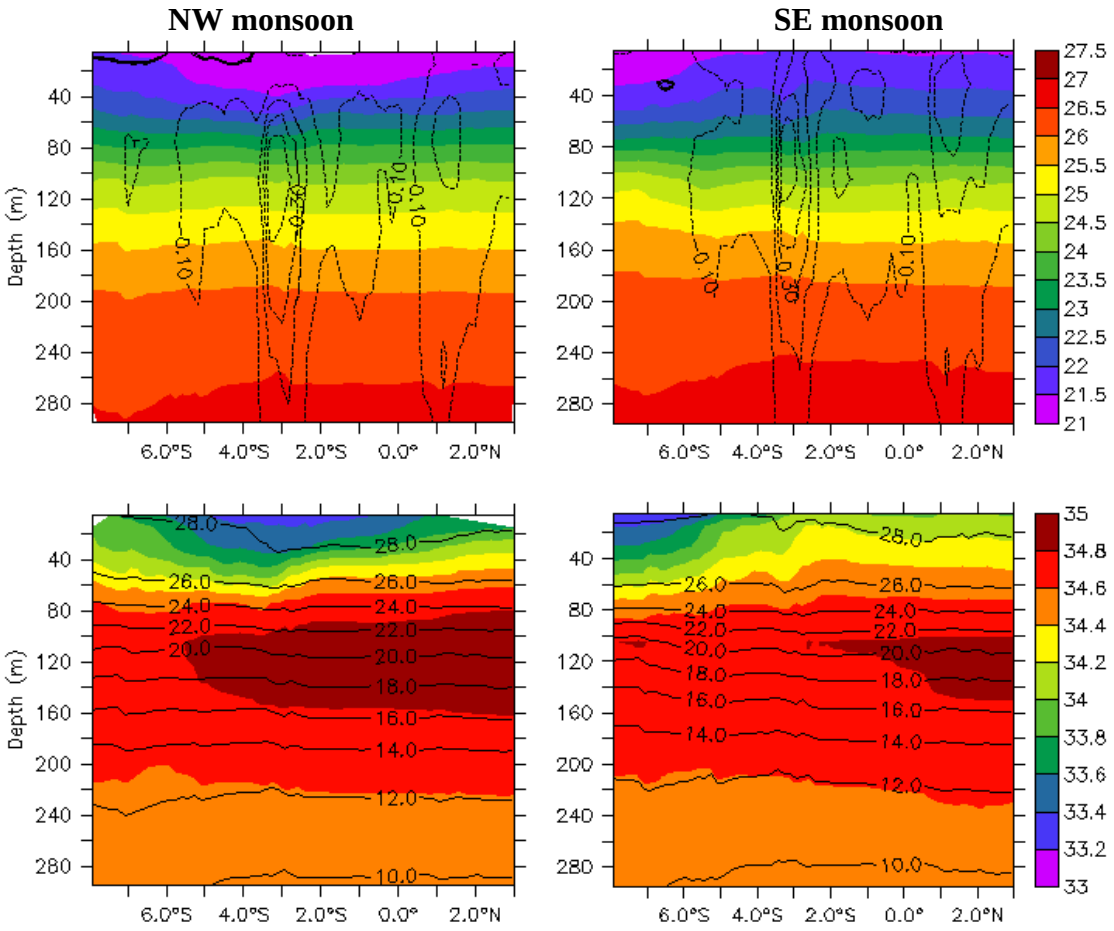

Figure 3-15 Zonal average of the along-channel section through Makassar Strait (115°E - 120°E) showing seasonal changes in density stratification (kgm^{-3}) with meridional velocity contours (ms^{-1}) (upper panel) and the salinity field (psu) with isotherms (°C) (lower panel) for the NW monsoon: November - February (left) and SE monsoon: May - August (right).

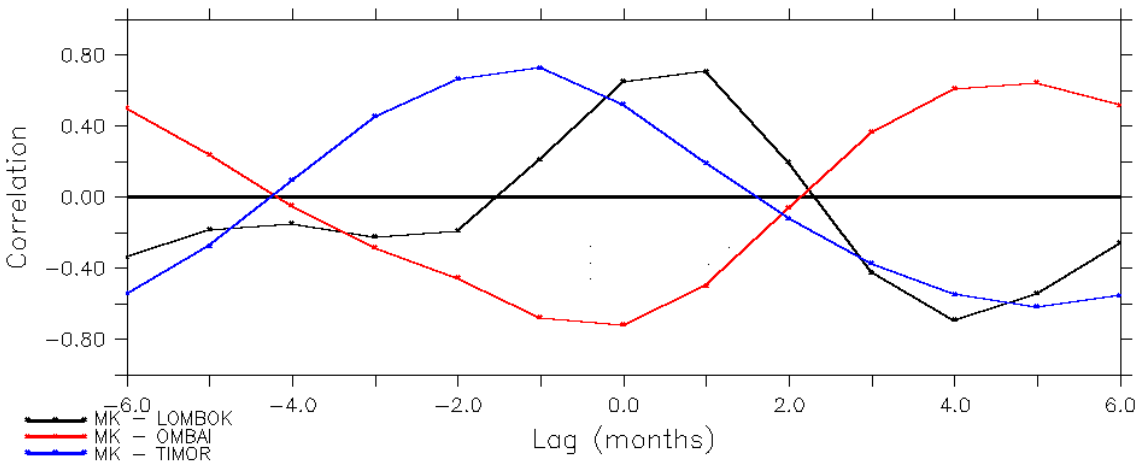

Figure 3-16 Lagged correlation between volume transport within Makassar Strait (MK) and outflow passages. For example, a positive correlation MK – LOMBOK at +1 month lag indicates that Makassar Strait transport is leading Lombok Strait transport by 1 month.

3.4.4 Density driven flow

Wyrtki [1987] suggested that the pressure difference between the Pacific and Indian Ocean forces the Throughflow and that variability of the ITF would be captured with an index of sea surface height difference between Davao on the east coast of Mindanao and Darwin on the north-western coast of Australia. *Potemra et al.* [1997] included sea level anomalies in West Pacific and south of Java together with the stations northwest of Australia and off coast of Philippines to get better index of ITF variability from seasonal to interannual time-scales. *Andersson and Stigebrandt* [2004] further argued that it is the difference in steric sea level between Pacific and Indian Ocean that forces the Throughflow by forming a downstream buoyant pool (DBP) in the North Australian Basin. Low buoyancy Pacific water fills the Indonesian Seas and it is drained by the sea level drop between the DBP and Indian Ocean. The geostrophic transport at the rim of the DBP is related to density anomaly between the DBP and Indian Ocean and is given by:

$$Q_l = \frac{g' H^2}{2 f(l)} \qquad 3\text{-}19$$

where $g' = g\frac{\Delta\rho}{\rho_0}$ is reduced gravity and $f(l)$ is the Coriolis parameter at the latitude l of the transport. The depth of the pool H is less or equal to the effective sill depth of the straits in the archipelago. The ITF magnitude is then given as difference between transports at northern and southern sides of the DBP:

$$Q_{ITF} = Q_N - Q_S \qquad 3\text{-}20$$

where Q_N and Q_S are geostrophic transports at the northern and southern latitude, respectively. Using hydrographic data to calculate steric height difference between Pacific and Indian Ocean, *Andersson and Stigebrandt* [2004] found an estimated of the ITF transport magnitude of about 10 Sv corresponding well to observations. However, this value was found when the West Pacific and North Australian Basin water are considered as single water mass and steric height was compared between the areas in North Australian Basin and central Indian Ocean (80°W-100°W, 6°S-6°N). Taking the depth of the DBP to be 1200 m as the depth of the Timor Strait, and reference temperature and salinity in the Pacific of T_{PAC}=2.73°C, S_{PAC}=34.60 psu and in North Australian Basin of T_{IND}=3.10°C, S_{IND}=34.70 psu, lead to steric height difference in boreal summer of about 4 cm while difference between North Australian Basin and central Indian Ocean was 18 cm.

Estimates of the ITF using steric height difference between Pacific and Indian Ocean could be an useful tool in assessing past climate changes in ITF magnitude. Changes in density stratification seem to be easier to estimate than wind field strength generally assumed to be the driving force of the Throughflow. Furthermore, the density driven flow is not included in the original *island rule* calculations and with different density stratification during the glacial periods might have a different role in governing the Throughflow.

Steric sea level difference between the West Pacific (WP) and East Indian Ocean (EIO) is analysed in the model and compared to the transport within Makassar Strait. This approach is different than originally suggested by *Wyrtki* [1987] since

it uses only density stratification and not wind forced contribution to sea level height. Steric height is calculated as:

$$h_{ster} = \rho_0 \int_0^H [\alpha(S,\theta,z) - \alpha(35,0,z)]dz \qquad 3\text{-}21$$

where reference depth H = 1000 m which is the depth of the sill in southern Makassar Strait. The areas taken as representative for WP and EIO are illustrated in Figure 3-17. Steric height field shows higher values in Pacific than the Indian Ocean. Mean annual value of steric height difference between WP and EIO is 2.2 cm, with maximum value of about 5.3 cm during the monsoon transition. This value seems to be insufficient to drive the flow of 9.3 Sv within Makassar Strait as predicted by the model. However, estimates of steric height difference are dependant on the area used in calculation and the reference depth. If the inflow region of MC near Philippine coast is taken instead of WP and region south from Java coast is used for EIO than maximum steric height difference can reach 20 cm which could be sufficient to drive significant part of the flow. The steric height in the central Indian Ocean could not be evaluated since this region is outside the model domain. Seasonal variations in Makassar Strait volume transport seem to be in good agreement with the estimated steric height difference variations (Figure 3-18).

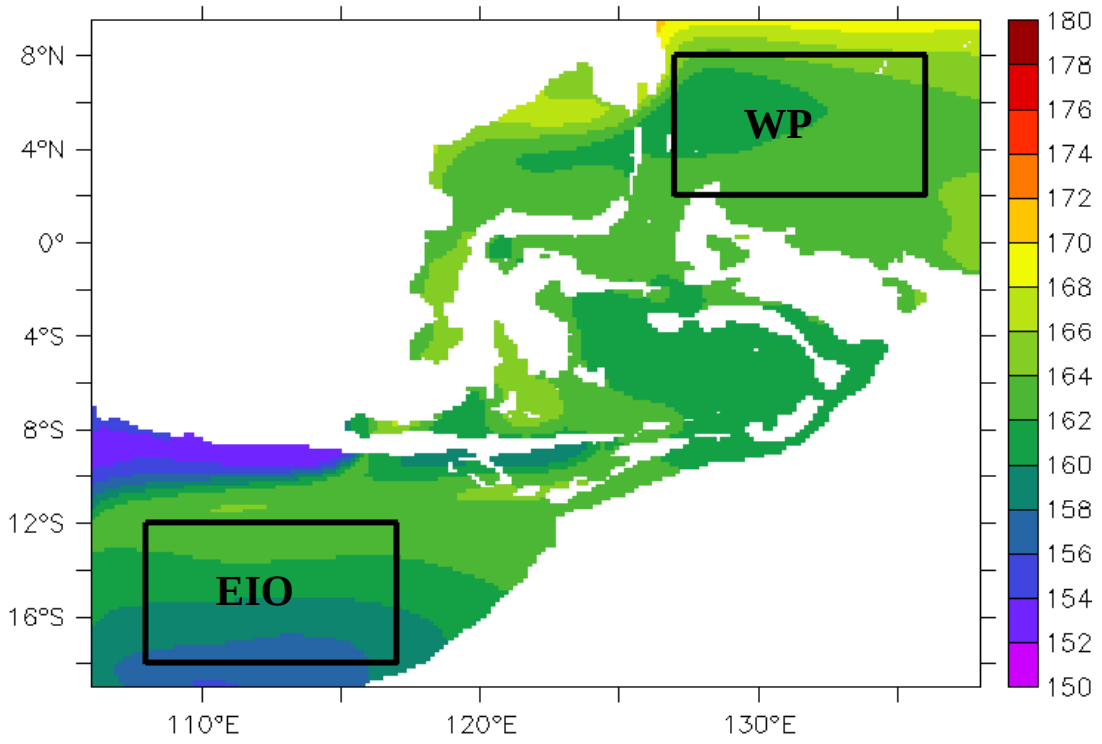

Figure 3-17 Mean steric height (cm) relative to 1000 m with indicated areas (black boxes) used in calculation of pressure difference in the model.

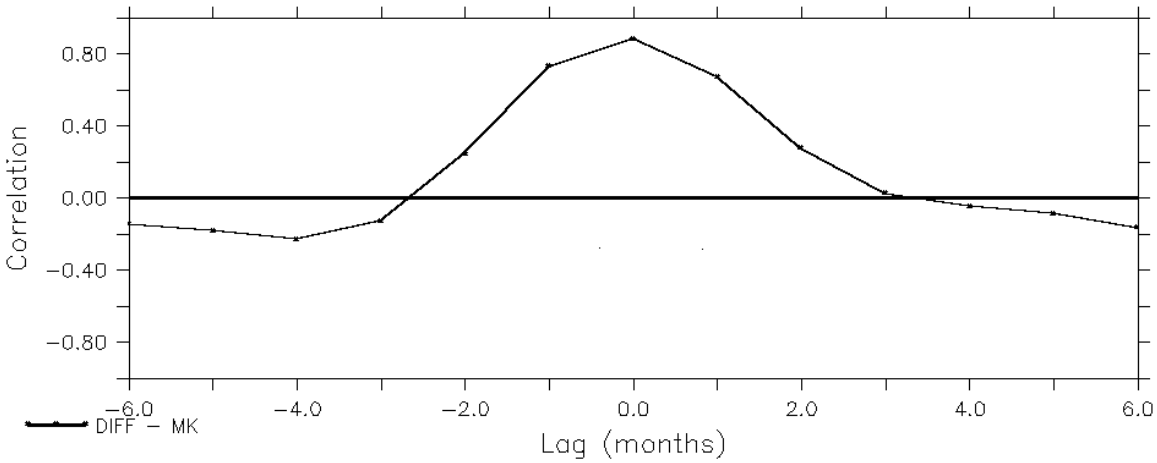

Figure 3-18 Correlation of steric height difference (DIFF = WP – IO) with Makassar Strait volume transport. Maximum positive correlation DIFF – MK at 0 month lag indicates that Makassar Strait transport is in phase with the DIFF.

The mean positive steric height difference between WP and EIO in the model suggests that the ITF could be driven by pressure gradients induced from the density field. This idea is further supported in the model where seasonal variations of the steric height difference show correlation with Makassar Strait transport. However, estimates of ITF transport from the density field are too small, suggesting that density difference is perhaps just one of the forcing mechanisms. However, calculation of density driven flow by integrating steric height from a defined depth and averaging over large areas is perhaps too simplified approach for describing the ITF. When only narrow coastal areas are taken into account, the estimates seem to give better results. This seems reasonable when considering that the bulk of the ITF originates from the narrow Mindanao Current, but contradicts the generally excepted view that the ITF must depend on large scale Pacific to Indian Ocean density difference. Moreover, the ITF profile is known to have a baroclinic structure within the thermocline maximum and it might be important to consider also different density layers when calculating steric height difference.

3.5 Outflow passages

3.5.1 Lombok Strait

The flow through Lombok Strait carries mainly surface and thermocline water towards the Indian Ocean. The mean flow at the surface reaches velocities of 1 ms^{-1} (Figure 3-19). In deeper layers velocities range from 0.6 to 0.2 ms^{-1} above the sill depth. Below 250 m the currents are decreased to almost zero. Comparison of the zonally averaged along-channel velocity with the vertical structure of the flow monitored during March 1997 and March 1998 [*Hautala et al.,* 2001] shows good agreement. However, the vertical profile of the flow in the model shows stable outflow throughout the year (Figure 3-20 and Figure 3-21) in contrast to same observations, e.g. the observed surface northward flow during December 1995 [*Hautala et al.,* 2001]. Temporary northward shifts in the flow have been also documented by *Murray and Arief* [1988]. The reversal of the flow is explained as the Ekman transport induced by westward passing cyclones in the Indo-Pacific basin raising the sea level on the Indian side of the Strait. Additional explanation is given through induced Kelvin waves on the eastern Indian Ocean boundary by remote forcing during the monsoon transition

periods (November/December, April/May) [*Hautala et al.,* 2001; *Sprintall et al.*, 2003]. Both forcing mechanisms are not included in the regional model.

The seasonal cycle of the Lombok Strait transport in the model correlates with Makassar Strait transport showing maximum of the flow from March to April (Figure 3-20). While the transport throughout the year is ~3.5 Sv, during the period of strongest outflow it shows values up to 5 Sv. Based on current meter data [*Murray and Arief*, 1988] the transport observed during the NW monsoon is approximately 1 Sv or less, while the maximum is in August and reaches 4 Sv. *Hautala et al.* [2001] found higher outflow values during the NW monsoon ranging 0.9 – 3.4 Sv for the estimates of transport in upper 200 m and pointed out that the 1.7 Sv value of the annual average [*Murray and Arief*, 1988] might be underestimated. Remember also that the modelled flow is overestimated because of the wider strait.

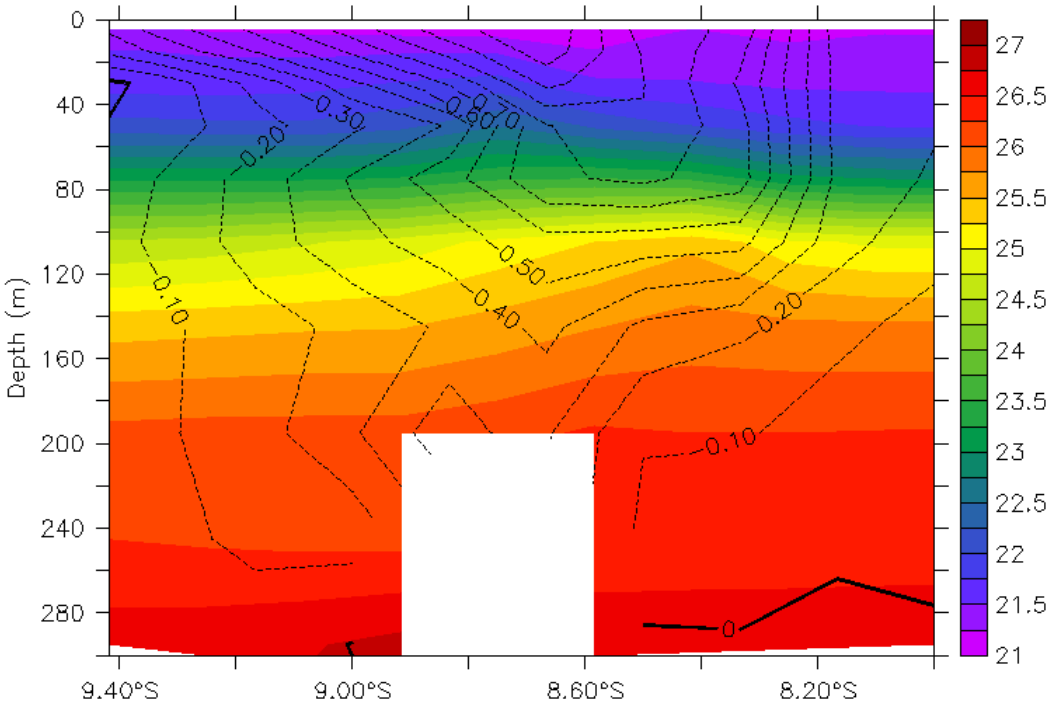

Figure 3-19 Along-channel section (115.7°E) of the mean annual density stratification (kgm^{-3}) and velocity field (ms^{-1}) in Lombok Strait with negative values indicating flow towards the Indian Ocean.

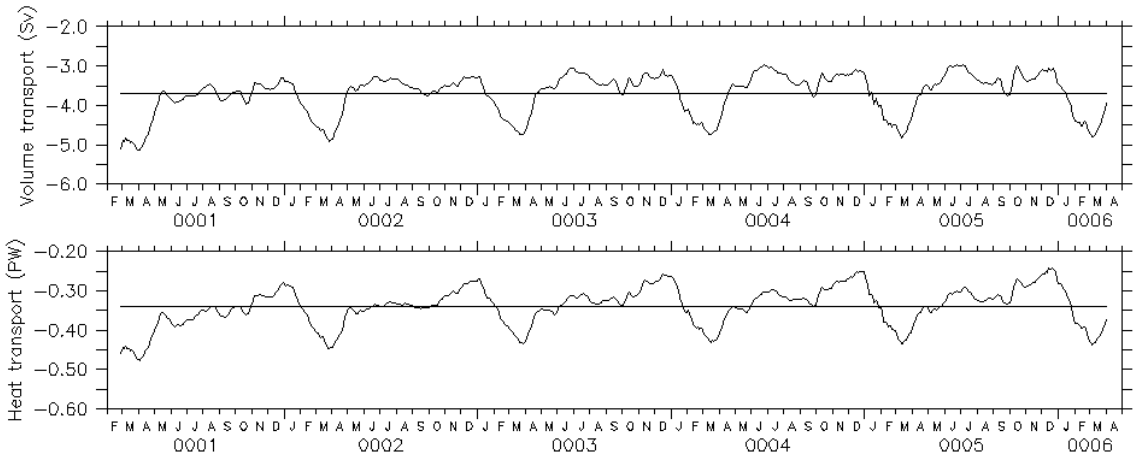

Figure 3-20 Lombok Strait volume (Sv) (top) and heat transport relative to 0°C (PW) (bottom) time-series.

Lombok Strait TS profiles show low salinity values in March characteristic for the NW monsoon period (Figure 3-21). The low salinity signal is generally observed in Lombok Strait from March to May, while a semi-annual signal is dominant in the temperature variations [*Sprintall et al.*, 2000]. Observed salinity minima, with values dropping up to 32 psu, were associated with strong river runoff near Lombok Strait following high precipitation in the region during the NW monsoon phase.

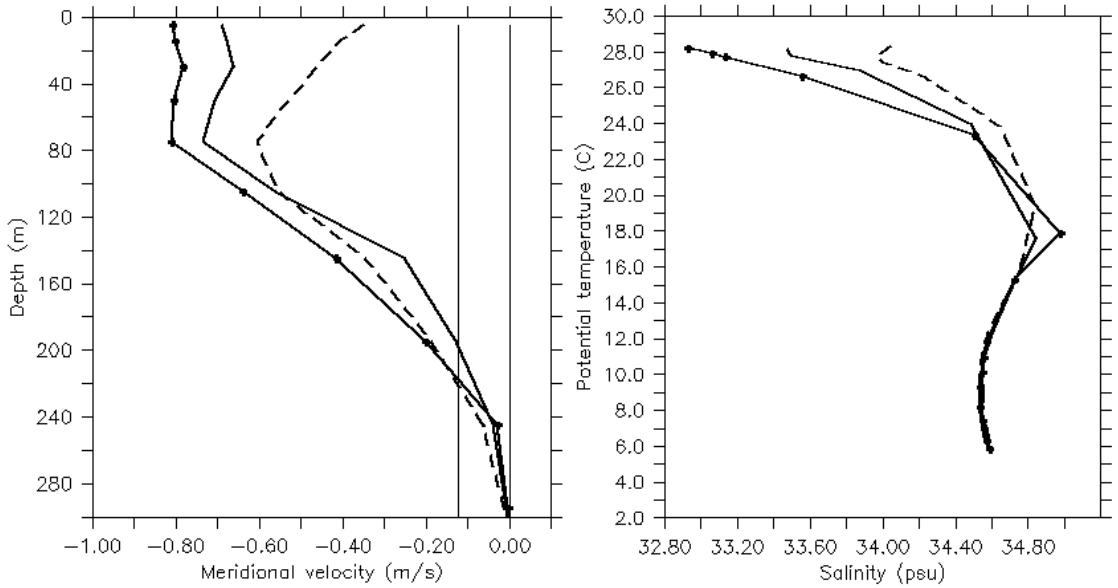

Figure 3-21 Lombok Strait seasonal velocity profile (ms^{-1}) and TS diagram for March (dot solid) and August (dash) and annual mean (solid line). Negative values of the velocity show southward transport.

Even though the model captures well the vertical profile of the flow and part of the seasonal variations, the dynamics of Lombok Strait Throughflow are probably not well represented in the model. The main reason is the inadequate representation of topography in the strait that leads to overestimated transport and simplified forcing that is not sufficient to capture the observed variability.

3.5.2 Ombai Strait

The flow through Ombai Strait carries mainly surface and intermediate waters towards the Indian Ocean. The seasonal cycle of the transport (Figure 3-22) shows strongest flow from June – September with southward transport exceeding 8 Sv during the SE monsoon phase and weak flow from December to March during the NW monsoon phase. The variability of the flow is mainly confined within the upper 150 m. Higher frequency variability is not captured in the model.

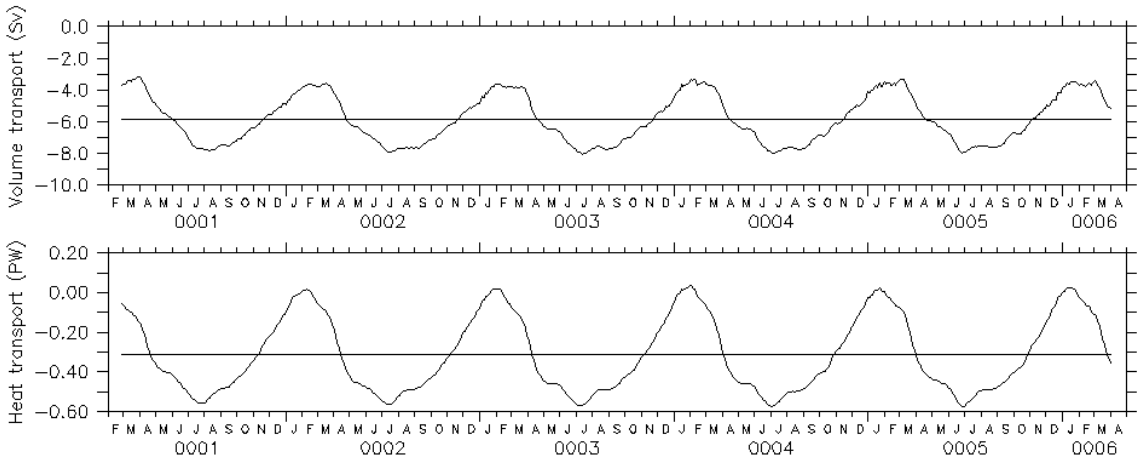

Figure 3-22 Ombai Strait volume (Sv) (top) and heat transport relative to 0°C (PW) (bottom) time-series.

A vertical cross section (Figure 3-23) illustrates surface intensified flow while the deep flow is week. However, monsoonal changes in the surface currents lead to reversals of the flow towards the Banda Sea during the NW monsoon phase (Figure 3-24) while intermediate water flow contributes to the net transport towards the Indian Ocean. Temperature and salinity profiles show small seasonal variations.

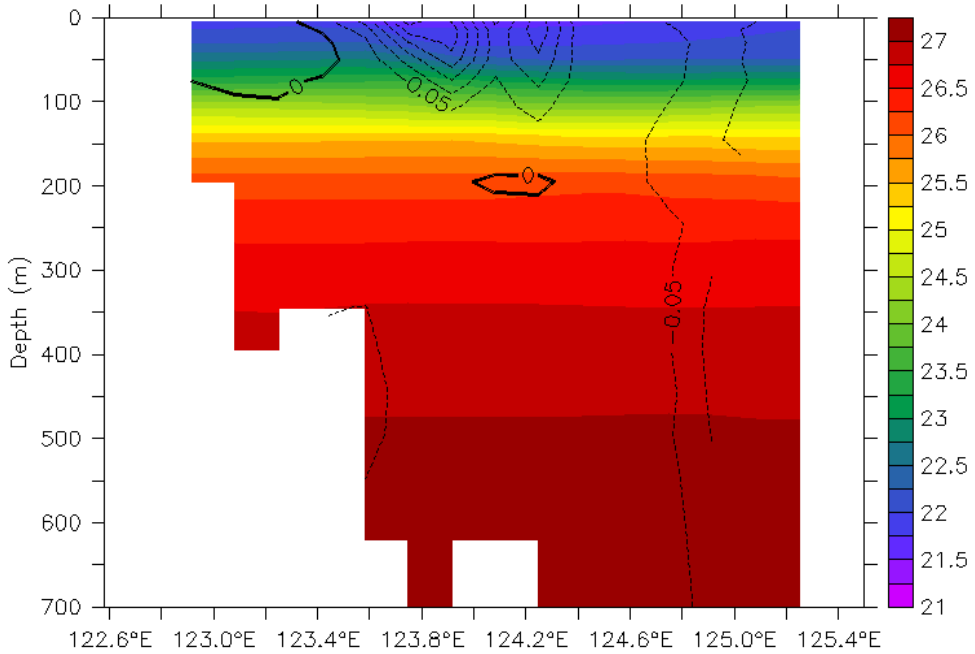

Figure 3-23 Ombai Strait cross section at 8.6°S with the mean annual density stratification (kgm^{-3}) and velocity field (ms^{-1}). Negative values indicate flow towards the Indian Ocean.

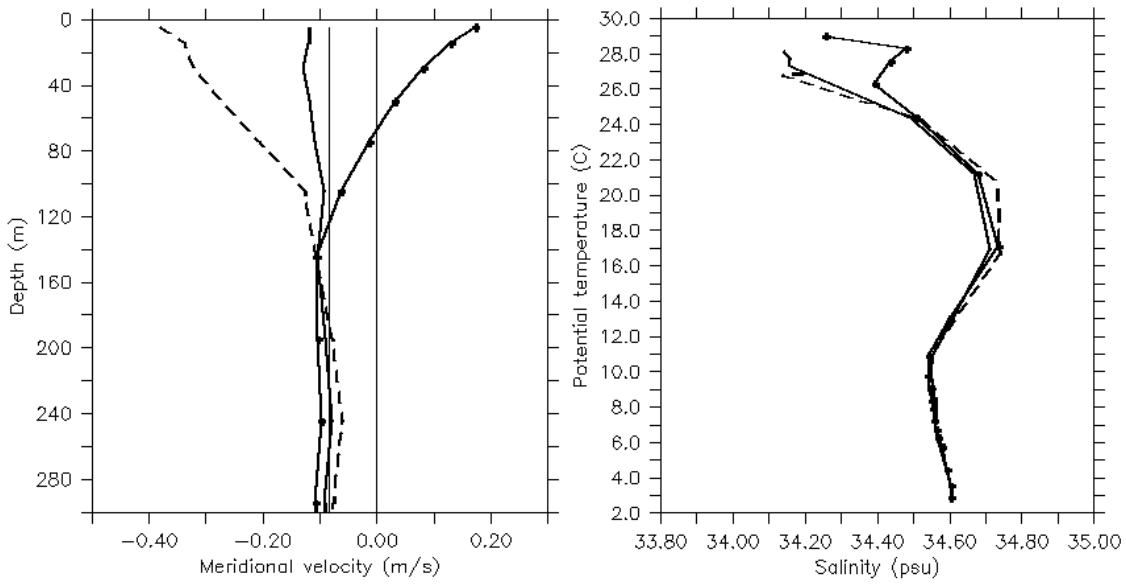

Figure 3-24 Ombai Strait mean (thick) and seasonal velocity profile (ms^{-1}) and TS diagram for August (dash) and March (dot) with negative values of the velocity indicating southward transport.

3.5.3 Timor Strait

The model results show underestimated mean volume transport values through the Timor passage (2.5 Sv) compared to the observational estimates (3.4 – 7 Sv) [*Creswell et al.*, 1993; *Molcard et al.*, 1996], while the larger part of the outflow (~ 6 Sv) exits through Ombai Strait. The mean coastal current in the model is weaker than predicted by the global model [ECCO MITgcm, *Menemenlis,* 2004] and as expected from the measurements. Possible explanations can be found in missing components of the transport from the northeastern Australian shelf region and closed communication with the South Pacific source through the Arafura Sea which could allow additional, although small, surface transport. Other reasons are the representation of the southern boundary as interpolated from the global model and overestimated transport through Lombok Strait.

The simulated seasonal cycle has strong outflow from December to March and weak flow from June to September (Figure 3-25). This is inconsistent with the observed seasonal changes in circulation of the Timor Strait which imply maximum of transport during SE monsoon period [*Creswell et al.*, 1993; *Molcard et al.*, 1996].

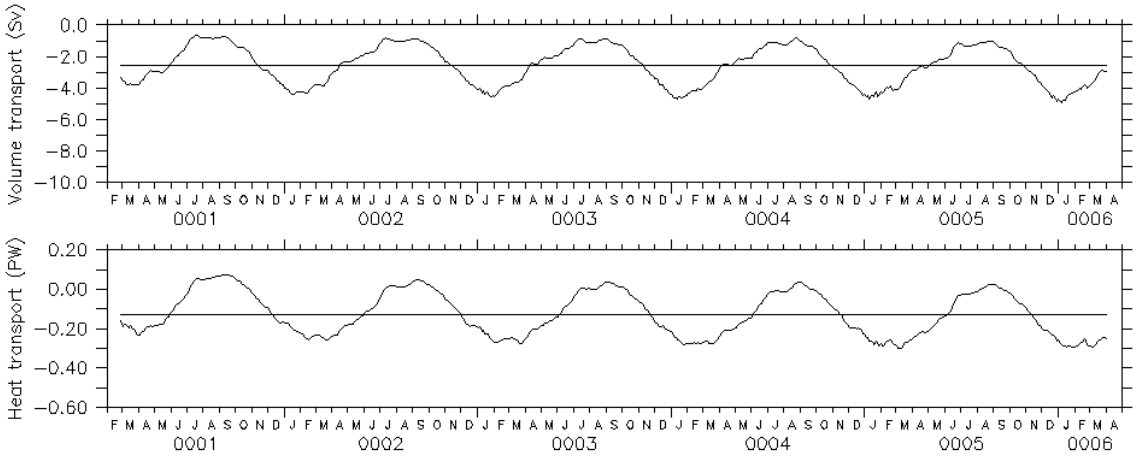

Figure 3-25 Timor Strait volume (Sv) (top) and heat transport relative to 0°C (PW) (bottom) time-series.

In order to analyse the circulation patterns in Timor Strait in the model, the flow dynamics are described by three separate layers: surface shelf current, coastal undercurrent between 30 and 200 m and deep water flow in the passage below 200 m. The upper layer flow is under strong influence of the monsoonal wind variations, while deep water currents are weak and show small changes.

Meridionally averaged temperature/salinity profiles (Figure 3-26) in Timor Strait show lower salinity values during the SE monsoon phase with the salinity minimum at subsurface levels.

Seasonal changes in the flow and density stratification are considered by looking at a vertical section across the strait at 126°E (Figure 3-27). During the NW monsoon the surface flow is weak and the outflow in subsurface and deep levels dominates. During the SE monsoon phase, the westward surface flow is intensified and low salinity surface water is transported towards the Indian Ocean which corresponds well to observations [*Creswell et al.*, 1993; *Molcard et al.*, 1996]. However, strong westward flow is confined in the upper 30 m and, below the surface an undercurrent in the opposite direction is formed, reducing the net outflow. The undercurrent is strongest between 50 and 90 m depth. The horizontal structure of the surface coastal current and the associated undercurrent is shown in Figure 3-28. During the SE monsoon phase a southward current is formed along the continental shelf that continues along the coast of Australia to join the Leuween current. Both currents are weak during the NW monsoon period.

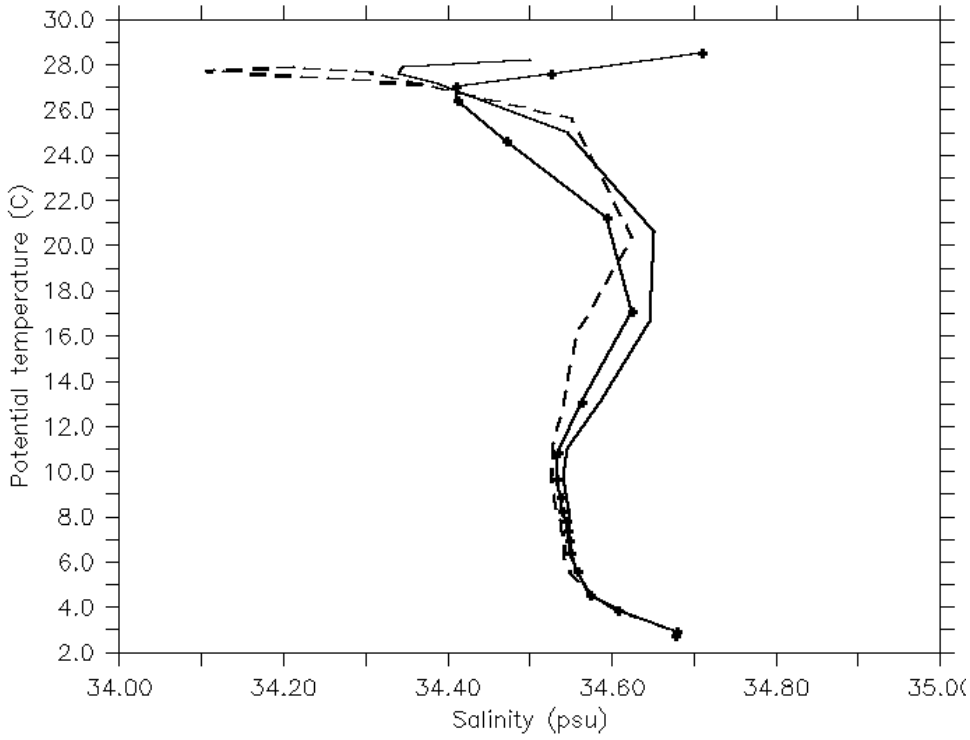

Figure 3-26 Timor Strait mean (thick) and seasonal TS diagram for August (dash) and March (dot).

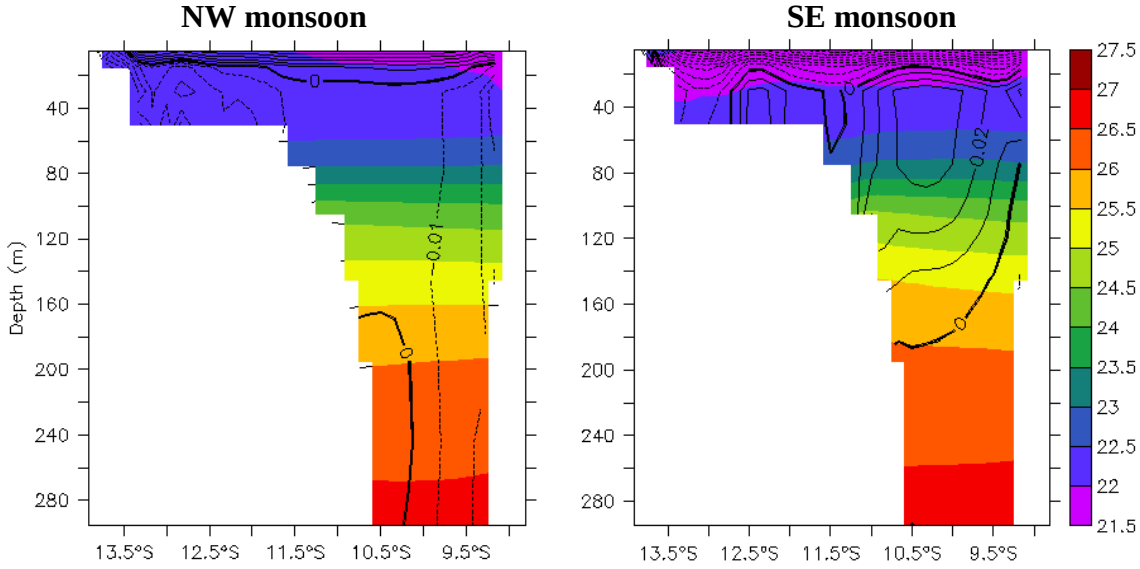

Figure 3-27 Seasonal changes in the circulation in Timor Strait and on the North Australian shelf. Density map across Timor Strait (126°E) and velocity contours for November - February (left) and May – August (right).

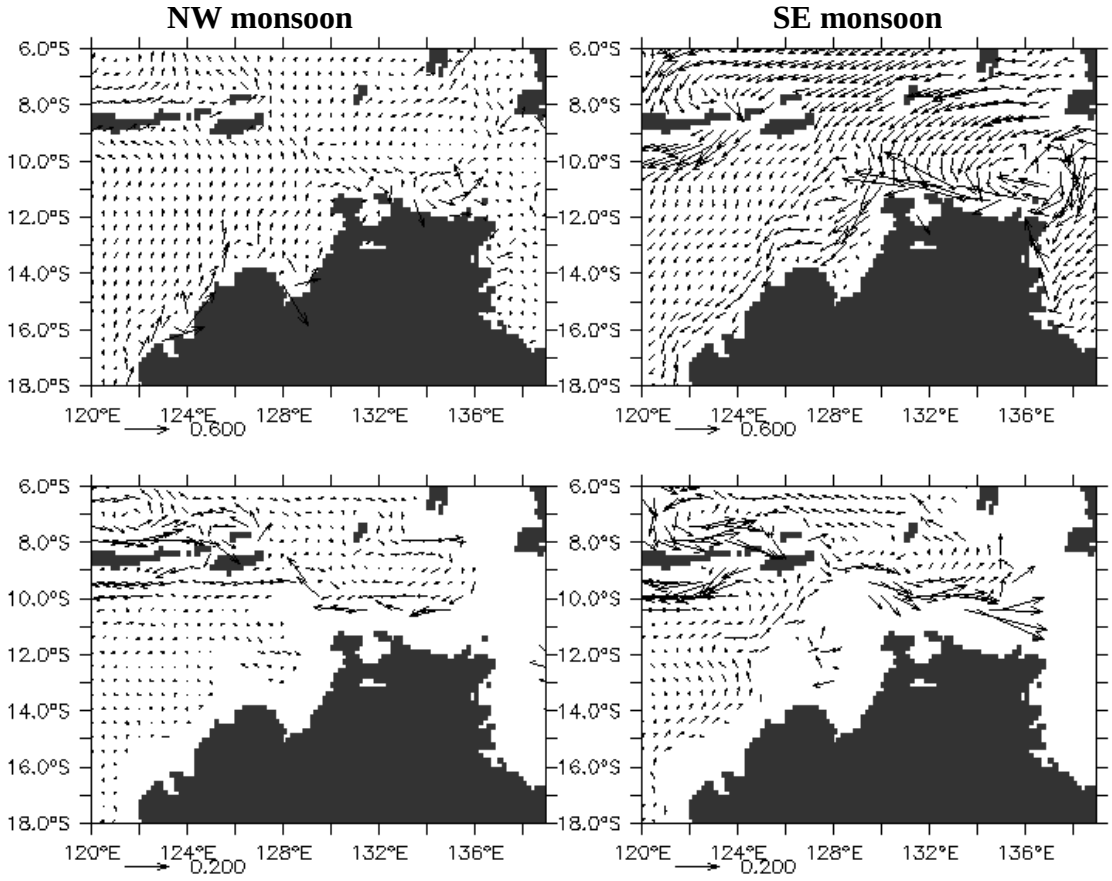

Figure 3-28 Surface coastal current (ms^{-1}) (upper panel) and the related undercurrent at 75 m (lower panel) along the North Australian shelf for the NW monsoon November - February (left) and SE monsoon May – August (right).

3.6 Sensitivity to boundary conditions

3.6.1 Wind forcing

Response of the model transport within Makassar Strait to the prescribed boundary transport for various scaling parameters with and without wind forcing is illustrated in Figure 3-29. The results show that Makassar Strait volume transport depends linearly on the prescribed total transport. The wind forcing does not significantly change the mean transport within Makassar Strait, but influences its variability. The linear regression of the transport values yields a correlation coefficient of R=0.99 and gives the following estimate of the transport within Makassar Strait (Q_{Mak}):

$$Q_{Mak} = 0.77 Q_{Tot} \qquad 3\text{-}22$$

where Q_{Tot} is the total inflow transport at the northern and eastern boundary.

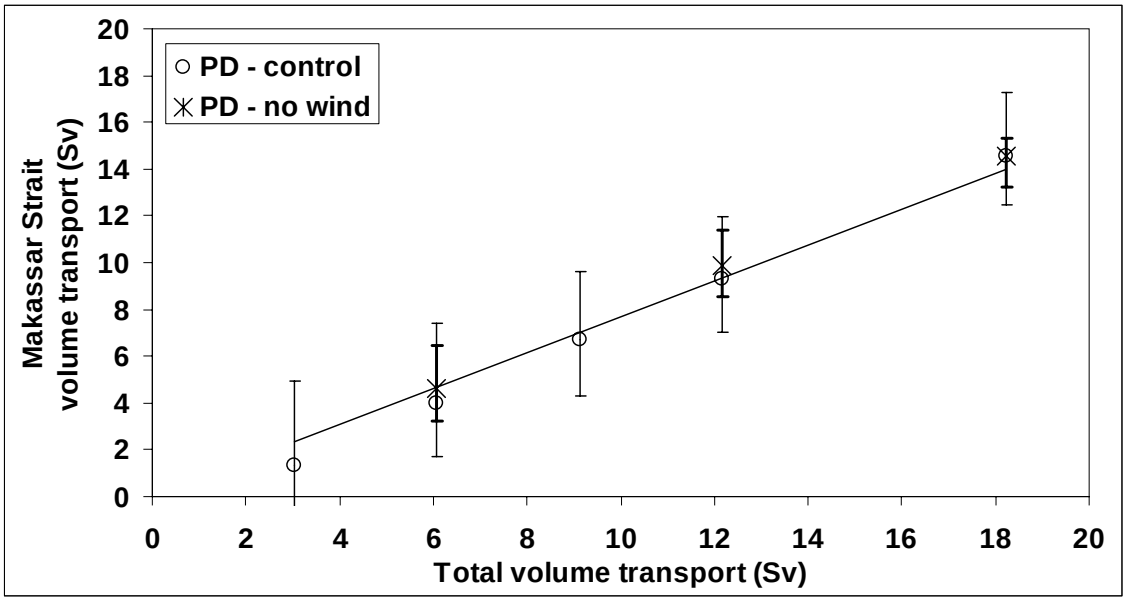

Figure 3-29 Response of the volume transport within Makassar Strait to scaling of the lateral boundary transport for PD – *control* experiment and PD – *no wind* experiment. The error bars indicate maximum and minimum values of the model transports.

The time-mean surface circulation through the Indonesian Seas in the PD – *no wind* experiment is similar to the PD – *control* simulation (Figure 3-30). The main effect of the wind forcing is an intensification of the inflow currents in the Celebes Sea surface, forming of gyres in the Java Sea, southern Makassar Strait and Flores Sea and surface outflow currents in the Banda Sea, North Australian shelf and East Indian Ocean.

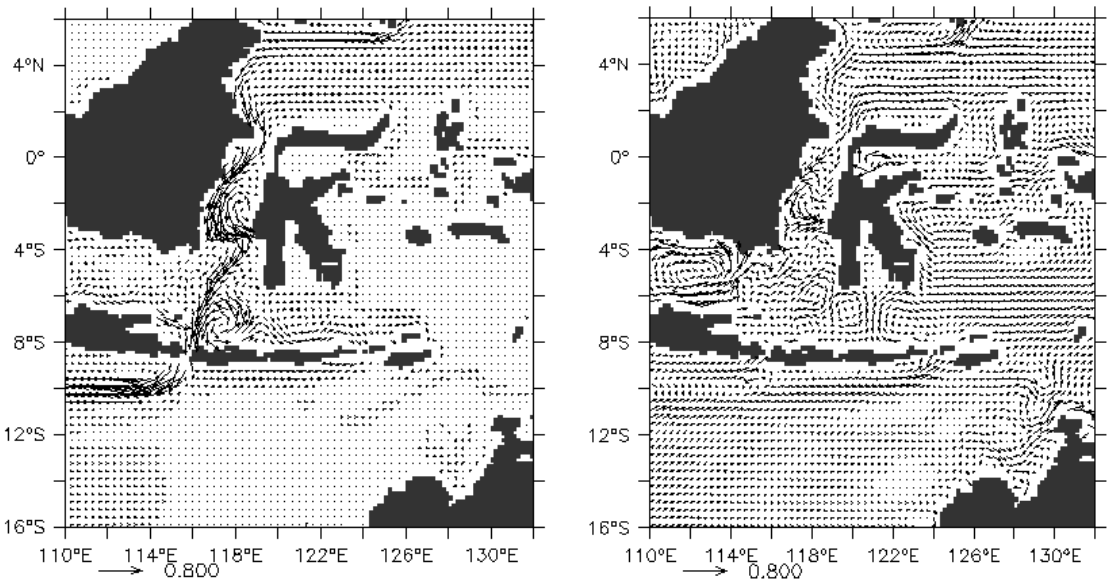

Figure 3-30 Mean annual surface circulation (ms^{-1}) in PD – *no wind* experiment (left) and difference in surface currents between the PD – *no wind* and PD – *control* experiment (right).

The monsoonal changes in the surface flow in Makassar Strait are investigated in the experiment without the wind forcing. Time-series of the volume and heat transport (Figure 3-31) in the PD – *no wind* experiment show small seasonal variations. Blocking of the surface flow in the southern Makassar Strait during the boreal winter due to the low surface salinity presence is significantly reduced in the absence of wind. This suggests that southeastward blowing winds during the NW monsoon push the low salinity surface waters from the Java Sea into the southern Makassar Strait initiating the blocking of the throughflow. The blocking of the flow has been assigned to density forcing assuming that the density gradient along the channel is sufficient to control the surface flow [*Gordon et al.*, 2003]. However, these results suggest that both wind and density forcing need to be taken into account when the seasonal patterns in surface circulation in Makassar Strait are considered.

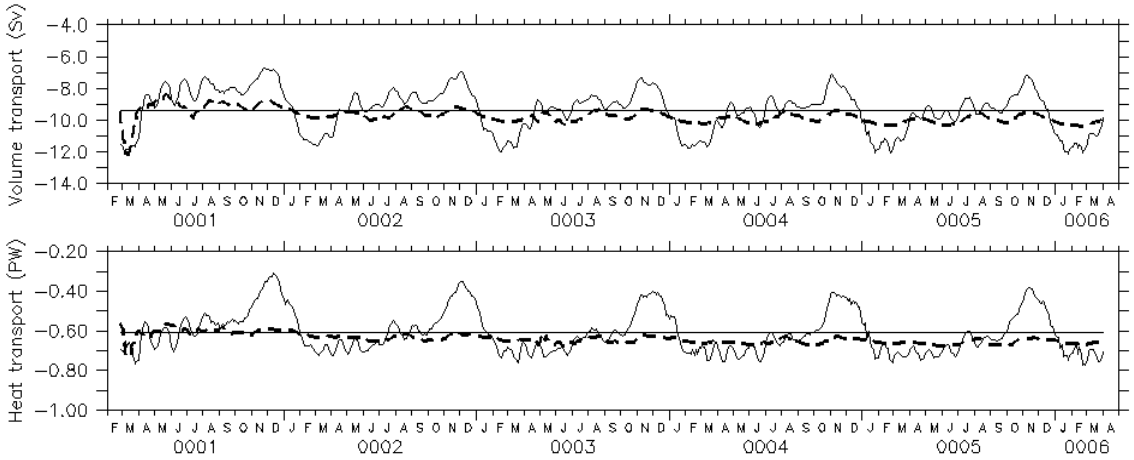

Figure 3-31 Volume and heat transport relative to 0°C variability within Makassar Strait for PD - *control* (thick) and PD – *no wind* experiment (dash).

3.6.2 Surface fluxes

In order to test sensitivity of ocean circulation and heat transport to the applied surface heat fluxes, four experiments with different representations of the surface boundary conditions are compared (Table 3-7). In the PD – *control* experiment restoring of temperature and salinity to monthly climatological values is applied (for descriptions see 2.3.2) and no additional surface fluxes are used. The relaxation time-scale is 30 days. In the PD – *no flux* experiment all surface fluxes are set to zero. In the PD – *heat flux* experiment only monthly net surface heat fluxes [NOAA NCEP/NCAR Reanalysis; *Kalnay et al.*, 1996] without surface restoring are applied. And, finally, in the PD – *rest + heat flux* experiment, the surface heat fluxes and restoring of temperature and salinity with 3 days restoring time-scale are used.

Table 3-7 Overview of the heat fluxes sensitivity experiments for the PD conditions.

Experiment	Net surface fluxes (Q_{net})	Restoring time-scale (τ)
PD – *control*	no	2592000 s
PD – *no flux*	no	no
PD – *heat flux*	monthly	no
PD – *rest. + heat flux*	monthly	259200 s

Interaction with the atmosphere in the model is then given by the surface heat flux (H_Q) resulting from the net surface fluxes adopted from the climatological estimates (Q_{clim}) and the relaxation fluxes:

$$H_Q = Q_{c\lim} + c_p \int_o^L \int_o^M \rho \frac{(\theta - \theta_{res})\Delta z}{\tau} dxdy \qquad 3\text{-}23$$

where θ is the model SST, θ_{res} is the climatological SST, Δz is the thickness of the surface layer (Δz = 5 m in the model), τ is restoring time-scale and L and M are width and length of the basin. Net surface heat flux Q_{clim} is given by the sum of the net upward shortwave radiation (Q_{sw}), net upward longwave radiation (Q_{lw}), latent (Q_{lh}) and sensible heat fluxes (Q_{sh}):

$$Q_{c\lim} = Q_{sw} + Q_{lw} + Q_{lh} + Q_{sh} \qquad 3\text{-}24$$

When only surface restoring is applied (PD – *control* experiment), the model surface heat fluxes are small and not sufficient to compensate cooling in the ocean interior (Figure 3-32). When climatological surface heat fluxes are applied (PD – *rest. + heat flux*), the model divergence is in good agreement with corresponding surface fluxes. However, when only climatological heat fluxes without surface restoring are applied (PD – *heat flux*), net heat transport in the ocean interior is increased, indicating that the heat fluxes are not in balance with the volume transport through the domain. This results in general warming of the ocean which can be seen in high SST produced in the PD – *heat flux* experiment (Figure 3-33).

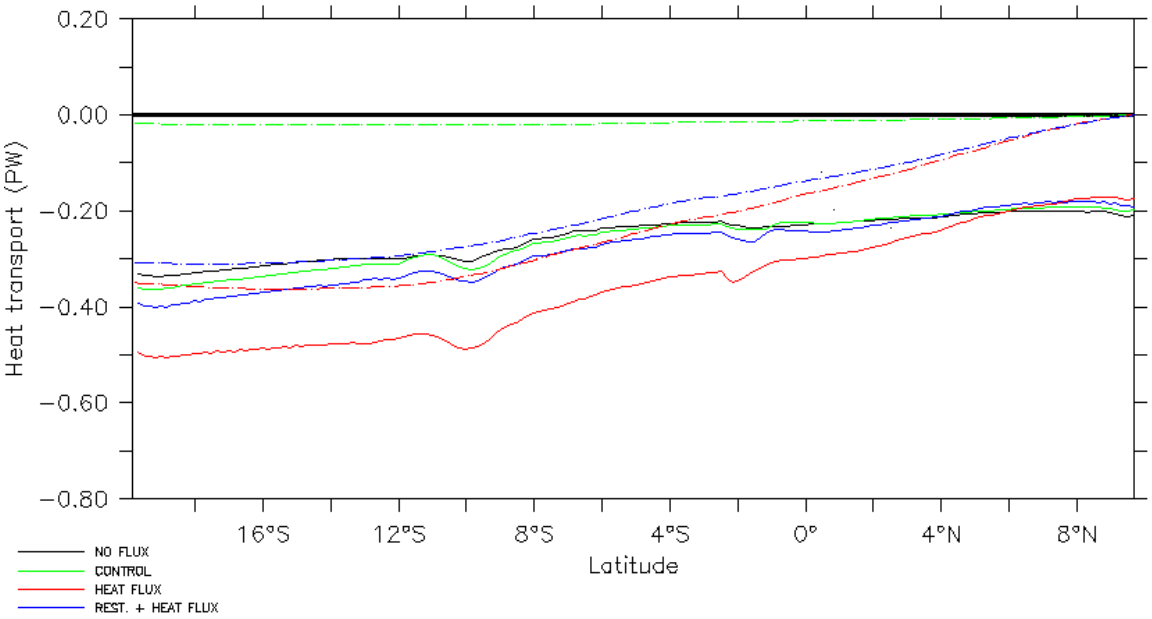

Figure 3-32 Net heat divergence Q_{net} (PW) is plotted for experiments with different representation of heat fluxes (full line). Corresponding zonally integrated surface fluxes are plotted in dash line.

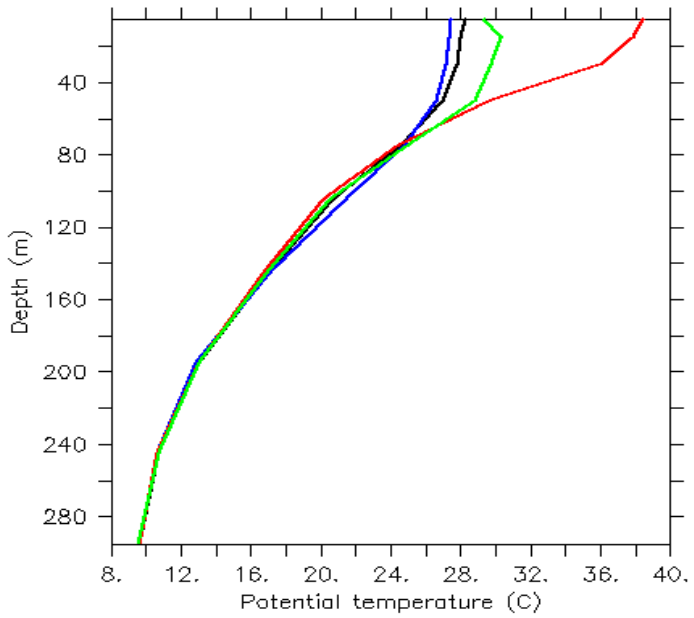

Figure 3-33 Average temperature profile (°C) in Makassar Strait at 3°S for the heat fluxes sensitivity experiments: PD – *control* (black), PD – *no flux* (blue), PD – *heat flux* (red), PD – *rest. + heat flux* (green).

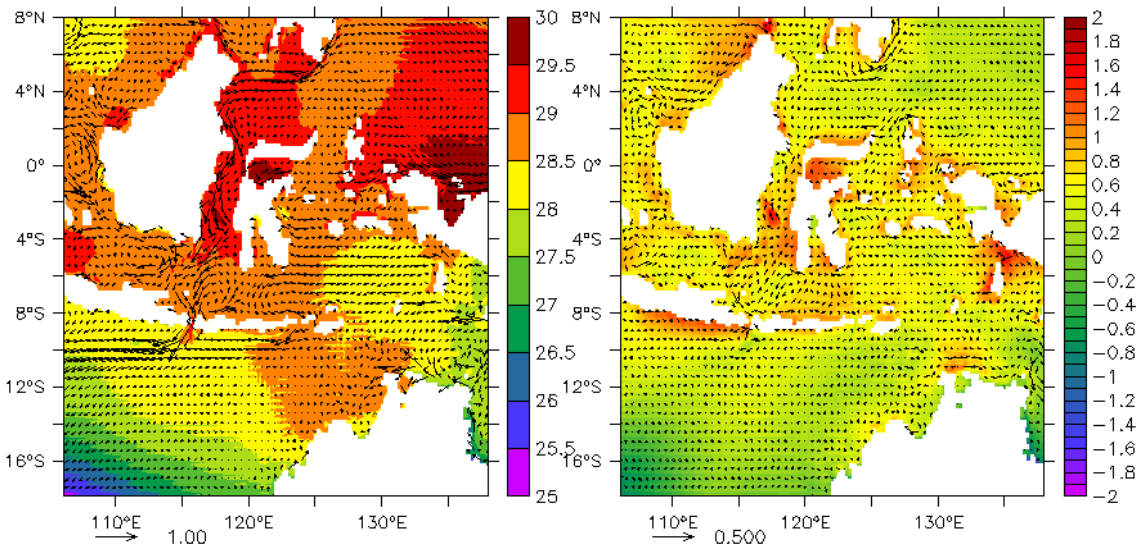

Figure 3-34 Mean SST (°C) and top layer circulation (ms^{-1}) in the PD - *rest. + heat flux* experiment (left) and anomaly between the PD – *control* and PD – *rest. + heat flux* simulation (right).

In the experiment PD – *rest.+ heat flux* (Figure 3-34) the mean SST is increased compared to the PD - *control* run. However, difference in the mean temperature and surface circulation is small possibly due to the strong surface restoring.

Even though, the absolute value of the heat transport differs between the heat fluxes experiments, the seasonal cycle of the heat fluxes is similar in the PD – *control* and PD – *rest. + heat flux* experiments (Figure 3-35). The annual cycle of the heat transport shows highest values during the boreal summer. The seasonal cycle of heat divergence at the ITF transect between 6°S – 4°S is compared to the NCEP/NCAR reanalysis climatological estimates (Figure 3-36). The seasonal cycle in PD – control simulation shows shift compared to observations, however the amplitude of variations in heat divergence is of same order of magnitude.

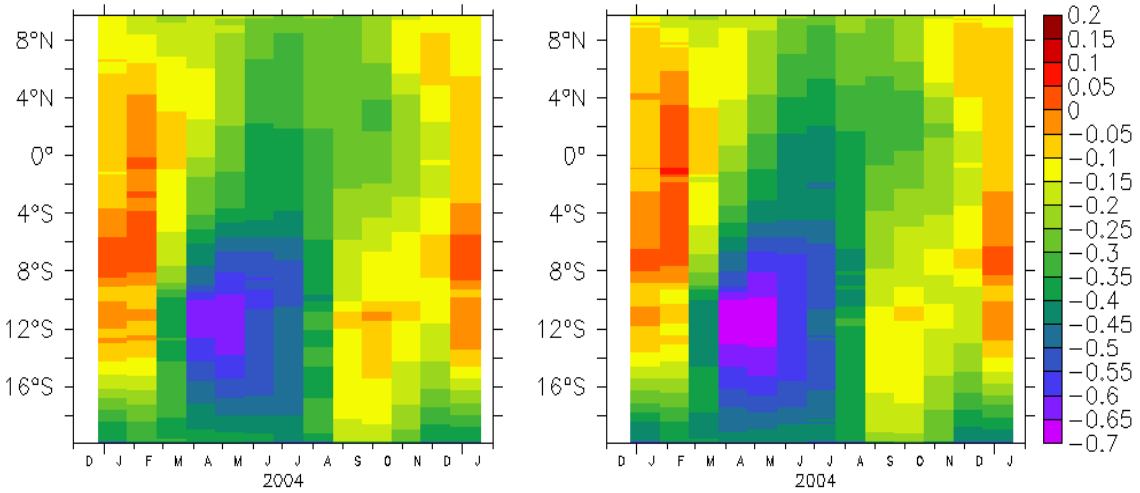

Figure 3-35 Annual cycle of the heat transport relative to 0°C (PW) in the PD – *control* (left) and PD – *rest. + heat flux* experiments (right).

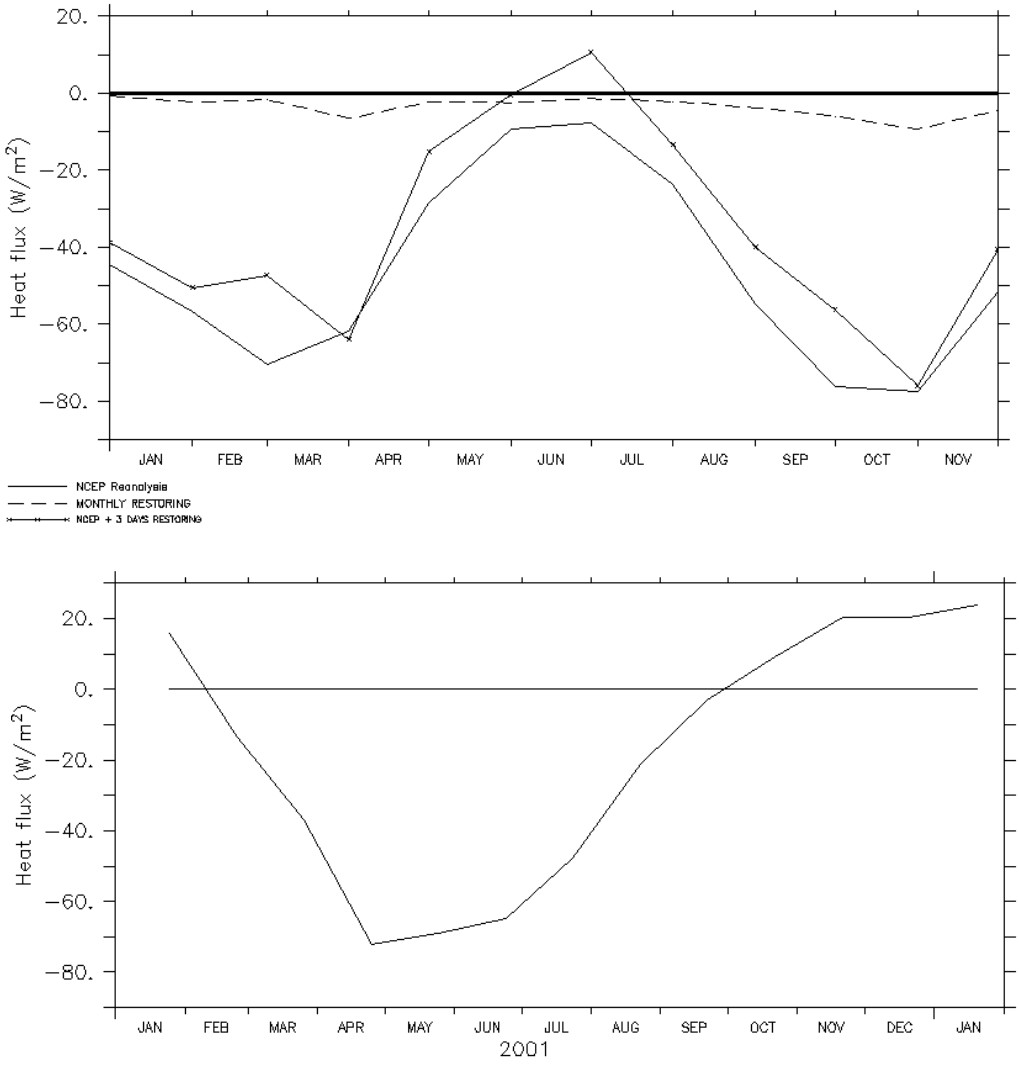

Figure 3-36 Seasonal cycle of zonally averaged surface heat flux at 5°S in the PD experiments compared to heat flux from NCEP/NCAR reanalysis [*Kalnay et al.*, 1996] (top) and heat divergence in the model between 6°S – 4°S calculated for the PD – *control* experiment (bottom). Positive values indicate heat flux from ocean to atmosphere.

3.6.3 Lateral boundary conditions

PD - *cyclic* experiment Here the sensitivity of the simulated circulation to seasonal variability in the inflow and outflow currents at the lateral boundaries is tested. Values of the volume and heat transport relative to 0°C for the main Indonesian passages are given in Table 3-8. The mean volume transport within Makassar Strait is slightly reduced and the transport between Sulawesi and New Guinea is increased. However, the mean circulation through the archipelago does not change significantly.

Table 3-8 PD – *cyclic* experiment volume and heat transport reference to 0°C. The numbers in brackets give minimum and maximum value of the transport. Positive values indicate southward transport towards the Indian Ocean.

	Volume transport (Sv)	Heat transport (PW)
Makassar Strait	8.6 ± 1.0 (6.6 – 10.7)	0.56 ± 0.08
Sulawesi – New Guinea	3.6 ± 1.6 (0.5 – 6.6)	0.12 ± 0.23
Lombok Strait	3.6 ± 0.7 (2.1 – 4.9)	0.33 ± 0.06
Ombai Strait	6.1 ± 1.7 (3.6 – 8.8)	0.30 ± 0.22
Timor Passage	2.9 ± 2.3 (-0.6 – 6.0)	0.13 ± 0.12
TOS	8.7 ± 1.1 (7.0 – 11.1)	0.42 ± 0.12
ITF	13.5 ± 0.7 (12.0 – 14.9)	0.82 ± 0.18

Changes in seasonality of the volume and heat transport within Makassar Strait and Timor Passage are illustrated in Figure 3-37. In experiment PD - *cyclic* the transport within Makassar Strait has its minimum during the NW monsoon period (November – February) as in the PD – *control* experiment. This is in accordance with the observed freshwater blocking in southern Makassar Strait during the NW monsoon phase [*Gordon et al.*, 2003]. The period of strong flow, with its maximum in March in the PD – *control* run, is now extended through the whole SE monsoon phase (April – August). This effect can be related to increased inflow at the lateral boundaries during boreal summer. The intensification of the flow, which terminates the blocking phase, appears slightly later in the PD – *cycli*c experiment compared to PD – *control*. This improves the agreement with the global high-resolution MIT ECCO model (see Figure 3-12). The transport in Timor Strait shows a shift in phase with the maximum of the flow appearing from February – June in experiment PD - *cyclic*. The seasonal variations of the flow in Timor Strait also show higher amplitude and possible reversals of the flow towards east when variability in the boundary currents is taken into account.

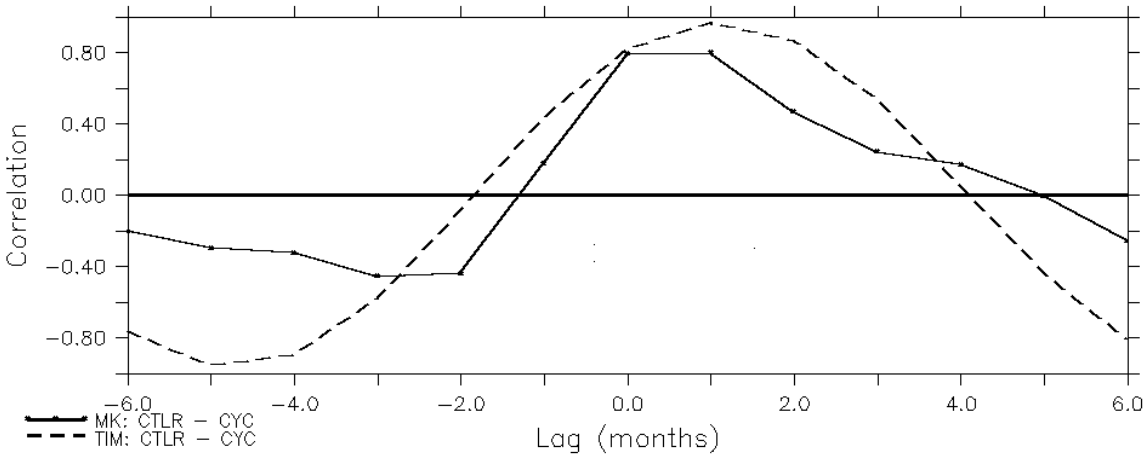

Figure 3-37 Correlation of the volume transport in Makassar Strait (thick line) and Timor Strait (dash line) between PD – *control* and PD – *cyclic* experiment. A positive correlation TIM: CTRL – CYC at +1 month lag indicates that Timor Strait transport in PD – *control* experiment is lagged by 1 month compared to the transport in PD – *cyclic* experiment.

PD – *ecco* experiment The simulated circulation in the PD - *ecco* experiment is shown in Figure 3-38. Given is comparison of the depth-integrated velocity and density field at 100 m depth representative for the main flow in the PD – *control* experiment. The current field in the PD – *ecco* simulation shows strong inflow from the northern boundary accounting for the strong MC which is mainly reverted towards the east into the NECC forming a gyre at the entrance of the Celebes Sea. The strong reversal of the flow into the NECC is not captured in the PD - *control* experiment. The density field in the PD – *ecco* experiment shows a sharp front that clearly separates the North Pacific inflow waters from the NECC. The horizontal density gradient induces strong zonal currents.

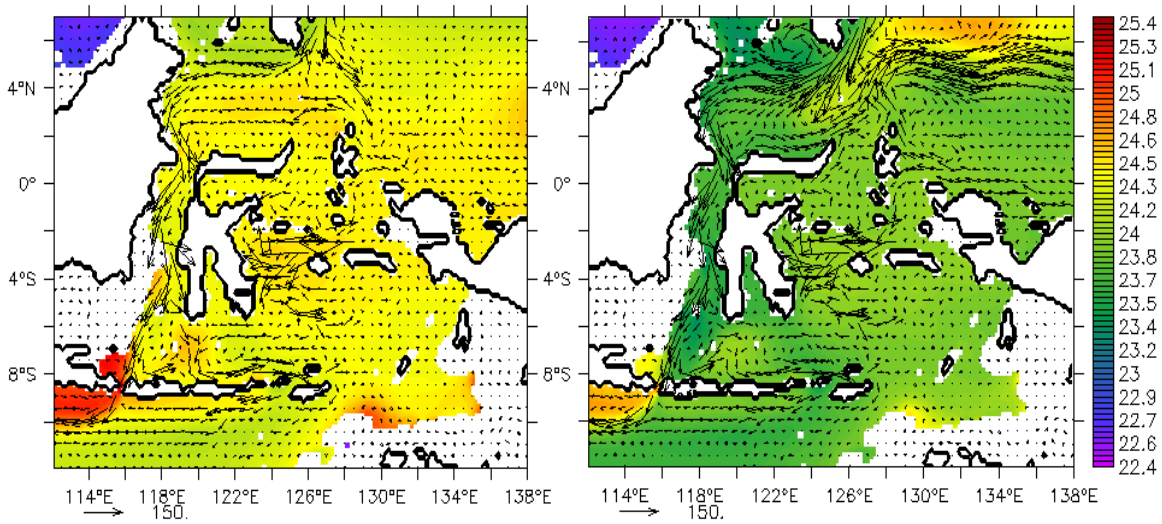

Figure 3-38 Mean depth-integrated velocity (m^2s^{-1}) and density field (kgm^{-3}) at 100 m depth in the PD - *control* simulation (left) and PD – *ecco* simulation (right).

Even though, the current system in the West Pacific appears considerably different in the two model simulations, the circulation inside the Indonesian Passages including Makassar Strait and the outflow passages does not seem to differ much. The seasonal variations within Makassar Strait and Timor Passage are similar to the PD - *control* run (Figure 3-29).

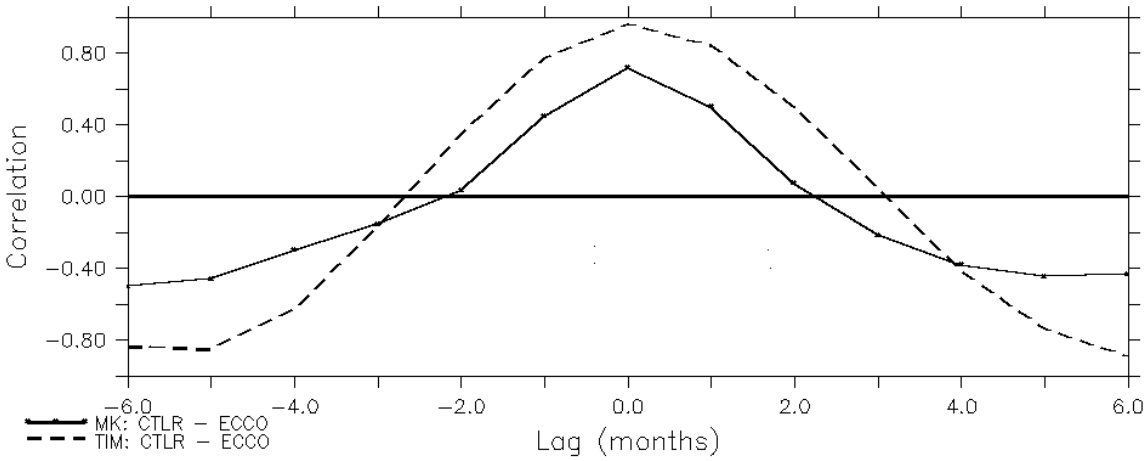

Figure 3-39 Correlation of the volume transport in Makassar Strait (thick line) and Timor Strait (dash line) between PD – *control* and PD – *ecco* experiment. A positive correlation MK: CTRL – ECCO at 0 month lag indicates that Makassar Strait transport in PD – *control* experiment is in phase with the transport in PD – *ecco* experiment.

The calculation of volume transport, given in Table 3-9, shows very small increase in transport through Makassar Strait and small increase of transport through Lombok Strait while the flow between Sulawesi and New Guinea and within Ombai Strait is reduced. However, larger differences appear in the vertical density stratification and velocity profiles that can be seen on transects through Makassar Strait (Figure 3-40). The flow in the upper 200 m is intensified in the PD – *ecco* simulation while the flow in intermediate levels (300 – 650 m) is decreased resulting in the increase in heat transport compared to the PD – *control* experiment. The density is decreased between 50 and 350 m with maximum difference of $\Delta\sigma$= 1 kgm^{-3} at 100 m depth where the flow is strongest signifying increased inflow of warm water. However, vertical profile of the flow and estimates of heat transport within Makassar Strait in the PD – *control* simulation seem to be in good agreement with observations [*Vranes et al.*, 2002] and this result can be taken as less realistic.

Table 3-9 PD – *ecco* experiment volume and heat transport reference to 0°C. The numbers in brackets give minimum and maximum value of the transport. Positive values indicate southward transport towards the Indian Ocean.

	Volume transport (Sv)	Heat transport (PW)
Makassar Strait	9.5 ± 1.1 (7.3 – 12.8)	0.76 ± 0.11
Sulawesi – New Guinea	0.8 ± 2.2 (-3.9 – 5.0)	0.01 ± 0.25
Lombok Strait	4.4 ± 0.5 (3.7 – 5.4)	0.42 ± 0.05
Ombai Strait	4.3 ± 1.4 (2.1 – 6.3)	0.28 ± 0.18
Timor Passage	2.5 ± 1.0 (0.9 – 3.9)	0.16 ± 0.10
TOS	6.6 ± 0.5 (5.6 – 7.4)	0.43 ± 0.11
ITF	11.9 ± 0.3 (11.2 – 12.8)	0.91 ± 0.13

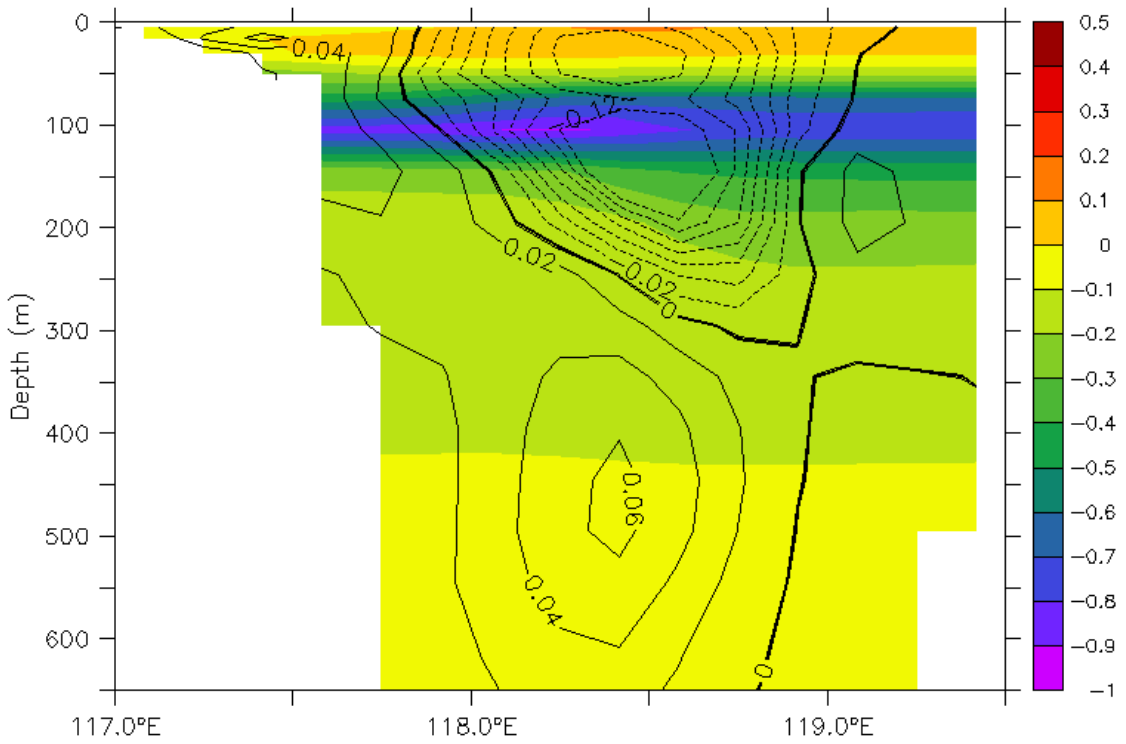

Figure 3-40 Difference in density stratification (kgm^{-3}) and velocity field (ms^{-1}) between the PD – *ecco* and PD – *control* experiment. Shown is across-channel section at 4°S in Makassar Strait. Dash lines indicate negative values.

Small difference in the volume transport within Makassar Strait between PD – *ecco* and PD – *control* experiment (0.2 Sv) indicate that representation of boundary currents is not crucial for the ITF volume transport. The net transport is set by prescribing Pacific to Indian Ocean transport and excess inflow water at the northern boundary in PD – *ecco* is returned into the equatorial Pacific. A high-resolution representation of the boundary currents is important if the West Pacific equatorial currents are analysed. However, low-resolution model can be equally used if the dynamics within the Indonesian Seas are investigated.

3.7 Conclusions

The dynamics of the ITF are investigated in the regional model using climatological boundary forcing for PD conditions. The regional model produces a mean circulation within the Indonesian Seas in reasonable agreement with the observations.

Mean volume and heat transport in Makassar Strait correspond well to measured values [*Gordon et al*., 1999; *Vranes et al.*, 2002]. Flow dynamics can be approximately described with a three-layer system. Maximum of the flow appears in subsurface levels between 50 and 150 m. The flow is in geostrophic balance except for the region near the equator. Seasonal variability of the transport is compared with observations [*Susanto et al.*, 2004] and global model simulation of MITgcm ECCO project intended to estimate the global ocean state [*Menemenlis*, 2004]. High-frequency variability and inter-annual variations in ocean dynamics are absent in the regional model forcing and for this reason, the results do not compare well in detail with the transport observations. However, the mean seasonal cycle is well represented and is in good agreement with the theory of monsoonal wind forced regime [*Gordon et al.*, 2003].

Temperature and salinity profiles correspond well with measurements including the seasonal cycle showing input of low salinity surface waters in the southern Makassar Strait during the NW monsoon phase [*Gordon and McClean*, 1999]. Due to the surface buoyant water present in the southern Makassar Strait, southward surface flow is reduced during boreal winter. Reversal of the wind in March allows intensified surface flow by eliminating low-salinity blocking and strong transport prevails during the SE monsoon phase. The timing of the transport maximum depends not only on the local dynamics, but also correlates with the large scale forcing introduced in the regional model by the seasonal cycle in lateral boundary currents. The response of the mean transport within Makassar Strait to the prescribed inflow at the lateral boundaries is linear. Wind forcing in the region does not effect the mean circulation significantly, however it is important factor in determining its seasonal variability.

Transport values through Lombok Strait are overestimated in the model due to the model horizontal resolution giving a wider cross-section of the passage than observed. The vertical profile corresponds well with observations [*Hautala et al.,* 2001] showing strong surface and thermocline outflow. The seasonal cycle of the flow has its maximum during the SE monsoon phase. However, observed reversals of the flow during the NW monsoon and intra-seasonal variability associated with induced coastal Kelvin waves are not captured in the model because of a lack of variability in the boundary conditions.

The flow through Ombai Strait shows relatively good agreement with observations with volume transport values higher by ~1 Sv than observational estimates [*Molcard et al.* 2001]. The seasonal cycle shows a maximum during the SE monsoon. The strongest variability of the flow appears in the upper 100 m while the deeper flow is weak but shows stable outflow. Surface currents show reversals towards the Banda Sea in the NW monsoon period in accordance with measurements [*Hautala et al.,* 2001].

The Timor Strait volume transport is underestimated in the model compared to the mooring measurements in the strait [*Creswell et al.*, 1993; *Molcard et al.*, 1996]. The model simulates well the formation of the strong current along the North Australian shelf region during the SE monsoon. However, in the model, undercurrent in opposite direction at the depths between 30 and 200 m is associated with the surface southward flow. Thus, the net outflow is reduced and the seasonal cycle of the flow is

compromised. However, the Timor Strait transport would be larger if the outflow through Lombok and Ombai Strait were smaller. The reduced Timor Strait outflow is partially a consequence of the overestimated transport through Lombok Strait considering that flow takes the westernmost pathway.

4. Impact of glacial sea-level changes on the Indonesian Throughflow

4.1 Introduction

The closure of the Indonesian passages has strong impact on the tropical climate as shown by the coupled AOGCM experiments [*Schneider and Barnett,* 1997; *Schneider*, 1998; *Wajsowicz and Schneider*, 2002]. During the LGM, lowering of the sea level by 120 m (see Figure 5-2) [*Hanebuth and Stattegger*, 2003; *Steinke et al.*, 2003] has significantly changed the topography of the Indonesian Gateways by reducing aperture of the main passages, decreasing depth of the main sills and changing land-sea distribution in the region [*De Deckker et al.*, 2002]. The question arises to what extent topographic changes during the LGM have impact on the ITF volume and heat transport. Based on the paleoclimatic evidence from the Indonesian Gateways [*Müller and Opdyke*, 2000; *Gingele et al.*, 2001a,b; *De Deckker et al.*, 2002; *Kuhnt et al.*, 2004] a reduction of the ITF transport during the LGM was proposed. Possible topographic blocking of the water masses exchange within Indonesian passages may be the reason for reduced transport and lead to a readjustment in the tropical ocean-atmosphere system during the glacial periods. However, role of topography must be considered in scope of glacial climate conditions which have significantly different climate forcing than the PD. Due to generally colder SST's by 2 - 5°C [*Lea et al.*, 2000; *Stott et al.*, 2002; *Rosenthal et al.*, 2003; *Visser et al.*, 2003] and possible absence of low salinity surface waters [*Martinez et al.*, 1997; 2002; *De Deckker et al.*, 2002], density stratification in the region might have been significantly different. Changes in monsoonal wind strength in the region [*van der Kaars et al.*, 2000; *van der Kaars et al.*, 2001; *Holbourn et al*., 2005] might effect wind forced circulation and also have impact on seasonal variations of the flow. Moreover, recent reconstruction of the SST and SSS in the eastern equatorial Pacific [*Koutavas et al.*, 2002] imply shifts in the tropical Pacific ocean-atmosphere system during the LGM that are analogous to the ENSO events. These findings have been supported with modelling results [*Otto-Bliesner et al.*, 2003; *An et al.*, 2004] suggesting that LGM background conditions are favourable to support large-amplitude self-sustained ENSO variations in the tropical Pacific. Taking the analogy with modern ENSO events [*Meyers*, 1996; *Murtugudde et al.*, 1998], ENSO conditions would generally lead to reduction in ITF transport by increasing westerly anomalies in wind stress over the Pacific. However, possible severe blocking of the Throughflow might, on the other hand, be one of the factors supporting the ENSO like pattern in the tropical Pacific.

In the previous chapter PD dynamics of the ITF are discussed and a high-resolution regional model with reference circulation for modern climate conditions in the Indonesian archipelago is developed. In this chapter, the results from the PD – control simulation are compared with the sensitivity experiment in which sea level lowering is taken into account, while maintaining the modern boundary conditions (PD – 120). In this way, impact of topographic changes is analysed separately from the impact of glacial climate conditions. The simulation of the ITF during the LGM includes both sea level lowering and glacial boundary conditions based on the global model experiment of the LGM climate [Paul and Schäfer-Neth, 2003]. Due to the large uncertainties in LGM surface forcing, especially in the ITF region, additional experiments are performed with boundary forcing taken from different global LGM simulations [Shin et al., 2003; Lohmann and Lorenz, 2000]. The main questions addressed in this chapter are whether the topographic changes can reduce the ITF

volume transport and in which way they impact seasonal variations and vertical structure of the flow and related heat transport from the Pacific to the Indian Ocean.

The Throughflow characteristics are analysed separately in Makassar Strait and outflow passages as in the previous chapter. Vertical transects across the main passages are provided illustrating simulated LGM hydrography and velocity structure together with anomalies between LGM and PD simulation which can be used for detailed comparison or as help in interpretation of the paleoceanographic data from the region.

4.2 Experimental setup

In PD – *120* experiment model forcing for the PD conditions is used and topography is reduced by 120 m in order to account for the sea-level change during the LGM. The bathymetry in the model is reduced uniformly from the bottom so the surface and intermediate forcing remained unchanged. The effect of missing bottom water for the mass balance at the lateral boundaries is small (~0.05 Sv).

Selection of boundary conditions and model configuration for the LGM experiments is described in sections 2.2 and 2.3. Overview of sensitivity experiments is given in Table 4-1.

Table 4-1 Glacial sea level lowering sensitivity experiments.

Experiment	Sea level change	Boundary Conditions
PD - *control*	0 m	PD
PD – *120*	– 120 m	PD
LGM	– 120 m	LGM

In addition to these experiments, LGM model simulation is repeated with different boundary forcing in order to test sensitivity of model circulation to the choice of the glacial boundary conditions. The experiments include sensitivity to wind stress forcing (LGM – *ECHAM3*), surface temperature and salinity (LGM – *NCAR*) and variations in lateral boundary transport (LGM – *cyclic*). The overview of the LGM sensitivity experiments is given in Table 4-2.

Table 4-2 Sensitivity experiments for LGM boundary conditions. ECHAM3 refers to wind stress forcing taken from the AGCM experiment with cooled tropics [Lohmann and Lorenz, 2002], MOM refers to the data derived from OGCM MOM simulation of Paul and Schäfer-Neth [2003] and NCAR refers to the coupled AOGCM experiment [Shin et al., 2003].

.

Experiment	Wind forcing	Surface SST and SSS restoring	Lateral transport
LGM – *ECHAM3*	ECHAM3	MOM	MOM constant
LGM – *NCAR*	NCAR CSM	NCAR CSM	MOM constant
LGM – *cyclic*	MOM	MOM	MOM annual cycle

4.3 Impact of topographic changes

4.3.1 Mean circulation

With the sea level lowered by 120 m in PD – *120* experiment, the mean current system through the Indonesian passages is similar as in the PD - *control* run (Figure 4-1). The main flow takes route through Makassar Strait and turns eastward towards the eastern outflow passages. The difference appears in the Banda Sea where deep water gyre is reduced and in exit passages, where currents through Lombok Strait are weaker and the flow towards the east is intensified especially in the Timor Strait.

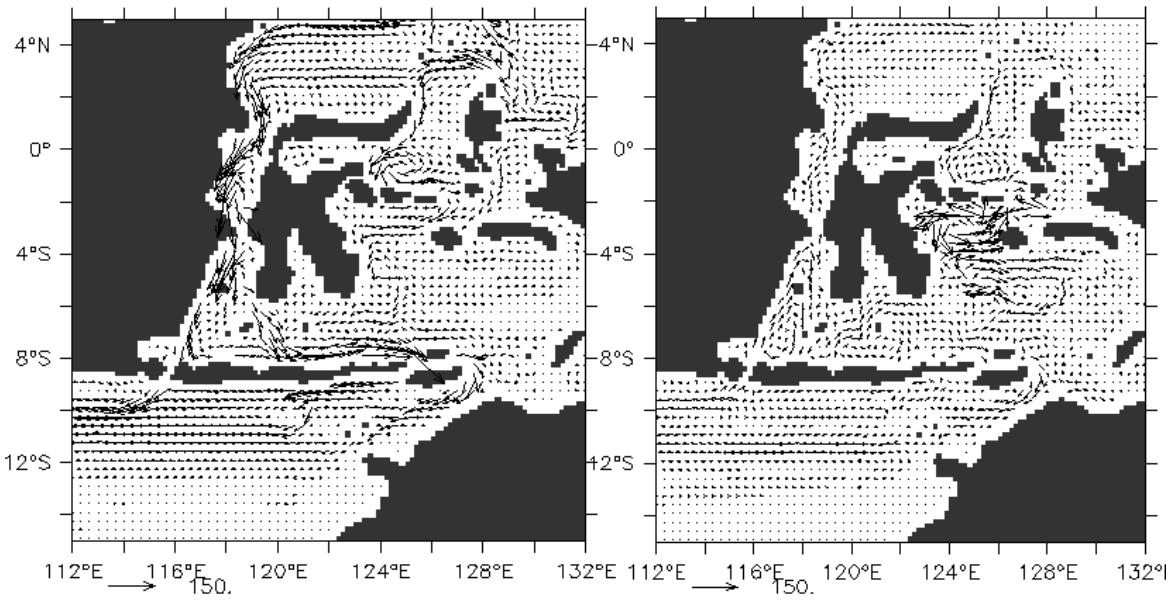

Figure 4-1 Mean annual depth-integrated flow (m^2s^{-1}) through the Indonesian Gateways in PD – *120* experiment (left) and difference in depth-integrated currents between PD – *120* and PD – *control* simulation (right).

Values of the mean volume and heat transport are given in Table 4-3. The mean volume transport through Makassar Strait does not change significantly with lowering of the topography. However, heat transport within Makassar Strait is increased by 0.05 PW compared to PD – *control* simulation. The volume transport through Lombok Strait is reduced by ~50 % and the related heat transport is decreased. The Ombai Strait transport does not change significantly while the Timor Strait transport is almost doubled. This leads to the increase in heat transport through eastern outflow passages of 0.15 PW.

Table 4-3 Volume and heat transport reference to 0°C in the PD - *120* simulation. The numbers in brackets give minimum and maximum value of the transport. Positive values indicate southward transport towards the Indian Ocean.

	Volume Transport (Sv)	Heat Transport (PW)
Makassar Strait	9.5 ± 2.2 (5.6 – 13.1)	0.66 ± 0.18
Sulawesi – New Guinea	2.7 ± 2.2 (0.9 – 6.5)	0.08 ± 0.25
Lombok Strait	1.8 ± 0.6 (0.7 – 2.4)	0.19 ± 0.06
Ombai Strait	5.6 ± 0.6 (4.5 – 6.6)	0.29 ± 0.06
Timor Passage	4.9 ± 0.5 (4.1 – 5.8)	0.30 ± 0.05
TOS	10.3 ± 0.5 (9.4 – 11.2)	0.58 ± 0.08
ITF	12.8 ± 0.5 (12.0 – 13.8)	0.83 ± 0.15

Since Makassar Strait volume transport seems not to be significantly effected with the topographic changes, the PD – *120* experiment is repeated with different values of the total transport prescribed at the boundary. The results are compared with the PD sensitivity experiments with the modern bathymetry (Figure 4-2). The same linear response of Makassar Strait volume transport to the net prescribed transport is found even if the sea level lowering is taken into account. However, transport values show higher variability in the PD – *120* experiments.

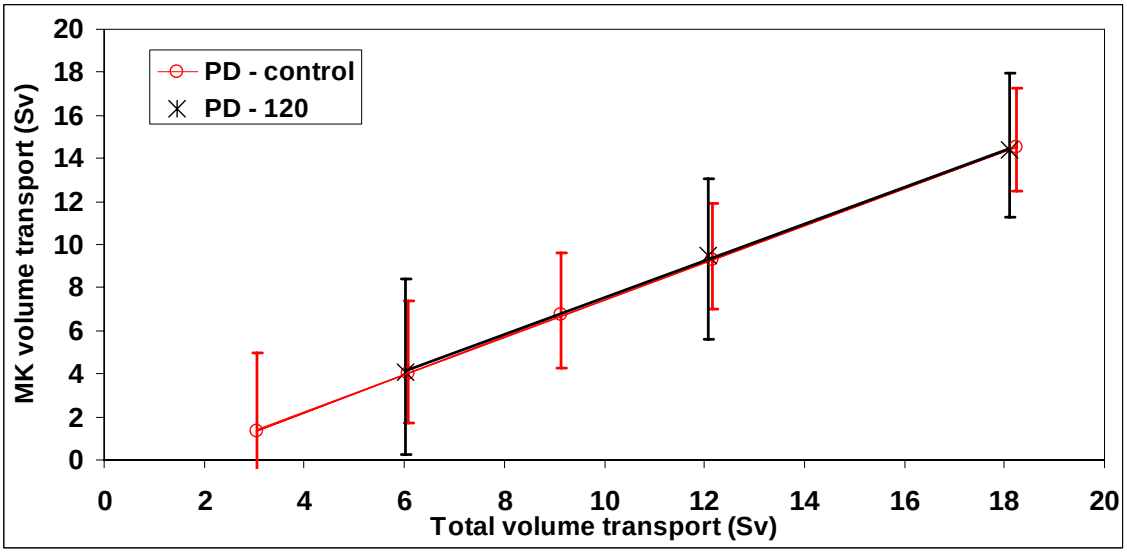

Figure 4-2 Response of the volume transport within Makassar Strait (MK) to scaling of the lateral boundary transport for PD – *control* (red) and PD – *120* experiment (black). The error bars indicate maximum and minimum values of the model transports.

Even though, topographic changes do not seem to changes significantly mean volume transport, they have impact on the net heat transport towards the Indian Ocean due to the modified vertical profile of the flow (see 4.3.3). The net increase in Makassar Strait heat transport is 8.2% compared to the PD – *control* simulation. In the PD – *control* experiment Makassar Strait carries 76.2% of the total volume transport. However, the heat transport values 83.3% of the total ITF heat transport since the flow

carries mainly surface and intermediate waters. For the similar volume transport, this value is increased to 88.8% in the PD – *120* experiment. The heat transport values within Makassar Strait are plotted against the total volume transport prescribed on the boundary for various values of the inflow transport (Figure 4-3). With given linear relationship of Makassar Strait volume and heat transport to the boundary forcing it is generally possible to estimate total ITF transport from the local measurements or reconstructions.

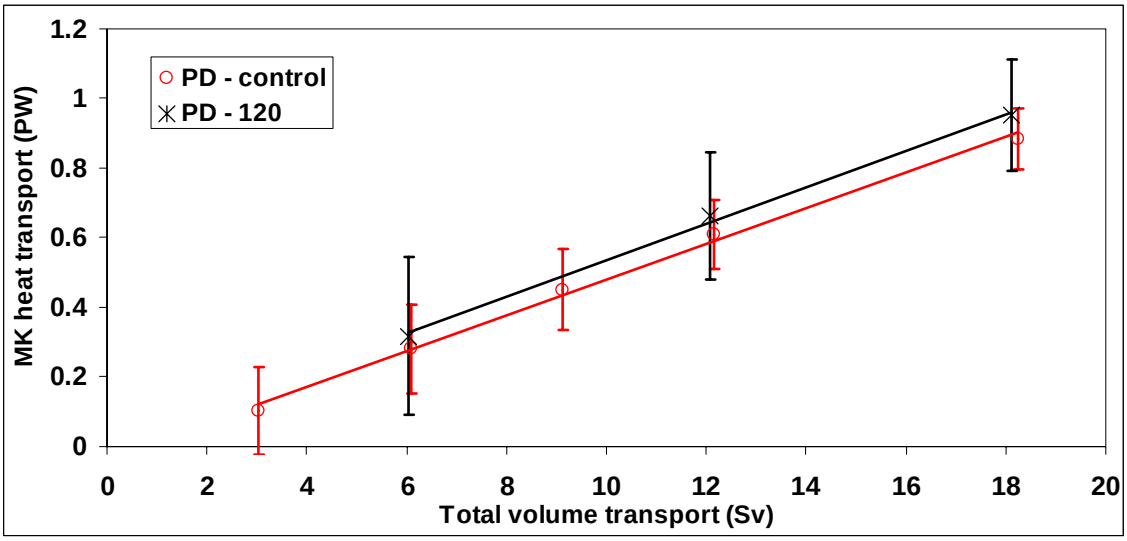

Figure 4-3 Response of the heat transport relative to 0°C within Makassar Strait (MK) to scaling of the boundary volume transport for PD – *control* experiment and PD – *120* experiment. The error bars indicate heat transport standard deviation.

4.3.2 Seasonal variability

The seasonal cycle of the transport within Makassar Strait is changed due to the sea level lowering (Figure 4-4). Maximum of transport appears from December to April during the NW monsoon phase and monsoon transition, and minimum of the flow appears from June to September during the SE monsoon phase.

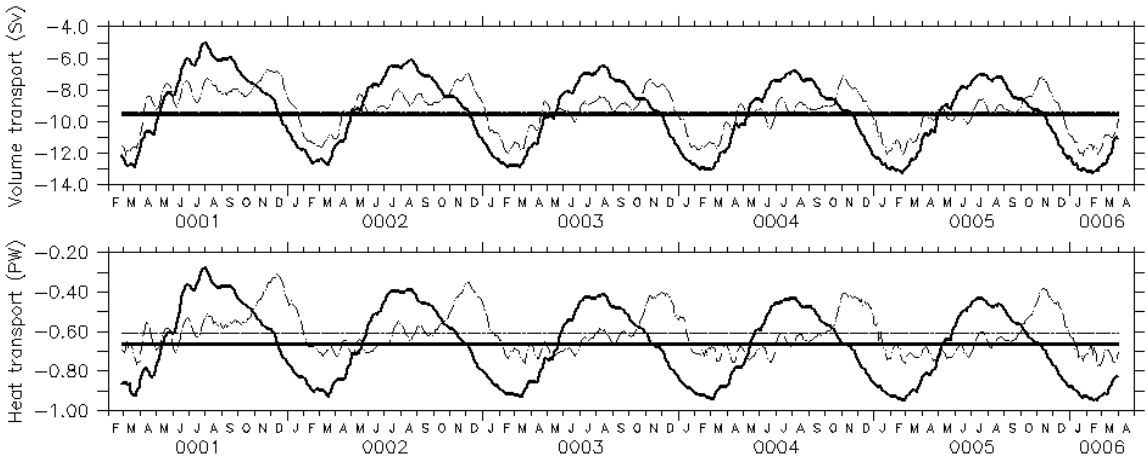

Figure 4-4 Makassar Strait volume (Sv) (top) and heat transport relative to 0°C (PW) (bottom) time-series in PD – *120* (thick) and PD – *control* (dash) experiment with negative values indicating southward transport.

During the NW monsoon, the surface flow through Makassar Strait is intensified with the southward winds within the Strait. Blocking of the surface flow due the low salinity Java Sea waters present in the PD – *control* simulation is absent since the shallow Java Sea is exposed during the LGM (Figure 4-5 left). During the SE monsoon, the wind reversal pushes the surface Banda Sea waters towards the southern Makassar Strait. The surface water piles up in the southern Makassar Strait since it is not able to flow into the Java Sea and the Lombok Strait is significantly closed (Figure 4-5 right). This results in blocking of the southward surface flow through Makassar Strait. In this way the seasonal cycle is reversed compared with the PD - *control* run and observations.

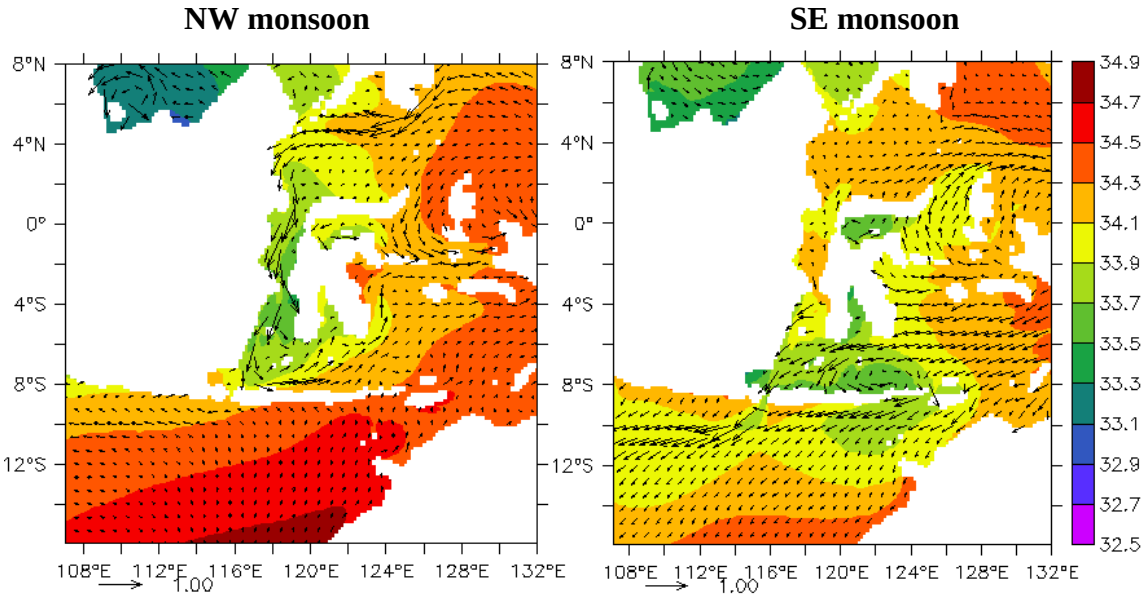

Figure 4-5 Seasonal changes in the surface circulation patterns when sea level is lowered (PD – *120* experiment). Surface salinity (psu) and currents (ms^{-1}) for ovember – February (top) and May – August (bottom) are illustrated.

With Lombok Strait transport significantly reduced due to the sea level lowering, the main outflow towards the Indian Ocean is provided through eastern exit passages. The time series of volume transport within main passages in PD – *120* experiment are correlated to the PD – *control* transports in order to estimate possible shifts in the seasonal cycles of the net outflow towards the Indian Ocean (Figure 4-6).

The eastern passages show higher transport values during the SE monsoon phase as expected from the PD – *control* simulation. The strong surface flow during the boreal summer seems to be related to local wind forcing and is not directly associated to the surface circulation in Makassar Strait. However, changes in seasonality within Makassar Strait might have impact on the ocean-atmosphere coupling within the Indonesian Seas and induce possible changes in the hydrological cycle. So far, no study has been done concerning seasonal interaction of the ITF with surface Indian Ocean circulation or feedbacks with the monsoonal system. Unfortunately, such mechanisms could not be investigated with the ocean only model and are out of scope of this study.

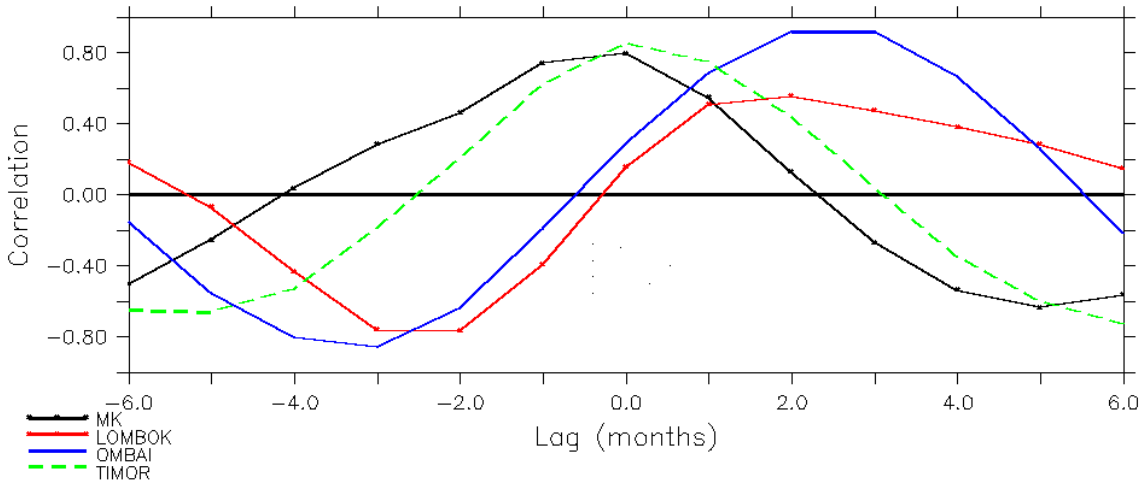

Figure 4-6 Lagged correlation of volume transport between PD – *120* and PD – *control* experiments for the main passages. For example, a positive correlation for MK at -1 month lag indicates that volume transport in Makassar Strait in PD - *120* leads the transport in PD – *control* by 1 month.

4.3.3 Vertical structure

The sea level lowering has significant impact on the vertical profile of the flow within Makassar Strait. With the shelf region exposed in the PD – *120* experiment, the main flow within Makassar Strait is constraint by the narrow and deep Labani Channel in the central of the passage (Figure 4-7). With the same boundary forcing as in the PD – *control* run, the velocities through the channel are increased, however, the net volume transport remains unchanged.

The shallow Dewakang Sill in the southern Makassar Strait controls the vertical structure of the flow. The reduction of the sill depth from 670 m to 550 m due to the sea level lowering results in intensification of the surface flow through the passage (Figure 4-8). Below the sill depth the transport is zero.

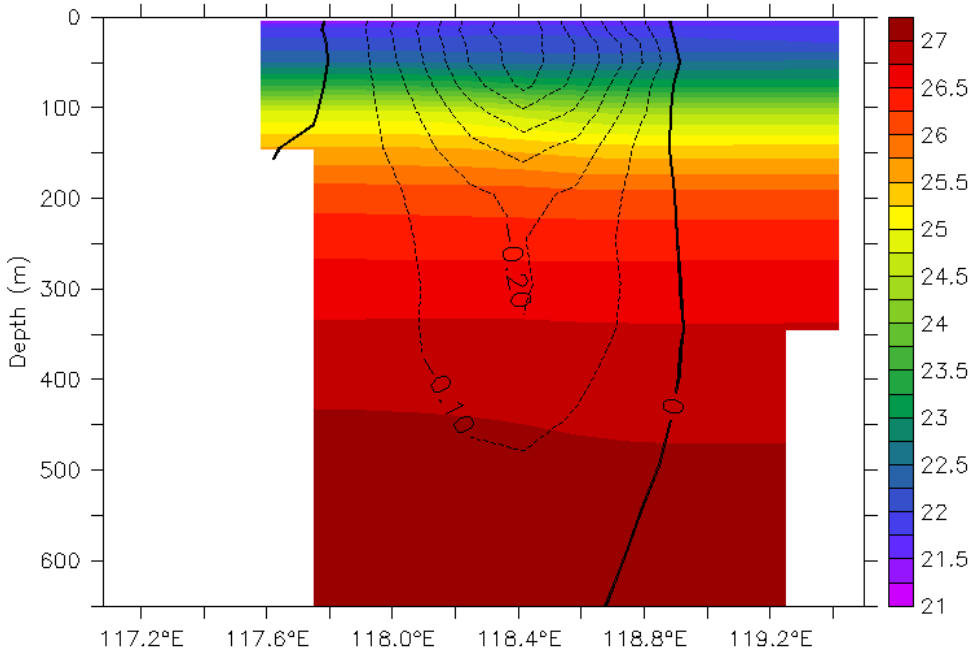

Figure 4-7 Density field (kgm^{-3}) and mean meridional velocity contours (ms^{-1}) in Makassar Strait at 4°S in PD – *120* experiment.

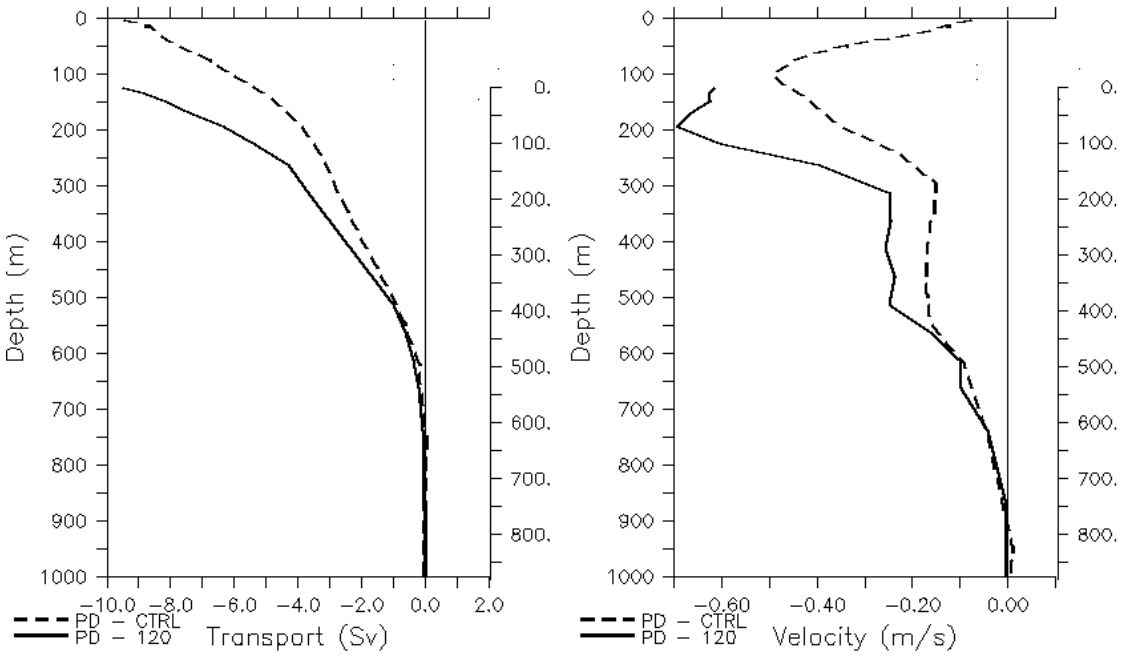

Figure 4-8 Makassar Strait cumulative transport (Sv) (left) and velocity profile (ms^{-1}) (right) at 4°S in PD – *120* (thick) and PD – *control* (dash) simulation. Negative values indicate southward transport. The right scale refers to the glacial topography.

Even though the topographic changes do not reduce the mean volume transport through Makassar Strait, changes in the vertical structure of the flow result in modified meridional heat transport. The intensified surface flow gives increase in net heat towards the Indian Ocean (Table 4-3).

Impact of changes in the vertical profile of the ITF on the Indian Ocean have been tested in the mixed-layer ocean model [*Song and Gordon*, 2004]. The vertical profiles of the transport within Makassar Strait in the PD - *control* run is similar to the thermocline intensified profile from model experiments of *Song and Gordon* [2004], while the lowered topography profile in the PD – *120* simulation resembles to the surface intensified profile (Figure 4-9).

The results of *Song and Gordon* [2004] show that the thermocline intensified transport leads to warming of the intermediate waters in the Indian Ocean by approximately 0.5°C. The total integrated meridional heat transport in the Indian Ocean is reduced by 0.1 PW. The magnitude of change is 25% as if the ITF was closed. This is a significant change considering that the change in the volume transport is just 1 Sv in the thermocline levels. However, the surface temperature signal in the Indian Ocean is small (maximum 0.05°C in the eastern Indian Ocean) and the net impact on the tropical climate is still not clear.

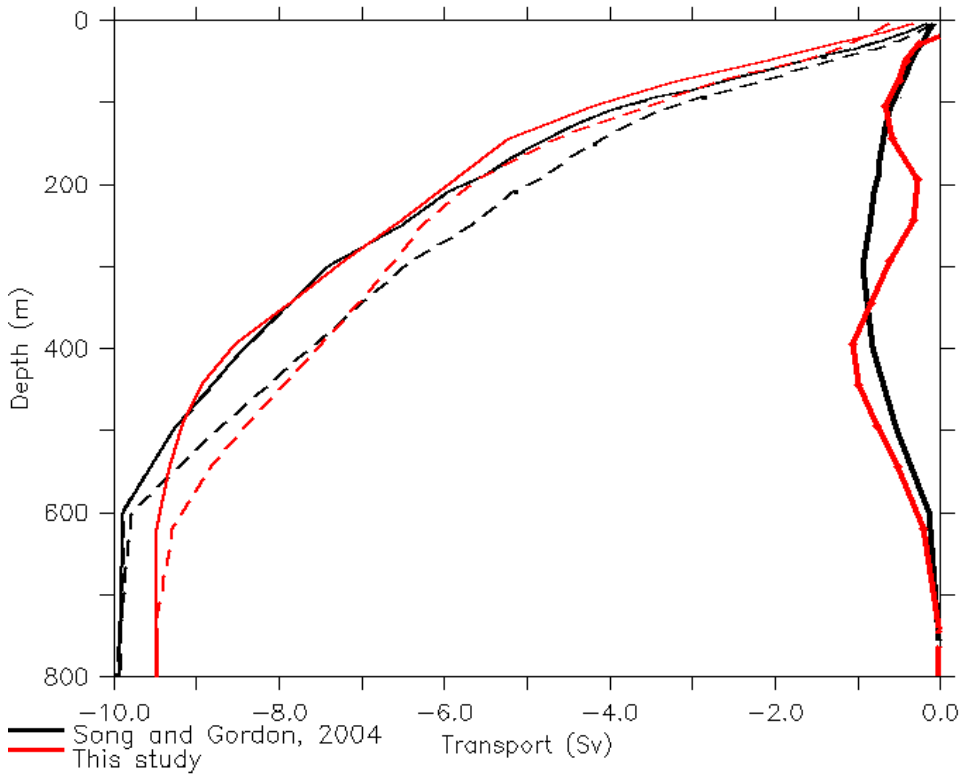

Figure 4-9 Vertical profile of the cumulative transport (Sv) within Makassar Strait from surface to bottom (red) for the PD – *control* experiment (dash), PD - 120 experiment (thin) and difference between two runs (thick). The profile is compared to the *Song and Gordon* [2004] results (black) with surface intensified (thin) and thermocline intensified (dash) transport.

4.4 Last Glacial Maximum simulation

4.4.1 Mean circulation

When glacial boundary conditions are taken into account in the LGM experiment, the model developed circulation is similar to the *PD – 120* simulation with the bulk of the ITF flowing through Makassar Strait, reduced Banda Sea deep water circulation and intensification of the flow through eastern outflow passages (Figure 4-10). However, the mean current field is weaker than in the PD – *control* experiment due to the reduced velocity values prescribed at the lateral boundaries to account for the LGM reduction in transport. Therefore, it is important to emphasize that the net LGM transport reduction is mainly set by the boundary conditions taken from the global OGCM MOM [*Paul and Schäfer-Neth*, 2003] and is not independent result of the regional model.

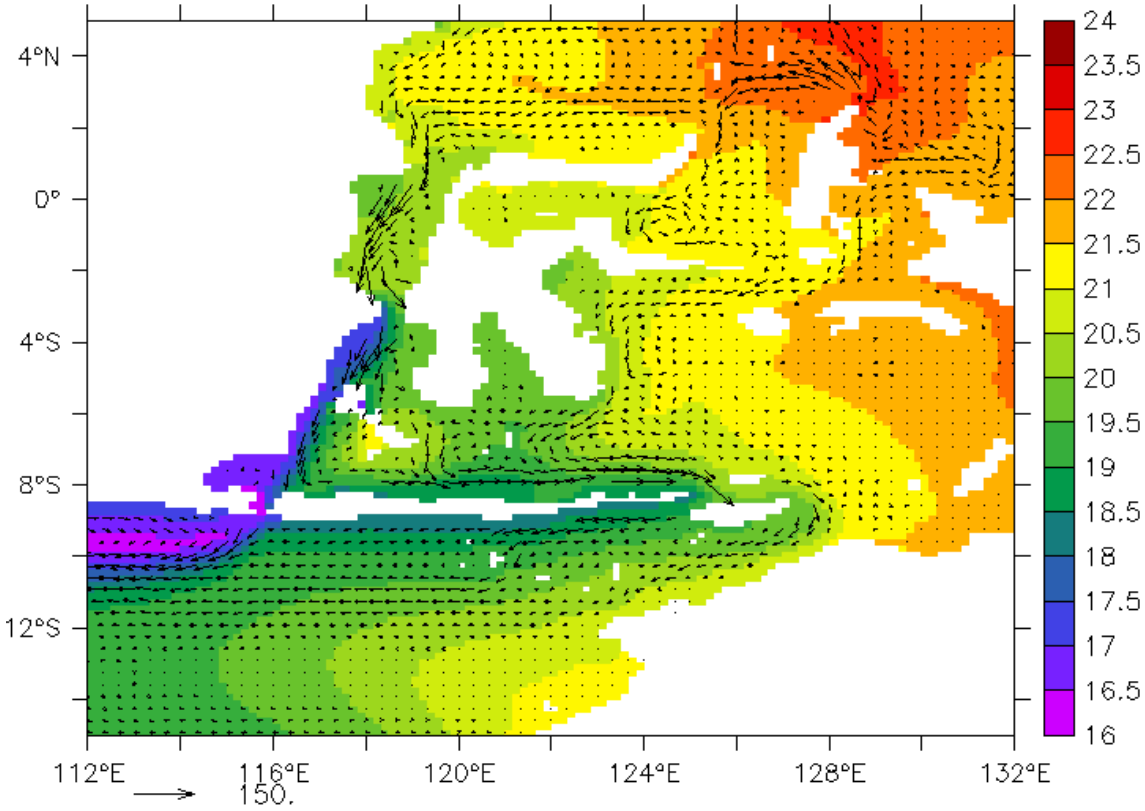

Figure 4-10 Mean depth-integrated circulation (m^2s^{-1}) and temperature (°C) at 100 m depth in the LGM experiment.

The transport values within the major passages and the net outflow at the sections in the Indian Ocean are given in Table 4-4. The volume transport in the LGM simulation within Makassar Strait is reduced by 34.4% compared to the PD – *control* experiment which is in agreement with the total reduction of the transport at the boundaries in the LGM experiment set to 2/3 of the PD value. The resulting Makassar Strait transport in the LGM experiment is 75.3% of the total ITF value. This result corresponds well to the PD – *120* experiments where the results suggest that glacial sea level lowering does not significantly change mean volume transport within Makassar Strait and that Makassar Strait transport depends linearly on the prescribed boundary transport (see 4.3).

Table 4-4 Volume and heat transport reference to 0°C in the LGM simulation. The numbers in brackets give minimum and maximum value of the transport. Positive values indicate southward transport towards the Indian Ocean.

	Volume Transport (Sv)	Heat Transport (PW)
Makassar Strait	6.1 ± 2.1 (2.7 – 9.4)	0.43 ± 0.23
Sulawesi – New Guinea	2.0 ± 2.1 (1.3 – 5.4)	0.05 ± 0.17
Lombok Strait	1.6 ± 0.8 (0.1 – 2.7)	0.16 ± 0.09
Ombai Strait	3.7 ± 0.9 (2.2 – 4.9)	0.17 ± 0.04
Timor Passage	2.8 ± 0.5 (1.8 – 3.8)	0.17 ± 0.05
TOS	6.6 ± 1.0 (4.9 – 8.2)	0.33 ± 0.06
ITF	8.7 ± 0.6 (7.1 – 10.1)	0.53 ± 0.14

The volume transport through Lombok Strait is similar to the PD – *120* experiment value. Ombai Strait transport is reduced by 37.3% compared to the PD – *control* experiment. Timor Strait transport is decreased compared to the PD – *120* experiment, however it remains similar to the PD – *control* value.

Net heat transport in the LGM simulation is reduced due to the lower volume transport values and colder temperatures. Impact of both surface and lateral boundary forcing on the ITF heat transport is analysed in section 4.5. Reduction of net heat transport within Makassar Strait is 29.5% compared to the PD – *control* experiment, while the total ITF heat transport is reduced by 34.2%.

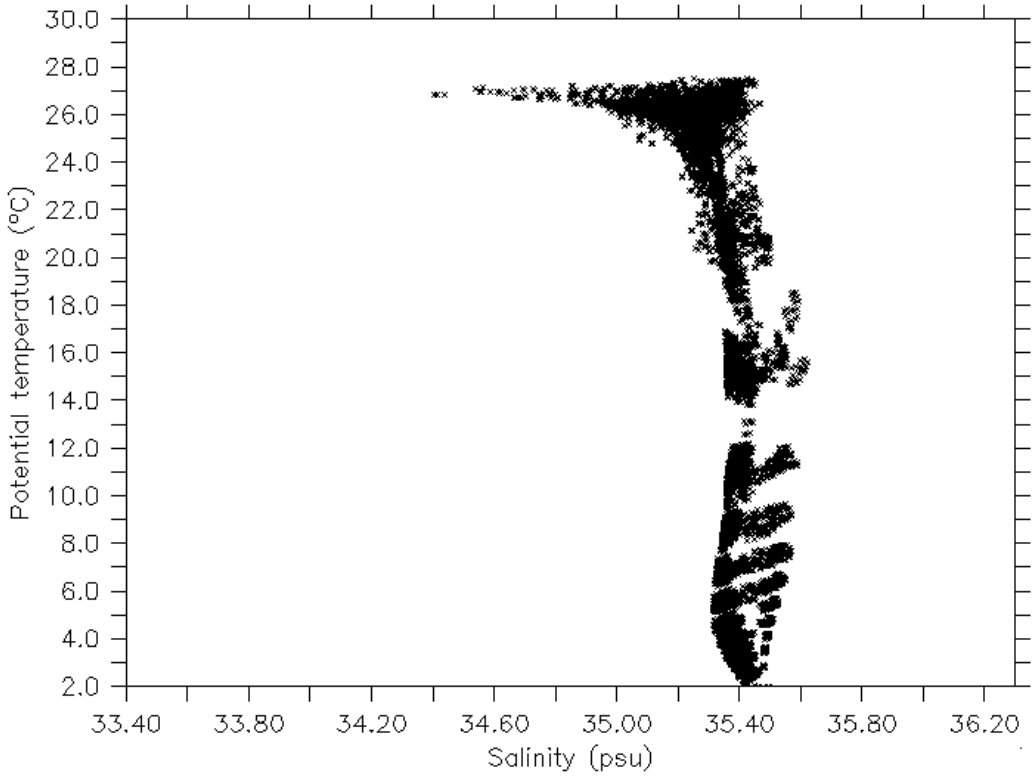

Figure 4-11 LGM potential temperature and salinity in the Indonesian Seas between 110°E – 135°E and 8°S – 0°. Note higher salinity values by 1 psu compared to PD – *control* run.

Temperature and salinity values in the LGM simulation show absence of low salinity surface water in the Indonesian Seas (Figure 4-11). The salinity values in the model are higher in average by 1 psu. Average salinity in the model in the LGM simulation is S_0=35.4 psu. The freshwater transport at 4°S referenced to average salinity S_0=35.52 psu is 0.041 ± 0.012·10^9 kgs^{-1}, while taking the PD value of S_0=34.64 psu the freshwater transport is 0.169 ± 0.010·10^9 kgs^{-1}. The magnitude of salt exchange is increased in LGM simulation compared to PD. However, the values are comparable only in a closed system and therefore net transport on the Indian Ocean should be analysed on the global scale. Relative contribution of different Pacific water masses in the Indonesian Seas is hard to analyse since the hydrographic data have considerably different values at the LGM and characteristics of the individual water masses should be redefined in scope of glacial climate conditions.

4.4.2 Seasonal variability

The seasonal variations in surface circulation in Makassar Strait are similar as in the PD – *120* experiment giving the strong surface outflow during the NW monsoon phase (Figure 4-12 left) and weak surface flow during the SE monsoon phase due to the accumulation of the Banda Sea waters in the southern Makassar Strait (Figure 4-12 right). Maximum of the transport appears from November to March, while minimum of the transport appears in September. In the LGM simulation, strong northward surface flow is developed near and across the equator during the SE monsoon. Intensification of the northward surface currents is most likely associated with the LGM wind field applied in the model. Analysis of the LGM atmospheric forcing simulated by the global AGCM [*Lohmann and Lorenz*, 2000] shows reduction in size and westward shift of the low pressure system in the western tropical Pacific resulting in intensified northward winds across the Indonesian Seas. These results have to be considered in scope of the whole tropical atmospheric system adjustment to glacial conditions and their impact on the local wind forcing should be taken with caution.

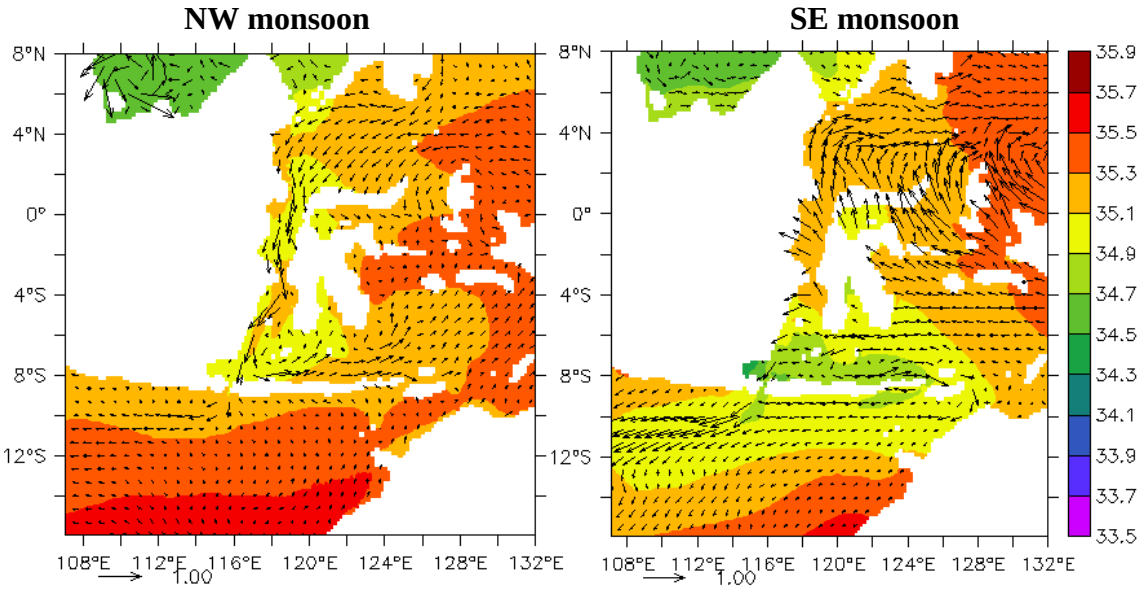

Figure 4-12 Monsoonal changes in surface circulation in LGM experiment for November – February (left) and May – August (right). Colour scale indicates salinity values (psu) and vectors velocity (ms^{-1}). Note higher salinity values in the LGM simulation.

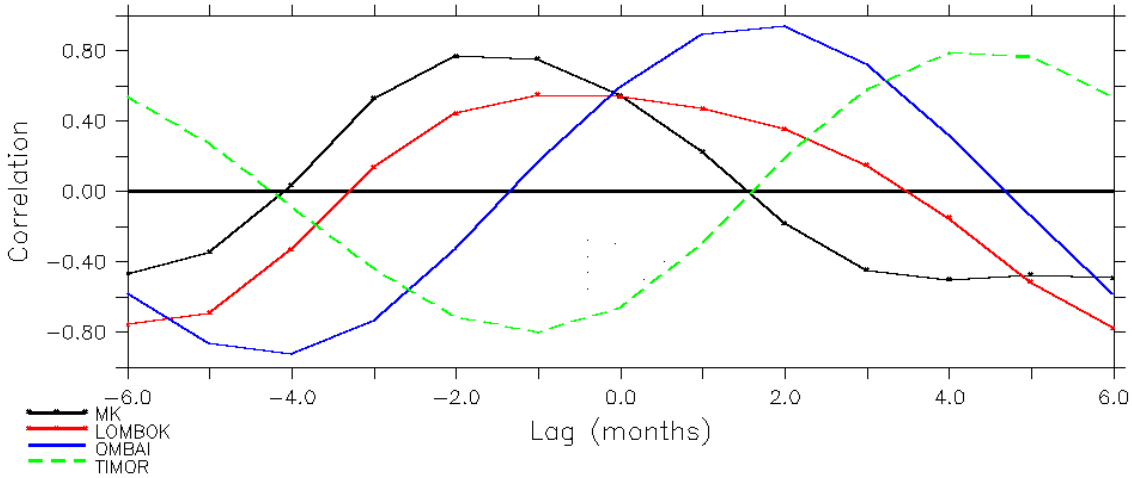

Figure 4-13 Lagged correlation of volume transport in the main passages between PD – *control* and *LGM* experiment. For example, a positive correlation for MK at -2 month lag indicates that volume transport in Makassar Strait in *LGM* simulation is leading the transport in PD – *control* experiment by 2 months.

The transport correlations between the PD – *control* and LGM simulations in the main passages are illustrated in Figure 4-13. The seasonal cycle of the flow in Lombok Strait in the LGM simulation shows strong outflow from December to April, while the weak flow appears from August to October. Changes in seasonal cycle in the Lombok Strait correspond to the changes in Makassar Strait seasonality in the LGM simulation giving maximum of the outflow during NW monsoon phase. Variations of transport in Lombok Strait are stronger when LGM forcing is taken into account giving almost zero outflow into the Indian Ocean in August/September.

Ombai Strait seasonal cycle of volume transport shows high outflow values from July to November and weak transport from March to May. The timing of strongest and weakest outflow appears during the monsoon transitions and is therefore shifted compared to the PD – *control* experiment. Timor Strait seasonal cycle of the flow differs significantly between the PD – *control* and LGM run. In the LGM simulation, volume transport is increased during the SE monsoon phase from April to September and decreased during the NW monsoon phase from November to February. The change in the seasonal cycle in this case seems not to be related with the changes in topography since the seasonal variations in the PD – *control* and PD - 120 experiments are similar.

4.4.3 Makassar Strait

Mean flow within Makassar Strait in the LGM simulation is weaker then the PD – control experiment. The flow is strongest in the upper 200 m (Figure 4-14). Intensification of the surface flow can be associated with the topographic changes as shown in PD – 120 experiment. The vertical profile of the flow is similar to the PD – 120 experiment, though the intermediate flow is reduced (Figure 4-16). Geostrophic balance gives good estimate of the vertical profile of the flow suggesting that magnitude of the ITF transport in LGM can be reconstructed from the density field within Makassar Strait.

Mean SST in Makassar Strait in the LGM simulation is reduced by 2°C (Figure 4-15 left). The deep water temperatures are colder by ~3°C, while changes in the thermocline are small. Salinity values in Makassar Strait are higher by ~0.8 psu

throughout the water column (Figure 4-15 right). The low surface salinity values associated with the presence of the Java waters are absent in the LGM simulation.

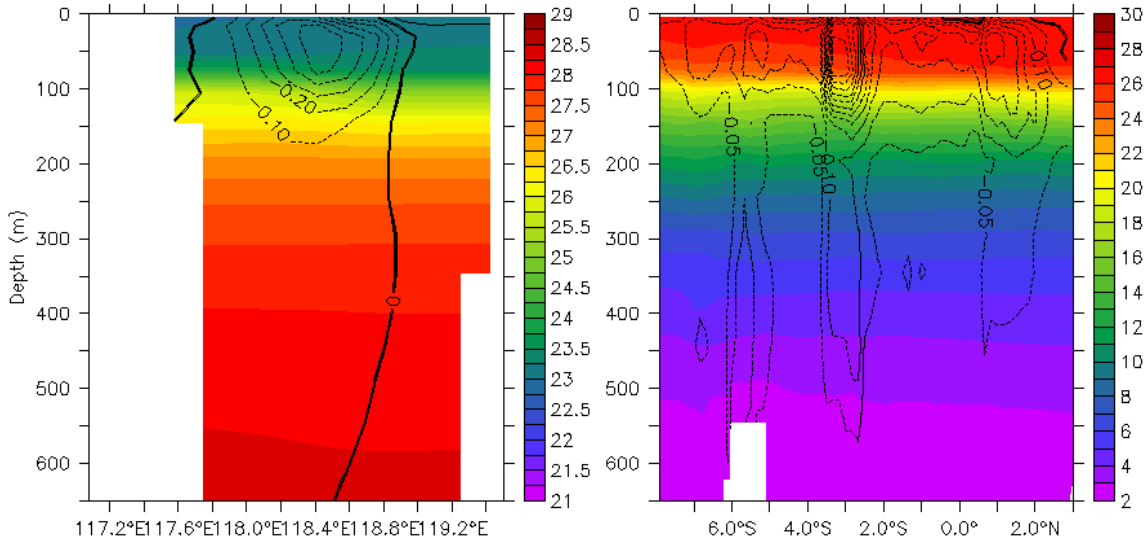

Figure 4-14 Makassar Strait mean density stratification (kgm-3) and velocity contours (ms-1) at 4°S (left) and zonally averaged temperature field (°C) with velocity contours (ms-1) in the LGM simulation.

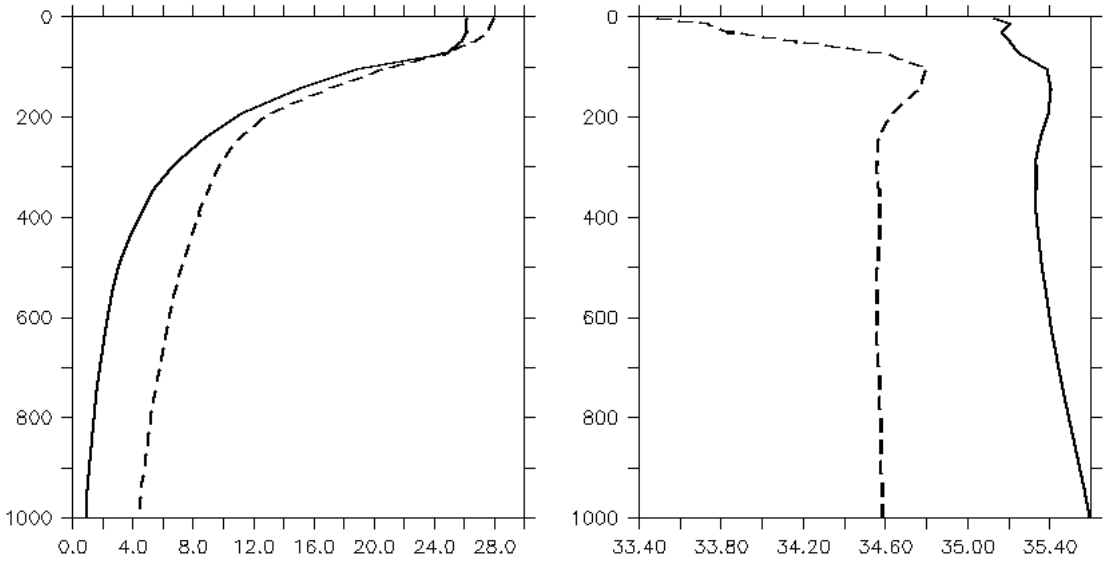

Figure 4-15 Makassar Strait temperature (°C) (left) and salinity (psu) (right) profile at 118.5°E, 4°S in LGM (thick) and PD - *control* (dash) simulations.

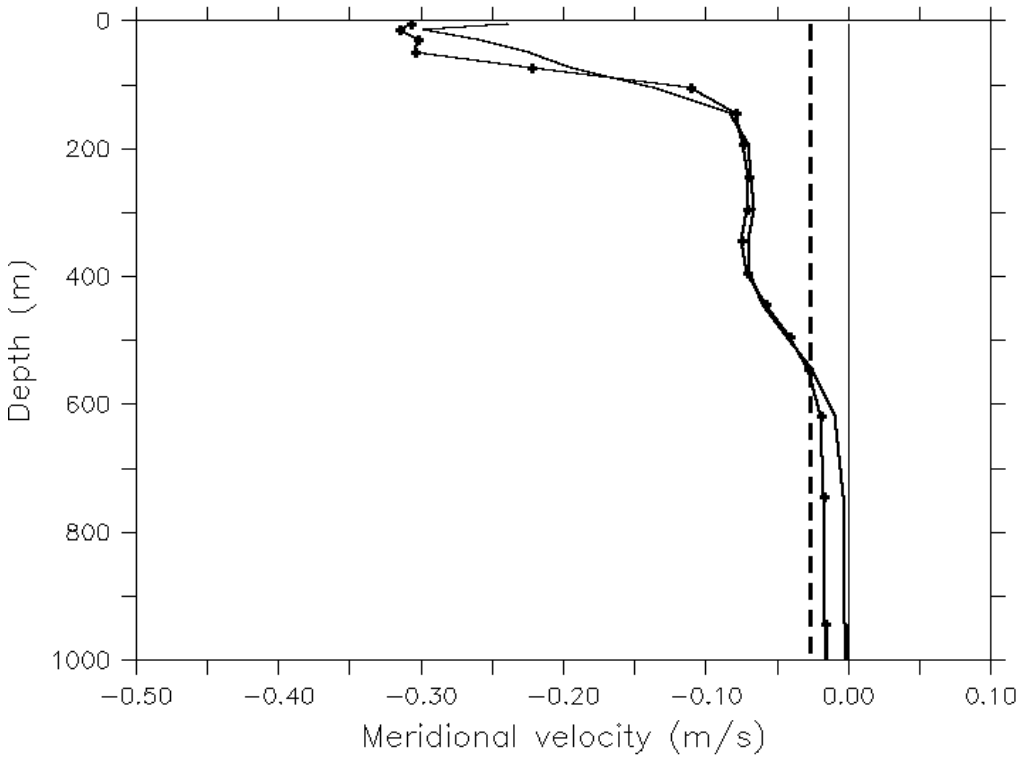

Figure 4-16 Geostrophic approximation of Makassar Strait velocity profile (dot solid line) in the LGM simulation compared to mean meridional velocity (ms^{-1}) (solid line) at 118.1°E, 4°S and its barotropic component (dash line). Negative values indicate southward velocities.

Density driven flow The density gradient between the West Pacific (WP) and East Indian Ocean (EIO) is analysed in the LGM simulation (Figure 4-17) and compared to the transport variations within Makassar Strait as in section 3.4.4.

The average steric height difference between WP and EIO is 11.6 ± 3.2 cm with reference level H=1000 m which is significantly higher than in the PD – *control* simulation (2.2 ± 1.6 cm). This would suggest increase in density driven transport in the LGM simulation. However, net transport simulated in the *LGM* experiment is reduced compared to PD – *control* run. The reduction in *LGM* experiment is related to barotropic flow as prescribed on the boundaries. Difference in density stratification in the LGM simulation might be result of reduced mixing of Pacific and Indian Ocean water masses which is consequence of reduced transport and topographic blocking. This result suggests that given theory of density forcing [*Andersson and Stigebrandt*, 2004] can not provide explanation for the reduced ITF magnitude at the LGM. Moreover it would lead to increase in LGM transport which is not expected.

Time correlation of steric height difference between WP and EIO variations and Makassar Strait volume transport in the LGM simulation shows lag of 1-2 months of the Makassar Strait transport (Figure 4-18), while in the PD simulation the variations were in phase. This result might be related to the different wind forcing used in the LGM simulation. If the *Wyrtki* [1987] hypothesis is considered, the variations of sea level difference between Pacific and Indian Ocean are governing the ITF variability. The steric height calculations include only density variations in sea surface height, but not the wind forced variations. Considerably different regional winds in the LGM simulation might change the expected signal in sea level.

The aim of this analysis was to examine proposed theory of the main forcing of the Throughflow during the glacial and to find possible analytical estimate of the ITF magnitude which could be used in past climate research. The PD estimates of the ITF magnitude using steric height difference are highly dependant on the region used in calculation. The model results show that the given theory of DBP drained by the sea level difference between Pacific and Indian Ocean [*Andersson and Stigebrandt*, 2004] could not be directly applied under glacial conditions. Despite its simplicity, this method seems unreliable to be used for estimating the Throughflow.

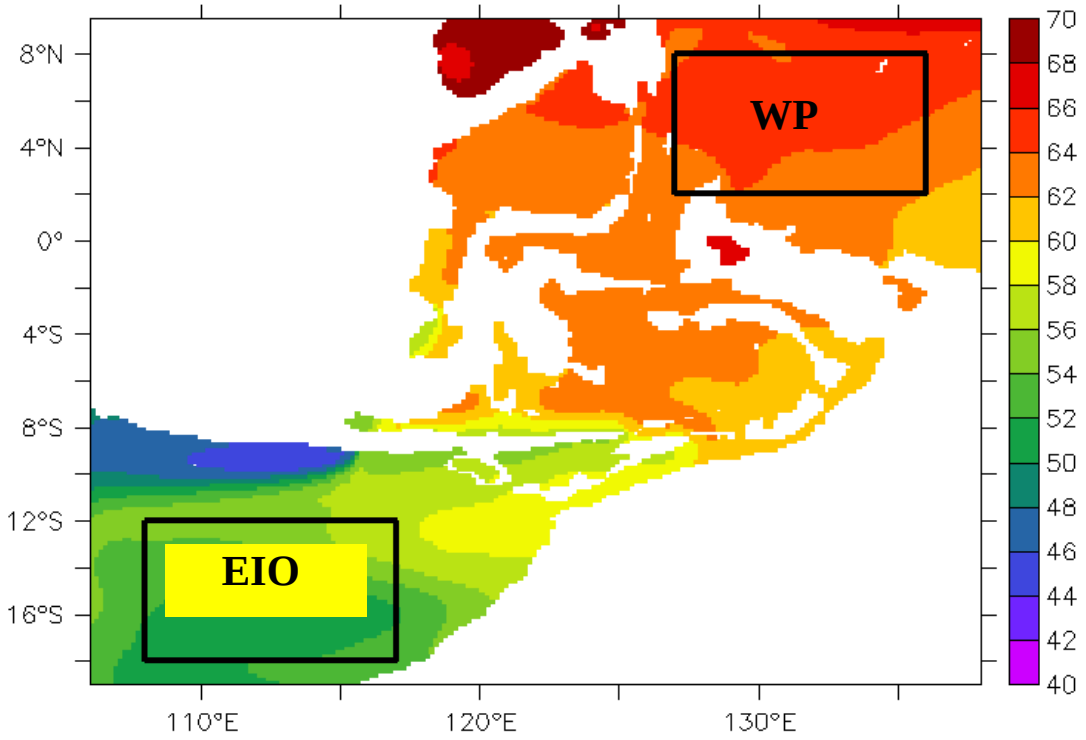

Figure 4-17 Mean LGM steric height (cm) reference to 1000 m with indicated areas (black boxes) used in calculation of pressure difference in the model.

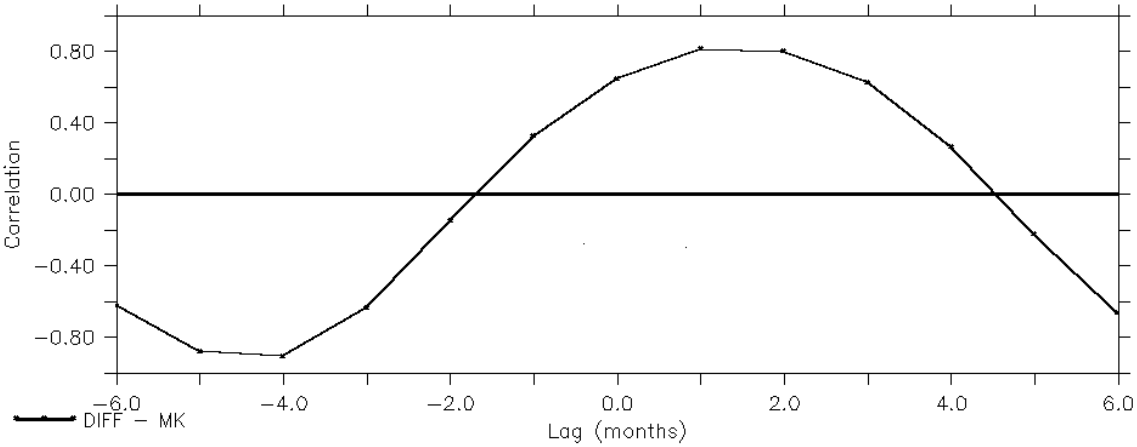

Figure 4-18 Lagged correlation of steric height difference between WP and EIO (DIFF) with Makassar Strait (MK) volume transport in LGM experiment. A positive correlation DIFF – MK at +1 month lag indicates that Makassar Strait transport lags DIFF by 1 month.

4.4.4 Lombok Strait

Changes in topography lead to decrease in flow through Lombok Strait by reducing the aperture of the passage as shown in the PD – *120* experiment (see section 4.3.1). The mean surface flow through Lombok Strait in the LGM simulation remains strong compared to the PD – *control* run. However, the flow is confined in the top 100 m (Figure 4-19) and below the sill depth the currents are decreased to almost zero.

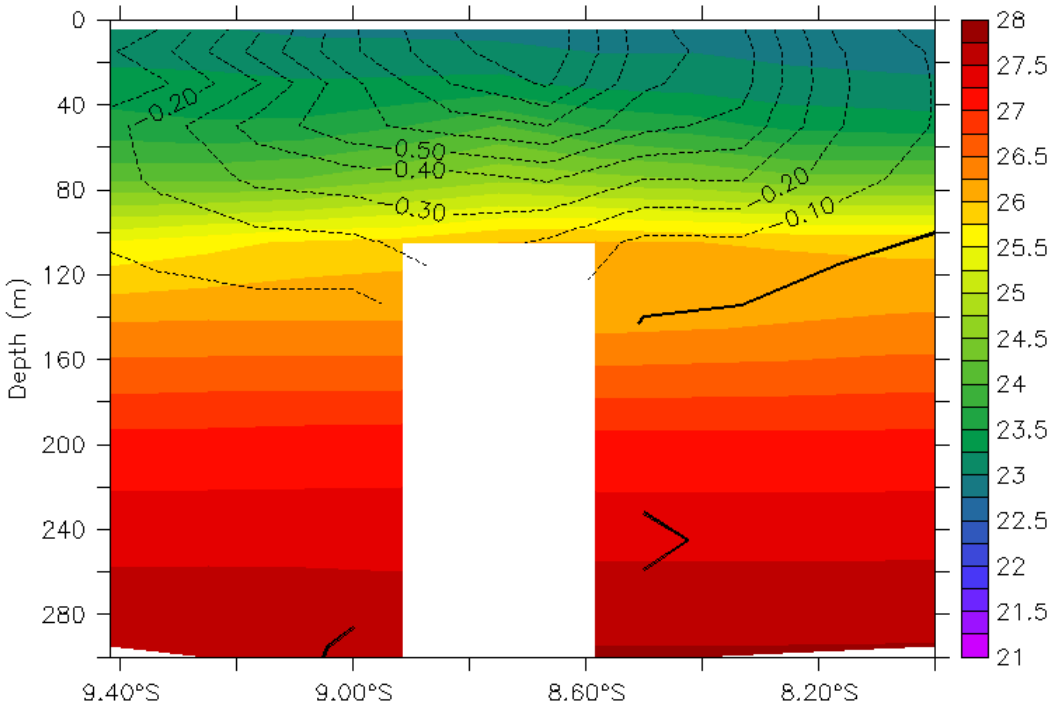

Figure 4-19 Lombok Strait along-channel mean annual density stratification (kgm^{-3}) and velocity field (ms^{-1}) at 115.7°E with negative values indicating flow towards the Indian Ocean.

Mean temperature profile in the Lombok Strait shows colder temperatures by ~ 2°C in the LGM simulation throughout the water column (Figure 4-20 left). Mean salinity values in Lombok Strait are higher by ~0.7 psu except for the surface salinity values which are increased by ~1.4 psu compared to the PD – *control* experiment (Figure 4-20 right). The observed low surface salinity values are associated with the strong river runoff in vicinity of Lombok Strait [*Sprintall et al.*, 2000]. River runoff is not included in the model and possible salinity minima at the LGM can not be excluded. Mean SSS increase in the Lombok Strait in the model is related to absence of low salinity Java waters and applied surface salinity restoring with higher values in the LGM simulation.

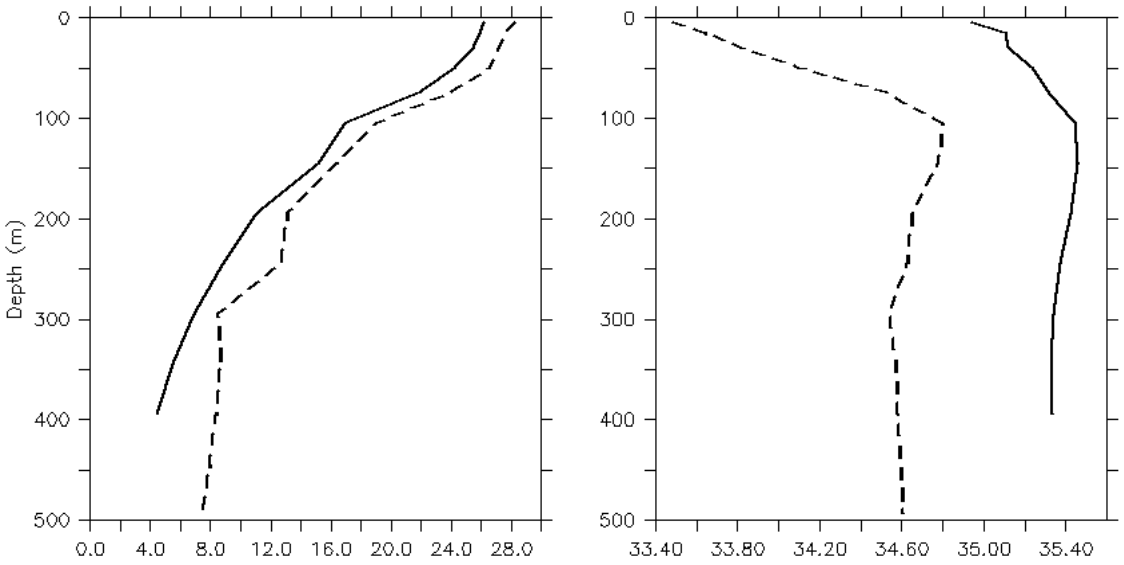

Figure 4-20 Lombok Strait temperature (°C) (left) and salinity (psu) (right) profile at 115.7°E, 9°S in LGM (thick) and PD - *control* (dash) simulations.

4.4.5 Ombai Strait

Mean flow through Ombai Strait in the LGM experiment shows reduced outflow towards the Indian Ocean compared to the PD - *control* run (Figure 4-21). The surface flow is intensified on the eastern side of the passage.

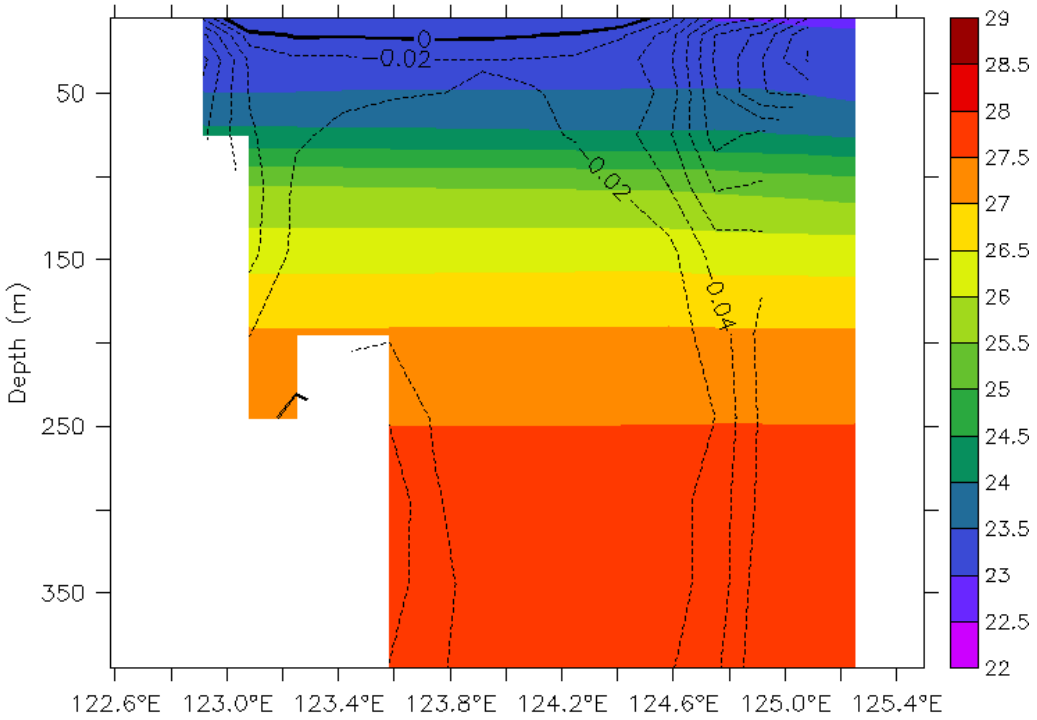

Figure 4-21 Ombai Strait cross section at 8.6°S with the mean annual density stratification (kgm^{-3}) and velocity field (ms^{-1}) in the LGM experiment. Negative values indicate flow towards Indian Ocean.

Temperature profile shows reduction in the SST by ~2°C and ~3°C colder temperatures in the deep part of the Strait in the LGM experiment (Figure 4-22).

Salinity values in Ombai Strait are increased by ~0.8 psu in the top layer, while even higher salinity anomaly (~1.2 psu) appears below 1200 m.

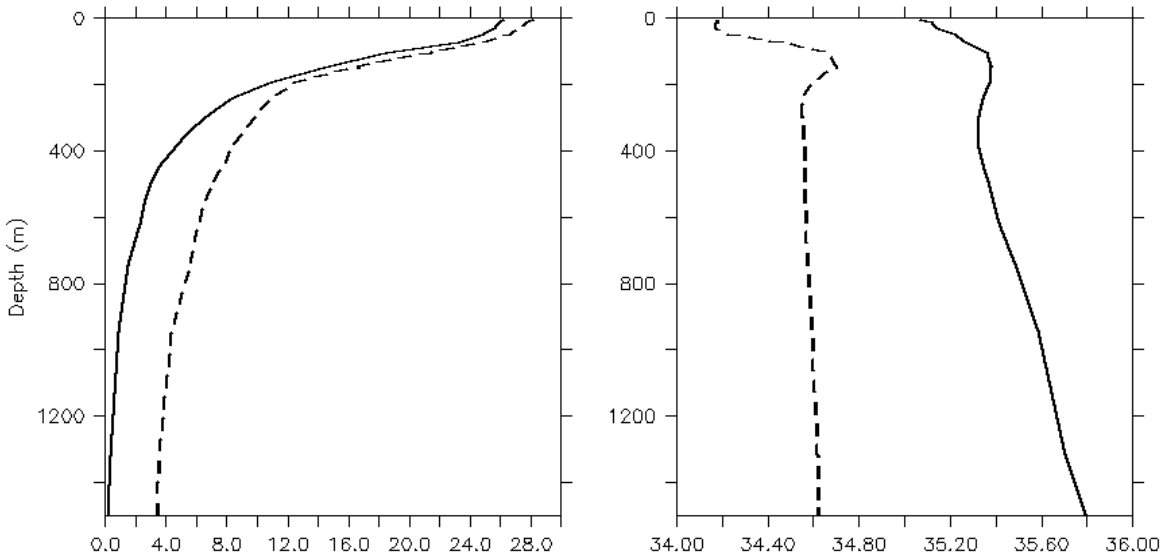

Figure 4-22 Ombai Strait temperature (°C) (left) and salinity (psu) (right) profile at 124.5°E, 8.6°S in LGM (thick) and PD - *control* (dash) simulations.

4.4.6 Timor Strait

Mean flow through the Timor Strait is significantly changed under glacial conditions. Shelf region and associated coastal currents are absent in the LGM simulation and the flow is confined in the central deep channel (Figure 4-23). The eastward current through the passage is intensified giving strong surface and intermediate water flow.

Temperature and salinity profiles are plotted for the location within the deep channel in Timor Strait (Figure 4-24). Comparison of simulated LGM temperature with PD – *control* run shows surface cooling of ~2°C and deep water cooling of almost 4°C. Thermocline levels show small difference in temperature stratification. Salinity values are higher between 0.9 at the surface to 1.2 psu at the deep levels.

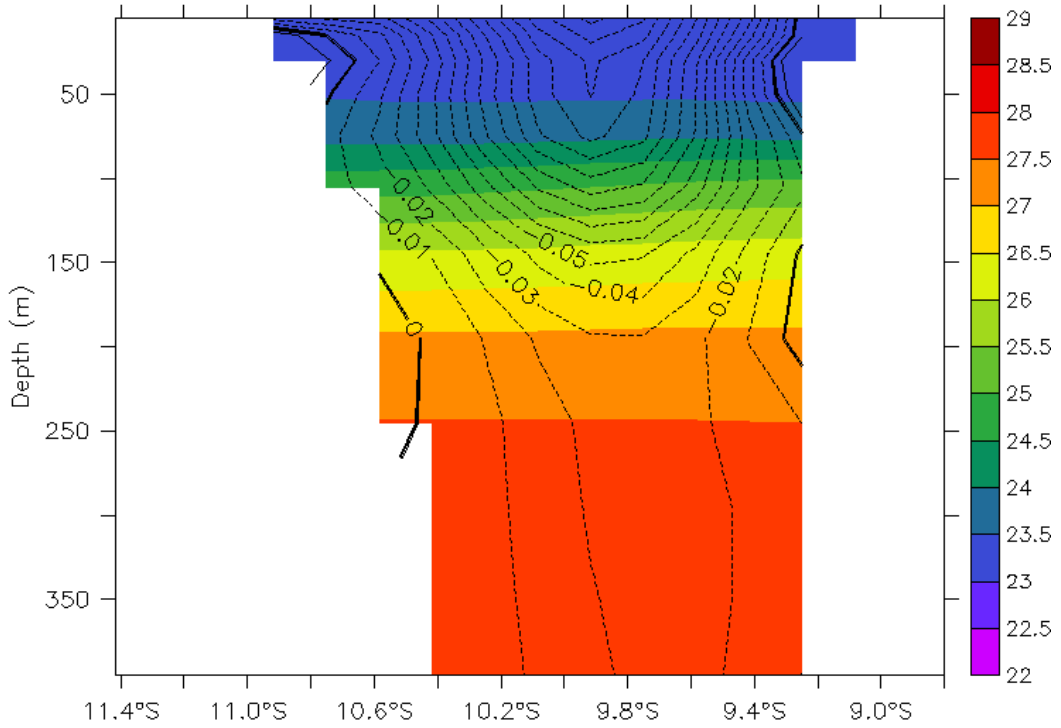

Figure 4-23 Timor Strait mean density field (kgm^{-3}) at 126°E and velocity contours (ms^{-1}) in the LGM simulation. Negative values indicate flow towards Indian Ocean.

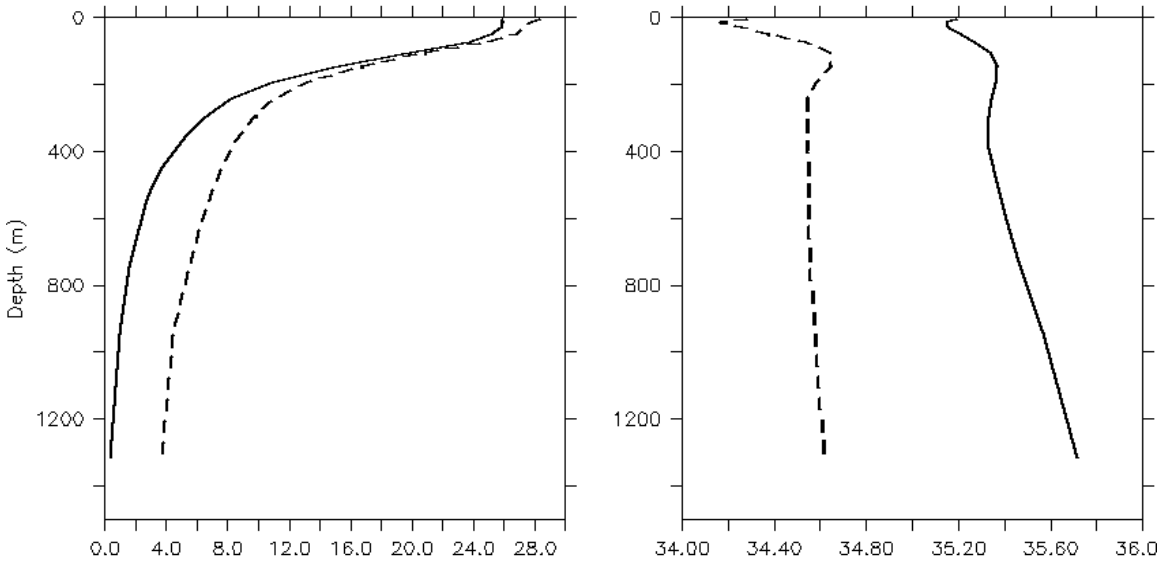

Figure 4-24 Timor Strait temperature (°C) (left) and salinity (psu) (right) profile at 125°E, 10°S in LGM (thick) and PD - *control* (dash) simulations.

In order to give general illustration of the changes in ITF hydrography and velocity structure in glacial simulation, TOS transect in Indian Ocean is analysed including both eastern exit passages. The position of transect is chosen for future detailed comparison of model results with paleoceanographic data.

The flow at the TOS transect in the LGM experiment shows main outflow in the top 200 m (Figure 4-25). The flow is intensified at the northern part of the transect.

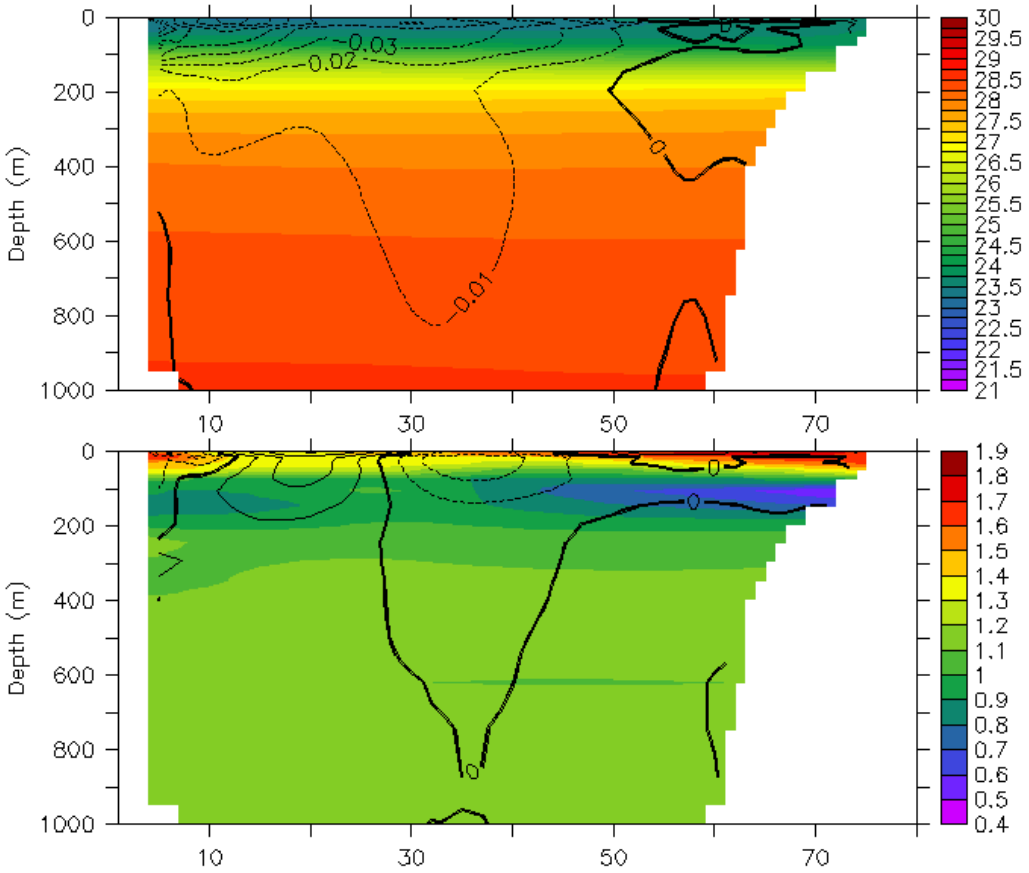

Figure 4-25 Density stratification (kgm^{-3}) and velocity contours (ms^{-1}) on the TOS transect in the LGM simulation (top) and difference between LGM and PD simulation (bottom). Negative values indicate flow towards the Indian Ocean. Values on the x axis indicate distance in 13.5 km from the Java coast

Comparison of the temperature field in the upper 200 m between LGM and PD – *control* experiment at the TOS transect (Figure 4-26) shows cooling in the surface levels by 2-3°C. Weaker cooling of ~ 1°C appears in the subsurface levels at 80 – 150m. Low salinity values in the LGM experiment are found at the TOS transect in the upper 100 m. However, salinity anomaly in the glacial experiment is strongest at the surface (~1 psu) while at 100 m depth salinity change is ~0.6 psu. Salinity maximum of 35.5 psu is found at 120 – 200 m depth.

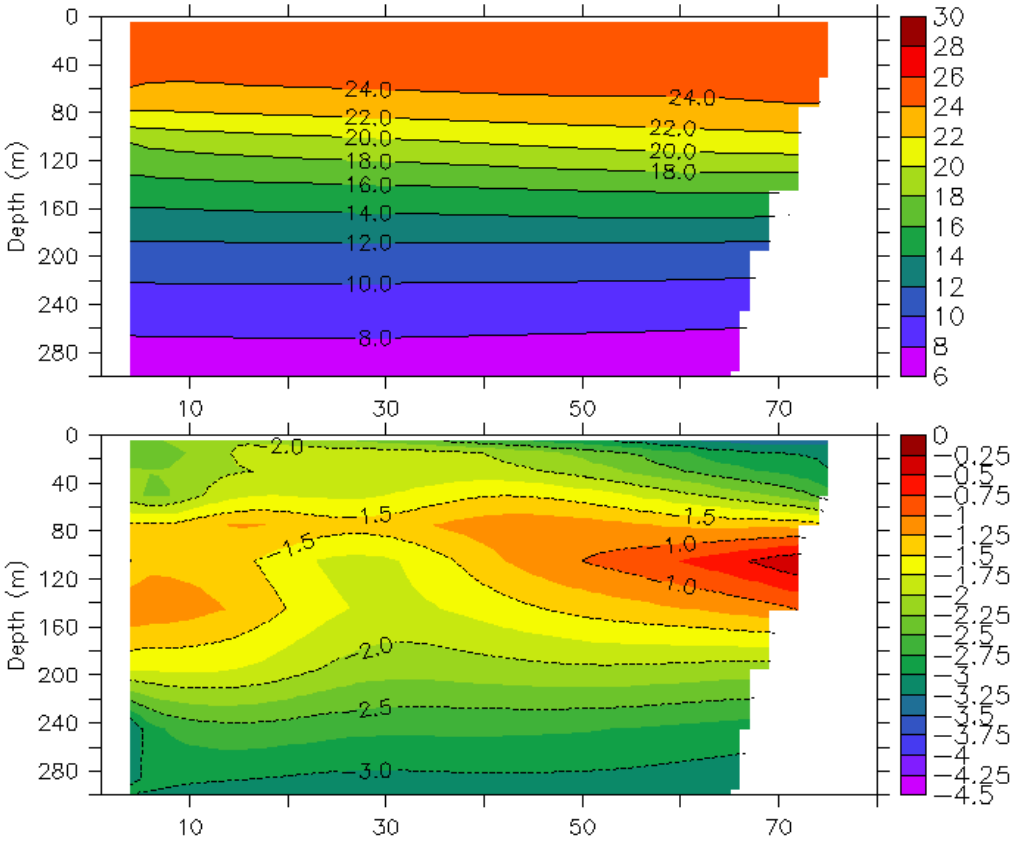

Figure 4-26 Upper 300 m temperature (°C) field at the TOS section in the LGM simulation (left) and temperature anomaly between the LGM and PD - control experiment (right).

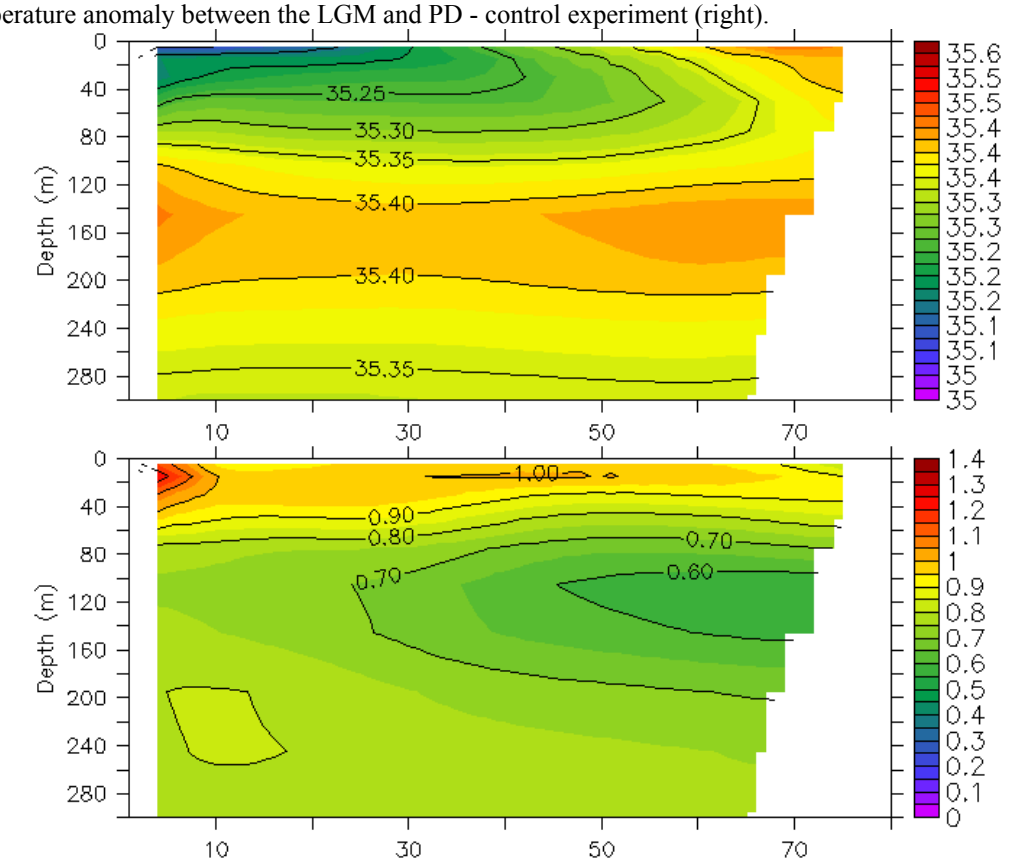

Figure 4-27 Salinity field (psu) in upper 300 m at the TOS section in the LGM simulation (left) and salinity anomaly between the LGM and PD - *control* experiment (right).

4.5 Sensitivity to glacial boundary conditions

4.5.1 LGM wind stress

The model developed LGM circulation shows higher amplitudes in transport within Makassar Strait and exit passages than in the PD – *control* experiment. The seasonal cycle of the volume transport is shifted compared to the PD - *control* and PD – *120* simulations. All these effects may be related to the changes in the wind forcing. To analysed relative importance of the choice of wind stress forcing to the glacial ITF, LGM and LGM – *ECHAM3* experiments are compared.

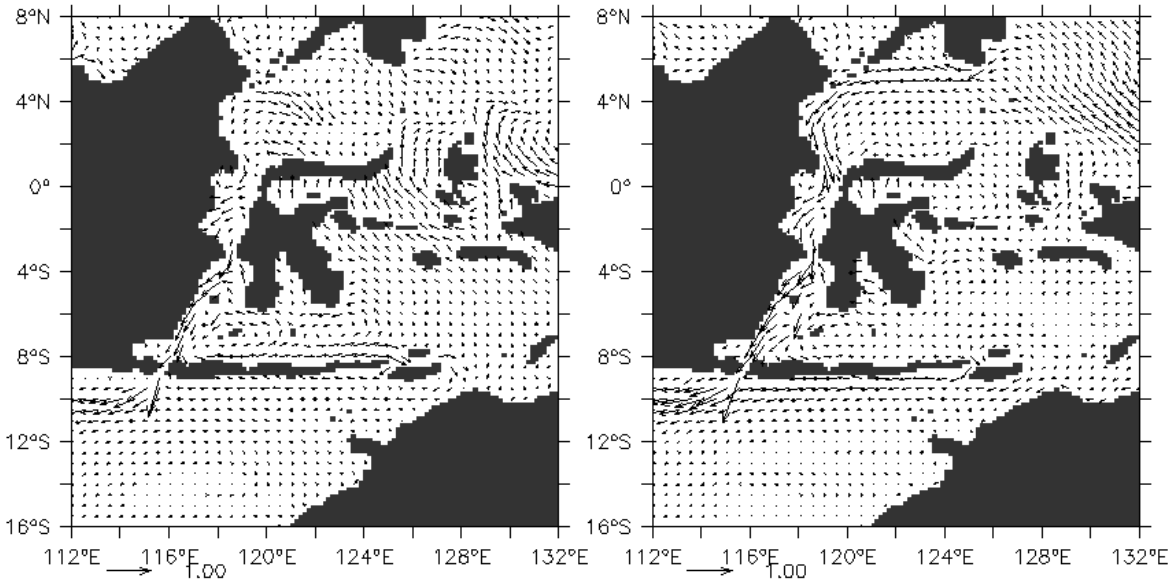

Figure 4-28 Mean surface circulation (ms^{-1}) in LGM (left) and LGM – *ECHAM3* simulation (right).

Mean surface circulation differs between the LGM and LGM – *ECHAM3* experiment (Figure 4-28). The northward flow across the equator is absent in the LGM – *ECHAM3* simulation, confirming that the currents are indeed associated with the applied glacial wind forcing and that this result should be taken with caution if the local glacial wind field is not well known. The coastal current in the Celebes Sea is developed in the LGM – *ECHAM3* simulation and southward flow through Makassar Strait is intensified compared to the LGM experiment.

The seasonal cycle of the volume transport in Makassar Strait shows difference between the two simulations with different glacial wind forcing (Figure 4-29). The strongest flow appears from September – November in the LGM experiment, while the high transport values appear from January – March in LGM – *ECHAM3* simulation. The amplitude of the volume transport in Makassar Strait is increased in LGM – *ECHAM3* simulation compared to both PD – *control* and LGM experiments. The increase in amplitude in volume transport in Makassar Strait might be related to the stronger along- channel wind field forcing used in the LGM – *ECHAM3* simulation.

However, the volume transport through eastern passages does not show large differences between the LGM and LGM – *ECHAM3* simulation. Even though the timing of maximum of transport is shifted from October in LGM experiment to November in LGM – *ECHAM3* simulation, the main seasonal variability is preserved and the amplitude is similar in both glacial wind experiments.

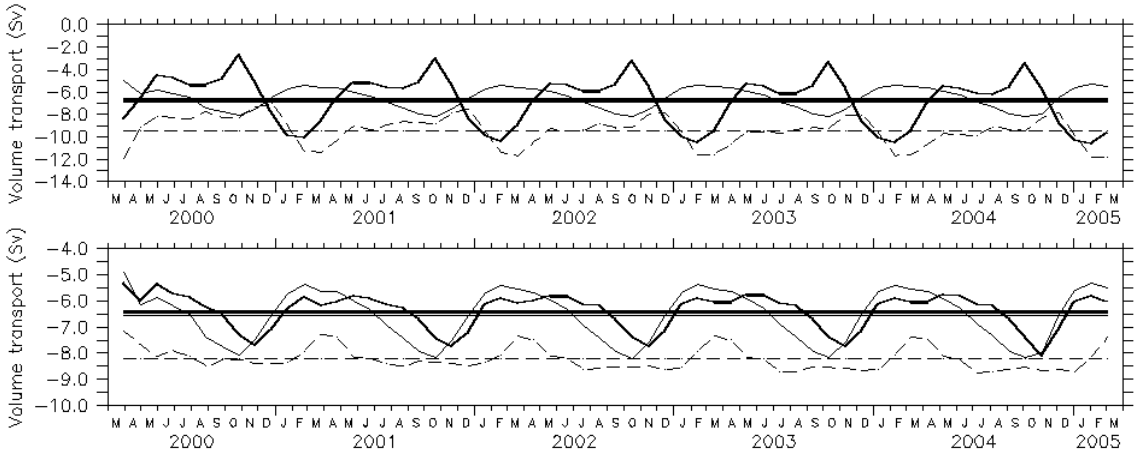

Figure 4-29 Time-series of the volume transport in Makassar Strait (up) and TOS (down) in LGM – *ECHAM3* (thick), LGM (thin) and PD – *control* experiment (dash).

The results suggest that the applied glacial wind forcing might have strong impact on the surface circulation and seasonal changes in the ITF region. Additional factor is the difference in global model estimates of the strength of the glacial wind field that can lead to large differences in amplitude of the ITF. Moreover, response of the transport variability to the glacial wind forcing differs between Makassar Strait and exit passages and should be considered separately. Without further constraints on the glacial wind field, the results of the LGM variability in the ITF should be taken with caution.

4.5.2 LGM surface forcing

The ITF heat transport is reduced in the LGM experiment compared to the PD – *control* and PD – *120* simulations, even though the glacial results suggest intensified surface flow. One of the possible causes may be found in the cooling of the SST at the LGM that could lead to decrease in heat transport. In order to estimate relative impact of the surface boundary conditions to the ITF heat transport, sensitivity experiment with different surface boundary forcing (LGM – *NCAR*) is compared to the LGM experiment.

Model developed temperature field at 30 m depth in the LGM – *NCAR* experiment shows generally colder temperatures by 1 - 2°C in the Indonesian Seas (Figure 4-30). In both LGM and LGM – *NCAR* experiment the ITF heat transport is reduced compared to the PD simulations. The estimate of Makassar Strait heat transport in two different representations of surface boundary conditions differs by 0.02 PW. This is considerably smaller than the difference between the PD and LGM experiment where the reduction in the heat transport is approximately 0.1 – 0.2 PW. The representation of the sea surface boundary conditions plays a secondary role in control of the ITF heat transport.

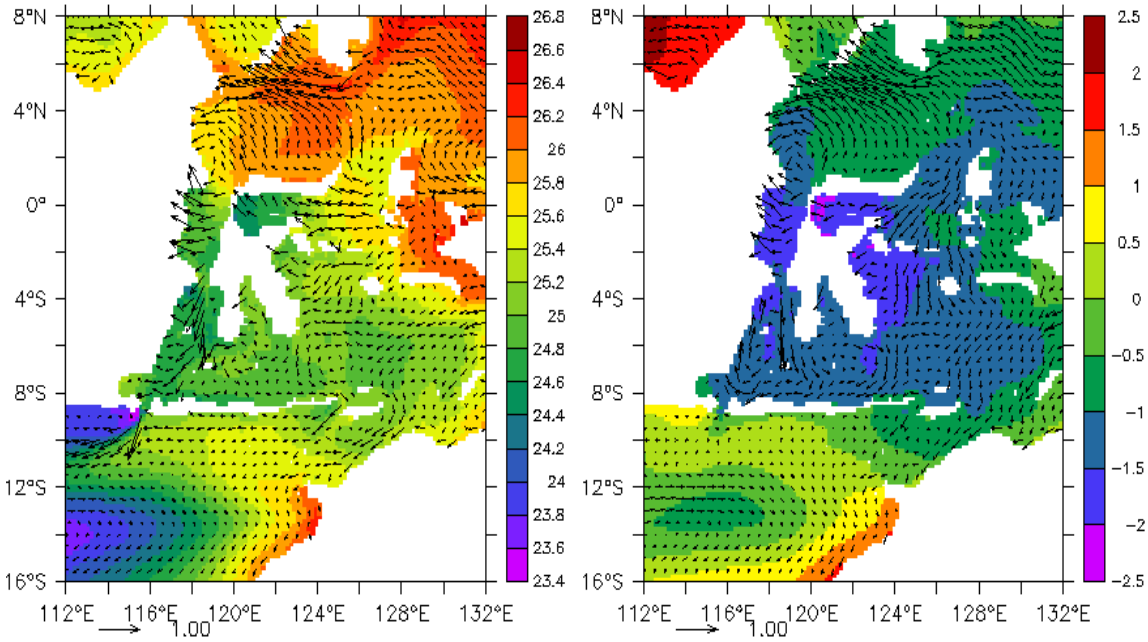

Figure 4-30 Mean surface circulation (ms^{-1}) and temperature at 30 m depth (°C) in LGM - *NCAR* experiment (left) and difference in circulation between LGM – *NCAR* and LGM simulation (right).

4.5.3 LGM lateral boundary conditions

The total ITF volume transport in the previous LGM experiments is held constant at the lateral boundaries. The sensitivity experiment (LGM – *cyclic)* is performed where the glacial boundary transport is interpolated from the monthly climatology of the LGM experiment of *Paul and Schäfer-Neth* [2003]. In this way, possible changes in the vertical structure of the current system during the LGM at the boundaries are taken into account and the transport is allowed to vary on the monthly time-scale.

With variable total transport at the lateral boundaries, Makassar Strait volume transport is reduced by ~1 Sv compared to the LGM experiment. Seasonal cycle of the volume transport is similar to the LGM simulation (Figure 4-31). Strong transport appears during the NW monsoon phase from November to April. Weak flow appears from July to October even if the boundary transport gives maximum of the flow from July to September (Figure 2-10).

Seasonal cycle of the volume transport at the eastern exit passages shows shift when variability in boundary transport is taken into account. Timing of the maximum of transport is in October in LGM experiment, while maximum of transport appears in August – September in LGM – *cyclic* experiment.

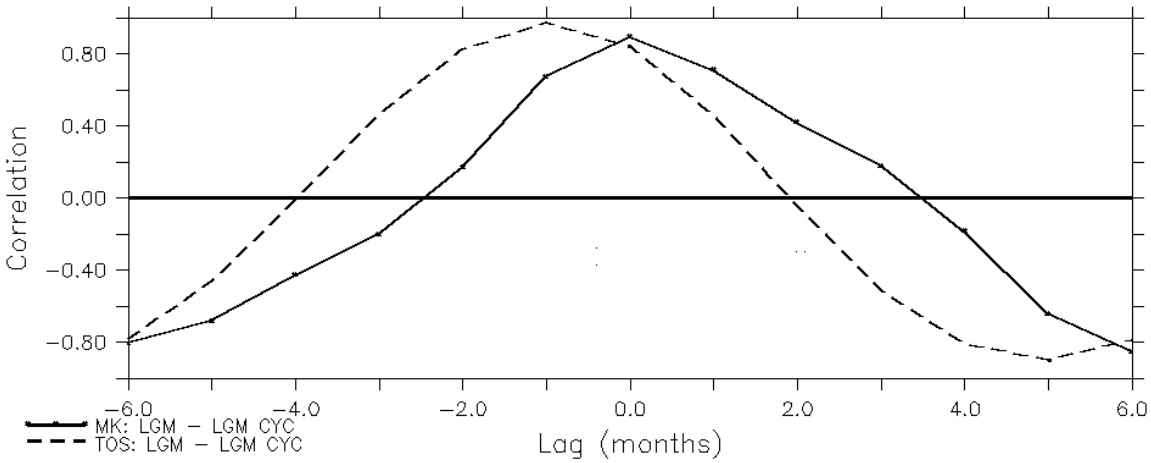

Figure 4-31 Correlation of the volume transport in the Makassar Strait and at the TOS transect between LGM and LGM – *cyclic* experiments. A positive correlation for TOS at -1 month lag indicates that volume transport at TOS transect in *LGM* simulation is lagging the transport in LGM – *cyclic* experiment by 1 month.

In all LGM simulations Makassar Strait heat transport is reduced compared to the PD. The heat transport is primarily dependent on the volume transport prescribed at the boundary and scales linearly even if the topographic changes are taken into account. Therefore, a reliable estimate of the total ITF volume transport at the LGM is necessary to calculate changes in the heat transport. In Figure 4-32 are given estimates of the heat transport within Makassar Strait for various representation of boundary conditions. The relative change between the PD and LGM simulation always shows reduction in the heat transport and the boundary forcing plays a secondary role.

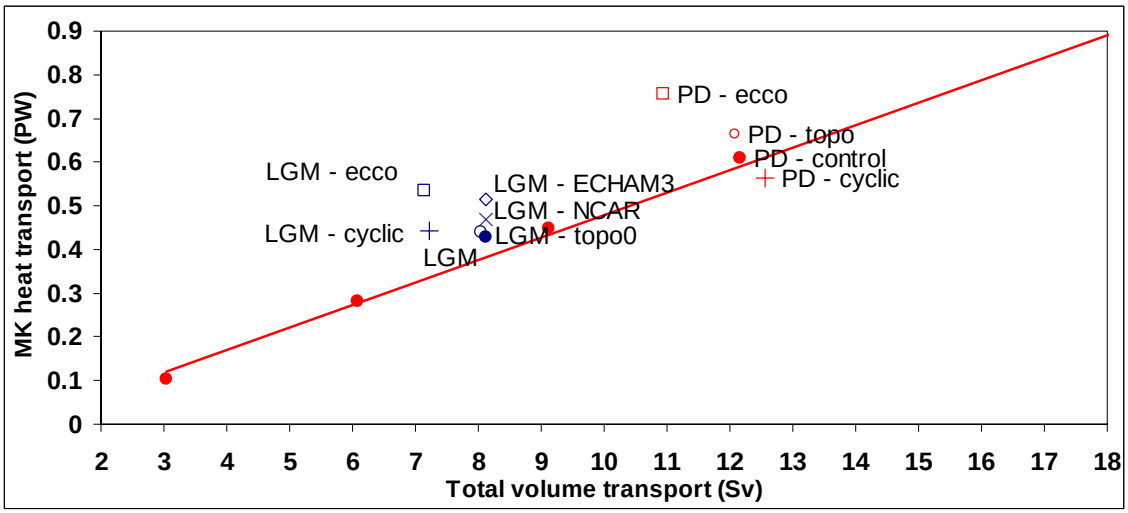

Figure 4-32 Response of the heat transport relative to 0°C within Makassar Strait (MK) to the prescribed volume transport at the lateral boundaries for LGM (blue symbols) and PD (red symbols) simulations. Linear trend line is calculated for PD - *control* experiments with scaling of boundary transport.

4.6 Conclusions

Impact of topographic changes during the LGM on the ITF heat and volume transport is investigated in the regional model. The model results show that the glacial sea level lowering alone does not seem to reduce volume transport within Makassar Strait. With the sea level lowered by 120 m, the flow through narrow, but deep channel in central Makassar Strait is intensified and net volume transport is similar as in the PD – *control* simulation. However, lowering of the sea level results in changes in vertical profile of the flow. Due to the shallowing of the sill in southern Makassar Strait, the flow in LGM simulation is more surface intensified which leads to an increase in heat transport towards the Indian Ocean. Even small changes in ITF vertical profile might have impact on the Indian Ocean heat balance [*Song and Gordon*, 2004]. However, this effect is small (~0.05 PW) compared to the experiment when glacial boundary conditions are applied and the heat transport within Makassar Strait is reduced by 0.18 PW. The glacial boundary conditions include cooling which can be one of the factors in decreasing the heat transport. A comparison of sensitivity experiments with surface forcing taken from different global LGM simulations [*Paul and Schäfer-Neth*, 2003; *Shin et al.,* 2003] gives small difference in heat transport (0.02 PW) suggesting that representation of boundary forcing plays a secondary role in controlling the heat transport. The primary factor determining the reduction of heat transport is the total ITF volume transport prescribed on the boundaries. The reduction of volume transport of about 1/3 of the PD value in the glacial boundary conditions is an estimate taken from global LGM model simulation [*Paul and Schäfer-Neth*, 2003] and does not seem to be related to local ocean dynamics. The steric sea level difference between the Pacific and Indian Ocean does not seem to be sufficient to explain changes in the volume transport. Moreover, the density difference between the Pacific and Indian Ocean is higher in the LGM simulation. The analytical model of the wind forced circulation around the island [*Godfrey*, 1989] could not be tested in the regional model due to the limited domain. What sets the net reduction in transport during the LGM still remains unclear.

The sea level changes have significant impact on seasonal variations of the surface flow in Makassar Strait resulting in reversed seasonal cycle compared to the PD monsoonal circulation. During NW monsoon the flow is intensified since the blocking of the surface flow by low salinity Java Sea waters in southern Makassar Strait is absent. During SE monsoon the flow is decreased due to accumulation of Banda Sea waters in southern Makassar Strait. The reversal of seasonal cycle is related to the topographic changes only, but could be further modulated with the local wind forcing during the LGM. Applied glacial wind forcing in the model suggests higher amplitudes in seasonal variations during the LGM. However, with large uncertainties in global model estimates of the strength of glacial wind field this result should be taken with caution. The dynamical aspects of the impact of changes in seasonal cycle within Makassar Strait on the climate system are not known. However, this mechanism should be taken into consideration when the local paleoclimatic evidence for the LGM is analysed.

5. Particle distribution patterns

5.1 Introduction

Marine biota and geochemical/sedimentological tracers are one of the primary sources of data for understanding past climate changes. Reconstructions of changes in ocean circulation and water masses properties largely depend on assumptions of particles distribution in the ocean. Beside ocean dynamics, numerous factors influence particle composition in the ocean such as terrestrial input, hydrological, chemical and sedimentation processes, as well as biological factors when marine organisms are used as a proxy. For a qualitative analysis of water samples or sediment core records, variety of different agents working together need to be taken into account and very often, the resulting signal is difficult to interpret. In this study, a regional OGCM with Lagrangian particle-tracing module is employed to simulate dispersal of particles within the Indonesian Gateways. The focus of the study is on the particles origins, pathways, residential time and velocity of propagation within the Indonesian Seas. The simulated particle trajectories are associated with ocean circulation only and can be therefore isolated from other factors.

One of the proxy for assessing past changes in the intensity of the ITF on glacial-interglacial time-scales are clay minerals eroded from the soil by rivers and wind action and entrained in the water masses circulating in the region [*Gingele et al.*, 2001a,b]. Transport of clay minerals mainly by surface and subsurface ocean currents can be observed by the patterns on the sea floor and give clues on the extent and propagation of the water masses. Clay mineral assemblages in sediment cores are closely related to the geology and weathering regime in the region and are therefore not only a proxy for the past changes in intensity of the ocean currents, but also for the nature of paleoclimatic processes of the adjacent land masses. For example, kaolinite and chlorite are entrained in the low salinity ITF waters on its way through the Indonesian Gateways and are transported into the Timor Passage, while local input in Timor Strait is characterized by illite. Reduction in kaolinite and chlorite reaching Timor Passage during the LGM may indicate reduced volume transport of the ITF, but also a reduction in the input of chlorite due to the drier conditions on land. Both ocean currents and weathering regime in the Indonesian Gateways are under influence of monsoonal wind variations (Figure 5-1). Changes in monsoonal wind forcing during the LGM as well as different land-sea distribution might result in different dispersal patterns during the glacial periods.

The analysis of particle trajectories by a regional ocean model can be helpful in several ways to interpret the paleoclimatic records. First of all, the impact of ocean dynamics on the particle dispersal can be isolated from other factors. For example, changes in the land-sea distribution, river runoff, local hydrological cycle and winds might influence the terrestrial input of particles in the ocean. The changes in terrestrial input at the LGM are not included in the regional model. However, impact of glacial climate conditions on ocean currents is taken into account giving a possibility to separate and quantify the ocean influence on particle distribution during the LGM.

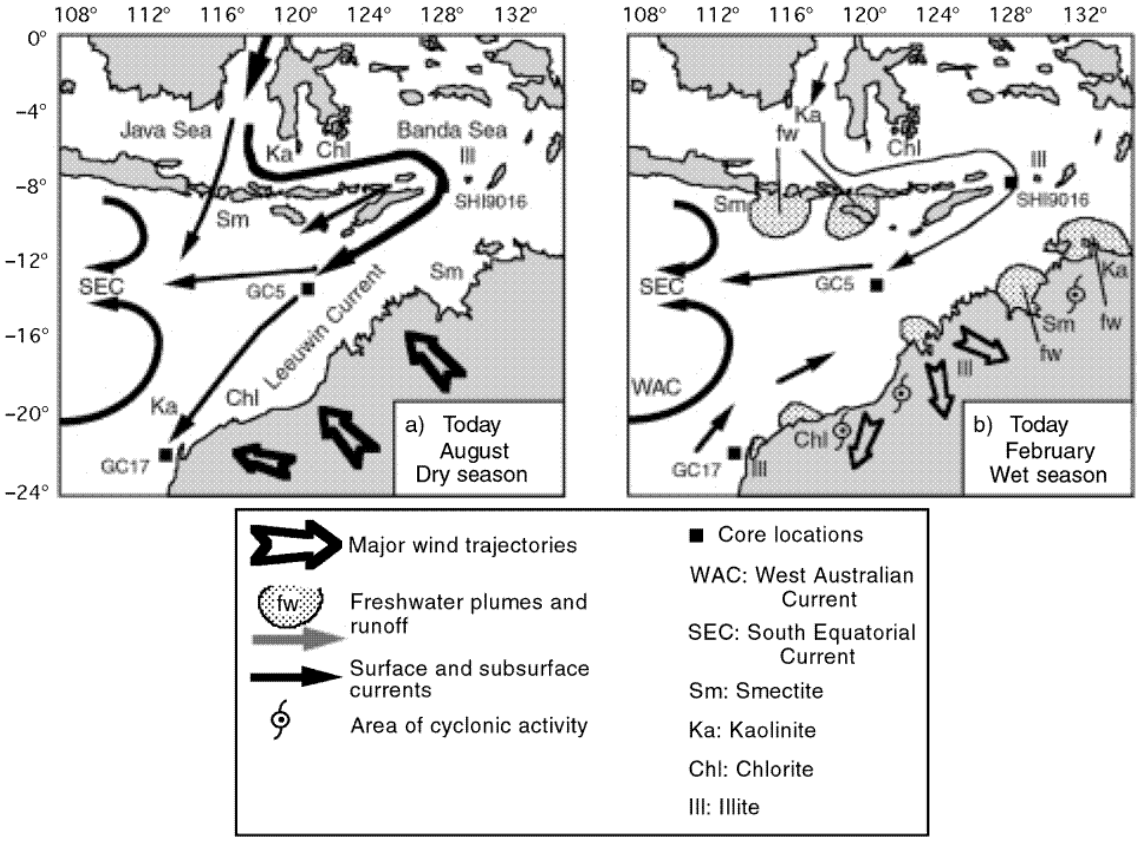

Figure 5-1 Present-day clay mineral sources and distribution within the Indonesian Gateways for SE monsoon phase (left) and NW monsoon phase (right). From *Gingele et al.* [2001].

For the reconstructions of global climate changes such as global ice sheet growth, basin scale changes in SST and SSS by analysing isotopic composition of the foraminifera, it is very important to distinguish between the local climatic influences and the global signal. Therefore, the sampling sites need to be carefully chosen. High-resolution OGCM experiments give main pathways of the particles showing the regions where the mean local dynamics in the ocean can be tracked. The particle distribution in the model gives information of spreading of the marine biota or tracers of different water masses within the region. This can help in the future to avoid sampling sites with high local impact or give hint for a possible good sampling site.

Sedimentation processes such as changes in accumulation rates related to grain size, bottom velocity and friction are not included in the model. However, established mean ocean circulation within the Indonesian Seas for modern and glacial conditions might be in the future used as a base for detailed sediment modelling in the possible regions of interest.

In order to help interpret continuous sediment records from the region, sensitivity experiments are designed to determine the influence of gradual topographic changes on glacial-interglacial time-scales on the particle distribution within the Indonesian Gateways. Based on the downcore records from the Sunda Shelf [*Geyh et al.*, 1979; *Hesp et al.*, 1998; *Hanebuth et al.*, 2000; *Hanebuth and Stattegger*, 2003; *Steinke et al.*, 2003], the sea level curve is derived indicating several distinct phases in sea level rise from the LGM to present-day (Figure 5-2). However, it needs to be noted that the recent revision of the sea level during the peak glacial results in a somewhat higher estimate of the sea level lowering (about 127 m compared to 120 m shown in the figure) and even an larger value of 136 m was considered [*Yokohama et al.*, 2000]. Moderate

increase in sea level is found since the last glaciation up to 16.5–14.5 ky ago followed by accelerated sea level rise associated with the flooding at 14.5–14 ky ago. From 14–8.5 ky ago sea level gradually increased reaching modern coastline position at 8.5–6 ky ago.

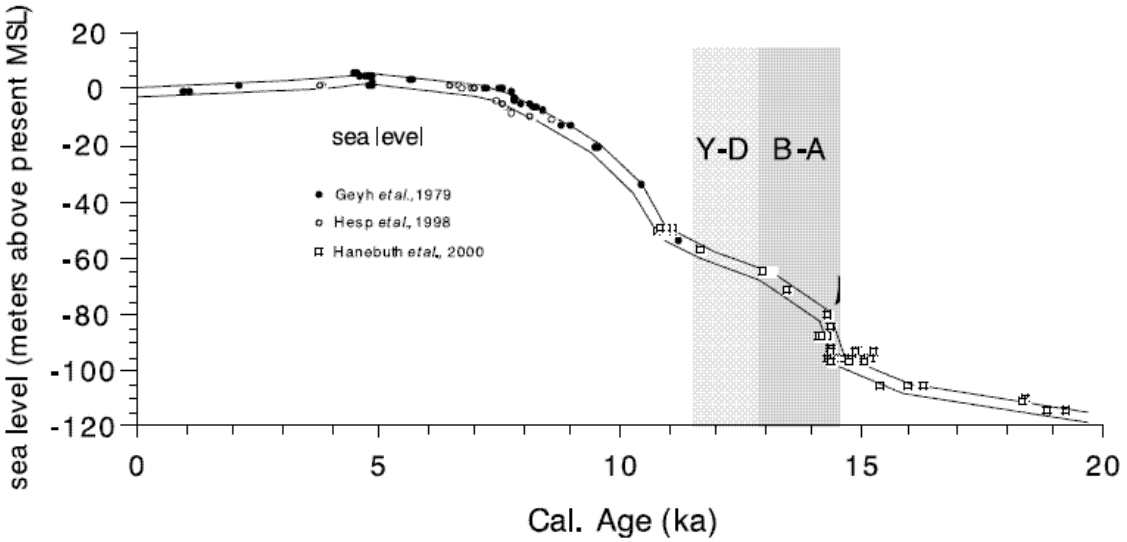

Figure 5-2 Estimated sea-level curve for the Sunda Shelf region compiled from *Geyh et al.* [1979], *Hesp et al.* [1998] and *Hanebuth et al.* [2000]. Shaded bars indicate the Younger Dryas (Y-D) and Bølling/Allerød (B-A) intervals (ages adopted from *Stuiver et al.* [1995]). From *Steinke et al.* [2003].

For this purpose, the high-resolution model simulates particle trajectories including 120 m sea level lowering corresponding to the LGM, 70 m sea level change associated with transition between Bølling – Allerød (BA) interval and Younger Dryas (YD) at 12.8 - 13.5 ky ago and 30 m sea level lowering as transition step to the Holocene and PD value. Unfortunately, boundary conditions for the transition periods are not well known and the model is in these cases forced by PD climate conditions. However, glacial particle trajectories are additionally simulated including both topographic changes and LGM climate conditions. Several seeding areas are used to characterize propagation of different water masses through the Indonesian Gateways. The trajectories are analysed for surface, subsurface, intermediate and deep drifters. Various timings of release are tested in order to capture seasonal variations in the circulation.

5.2 Experimental setup

General description of the Lagrangian particle-tracing module is given in section 2.4, while model configuration and boundary conditions for PD - *control* and LGM experiments are described in section 2.3.

The particles are released in four seeding areas (Table 5-1). The Celebes Sea (CS) for testing the dispersal inside the Indonesian Gateways, Mindanao Sea as representative for North Pacific (NP) source water, New Guinea area for the South Pacific (SP) source water and eastern Indian Ocean (IO). The floats are released at surface (5 m), subsurface (105 m), intermediate (395 m) and deep level (945 m) with at least 500 floats per level. Even though no biota are found at the deeper levels (395 m, 945 m), the trajectories of deep floats are simulated to illustrate pathways and spreading of the intermediate and deep water masses. For example, possible increase in number of SP intermediate and deep drifters spread into the Indonesian Seas may indicate higher contribution of the SP source to the ITF.

Table 5-1 Setup of Lagrangian drifters.

Seeding area	Release location	Depth level (m)	Number of floats per level
Indian Ocean (IO)	111°E – 115°E 16°S – 12°S	5	775
Celebes Sea (CS)	119.5°E – 124.5°E 1.5°N – 4.5°N	5, 105, 395	589
North Pacific (NP)	127°E – 130.2°E 4°N – 8°N	5, 105, 395, 945	500
South Pacific (SP)	134.9°E – 138°E 0°N – 4°N	5, 105, 395, 945	500

Sensitivity experiments are designed to test impact of the topographic changes on particle trajectories, seasonal variations in particle dispersal and influence of glacial climate conditions. In the experiment FLT – *control*, particle distribution is analysed for the modern climate conditions using different seeding areas and timing of release (Table 5-2). Simulated particles trajectories are compared to the observed seasonal patterns of the Indian Ocean surface drifters [*Michida and Yoritaka*, 1996]. For testing the particle pathways inside the Indonesian Gateways and in the Indian Ocean, PD – *control* configuration of the model is used. PD – *ecco* configuration (section 3.2) is used for testing particle trajectories originating in Pacific since the equatorial currents seem to be better represented when the lateral velocities are taken from a higher resolution model [MITgcm ECCO project, *Stammer et al.*, 2003] (for results see section 3.6.3).

Impact of topographic changes is tested in FLT – *120* experiments where modern boundary conditions are used and the sea level is lowered by 30 m, 70 m and 120 m. In the FLT – *seasonal* experiments, monsoonal patterns in surface particle distribution are simulated under PD and LGM boundary conditions with additional experiment PD – *120* using PD climate conditions and glacial topography. To capture seasonal variations in surface particle dispersal, the floats are released every 2 months in the CS and the exchange of particles through the Makassar Strait is investigated. Glacial particle trajectories are further analysed in the FLT – *LGM* experiments taking into account different seeding areas, depth and timing of release.

Table 5-2 Float experiments overview.

Experiment	Experiment configuration	Release location	Timing of release
FLT – *control*	PD – *control*	IO, CS	May, November
	PD – *ecco*	NP, SP	March
FLT – *120*	PD – *control*	CS	May
	PD – *30*		
	PD – *70*		
	PD – *120*		
FLT – *seasonal*	PD – *control*	CS	January, March, May, July,
	PD – *120*		September, November
	LGM		
FLT – *LGM*	LGM	CS	May
	LGM – *ecco*	NP, SP	March

5.3 Present-day particle trajectories

FLT – *control* Particle trajectories, velocity of propagation and seasonal patterns in distribution are analysed for the modern climate conditions using different seeding areas and timing of release. In Figure 5-3 is shown propagation of thermocline drifters representing the main flow through the Indonesian Seas for a 1 year period. The majority of floats (80%) released in CS at 105 m depth flow southward through Makassar Strait. Small number of floats (4%) is returning into the Pacific Ocean. The floats reach Indian Ocean after 4 months from the release by exiting through Lombok Strait. The drifters pass through Ombai Strait after approximately 6 months, while they reach Timor Strait after more than 1 year. Substantial number of drifters does not flow through Makassar Strait (26%) and resides in CS. The remaining floats are either recirculated within eddies in CS, enter the Sulu Sea at northern part of CS or reach the coast and are excluded from further analysis.

The mean velocities of the particles passing through Makassar Strait in 1 year period after being deployed in May in CS, and the mean velocity of drifters released in NP and SP in March during 22 months period are given in Table 5-3. The particle velocities indicate total magnitude of velocity (V) derived from zonal (u_{vel}) and meridional (v_{vel}) particle velocity components:

$$V = \sqrt{u_{vel}^{\ 2} + v_{vel}^{\ 2}} \qquad 5\text{-}1$$

The average surface velocity within Makassar Strait is calculated by taking into account floats released every two months during 1 year period and averaged through the 22 months period. Maximum velocity of surface particles in the Makassar Strait reaches 190 cms^{-1}, while maximum velocity of thermocline floats is 80.2 cms^{-1}.

Table 5-3 Mean particle velocity (cms^{-1}) in FLT – *control* experiments

Depth	Makassar Strait (115°E-120°E, 6°S-2°N)	Released in NP	Released in SP
5 m	28.4 ± 22.8	29.4 ± 25.1	16.1 ± 10.9
105 m	17.5 ± 12.9	16.0 ± 14.7	11.4 ± 9.8
395 m	11.5 ± 7.5	4.5 ± 3.8	3.9 ± 2.6
945 m		2.7 ± 1.8	2.5 ± 1.5

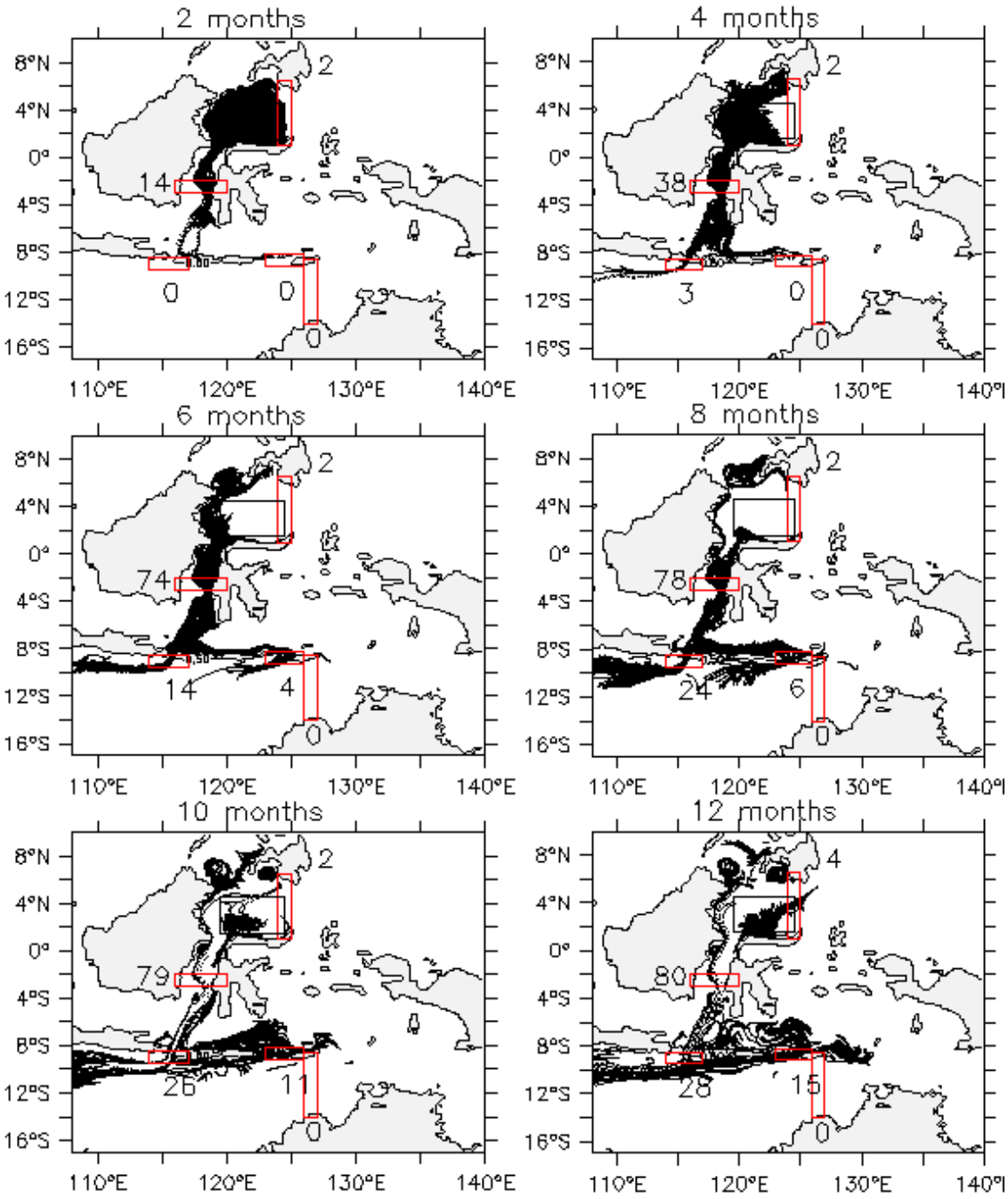

Figure 5-3 Temporal evolution of particle dispersal through the Indonesian Gateways under PD climate conditions. The floats are released in May at 105 m depth. Numbers indicate percent of individual floats passing through the main passages (red boxes) after deployment in CS (black box).

The particles released in NP (Figure 5-4 left) enter CS and propagate through Makassar Strait into the Indian Ocean. However, large part of the floats remains on the Pacific side and flows eastward following the NECC. The number of drifters entering the Indonesian Seas depends on the depth of the drifters and moreover, on the time of release for the surface floats (discussed in 0). For the surface drifters released in March, 86% of the drifters enter the CS and flow towards the Indian Ocean taking the westernmost route. Only 10% of the surface drifters released in NP reach Indian Ocean in the period of almost 2 years. The remaining drifters that enters Indonesian Seas is recirculated in Celebes and Sulu Sea, while part of floats passing through Makassar Strait enter Java Sea and flows northward around Borneo.

Even though large part of the floats released at 105 m depth is reversed towards the east (54%) and does not reach Indonesian Seas, the number of drifters entering Indian Ocean (17%) is larger than for the surface floats suggesting high velocity of propagation and weaker recirculation. The maximum velocity of the particle released in NP is almost 225 cms^{-1}, while thermocline drifters reach 122.5 cms^{-1}.

Small number of intermediate water drifters (17%) enters CS. With Lombok Strait closed at 395 m depth, the drifters follow eastern pathway, entering the Indian Ocean through Ombai Strait after approximately 7 months.

The SP drifters do not seem to propagate significantly into the Indonesian Seas (Figure 5-4 right). Only 2% of the floats enter the Seram Sea near Halamhera at 105 m depth from the SP source with additional 1% of surface floats coming originally from the NP. This is consistent with findings of *Lukas et al.*, [1991] and *Gordon and Fine*, [1996] suggesting the North Pacific source of the ITF and small contribution of South Pacific waters. The SP drifters flow westward towards the Indonesian archipelago, but are reverted near Halmahera into the NECC.

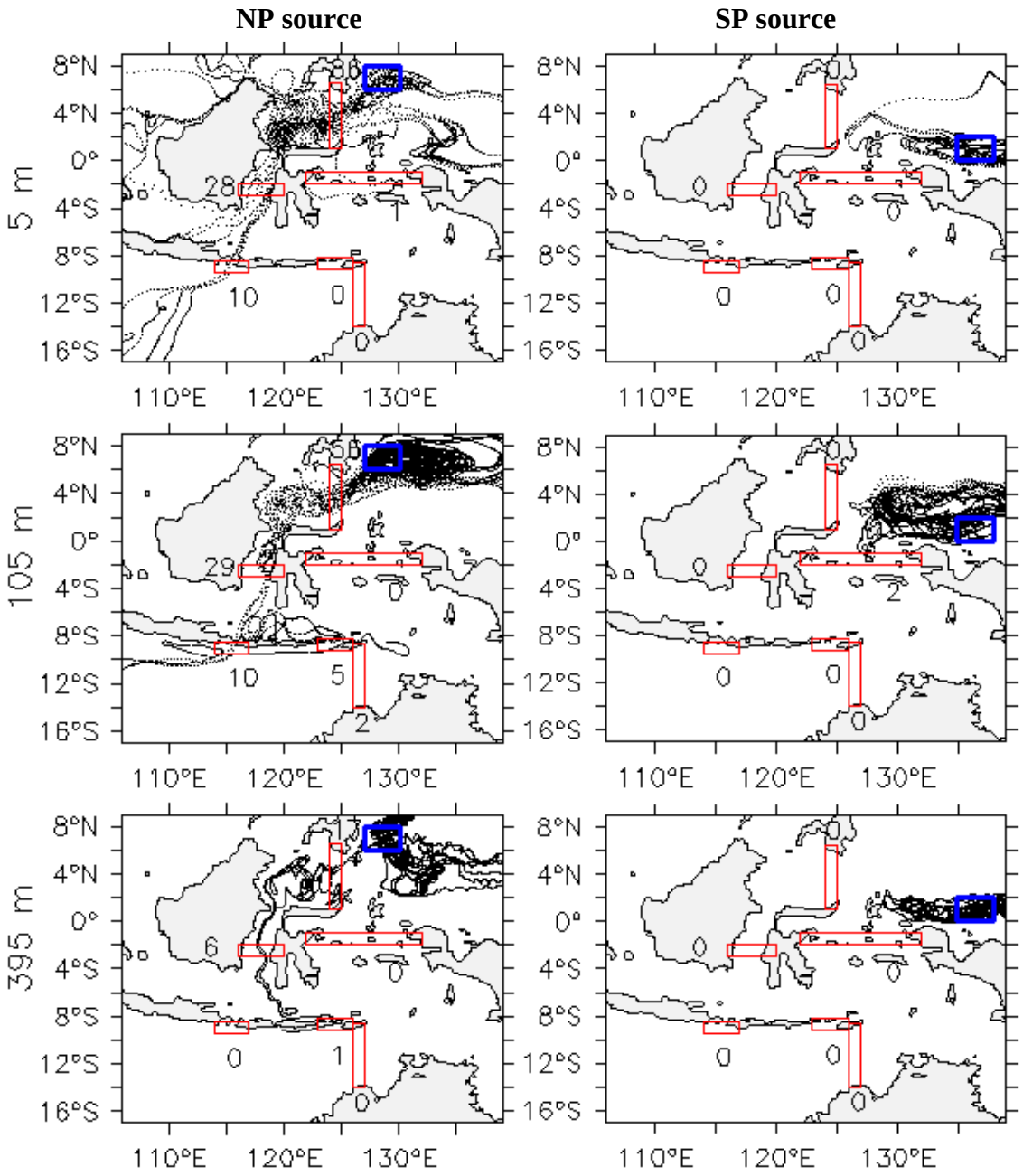

Figure 5-4 Particle trajectories at 5 m (top), 105 m (middle) and 395 m depth (bottom) released in NP (left) and SP (right) (blue boxes) for PD climate conditions. Numbers indicate percent of individual floats passing through the main passages (red boxes) within 22 months period. The floats are released in March.

The trajectories of surface drifters released in eastern Indian Ocean have been investigated within the JEXAM program to illustrate the surface current filed and its seasonal changes in the ITF area and in the tropical Indian Ocean [*Michida and Yoritaka*, 1996]. Surface drifters deployed between 1990 and 1993 show distinct seasonal patterns of surface trajectories. The floats released in May circulate within eddies in the eastern Indian Ocean and flow further towards west and southwest (Figure 5-5 top). The floats released in November drift northward and eastward entering inside the Indonesian Seas (Figure 5-5 bottom). The measured eastward velocity component of the drifters that enter Indonesian Seas was generally between 20 - 50 cms^{-1}.

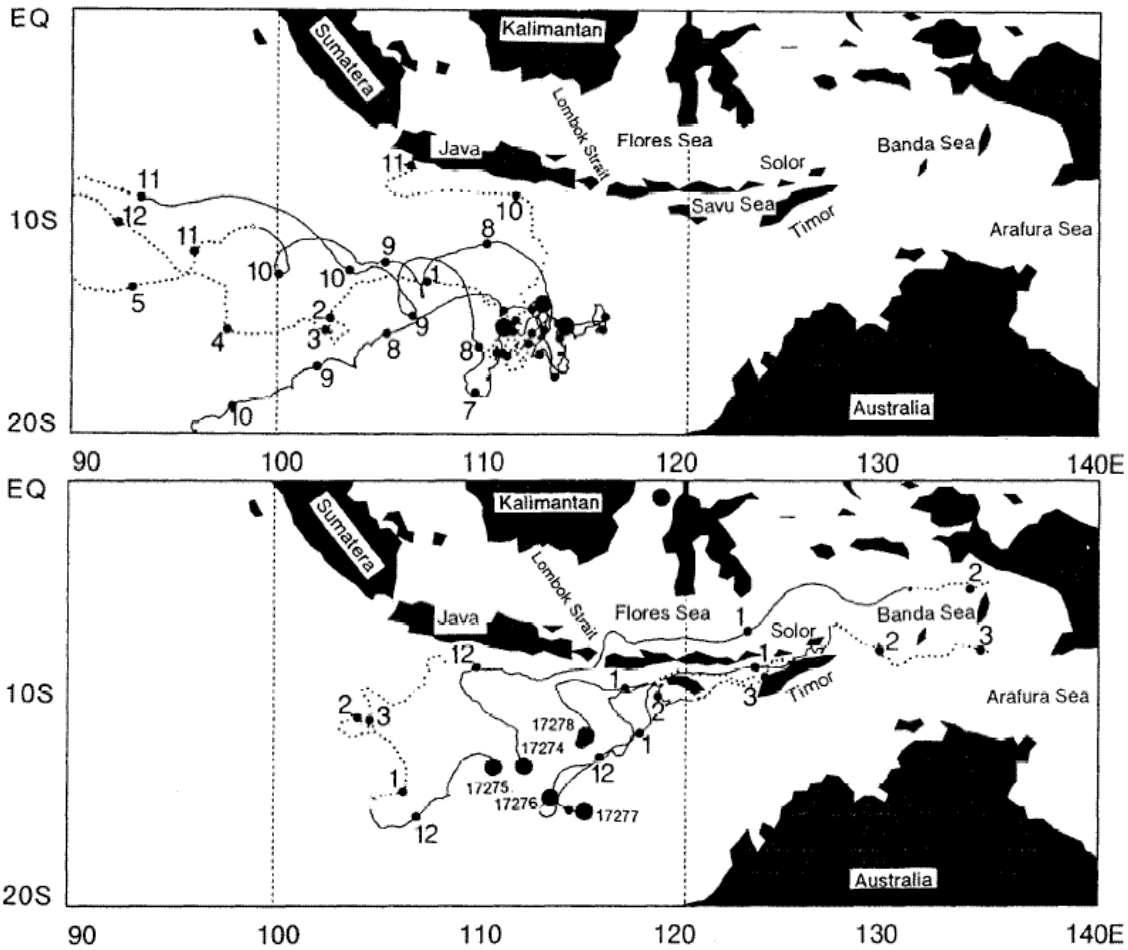

Figure 5-5 Trajectories of surface drifters deployed in East Indian Ocean in May 1991 (top) and November 1993 (bottom). The large solid circles mark deployment location. Small solid circles mark the locations of the first day of every month with the month number. From *Michida and Yoritaka*, [1996].

A similar experiment is performed with the regional model with floats released in IO in May and November (Figure 5-6). Initial position of the floats is shifted slightly east to avoid immediate interaction with the model boundaries. The seasonal pattern in float trajectories is in relatively good agreement with observations. However, the floats released in May in the model experiment are propagating faster and further southwest compared to the observed westward trajectories. Possible reason is applied climatological wind forcing in the model that might differ from the actual winds in given years. The northward trajectories of the drifters released in November are simulated well except for the Lombok Strait where the northward flow is suppressed by the strong southward outflow.

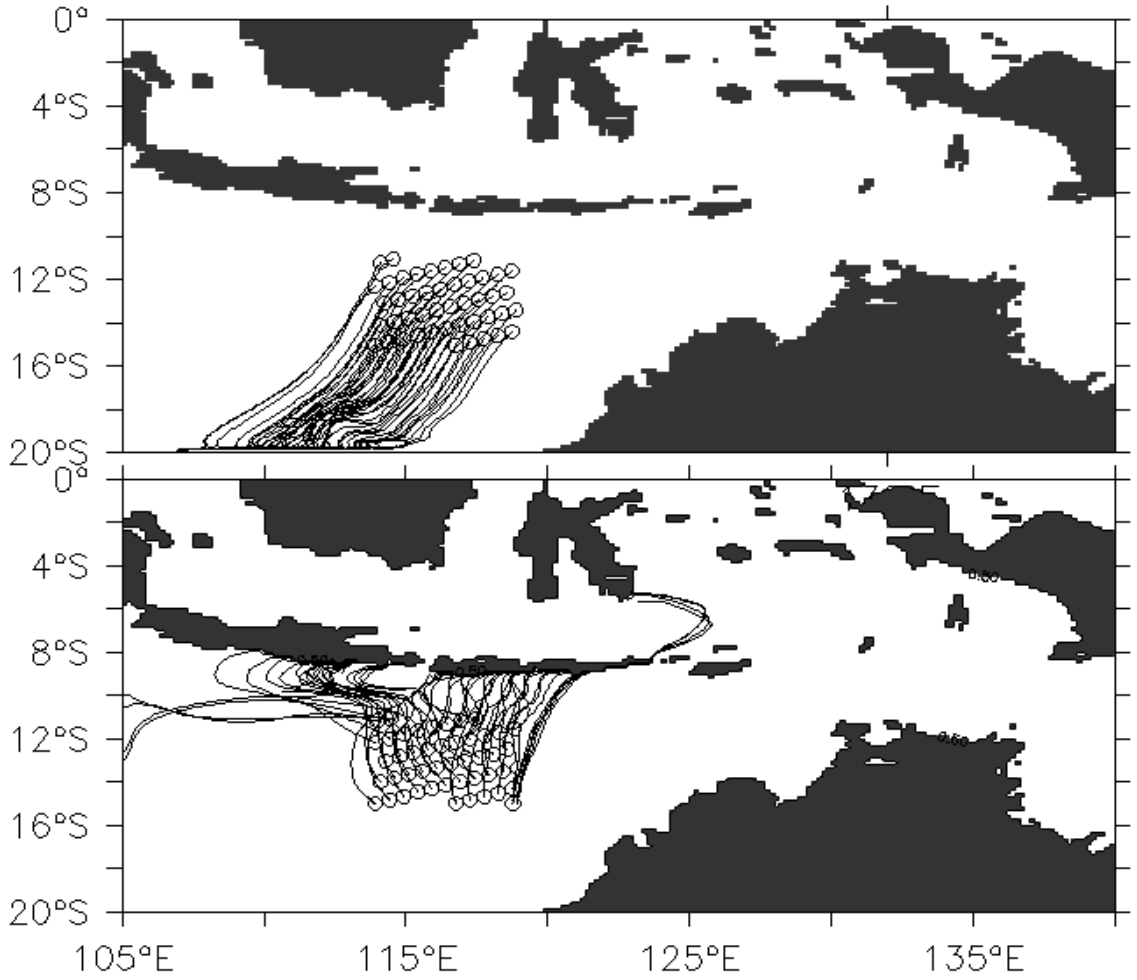

Figure 5-6 Seasonal changes in trajectories of the Indian Ocean surface drifters for SE monsoon (top) and NW monsoon phase (bottom). The float trajectories are plotted for period May to September (top) and November to April (bottom). Circles indicate deployment locations.

5.4 Impact of sea level lowering on particle exchange

FLT – *120* Dispersal of surface particles for the 0 m, 30 m, 70 m and 120 m sea level lowering is illustrated in Figure 5-7. Major part of floats released in May in CS flows eastward into the Pacific (~ 80%). Number of drifters passing through Makassar Strait is gradually decreasing with the lowering of the sea level. For the PD conditions, most of the float trajectories in the Indonesian Seas recirculate around Borneo. During the SE monsoon phase, when the floats are released, the surface drifters in the southern Makassar Strait are pushed into the Java Sea and flow further north towards the South China Sea. During the NW monsoon phase, the drifters are again pushed southward into Makassar Strait. At the 30 m sea level lowering, the communications with the South China Sea is blocked, restricting the circulation around Borneo. The floats are accumulating in the Java Sea and part of the floats passes through the Lombok Strait into the Indian Ocean. At 70 m sea level lowering, the Java Sea is exposed resulting in reduced exchange of particles in the southern Makassar Strait. This dispersal pattern remains similar when glacial topography is taken into account.

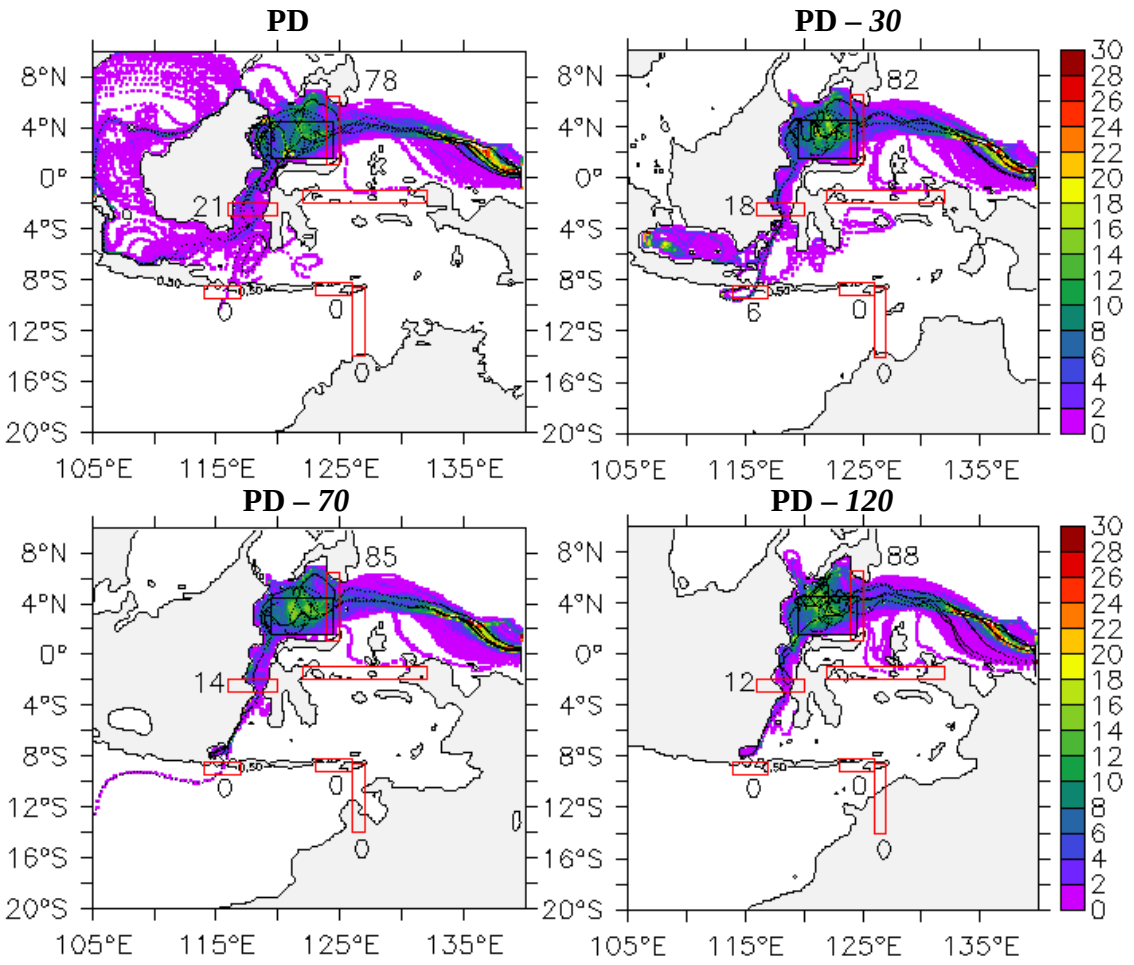

Figure 5-7 Surface floats distribution for sea level lowering of 0 m (upper left), 30 m (upper right), 70 m (lower left) and 120 m (lower right). The floats are released in May in CS (black box). Numbers indicate percent of individual floats passing through the main passages (red boxes). Colour scale represents probability in percent of finding a particle in the area within 1 year period.

The particle trajectories at the 105 m show significantly different dispersal patterns than the surface trajectories (Figure 5-8). The particle exchange through Makassar Strait at 105 m depth shows small differences with the changes in topography (2 – 6 %). Large difference appears in redistribution of the particles between the exit passages. The exchange of particles through Lombok Strait gradually decreases with the sea level lowering and is reduced by 71% when topography is lowered form 0 to 120 m. With restricted exchange through Lombok Strait, the particles take route towards east. Number of drifters passing through Ombai Strait increases by 5% at 70 m sea level lowering compared to PD value. With the 120 m reduced sea level the particle exchange through Ombai Strait does not seem to increase, but the probability of finding particles in the Timor Strait is significantly larger (by 29% compared to PD value). The Timor Strait plays major role in exchange of particles when glacial topography is taken into account. However, all the experiments are performed with PD climate conditions and when glacial reduction in transport is considered, the net impact of topography on particle exchange might be reduced. Additional remark needs to be made that analysis is done for a 1 year period after which approximately 28% of particles passing through Makassar Strait still resides in the Indonesian Sea.

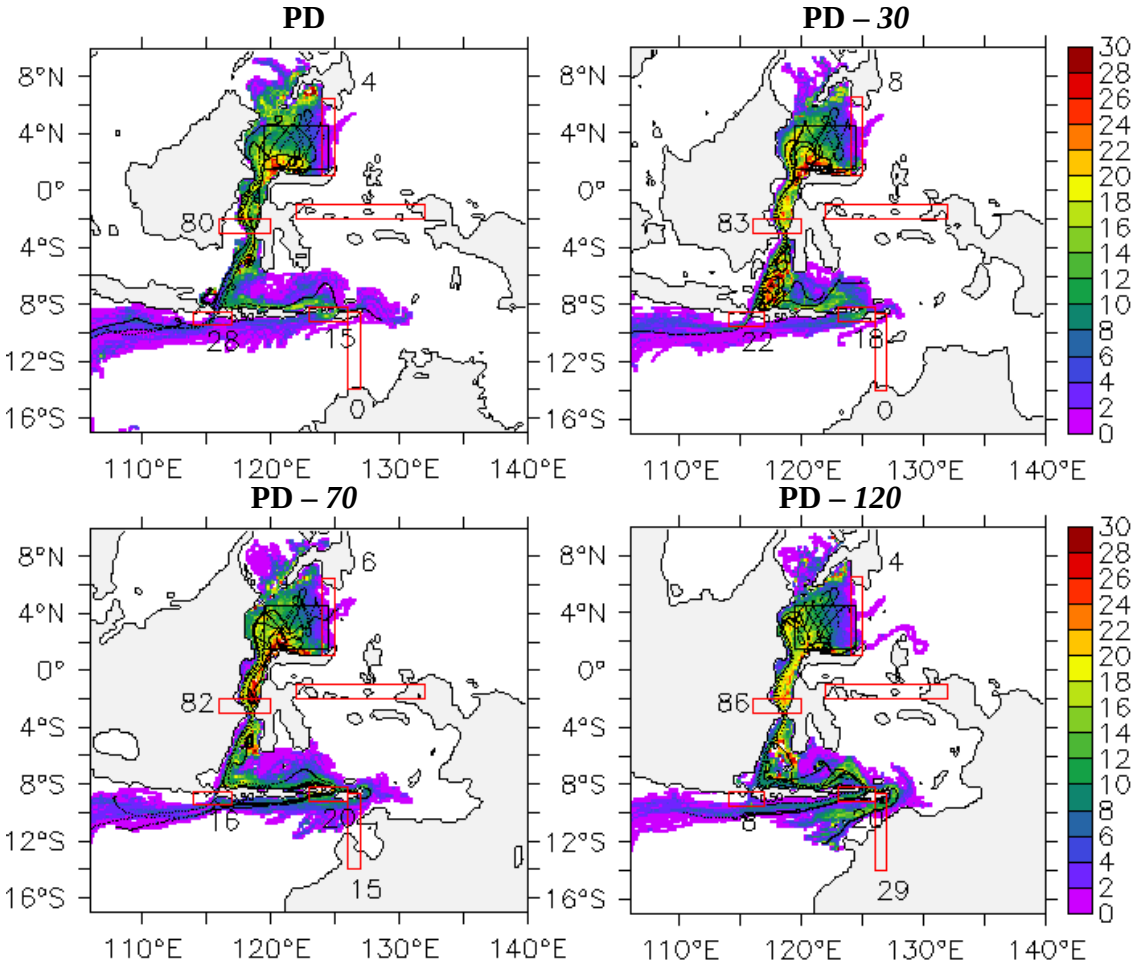

Figure 5-8 Floats distribution at 105 m depth for sea level lowering of 0 m (upper left), 30 m (upper right), 70 m (lower left) and 120 m (lower right). The floats are released in May in CS (black box). Numbers indicate percent of individual floats passing through the main passages (red boxes). Colour scale represents probability in percent of finding a particle in the area within 1 year period.

5.5 Seasonal patterns in surface distribution

FLT – *seasonal* The glacial sea level lowering has strong impact on seasonal variability in surface circulation in Makassar Strait. The seasonal patterns in exchange of surface particles through Makassar Strait might be significantly different in glacial periods. To test seasonal variations in the particle distribution through Makassar Strait with topographic changes and glacial climate conditions taken into account, the floats have been released in CS every 2 months for a period of 1 year. The particle distribution is given for NW monsoon phase from November to February with particles released in November and January (Figure 5-9 left) and SE monsoon phase from May to August with particles released in May and July (Figure 5-9 right).

In the PD simulation (Figure 5-9 top), the surface floats released in November and January do not propagate through the southern Makassar Strait, but circulate in northern part of the passage and CS or are reflected into the Pacific. The floats released in May and July are able to flow through Makassar Strait and are entering into the Java Sea. However, the maximum number of particles (41%) passing through Makassar Strait in PD experiment is not during the SE monsoon phase, but during monsoon transition from March to May as the period of the strongest outflow in the regional model.

When the topography is lowered (Figure 5-9 middle), the number of floats released in November and January that passes through Makassar Strait is almost doubled and smaller number of floats is reflected into the Pacific. However, the floats released in May and July mainly join NECC and just small number is able to flow through Makassar Strait. When the LGM boundary conditions are taken into account (Figure 5-9 bottom), the velocity of the surface floats is reduced and exchange of the particle through Makassar Strait during the NW monsoon is decreased. The floats released during the SE monsoon do not propagate into Makassar Strait, but are flowing northward. The northward intensification of particle dispersal released in May and July differs from PD particle dispersal and might be related to the applied glacial wind forcing. With large uncertainties in the local wind field during the LGM, this feature should be taken with caution.

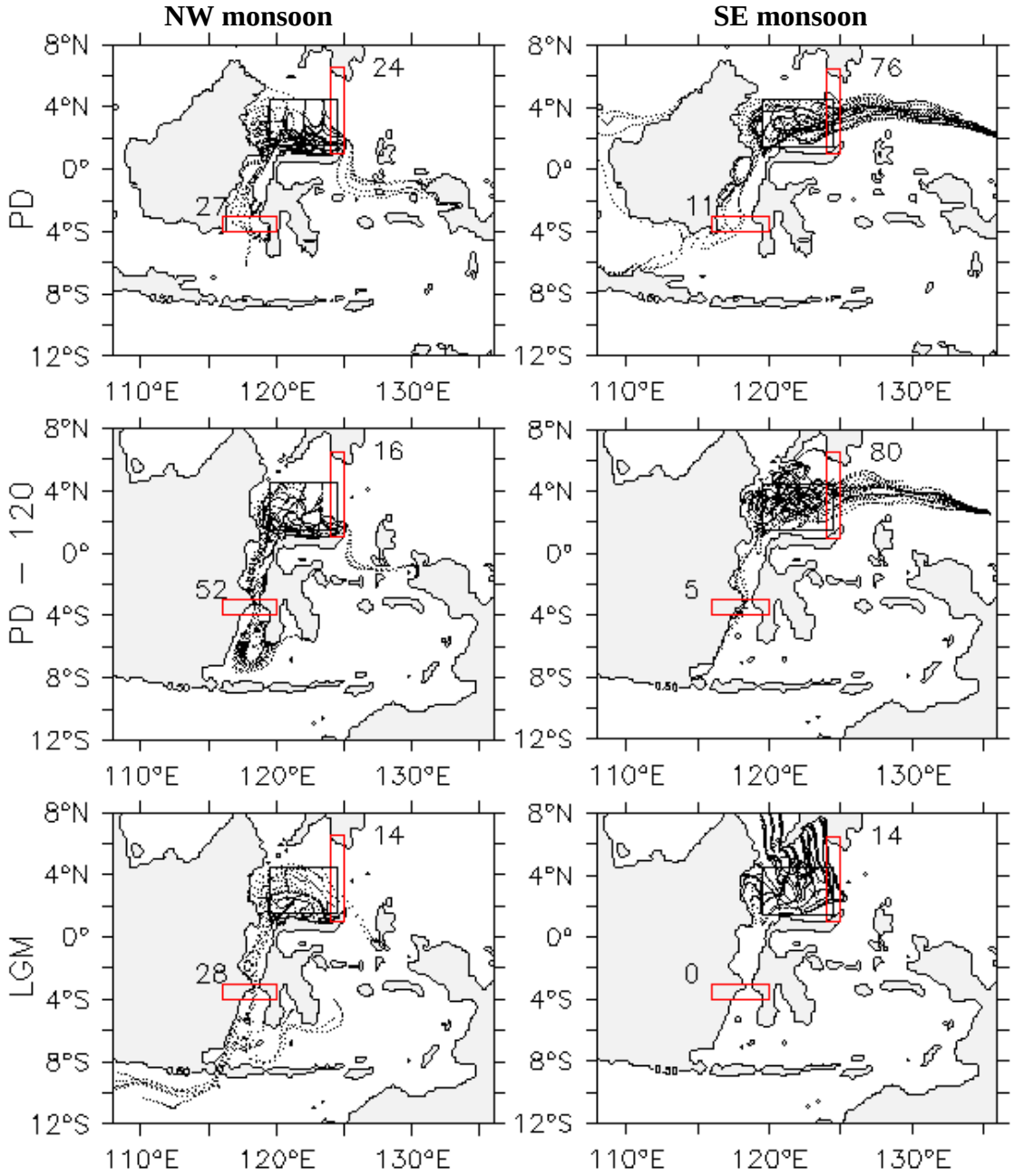

Figure 5-9 Seasonal patterns in surface float distribution for PD – *control* (top), PD – *120* (middle) and LGM experiment (bottom) for NW monsoon (November to February) (left) and SE monsoon (May to August) (right). Numbers indicate percent of individual floats passing through Makassar Strait and exiting Celebes Sea (red boxes). Plotted are particle trajectories for every 20 floats.

5.6 Glacial particle trajectories

FLT – *LGM* The mean particle pathways within the Indonesian Gateways for glacial climate conditions are compared with PD particle trajectories on surface, thermocline and intermediate water depths (Figure 5-10). The surface particle trajectories include analysis of floats released in CS every two months during one annual cycle in order to take into account seasonal variations in particle distribution. The particle exchange through Makassar Strait during 1 year period is decreased by 7% in glacial simulation. Overall, small number of particles (3%) reaches Indian Ocean through Lombok Strait. Maximum velocity of surface particles passing through Makassar Strait in glacial simulation reaches 167 cms^{-1}.

The drifters at 105 m depth have maximum velocity of 88.4 ms^{-1} in glacial simulation. The number of floats passing through Makassar Strait is reduced by almost 20% of total number of drifters and exchange through Lombok Strait is decreased by 43% relative to the PD value. The exchange of particles through eastern passages is reduced as expected from the PD – *120* experiment indicating reduced transport through the Makassar Strait. Mean velocity of propagation for the drifters in glacial simulations are given in Table 5-4.

The floats drifting at 395 m depth show similar pattern of distribution in both PD and LGM simulation. However, number of floats passing through Makassar Strait and reaching the Indian Ocean is reduced in glacial simulation by approximately ~17% and the velocity of the particles is decreased. The particles released in CS in glacial simulation reach Indian Ocean after approximately 10 months at intermediate depths compared to 3 months in the thermocline depths.

The deep water particles at 945 m depth released in the Pacific do not propagate into the Indonesian Seas during the 3 year period of simulation. The maximum velocity of the deep water floats does not exceed 13 cms^{-1} in both PD and glacial simulation.

Table 5-4 Particles velocity (cms^{-1}) in FLT – *LGM* experiment

Depth	Makassar Strait (115°E-120°E, 6°s-2°N)	Released in NP	Released in SP
5 m	40.1 ± 32.4	30.0 ± 21.1	10.9 ± 9.8
105 m	20.9 ± 15.9	9.5 ± 8.2	8.5 ± 4.5
395 m	7.9 ± 5.6	1.7 ± 1.9	2.7 ± 2.2
945 m		1.4 ± 1.0	1.3 ± 0.8

Glacial particle trajectories are examined for the floats originating in the NP and SP (Figure 5-11). The surface floats distribution released in March is significantly different than the PD pattern (Figure 5-4) showing eastward flow of NP drifters and northward reversal of SP drifters. The resulting surface particle dispersal is probably influenced by the glacial wind forcing and might not be reliable.

At 105 m depth, the NP floats enter Indonesian Gateways and follow the main pathway through Makassar Strait exiting into the Indian Ocean through Ombai and Timor Strait 20 months after the release. The total number of floats reaching Indian Ocean is reduced by half relative to the PD simulation. A significant number of drifters enter Indonesian Seas through the eastern pathway between the Halmahera and Celebes carrying 9% of floats with the origin in NP. Only 0.4% of the SP floats propagate in the Indonesian archipelago during the period of 2 years. The particles released in NP reach Indian Ocean after 6 months at 105 m depth and after 31 months at 395 m.

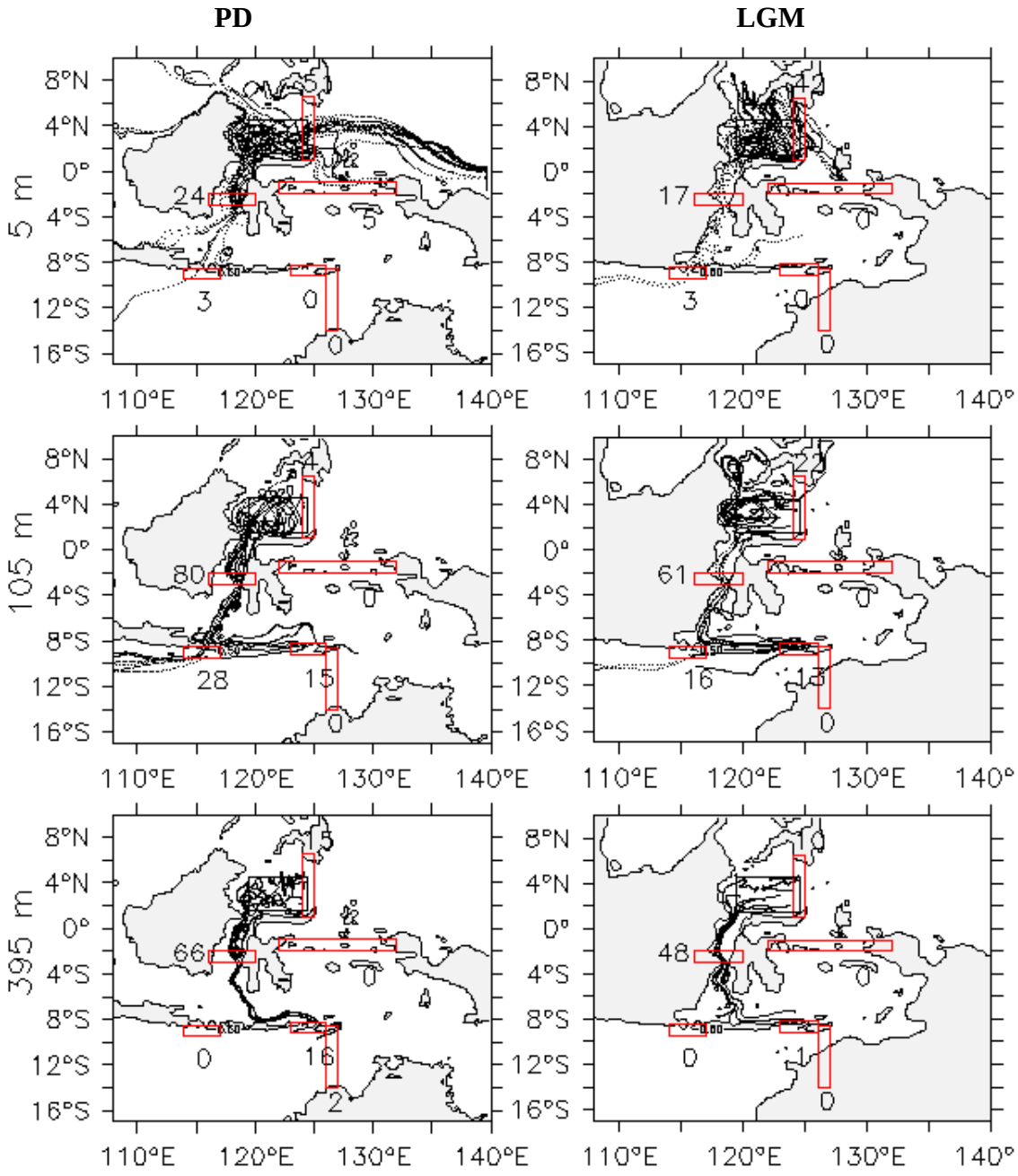

Figure 5-10 Main pathways of surface (top), 105 m (middle) and 395 m drifters (bottom) for PD – *control* (left) and LGM experiment (right) with numbers indicating percent of individual floats passing through the main passages (red boxes) within 1 year period. The floats are released in CS in May for subsurface and intermediate water drifters and every two months for surface floats.

The analysis of the particle trajectories shows that SP source does not seem to have different importance under glacial conditions. If the surface trajectories are excluded taking into account that they might be effected significantly with the unreliable surface glacial forcing, the thermocline and intermediate water trajectories could possible give more reliable estimates. The representation of the glacial climate conditions at the lateral boundaries could, however influence the result in possible changes in deeper water trajectories. The LGM experiment configuration used to simulate Lagrangian particle trajectories assumes same spatial representation of boundary currents with reduced total transport and glacial density stratification. However, this might be a realistic estimate considering that only large changes in

Gateways configuration such as southward shift of the Halmahera Island would lead to redistribution between NP and SP source [*Cane et al.*, 2001].

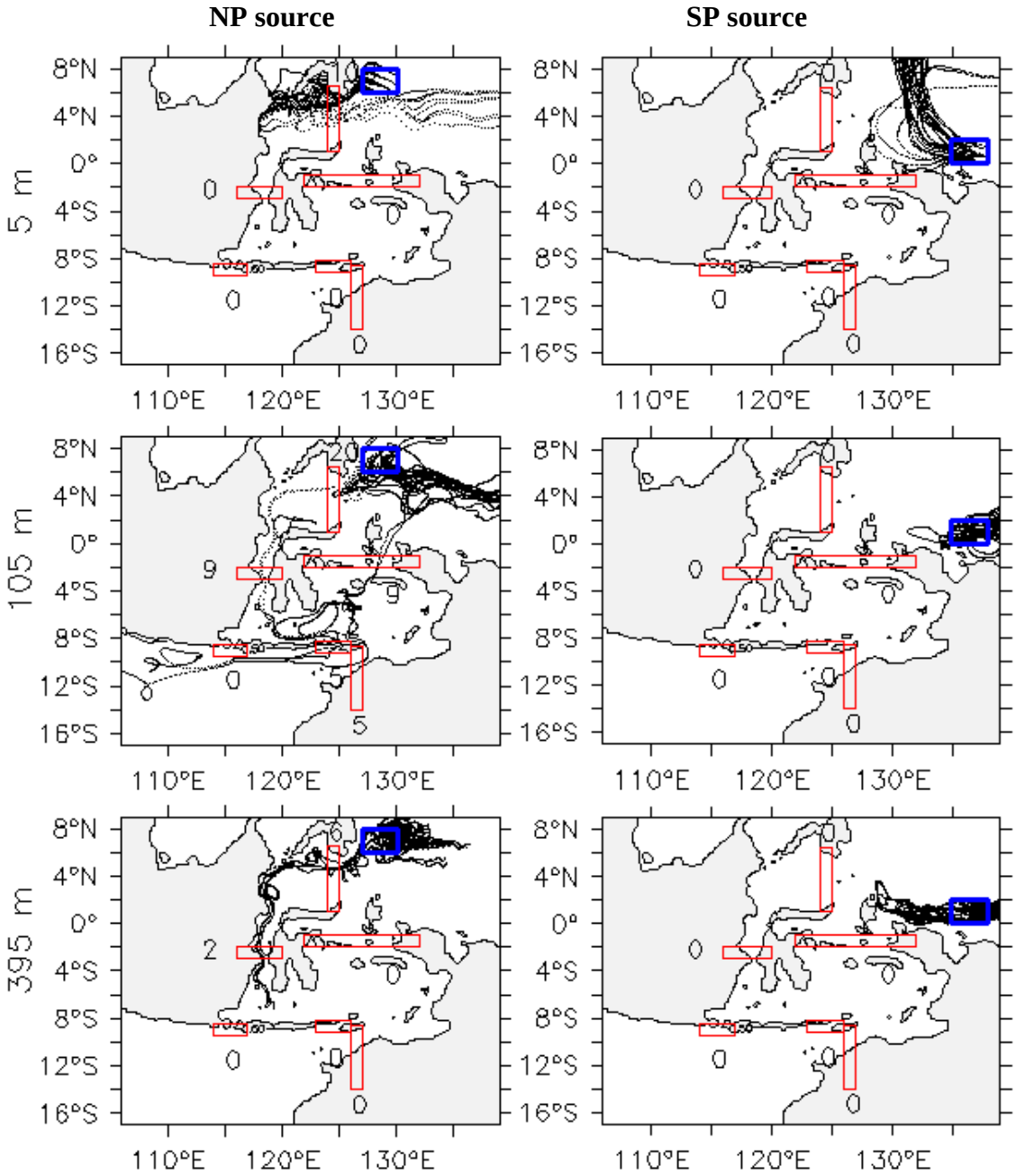

Figure 5-11 Glacial particle trajectories at 5 m (top), 105 m (middle) and 395 m depth (bottom) released in NP (left) and SP (right) (blue boxes). Numbers indicate percent of individual floats passing through the main passages (red boxes) within 22 months period. The floats are released in March.

5.7 Conclusions

Regional ocean model experiments using Lagrangian particle-tracing module give sensitivity of particle distribution through the Indonesian Gateways to the topographic changes on glacial-interglacial time-scales. The particle dispersals show different patterns depending on the location, depth and timing of deployment.

The model simulated trajectories for the PD conditions show that the main pathway of the Throughflow waters follows the route from the NP into CS and through Makassar Strait. The velocity of particles decreases with depth. Average velocity of particle propagation through the Makassar Strait under PD conditions is approximately 28 cms^{-1}, 18 cms^{-1}, 12 cms^{-1} for the surface (5 m), thermocline (105 m) and intermediate (395) water depths, respectively. The surface and thermocline drifters exit into Indian Ocean through Lombok Strait after approximately 2–4 months (for thermocline drifters) since the release in CS. The thermocline and intermediate drifters pass eastward through Ombai and Timor Strait and reach the Indian Ocean after 4–10 months (for thermocline drifters) since the release in CS.

Even though surface particles have highest velocities of propagation, small number of drifters reaches the Indian Ocean (~3%) after release in CS. The surface trajectories show recirculation inside the Celebes, Java and Flores Sea and are under high influence of the local wind variations. With applied monthly climatological wind forcing, the highest number of surface particles is propagated through Makassar Strait during transition between NW and SE monsoon phase. During the SE monsoon phase, the surface particles flow westward into the Java Sea and recirculate around Borneo.

In order to validate the simulated surface pathways, the seasonal variations in trajectories of surface particles are compared to existing drifter trajectories observations in the East Indian Ocean [*Michida and Yoritaka*, 1996]. The simulated trajectories of IO floats are in relatively good agreement with the observed trajectories showing northward and northeastward propagation during the NW monsoon phase and southwestward propagation during SE monsoon phase. The differences between the observed and simulated trajectories might be associated to the climatological forcing which differs from the observed wind field. For this reason, the simulated trajectories do not show westward particles propagation during the SE monsoon phase and the northward propagation of the surface drifters through Lombok Strait during the NW monsoon phase.

Gradual lowering of the sea level leads to changes in the exchange of the particles through the main passages. At 30 m sea level change, the circulation of the surface floats around Borneo is blocked, indicating a stage where no communication with the China Sea could be established. Higher number of particles enters Indian Ocean (~6%) through the Lombok Strait and particles propagate into the Banda Sea. Lowering of the sea level by 70 m further decreases the surface particle exchange through the Makassar Strait into the Flores Sea by reducing the width of the channel. At the thermocline depth (105 m), severe change in particle exchange can be found at 70 m sea level change, when the Java Sea is exposed and the Lombok Strait is significantly closed. The eastward propagation of the particles is intensified. However, realistic assumptions on particles velocities and exchange through the eastern passages depend crucially on the applied boundary conditions that are not well know for this stage. With the assumption of similar volume transport of the ITF as for the modern conditions, the increase of particle originating in CS that pass through Timor Strait in period of 1 year is about 15% and increases to 30% for the sea level lowering of 120 m. This change could

be possibly detected in the sediment patterns in the Timor Strait already at the 70 m sea level change. In this case content of kaolinite and chlorite as tracers of ITF could be increased. However, expected decrease in ITF volume transport under glacial conditions would reduce the net effect.

The sediment records in Timor Strait show reduction of kaolinite and chlorite during the glacial [*Gingele et al.*, 2001a,b]. The reduction was assumed to be associated with weaker glacial ITF volume transport, but also to decreased input of kaolinite and chlorite injected by Western Australian rivers due to drier conditions at the LGM [*De Deckker et al.*, 2002]. In the FLT – *LGM* experiment where reduced ITF transport and topographic changes are taken into account, the number of particles passing through Makassar Strait is reduced by ~20% at the thermocline level. However, large percent of the floats exits through Lombok Strait and exchange of particles through Ombai and Timor Strait is similar or just slightly reduced compared to the PD conditions. Larger reduction in transport of particles is found only at intermediate levels (~15 %). When surface trajectories are considered, it needs to be noted that particles originating from Makassar Strait do not seem to enter directly into eastern passages, but are being pushed back and forth from Flores to Banda Sea by the seasonal winds. These results indicate that the reduction in kaolinite and chlorite in Timor Strait cores might be just partly related to the reduced ITF transport at the glacial. Local terrestrial input might play a significant role especially if it is assumed that the clay minerals are mainly entrained into the shallow water masses.

Glacial topographic changes have large impact on seasonal patterns of surface particle distribution which have not been considered previously when investigating sediment cores. The absence of Java Sea during the LGM leads to reversal of the seasonal cycle in surface circulation within Makassar Strait. Weak propagation of surface particles through the Makassar Strait is found during the SE monsoon, while the NW monsoon propagation is expected to be intensified during glacial period. The SE monsoon phase is usually characterized to be the phase of strong ITF transport. However, NW monsoon phase is characterized by high precipitation rate and therefore intensified river runoff and increased terrestrial input. If these results are taken into account, the signal of hydrological cycle might be compromised by the blocking of the flow during the SE monsoon phase leading to overall reduced distribution of surface tracers further downstream. These findings should be considered when analysing sedimentological tracers from the Makassar Strait.

The model experiments with particles released in North and South Pacific show that the ratio between the NP and SP origin of the particles is not significantly changed under glacial conditions. The NP drifters are dominantly present inside the Indonesian archipelago in both PD and LGM experiments. Possible redistribution between NP and SP source could be expected only with severe changes in West Pacific equatorial currents or Gateway configuration [*Cane et al.*, 2001].

6. Indonesian Throughflow in existing LGM model simulations

6.1 LGM model simulations

General circulation models of the climate system are powerful tool for understanding mechanisms of climate change. Large number of paleoclimatic evidence of the LGM climate provided possibility for testing the performance of the GCMs. Ability of the GCMs to realistically simulate climate system not only helps interpret paleoclimatic records and past climate changes, but could be used for future long-term climate predictions. Due to complexity of the climate system, accurate simulations of LGM climate and consistent explanation of climate changes on glacial-interglacial time-scale are a difficult task and LGM climate models are under constant development.

The LGM climate conditions generally imply changes in orbital forcing [*Berger*, 1978], reduced concentration of greenhouse gases (CO_2=200 ppm compared to 345 ppm PD value, or 280 ppm pre-industrial value) and global ice sheet growth resulting in orographic difference, changes in land-sea albedo, lowering of the sea level and land-sea distribution [*Peltier*, 1994].

The CLIMAP [1981] reconstructions of the SSTs during the LGM were applied as boundary conditions to simulate glacial climate using AGCMs. Comparison of AGCM simulations and paleoclimatic data in the Paleoclimate Modeling Intercomparison Project (PMIP) [*Pinot et al.*; 1999] pointed out to importance of the ocean circulation for simulating long-term climate changes showing better agreement with the data when ocean dynamics are included in the model.

Early experiments to investigate physical processes that govern LGM climate without interfering the surface boundary conditions were made by using atmosphere-mixed layer ocean models with simple ocean dynamics and heat and water budget model on the land surface [*Manabe and Broccoli*, 1985].

The most recent paleoclimate models are fully coupled atmosphere-ocean GCMs which include sea-ice dynamics and thermodynamics, land surface biophysics and hydrology models [*Kim et al.*a,b, 2002; *Kitoh and Muarakami*, 2002; *Hewitt et al.*, 2001; 2003; *Shin et al.*, 2003] and are used to simulate changes in marine biology and carbonate cycle as well [*Ewen et al.*, 2004]. However, for studying climate processes, computationally expensive coupled climate models have been often successfully substituted by models of intermediate complexity with simplified atmospheric [*Weaver et al.*, 2001] or oceanic dynamics [*Ganopolski et al.*, 1998].

6.2 Tropical climate at the LGM

One of the most important issues in understanding the LGM climate is quantifying the cooling of the tropics which is fundamental for atmospheric and oceanic circulation regimes by influencing energy transfer from the equator to the poles. LGM model simulations and reconstructions of the SSTs in the tropics show large disagreement. Early estimates of the tropical cooling [CLIMAP; 1981] indicated very small changes compared to modern climate (less than 1°C). PMIP simulations [*Pinot et al.*; 1999; *Broccoli*, 2000] with coupled atmosphere and mixed-layer ocean models produced larger cooling (1°C - 3.5°C) more consistent with the terrestrial data than in the models which used CLIMAP reconstructions as surface boundary conditions. Moderate

cooling of the WPWP (2-3°C) is found in the coupled AOGCMs [*Weaver et al.*, 2001; *Kitoh and Muarakami*, 2002; *Shin et al.*, 2003] in broad agreement with recent paleoclimatic reconstructions (see *Kuhnt et al.* [2004] for overview). Colder tropical temperatures at the LGM could be associated with the lowered greenhouse gases concentration explaining half of the simulated cooling in the LGM simulation [*Shin et al.*, 2003] and partly to atmosphere-ocean interaction including export of cold air from the continent.

Simulations of glacial changes in hydrological cycle show decrease in mean annual precipitation over land and generally more arid conditions during the LGM. However, tropical changes in precipitation are dependant on surface temperatures anomalies showing stronger decrease in precipitation as result of cooling in SSTs [*Pinot et al.*; 1999; *Lohmann and Lorenz*; 2000]. The precipitation anomalies are not spatially uniform and models predict different regional patterns. With moderate tropical cooling, negative precipitation anomalies and increase in SSS in the Indonesian Seas are found as consequence of eastward shift of the WPWP and tropical centres of deep convection [*Kitoh and Muarakami*, 2002]. The eastward displacement of tropical circulation system is manifested in positive SST and precipitation anomalies in the central equatorial Pacific, large westerly anomalies of the surface wind over the tropical central Pacific and weakened Walker circulation.

Coupled ocean-atmosphere climate models have been used to investigate ENSO intensity under glacial climate conditions [*Kim et al.*a,b, 2002; 2003; *Liu et al.*, 2000; 2002; *Otto-Bliesner et al.*, 2003; *Timmermann et al.*, 2004]. *Kim et al.* [2002; 2003] found large tropical cooling of about 6.5°C in relative agreement with proxy estimates from various sources (pollen, tropical ice core, planktonic assemblages). They associated ocean dynamics in the tropical Pacific to the mean La Niña-like response. *Timmermann et al.* [2004] found as well La Niña-like pattern for the LGM tropical climate with enhanced trade winds and ocean currents due to orographic difference in LGM simulation. However, inadequate representation of atmospheric dynamics in the model of intermediate complexity (ECBilt-CLIO) underestimates tropical variability [*An et al.*, 2004]. Analysis of ENSO variations [*An et al.*, 2004] using background conditions from different LGM simulations [*Timmermann et al.* 2004; *Shin et al.*, 2003] shows that LGM climate conditions are favourable to enhance large amplitude interannual ENSO variability and that LGM tropical climate was probalby more El Niño-like. Simulation of LGM climate by NCAR CSM [*Liu et al.*, 2002; *Otto-Bliesner et al.*, 2003] shows intensified ENSO variability over the last glacial-interglacial cycle which is not correlated to the mean sea ocean temperature change but to the zonal and vertical gradients of ocean temperature. Tropical Pacific zonal SST gradient is weakened in the LGM simulation and upwelling and sharpening of tropical thermocline is found in the eastern Pacific. The temperature gradients in the tropical Pacific agree well with recent proxy record analysis supporting the El Niño-like pattern during the LGM [*Koutavas et al.*, 2002; *Stott et al.*, 2002].

Mean El Niño-like pattern in the tropical Pacific is expected to result in reduced ITF transport due to weakening of the trade winds that build high sea level in the western Pacific [*Clark and Liu*, 1993; *Meyers*, 1996]. The changes in zonal temperature gradients across the equatorial Pacific could additionally effect sea level in the western Pacific by changing the density structure.

6.3 ITF representation in the global LGM model simulations

Existing model simulations of the glacial climate suggest that the ITF was reduced during the LGM. However, amount of reduction in the ITF varies significantly between the models (Table 6-1). The AOGCM UVic [*Weaver et al.*, 2001] predicts small difference in the ITF (9.2%) between the control and LGM simulation. A possible explanation might be found in the missing atmospheric dynamics with the same wind forcing used in present-day and glacial experiment. The OGCM LGS [*Maier-Reimer et al.*, 1993] experiment gives similar values of transport as used in the regional model, as well as the LGM reduction in transport. The NCAR CSM simulation overestimates the Throughflow magnitude for PD. However, relative reduction between PD and glacial simulation (24.9%) is comparable with other model experiments.

Table 6-1 ITF volume transport (Sv) in global LGM model experiment.

Model	Present-day	LGM	Reduction by
OGCM MOM *Paul and Schäfer-Neth* [2003]	17.1	10.2	40.4%
OGCM LGS *Maier-Reimer et al.* [1993]	9.7	6.6	32.0%
AOGCM UVic *Weaver et al.* [2001]	18.5	16.8	9.2%
NCAR CSM *Shin et al.* [2003]	26.5	19.9	24.9%

The regional model results in this study show that glacial sea level lowering is not sufficient to reduce the net volume transport from the Pacific to the Indian Ocean. However, variety of global LGM simulations [*Maier-Reimer et al.*, 1993; *Weaver et al.*, 2001; *Liu et al.*, 2002; *Shin et al.*, 2003; *Paul and Schäfer-Neth*, 2003] and paleoclimatic records from the Indonesian Gateways [*Müller and Opdyke*, 2000; *Gingele et al.*, 2001a,b; *De Deckker et al.*, 2002] indicate that the ITF was reduced during the glacial periods. Excluding regional dynamics, several possible mechanisms can be considered to influence the ITF magnitude during the LGM:

- changes in glacial wind over the Pacific effecting wind forced circulation around the island,
- reduction in pressure gradient between Pacific and Indian Ocean induced by density anomalies,
- ENSO like conditions in the tropical Pacific during the LGM influencing wind field and temperature gradients,
- possible reduction in the global THC.

Some of the mechanisms are further analysed in the available global LGM simulations [OGCM MOM; Paul and Schäfer-Neth [2003] and NCAR CSM; Shin et al. [2003]).

6.4 Wind forced circulation around island

The existing theory of the wind forced circulation around the island [*Godfrey*, 1989; *Wajsowicz,* 1993a] is tested here by using the global model results. The ITF volume transport is estimated based on the *island rule* formulation taken from *Wajsowicz* [1993a]. The Throughflow magnitude can be estimated for the climatological mean circulation assuming there exists a level of no motion above all topography by:

$$\Psi_0(t) = \frac{-1}{(f_N - f_S)} \oint_{\partial D+\partial I} \frac{\tau(x,y,t)\cdot dl}{\rho_0} \qquad 6\text{-}1$$

where $\Psi_0(t)$ is the depth integrated stream function, f_N and f_S are the values of the Coriolis parameter at y_N and y_S the northernmost and southernmost latitudes of the island, respectively, dl is an infinitesimal line element tangential to ∂D and ∂I, ρ_0 is mean water density and τ(x,y,t) is the wind stress. The path integrals ∂D and ∂I along the east coast of Australia cancel so the wind stress needs to be integrated along the path over the South Pacific and west coast of Australia (Figure 6-1). The circulation around New Zeeland is neglected assuming that its contribution to the total circulation around Australia would be small. Topographic effects in the Indonesian Gateways are not considered taking into account that global models do not have appropriate representation of topography in Indonesian archipelago.

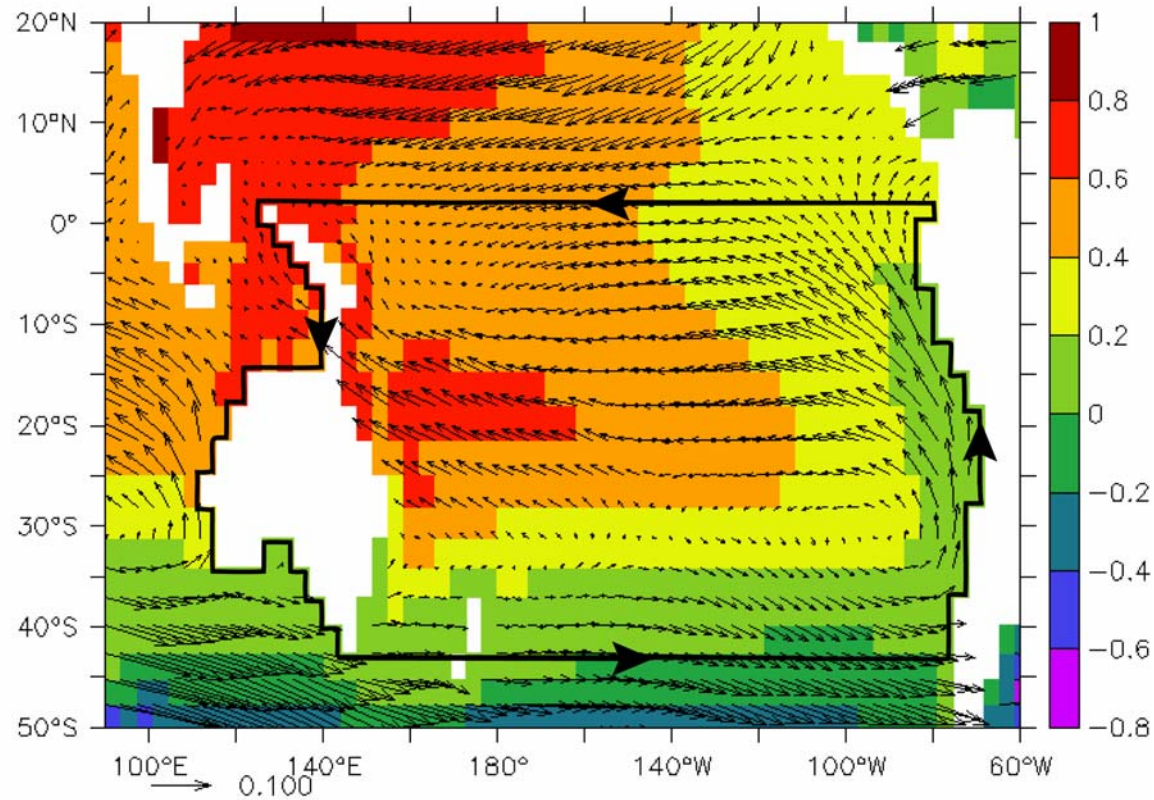

Figure 6-1 Mean sea surface height (m) and path used in *island rule* calculation in the OGCM MOM [*Paul and Schäfer-Neth*, 2003] are illustrated together with the mean wind stress field (Nm^{-2}) from NCEP climatology [*Kalnay et al.*, 1996] used as forcing in PD simulation.

The estimate of the wind induced Throughflow is compared to the global model results from OGCM MOM [*Paul and Schäfer-Neth*, 2003] and NCAR CSM [*Shin et al.*, 2003] for PD and LGM conditions. The wind field used to force the OGCM MOM

under PD conditions is taken from NCEP/NCAR Reanalysis [*Kalnay et al.*, 1996], while the LGM wind includes glacial anomaly from the AGCM ECHAM3 [*Lohmann and Lorenz*, 2000]. The estimates of the ITF transport are given in Table 6-2.

Table 6-2 ITF volume transport (Sv) calculated from the *island rule*.

Model	Present-day	LGM	Reduction (Sv)
OGCM MOM *Paul and Schäfer-Neth* [2003]	10.0 ± 1.4	4.7 ± 2.3	5.3
NCAR CSM *Shin et al.* [2003	20.3 ± 6.5	19.5 ± 6.6	0.8

The estimates of the ITF transport calculated from the *island rule* partly agree with model results. The magnitude of the transport is higher by approximately 6 Sv in OGCM MOM. The errors could be possibly induced by calculation of the wind field on a low resolution horizontal grid. However, reduction in LGM transport derived from the wind balance of about 5 Sv is comparable to model reduction of about 7 Sv.

The *island rule* estimates of ITF transport in NCAR CSM simulation are as well lowered by 6 Sv compared to the model results, but give very small reduction between PD and LGM simulations. The reason for similar estimates in ITF transport is small difference in wind field between the PD and LGM experiment (Figure 6-2). This indicates that reduction of the Throughflow in NCAR CSM simulation is not related to the wind field. The reduction could possibly be associated to weakened meridional overturning circulation at the LGM compared to the modern control run [*Shin et al.*, 2003]. Considering that the ITF belongs to returning branch of the global conveyor belt, a weaker global thermohaline circulation would reduce net ITF transport. However, deep-ocean acceleration used during ocean spin-up in the LGM simulation could induce errors in simulating global thermohaline circulation in NCAR CSM model.

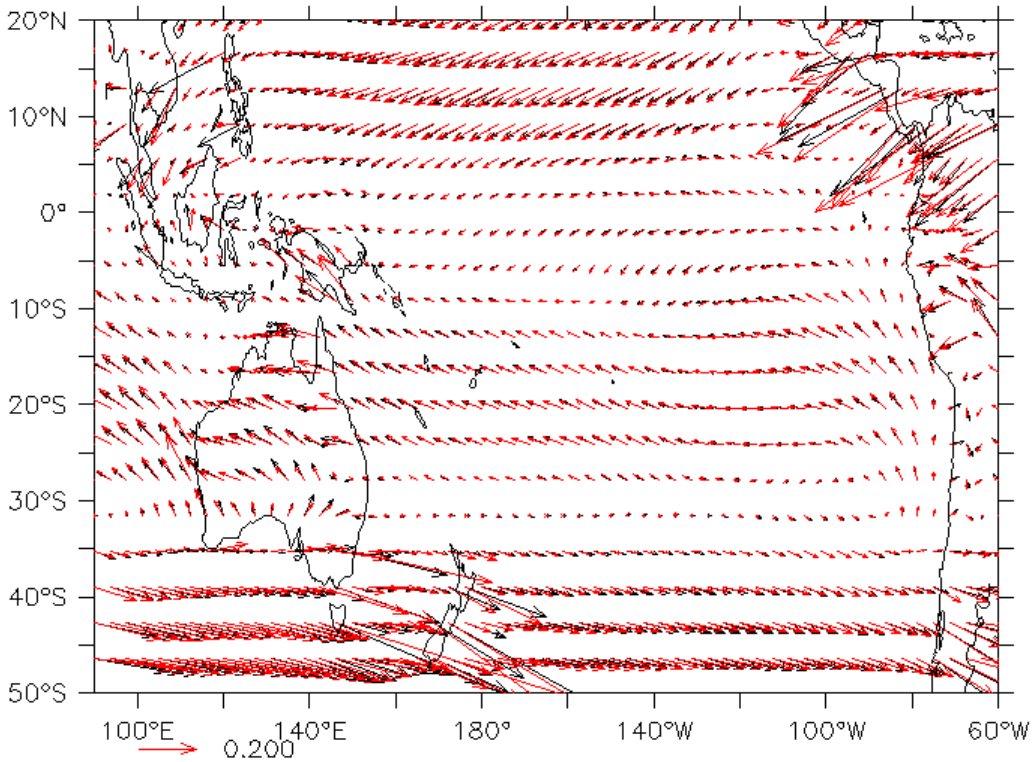

Figure 6-2 Mean wind stress over the Pacific taken from coupled NCAR CSM [*Shin et al.*, 2003] for PD (black) and LGM (red) conditions.

6.5 Pacific to Indian Ocean density difference at the LGM

Cooling of the WPWP and absence of low salinity surface waters in the ITF region might induce different pressure difference between the Pacific and Indian Ocean during the LGM. The density driven flow was discussed in scope of regional model in sections 3.4.4 and 4.4.3. However, large scale changes such as formation of the ITF waters in the North Pacific could not be investigated in the regional model.

Density driven flow is analysed in the global OGCM MOM [Paul and Schäfer-Neth, 2003] and NCAR CSM [*Shin et al*., 2003] simulations for PD and LGM conditions. The areas where Mindanao Current is formed in the subtropical Pacific shows highest values of steric height indicating high pressure. The low pressure region is defined in the East Indian Ocean similar to the regional model experiments.

The steric height difference between MC and IEO relative to 1000 m is larger in NCAR simulation (36.1 ± 8.8 cm) compared to the MOM simulation (25.4 ± 4.2 cm) indicating higher transport. In the LGM simulations the steric height values in the Pacific and Indian Ocean are generally reduced compared to the PD run. However, difference in steric height between MC and IEO in NCAR CSM simulation has higher values (58.3 ± 8.5 cm) compared to the control run even if the ITF transport is reduced, while in the MOM model the values are lower (19.3 ± 4.1 cm).

Reduced difference in density could partly explain reduction in ITF transport in MOM model. This is, however, not true for the NCAR CSM where reduction in ITF transport does not seem to be related to density difference. Simple correlation of the steric height differences and resulting ITF transports is not consistent between the models and the theory requires further revision. Selection of the areas used in calculating the steric height difference could be critical for estimating ITF variations. Therefore, analysis of the water mass characteristics and dynamics of circulation in the North Pacific where ITF is formed and in the East Indian Ocean could give more insight to what extent the ITF is density controlled.

Comparison of LGM model results does not give clear answer what controls the ITF during the LGM. Weakened wind stress forcing over the Pacific could partly explain reduction of the Throughflow transport in the OGCM MOM. However, reduced ITF is found even in the LGM models where glacial change in the wind field is small (NCAR CSM) or not included (UVic). The density difference in the LGM simulations between the West Pacific and East Indian Ocean gives ambiguous results showing reduction of the density driven flow in OGCM MOM, but increase in density difference in NCAR CSM and the regional model. The reduction of the ITF transport could possibly be reflection of weakened global thermohaline circulation in some of the model simulations. However, in scope of tropical climate, the changes in ITF transport might be associated to El-Niño-like conditions in the tropical Pacific during the LGM changing both the wind field and density gradients in the Pacific and Indian Ocean. This aspect needs to be further analysed in the coupled ocean-atmosphere models.

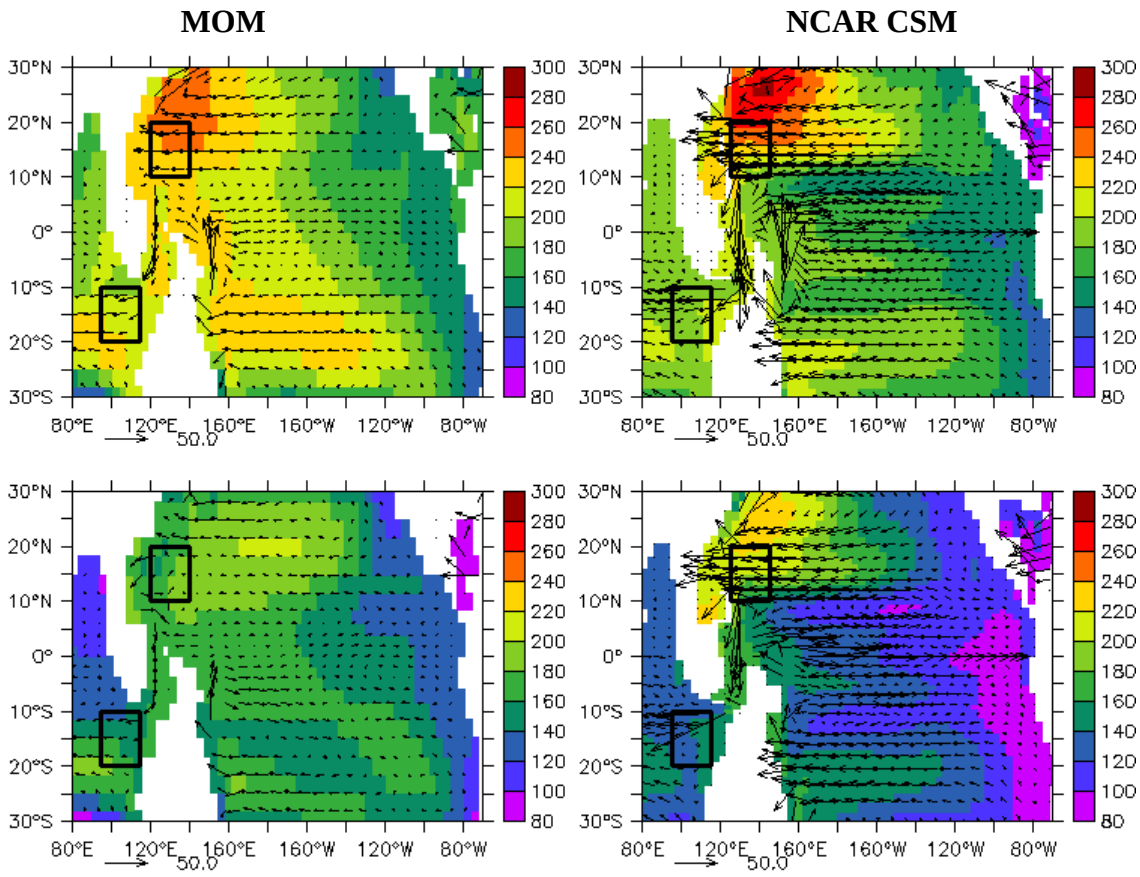

Figure 6-3 Steric height reference to 1000 m and depth integrated velocity field (m^2s^{-1}) with indicated areas (black boxes) used in calculation of pressure difference in the model for PD (top) and LGM (bottom) conditions.

6.6 Application of regional model results in the global model

Most of the climate GCM models used for assessing past climate changes have inadequate representation of the Indonesian Passages due to the low resolution of the models [*Weaver et al.*, 2001; *Shin et al.*, 2003; *Paul and Schäfer-Neth*, 2003]. The Indonesian Gateways are generally represented by a simple deep and wide passage. This leads to large errors in mean volume transport which is usually overestimated compared to observations. As a result, heat and freshwater balance between Pacific and Indian Ocean are compromised.

The regional model estimates 9.3 Sv of mean volume transport within Makassar Strait for PD conditions, which agrees well with observations, and 6.1 Sv for LGM conditions accounting for 75% of the total ITF transport. The topography of the Indonesian Gateways in the low resolution models could be changed to give more realistic ITF transport.

The vertical profile of cumulative transport in OGCM MOM [*Paul and Schäfer-Neth*, 2003] and NCAR CSM [*Shin et al.*, 2003] experiments is compared with the regional model results for PD and LGM simulations (Figure 6-4). The regional model profile shows no significant transport below 1000 m depth, while bulk of the flow can be found above 670 m (550 m in LGM experiment) as the depth of the sill in southern Makassar Strait. In the global simulations deep water transport is much higher and total magnitude of the Throughflow is increased. Correct representation of ITF vertical profile might be important for the Indian Ocean circulation and heat balance and

should be reconsidered in the global LGM experiments. Moreover, the regional model results show shift of the strongest flow from thermocline to surface levels in the LGM experiment which might have additional impact on the Indian Ocean circulation.

The regional model results suggest reversal of seasonality of the transport in Makassar Strait due to the topographic changes during the LGM. This mechanism is not captured in the global LGM simulations. However, it is not well known to what extent changes in seasonal variations of the ITF have impact on ocean and atmospheric circulation.

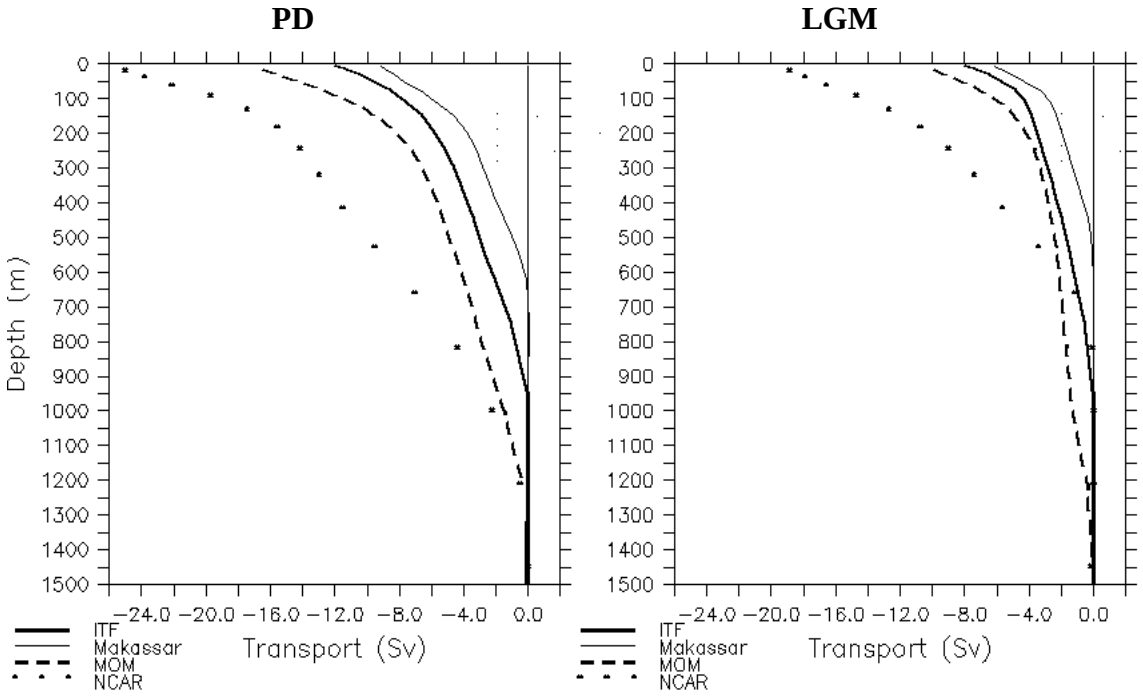

Figure 6-4 ITF cumulative transport (Sv) for PD (left) and LGM (right) boundary conditions from regional model in Makassar Strait (thin), ITF transect (thick), OGCM MOM [*Paul and Schäfer-Neth*, 2003] (dash) and NCAR CSM [*Shin et al.*, 2003] (dot).

In this study, glacial changes in sea surface temperature and salinity could not be investigated with ocean model and atmospheric conditions needed to be prescribed. However, glacial cooling and changes in hydrological cycle are important factors in understanding tropical climate at the LGM. The regional model results suggest strongest impact of the ITF on the surface and thermocline circulation in the Indian Ocean which could be different than the PD considering that the ITF is more surface intensified in the LGM simulation. Possible interactions with the atmosphere remain a task to be investigated in the coupled ocean-atmosphere models.

7. Summary

The focus of this study was on the impact of topographic changes in the Indonesian Gateways on glacial-interglacial time-scales on the Pacific to Indian Ocean water masses exchange. A regional high-resolution model [MITgcm; *Marshall et al.,* 1997a, b] has been employed to investigate ITF dynamics under modern and glacial climate conditions. Sensitivity of the circulation to glacial topographic changes is tested by reducing the bathymetry by 120 m in order to account for the LGM sea level lowering, while LGM simulation included both sea level lowering and glacial boundary forcing. The results from the regional model are compared with global model simulations and data where available and control of the ITF in scope of tropical climate changes during the LGM is discussed. In addition, a Lagrangian particle tracing module is used in order to assess possible changes in particle dispersal during the glacial periods which could provide help in interpretation of paleoclimatic records from the region.

7.1 Present-day ITF dynamics

The bulk of the flow (about 75% of the total ITF volume transport) takes route through Makassar Strait. Deep water flow enters the Indonesian region through the Lifamatola Passage between the Celebes and Halmahera. The mean volume, heat and freshwater transport are directed towards the Indian Ocean. Analysis of water mass characteristics confirms that the ITF transport is fed from the North Pacific (7.1 Sv compared to 2.8 Sv from South Pacific). Even though, the low salinity values of Indonesian surface waters dominate the freshwater transport towards the Indian Ocean, the North Pacific Thermocline characterized by the salinity maximum indicates increase in salt input into the Indian Ocean at the levels between 100–200 m. The contribution of salt input from South Pacific Thermocline is small. The volume transport value of 9.3 ± 1.3 Sv and associated meridional heat transport relative to 0°C of 0.61 ± 0.10 PW agree well with measurements within Makassar Strait [*Gordon et al*., 1999; *Vranes et al.*, 2002]. The flow through Lombok Strait is somewhat overestimated in the model (3.7 ± 0.5 compared to 1.7 ± 1.2 Sv observed [*Murray and Arief*, 1988]) possibly due to the increased width of the passage due to the model resolution. Consequently, the transport through Timor Strait is lower than expected (2.5 Sv compared to observational estimates of 3.4 – 7 Sv [*Creswell et al.*, 1993; *Molcard et al.*, 1996]), while the larger part of the outflow exits through Ombai Strait. Mean transport through Ombai Strait (5.9 ± 1.5 Sv) is in reasonable agreement with observations [5.0 ± 1.0 Sv; *Molcard et al.*, 2001].

The seasonal variations of the flow within Makassar Strait are governed by monsoonal wind changes. The maximum of the flow appears in March during the wind reversal from the NW to the SE monsoon. Throughflow remains strong during the boreal summer (May – August). Minimum flow appears during the boreal winter in the NW monsoon period (November - February). Excluding high frequency and interannual variability, the regional model have similar seasonal variations of the volume transport compared to global model simulation of similar resolution [Cube Sphere MIT ECCO experiment; *Menemenlis et al.*; 2004]. The timing of the maximum of transport in the regional model appears earlier than expected from the global model. However, better agreement is found when variations in transport at the lateral boundaries are included. The seasonal variations in the exit passages show strong outflow during

the SE monsoon phase except for the Timor Strait where strong undercurrent in opposite direction is formed. A maximum positive correlation between Makassar and Lombok transport indicates lag of 1 month of the Lombok Strait transport compared to the Makassar Strait. The flow through Ombai Strait lags the flow in Makassar Strait by 4–5 months, while flow through Timor Strait leads the flow in Makassar Strait by 1–2 months.

The seasonal changes of surface circulation in Makassar Strait agree well with observed monsoonal patterns [*Gordon et al.*, 2003]. From November to February the eastward wind in the Java Sea pushes low salinity water into the southern Makassar Strait. The surface flow is reduced despite southward blowing, along-channel winds because increase in sea surface height in southern Makassar Strait blocks southward flow. Reversal of the wind during the northern hemisphere summer pushes the low-salinity waters back into the Java Sea and allows southward surface layer transport. Even though, surface blocking of the flow is forced by density gradient along the channel, the role of the local winds is important for distributing the buoyant waters.

An additional effect of the buoyant surface water piling up in southern Makassar Strait is the shift of the main flow from the surface into thermocline levels. Maximum of the flow is between 50 and 150 m. The model developed vertical profile of the flow with subsurface maximum agrees well with the observations [*Waworuntu et al.*, 2001; *Gordon et al.*, 2003] indicating highly baroclinic structure. The flow within Makassar Strait is in approximate geostrophic balance except for the region near the equator. The slope of the internal density surfaces forces baroclinic shear in the northward direction at intermediate levels and reduces the thermocline flow. The flow below the sill depth (~ 670 m) in the southern Makassar Strait is almost zero. The geostrophic approximation of the flow seems to be in good agreement with the mean model profile and in this way density field and sea level height within Makassar Strait can be used to estimate the magnitude of the Throughflow. Along-channel gradients in the density field seem to be very small and possible hydraulic control of the flow at the sill is therefore, hard to validate. However, hydraulic control cannot be completely excluded since small density gradients in the equatorial regions could be sufficient to drive the flow. The calculations of the JEBAR term in the model give approximate value of 2.1 ± 0.5 Sv of topographic effects in the Makassar Strait on the ITF transport. However, estimate of the topographic effects is highly dependant on the parameters used in calculation.

The vertical profile of the flow in Lombok Strait the model shows stable outflow throughout the year in contrast with observations [*Murray and Arief*, 1988; *Hautala et al.,* 2001; *Sprintall et al.*, 2003], which show temporary reversals of the flow due to the Ekman transport induced by westward passing cyclones raising the sea level on the Indian side of the Strait or induced Kelvin waves on the eastern Indian Ocean boundary during the monsoon transition periods (November/December, April/May). Even though the model captures well the vertical profile of the flow and part of the seasonal variations, the dynamics of Lombok Strait Throughflow are probably not well represented in the model due to the inadequate representation of topography and simplified forcing that is not sufficient to capture the observed variability.

The flow through Ombai Strait carries mainly surface and intermediate waters towards the Indian Ocean showing main variability of the flow within the upper 150 m. Except high frequency variability, mean seasonal variations of the transport within Ombai Strait are in good agreement with observations [*Sprintall et al.*, 2000; *Hautala et al.* 2001].

Possible reasons for underestimated transport through Timor Strait except overestimated transport through Lombok Strait can be found in closed transport from the northeastern Australian shelf region which does not allow flow through the Arafura Sea that could account for additional, although small, surface transport and possible inadequate representation of the southern boundary as interpolated from the global model. The vertical structure of the flow shows development of surface southward current along the continental shelf during the SE monsoon that continues along the coast of Australia to join the Leuween current. The low salinity surface water is then transported towards the Indian Ocean which corresponds well to observations [*Creswell et al.*, 1993; *Molcard et al.*, 1996]. However, strong surface flow is confined in the upper 30 m and, below the undercurrent in the opposite direction is formed with maximum between 50 and 90 m depth, reducing the net outflow. During the NW monsoon the surface flow is weak and the outflow in subsurface and deep levels dominates.

7.2 ITF during the LGM

With the sea level lowered by 120 m the volume transport within Makassar Strait is not significantly changed. Possible topographic blocking of the flow in Makassar Strait was expected to increase the flow between Sulawesi and New Guinea in the model. However, this was not the case and relative distribution of the total transport between the western (Makassar Strait) and eastern pathway (Sulawesi-New Guinea) remained almost the same. This experiment was repeated with scaling of boundary transport by factors 1.5 and 0.5 in order to test possible sensitivity to the transport magnitude. However, the results were similar showing that Makassar Strait volume transport responds linearly to prescribed total boundary transport and that glacial sea level lowering is not sufficient to reduce the flow within Makassar Strait. The redistribution of the transport appears in the exit passages were transport through Lombok Strait is reduced by about 50% and flow through eastern passages is intensified.

Glacial topographic changes seem to have two important impacts on the ITF. First they modify its seasonal variations and secondly they influence the vertical profile of the flow and related heat transport.

The seasonal variations of the surface flow in Makassar Strait are reversed with the lowering of topography. During NW monsoon phase the flow is intensified since the blocking of the surface flow by low salinity Java Sea waters in southern Makassar Strait is absent. During SE monsoon the flow is decreased due to accumulation of Banda Sea waters in southern Makassar Strait. This result is associated with the topographic changes, but could be further modified under glacial climate conditions. Even though it is not clear to what extent this mechanism can influence the climate system it should be taken into consideration when the local paleoclimatic evidence for the LGM is analysed. So far, no study has been done concerning seasonal interaction of the ITF with surface Indian Ocean circulation or feedbacks with the monsoonal system. Unfortunately, such mechanisms could not be investigated with the ocean model and remain as future task for coupled tropical ocean-atmosphere modelling.

Vertical profile of the flow is surface intensified when the sea level is lowered. The reduction of sill depth in the southern Makassar Strait (from 670 m to 550 m) and absence of low salinity waters when Java Sea is exposed results in shift of the main flow towards the surface. This results in increase in meridional heat transport

towards the Indian Ocean since more surface water is being transported. The net increase in Makassar Strait heat transport is 8.2% compared to the modern simulation. Relatively small changes in ITF vertical profile might lead to significant changes in Indian Ocean circulation and heat balance especially in the upwelling regions [*Song and Gordon*, 2004]. However, the surface temperature signal in the Indian Ocean is expected to be small (maximum 0.05°C in the eastern Indian Ocean) and the net impact on the modern tropical climate is still not clear.

However, increase of heat transport due to the surface intensification of the ITF is small (~0.05 PW) compared to experiment when glacial boundary conditions are applied and the heat transport within Makassar Strait is reduced by 0.18 PW. The reduction is mainly associated with the decrease of volume transport in the LGM simulation. The reduction of volume transport of about 1/3 of the PD value in the glacial boundary conditions is an estimate taken from global LGM model simulation [*Paul and Schäfer-Neth*, 2003] and is not an independent result of the regional model. Since the meridional heat transport depends crucially on the prescribed volume transport, a reliable estimate of the glacial heat transport changes can be achieved only when LGM value of the ITF volume transport is well constrained. So far, regional model results give dependence of the Makassar Strait heat transport to the total volume transport for modern and glacial topography. With given linear relationship of Makassar Strait volume and heat transport to the boundary forcing it is generally possible to estimate total ITF transport from the local measurements or reconstructions.

In the LGM simulation, the seasonal variations in surface circulation in Makassar Strait are similar as in the experiment with lowered sea level giving the strong surface outflow during the NW monsoon phase and weak surface flow during the SE monsoon phase due to the accumulation of the Banda Sea waters in the southern Makassar Strait. Maximum of the transport appears from November to March, while minimum of the transport appears in September. The seasonal cycle of the flow in Lombok Strait shows strong outflow from December to April, while the weak flow appears from August to October. Changes in seasonal cycle in the Lombok Strait correspond to the changes in Makassar Strait seasonality in the LGM simulation giving maximum of the outflow during NW monsoon phase. Variations of transport in Lombok Strait are stronger when LGM forcing is taken into account giving almost no southward flow in August/September. Ombai Strait seasonal cycle of volume transport shows high outflow values from July to November and weak transport from March to May. The timing of strongest and weakest outflow appears during the monsoon transitions and is therefore shifted compared to PD. Timor Strait seasonal cycle shows increase of volume transport during the SE monsoon phase from April to September and decreased during the NW monsoon phase from November to February. With variable total transport at the lateral boundaries, Makassar Strait volume transport is reduced by ~1 Sv compared to the LGM experiment, however seasonal cycle of the transport variations is similar to the LGM simulation.

The mean circulation in the glacial simulation is weaker due to the reduced velocity values prescribed at the lateral boundaries to account for the LGM reduction in transport. The volume transport in the LGM simulation within Makassar Strait is reduced by 34.4% compared to PD value and carries 75.3% of the total ITF transport at the LGM. The volume transport through Lombok Strait does not change compared to the experiment with lowered sea level. However, transport through Ombai Strait is reduced by 37.3% compared to the PD value and Timor Strait transport is decreased compared to the experiment with lowered sea level. However it remains similar to the PD value. Strong northward surface flow is developed near and across the equator

during the SE monsoon. Intensification of the northward surface currents is most likely associated with the LGM wind field applied in the model. Difference in strength of the glacial wind stress between global model simulations [*Lohmann and Lorenz*, 2000; *Shin et al.*, 2003] leads to large differences in amplitude of the ITF. Without further constraints on the glacial wind field, the results of the LGM variability in the ITF should be taken with caution.

The vertical profile of the flow within Makassar Strait shows surface intensification as in the experiment with the lowered sea level, however the intermediate flow is reduced. Geostrophic balance provides a good estimate of the flow suggesting that the ITF transport magnitude at the LGM can be reconstructed from the density field within Makassar Strait. Mean SST in Makassar Strait in the LGM simulation is reduced by 2°C. The deep water temperatures are colder by ~3°C, while changes in the thermocline are small. Salinity values in Makassar Strait are higher by ~0.8 psu and low surface salinity values associated with the presence of the Java waters are absent.

The flow through Lombok Strait is confined in the top 100 m. Mean temperature is reduced by ~ 2°C, while salinity values are higher by ~0.7 psu except for the surface salinity values which are increased by ~1.4 psu compared to PD simulation. The observed low surface salinity values are associated with the strong river runoff in vicinity of Lombok Strait [*Sprintall et al.*, 2000]. River runoff is not included in the model and possible salinity minima at the LGM can not be excluded.

The vertical structure of flow through Timor Strait is changed under glacial conditions. Shelf region and associated coastal currents are absent in the LGM simulation and the flow is confined in the central deep channel. The eastward current through the passage is intensified giving strong surface and intermediate water flow. Surface temperature is cooler by ~2°C, while deep water is colder by of almost 4°C. Thermocline levels show small difference in temperature stratification. Salinity values are higher between 0.9 at the surface to 1.2 psu at the deep levels.

The flow at the TOS transect, that include Timor and Ombai Strait, shows main outflow in the top 200 m. The flow is intensified at the northern part indicating development of coastal current joining SEC. Comparison of the temperature field in the upper 200 m between LGM and PD experiment shows cooling in the surface levels by 2-3°C. Weaker cooling of ~ 1°C appears in the subsurface levels at 80 – 150m. Low salinity values in the LGM experiment are found in the upper 100 m. However, salinity anomaly in the glacial experiment is strongest at the surface (~1 psu) while at 100 m depth salinity change is ~0.6 psu. Salinity maximum of 35.5 psu is found at 120 – 200 m depth.

Analysis of forcing mechanism that control the ITF magnitude did not lead to unique answer to what sets the reduction of the ITF transport during the LGM.

Mean steric height difference between the Pacific and Indian Ocean [*Wyrtki*, 1987; *Andersson and Stigebrandt*, 2004] could not account for the total ITF transport in PD simulation except if the narrow regions of the MC and south of Java coast are taken as reference areas. In the LGM simulation the steric height difference is enhanced (10.9 cm compared to 2.2 cm for PD) suggesting increase in density driven transport. However, net transport in the LGM experiment is reduced compared to PD. The reduction is associated to weaker barotropic flow prescribed on the boundaries and difference in density stratification in the LGM simulation might be result of reduced mixing of Pacific and Indian Ocean water masses. The same method applied in the global LGM simulations showed that small difference in steric height in OGCM MOM [*Paul and Schäfer-Neth*, 2003] could partly account for transport reduction

between the PD and LGM. However, in the NCAR CSM [*Shin et al.*, 2003], the difference in steric height is higher in the LGM simulation compared to PD indicating that other mechanism controls reduction in the ITF in the NCAR LGM simulation. In general, estimates of the ITF magnitude by calculating steric height differences are highly dependant on the region used in calculation and revision of the method should be made by further investigating the water masses properties and circulation in the North Pacific where ITF is formed and in the East Indian Ocean.

Application of the Godfrey's *island rule* to estimate the Throughflow magnitude under glacial climate conditions just partly explained ITF reduction in the global LGM models. The magnitude of the transport in PD simulation is underestimated by approximately 6 Sv in OGCM MOM and NCAR CSM. The errors could be possibly induced by calculation of the wind field on a low resolution horizontal grid. In the OGCM MOM, the glacial wind balance could account for about 5 Sv of ITF transport reduction from 7 Sv simulated with the model. In the NCAR CSM, very small reduction in ITF transport is estimated according to the *island rule* since wind field is similar in PD and LGM experiment. The reduction in NCAR CSM could possibly be associated to weakened meridional overturning circulation at the LGM compared to the modern control run. However, deep-ocean acceleration used during ocean spin-up in the LGM simulation could induce errors in simulating global thermohaline circulation in NCAR CSM model.

Recent theory of El-Niño-like conditions in the tropical Pacific during the LGM [*Otto-Bliesner et al.*, 2003; *An et al.*, 2004] supported with paleoclimatic reconstruction [*Koutavas et al.*, 2002; *Stott et al.*, 2002] could give explanation for the reduced ITF transport. In this case, both glacial changes in wind field and density structure in the Pacific and Indian Ocean should be considered. This aspect needs to be further analysed in the coupled ocean-atmosphere models.

7.3 Particle trajectories and exchange of marine biota

The model simulated particle tracing trajectories for the PD conditions show main pathway of the Throughflow tracers following the route from the NP into CS and through Makassar Strait. Small number of floats (4%) released in CS at 105 m is returning into the Pacific Ocean. The majority of floats (80%) flow southward through Makassar Strait, while the rest of drifters are recirculated within eddies in CS or enter the Sulu Sea. The floats at thermocline levels reach Indian Ocean after 4 months from the release by exiting through Lombok Strait. The thermocline and intermediate drifters pass eastward through Ombai and Timor Strait and reach the Indian Ocean after 4 – 10 months since the release in CS. Only 10% of the surface drifters released in NP reach Indian Ocean in the period of almost 2 years. The number of drifters entering Indian Ocean at thermocline levels (17%) is larger than for the surface drifters indicating high velocities of propagation.

The surface drifters trajectories show strong seasonal variations and recirculation inside Indonesian Seas. The surface floats passing through Makassar Strait enter Java Sea and recirculate around Borneo. The surface floats released in November and January do not propagate through the southern Makassar Strait, but circulate in northern part of the passage and CS or are reflected into the Pacific. The floats released in March and during the SE monsoon phase flow southward through Makassar Strait. This is in agreement with the low salinity blocking of the surface flow in the southern Makassar Strait during the NW monsoon phase. The SP drifters do not seem to propagate

significantly into the Indonesian Seas. Only 2% of the floats enter the Seram Sea near Halamhera at 105 m depth from the SP source with additional 1% of surface floats coming originally from the NP. This is consistent with findings of *Lukas et al.*, [1991] and *Gordon and Fine*, [1996] suggesting the North Pacific source of the ITF and small contribution of South Pacific waters. The SP drifters flow westward towards the Indonesian archipelago, but are reverted near Halmahera into the NECC. The seasonal pattern in float trajectories is in relatively good agreement with observations of surface trajectories in the eastern Indian Ocean [*Michida and Yoritaka*, 1996] showing westward propagation during SE monsoon phase and northward flow during NW monsoon phase. However, the floats released in May in the model experiment are propagating faster and further southwest compared to the observed westward trajectories. Possible reason is applied climatological wind forcing in the model that might differ from the actual winds in given years. The northward trajectories of the drifters released in November are simulated well except for the Lombok Strait where the northward flow is suppressed by the strong southward outflow.

Under glacial climate conditions, the main pathway of the ITF tracers is similar as in the PD simulation, however the velocity of propagation of the floats are reduced. Average velocity of propagation for thermocline floats released in NP is 9.5 cms^{-1} compared to 16.0 cms^{-1} for PD. Number of particles passing through Makassar Strait is reduced by ~20% at the thermocline level. Large percent of the floats exits through Lombok Strait and exchange of particles through Ombai and Timor Strait is similar or just slightly reduced compared to the PD conditions.

When surface trajectories are considered, it needs to be emphasized that particles originating from Makassar Strait do not seem to enter directly into eastern exit passages, but are being pushed back and forth from Flores to Banda Sea by the seasonal wind variations. These results indicate that the reduction in clay minerals as tracers of Throughflow (kaolinite and chlorite) found in Timor Strait sedimentation patterns might be just partly related to the reduced ITF transport at the LGM. Local terrestrial input might play a significant role especially if it is assumed that the clay minerals are mainly entrained into the shallow water masses.

Glacial topographic changes have large impact on seasonal patterns of surface particle distribution. The absence of Java Sea during the LGM leads to reversal of the seasonal cycle in surface circulation within Makassar Strait and weak propagation of surface particles is found during the SE monsoon, while the NW monsoon propagation is expected to be intensified during glacial period. The SE monsoon phase is today characterized by strong ITF transport, while NW monsoon phase is characterized by high precipitation rate and therefore intensified river runoff and increased terrestrial input. If these results are taken into account, the signal of hydrological cycle might be compromised by the blocking of the flow during the SE monsoon phase. These findings should be considered when analysing sedimentation patterns in the Makassar Strait. Unfortunately detailed comparison with sedimentological and micropaleontological evidence could not be made since small number of data from the ITF region is retrieved.

The probability of finding NP and SP drifters in the Indonesian Seas does not seem to be changed during the LGM. The glacial climate conditions at the lateral boundaries could influence this result since same spatial representation of boundary currents is applied, while velocities where uniformly reduced and glacial density stratification is taken into account. However, this might be a realistic estimate considering that only large changes in Gateways configuration such as southward shift of the Halmahera Island would lead to redistribution between NP and SP source [*Cane et al.*, 2001].

8. Conclusions

The aim of this study was to determine the impact of glacial topographic changes in the Indonesian Gateways on volume and heat transport between Pacific and Indian Ocean and its influence on dispersal of marine biota and tracers in the region. The study is based on regional high-resolution MIT GCM results for PD and LGM conditions. The main findings are:

- Makassar Strait carries about 75% of the total ITF transport both under PD and glacial conditions. Glacial sea level lowering does not significantly reduce the volume transport within Makassar Strait. The transport through Lombok Strait is reduced by half and the shallow water transport towards the Indian Ocean is blocked. The main outflow takes route through Ombai and Timor Strait.
- Due to glacial topographic changes, seasonal cycle of the surface flow in Makassar Strait is reversed since the low salinity waters from Java Sea are absent. This results in intensified flow during NW monsoon phase and weak flow during SE monsoon phase.
- Reduced sill depth in southern Makassar Strait and absence of buoyant surface water leads to surface intensified flow under glacial conditions. With the similar volume transport, the heat transport within Makassar Strait is increased by ~ 8%. However, the effect of increase is small if the glacial reduction in volume transport is taken into account resulting in net decrease of heat transport by 30%.
- The magnitude of the ITF transport can be estimated using geostrophic approximation within Makassar Strait. However, regional dynamics seem not to provide explanation what sets the glacial reduction of the ITF.

Analysis of particle tracing trajectories showed that velocity of propagation and exchange of particles through the main passages is generally reduced under glacial climate conditions. Number of thermocline drifters passing through Makassar Strait is reduced by ~20%. Small number surface drifters entering from the North Pacific exit through Lombok in both PD and LGM simulation and are mainly recirculated inside the Indonesian Seas. The presence of surface and thermocline ITF tracers in the eastern exit passages is similar or slightly reduced compared to PD suggesting that glacial-interglacial changes of shallow waters characteristics in Timor Strait reflect local climatic influence. The seasonal pattern of surface trajectories within Makassar Strait is changed under glacial climate conditions indicating reduced exchange of particles within Makassar Strait during the SE monsoon phase and intensified propagation during the NW monsoon which could have effect on sedimentation patterns in the region. Probability of finding particles originating in North Pacific and South Pacific is not significantly changed under glacial conditions.

9. Outlook

The regional ocean model results left unanswered question what controls the ITF magnitude during the LGM. Several aspects could not be addressed with the regional model and need further attention. Response of the ITF to following forcing mechanisms should be considered:

- changes in Pacific wind field during the LGM,
- glacial changes in density stratification in tropical Pacific and Indian Ocean,
- relationship between ITF and possible ENSO like pattern during the LGM,
- glacial changes in global thermohaline circulation.

Although some of the forcing theories have been analysed in this work, the results seem to vary between the models and do not give consistent explanation. A more complete theory is needed for better understanding of ITF dynamics at the LGM.

The regional model results suggest strongest impact of the ITF on surface and thermocline circulation in the Indian Ocean. Possible interactions with atmosphere remain a task to be investigated in the coupled ocean-atmosphere models. However, more realistic representation of the ITF in the low resolution models is necessary for testing the sensitivity of tropical climate system to changes in the ITF. This includes realistic values of transport magnitude, possible changes in seasonality during the LGM and correct representation of vertical profile of the flow which could be more surface intensified due to the sea level lowering.

The ITF dynamics are still a challenge for physical oceanographers and the high resolution model used in this work can be further applied for process studies such as investigating frictional effects, impact of different mixing parameterizations including tides on modifying the water masses properties in the Indonesian Seas [*Hatayama et al.*, 1996; *Susanto et al*., 2000; *Schiller*, 2004]. Some of the short-time scale phenomena could not be captured in the model due to simplified forcing. However, intraseasonal fluctuations due to remote forcing from Indian Ocean [*Sprintall et al*., 2000] and eddies [*Qiu et al*., 1999; *Wijffels et al.*, 2000] could potentially account for large amplitudes of the flow. The performance of the regional model to realistically simulate ITF variability could be further improved by including intraseasonal variations in wind field and boundary conditions.

The regional model gives opportunity for direct comparison of water masses properties in the main passages with paleoclimatic reconstructions of ocean temperature, salinity and thermocline depth during the LGM. For comparison and interpretation of the sedimentological/paleontological data from the region, the simulated circulation in the Indonesian Seas for PD and LGM conditions can be used as a reference for more detailed sediment modelling. This could include analysis of bottom velocities, sedimentation processes such as changes in accumulation rates related to grain size and bottom friction that could be very helpful in data analysis.

10. Appendices

Appendix A List of acronyms

Abbreviation	Replacement Text
AGCM	Atmospheric General Circulation Model
AOGCM	Atmosphere-Ocean General Circulation Model
BA	Bølling – Allerød
CLIMAP	Climate Long Range Investigation, Mapping and Prediction
CS	Celebes Sea
CS	Cube Sphere
CSM	Climate System Model
DBP	Downstream Buoyant Pool
EIO	East Indian Ocean
ENSO	El-Niño Southern Oscillation
HE	Halmahera Eddy
IO	Indian Ocean
IPWP	Indo-Pacific Warm Pool
ITF	Indonesian Throughflow
JEBAR	Joint Effect of Baroclinicity and Relief
LGM	Last Glacial Maximum
MC	Mindanao Current
ME	Mindanao Eddy
MK	Makassar Strait
NECC	North Equatorial Countercurrent
NP	North Pacific
NW	Northwestern
OBC	Open Boundary Conditions
OGCM	Ocean General Circulation Model
PD	Present-day

SE	Southeastern
SEC	South Equatorial Current
SP	South Pacific
SSH	Sea Surface Height
SSS	Sea Surface Salinity
SST	Sea Surface Temperature
THC	Thermohaline Circulation
TOS	Timor and Ombai Strait
TS	Temperature Salinity
WOA	World Ocean Atlas
WP	West Pacific
WPWP	West Pacific Warm Pool
YD	Younger Dryas

Units

1 ky	10^3 years
1 PW	10^{15} W
1 Sv	10^6 m^3s^{-1}

Appendix B Model Formulation

Appendix B.1 Primitive equations

The model formulation is based on the non-hydrostatic form of the incompressible Boussinesq equations in z-coordinates. The following hydrostatic primitive equations are used to describe oceanic motion:

Equations of motion in horizontal:

$$\frac{D\vec{v}_h}{Dt} + f\hat{k} \times \vec{v}_h + \frac{1}{\rho_c}\nabla_z p = \vec{F} \qquad 10\text{-}1$$

Equation of motion in vertical:

$$\varepsilon_{nh}\frac{Dw}{Dt} + \frac{g\rho}{\rho_c} + \frac{1}{\rho_c}\frac{\partial p}{\partial z} = \varepsilon_{nh}F_w \qquad 10\text{-}2$$

Equation of continuity:

$$\nabla_z \cdot \vec{v}_h + \frac{\partial w}{\partial z} = 0 \qquad 10\text{-}3$$

Equation of state:

$$\rho = \rho(\theta, S, p) \qquad 10\text{-}4$$

Equation for potential temperature:

$$\frac{D\theta}{Dt} = Q_\theta \qquad 10\text{-}5$$

Equation for salinity:

$$\frac{DS}{Dt} = Q_S \qquad 10\text{-}6$$

Hydrostatic formulation is achieved by setting $\varepsilon_{nh} = 0$. The ocean properties are defined as following: $\vec{v}_h = (u, v, 0)$ is the horizontal component of velocity, w is the vertical velocity, g is the gravity constant, f is the Coriolis parameter, p is the pressure, ρ is the density of water, ρ_c is a constant reference density, $\vec{F}$ and F_w are the forcing and dissipation terms of velocity in horizontal and vertical respectively, θ is the potential temperature of the ocean, Q_θ are forcing and dissipation of potential temperature, S is the salinity of the ocean and Q_S are the forcing and dissipation of salinity.

11. Bibliography

Adcroft, A.J., Hill, C.N. and J. Marshall, 1997: Representation of topography by shaved cells in a height coordinate ocean model, *Mon. Wea. Rev.*, vol 125, 2293-2315.

An, S.-I., A. Timmermann, L. Bejarano, F.-F. Jin, F. Justino, Z. Liu, and A. W. Tudhope, 2004: Modeling evidence for enhanced El Niño–Southern Oscillation amplitude during the Last Glacial Maximum, Paleoceanography, 19.

Andersson, H. C. 2003: Effects of topography on ocean thermohaline circulation and of climate Variability on Baltic Sea water exchange, Doctoral Thesis, A84 2003, Göteborg University, Sweden, 172 pp.

Andersson, H. C. and A. Stigebrandt 2003: Regulation of the Indonesian throughflow by baroclinic draining of\tab the North Australian Basin, Deep-Sea Res (under revision).

Arief, D., S. P. Murray, 1996: Low-frequency fluctuations in the Indonesian Throughflow through Lombok Strait, *J. Geophys. Res.,*101(C5) 12455-12464.

Barrows, T., & Juggins, S., 2005: Late-glacial maximum sea surface temperatures around the Australian margin and Indian Ocean. Quaternary Science Reviews, 24, 1017-1047.

Barrows, T. T., Juggins, S., De Deckker, P., Thiede, J. and Martinez, J. I., 2000: Sea-surface temperatures of the southwest Pacific Ocean during the last glacial maximum. *Paleoceneanography,* 15(1): 95-109.

Berger, A. L. 1978: Long-term variations of daily insolation and Quaternary climatic changes. J Atmos Sci 35: 2362–2367.

Bingham, F. M., Lukas, R., 1994: The Southward Intrusion of North Pacific Intermediate Water along the Mindanao Coast, *Journal of Physical Oceanography*, 24, 141-154.

Bohren, C. F., and B. A. Albrecht, 1998: Atmospheric Thermodynamics, 402 pp., Oxford Univ. Press, New York.

Broccoli AJ, Marciniak EP, 1996: Comparing simulated glacial climate and paleodata: a reexamination. Paleoceanography 11: 3–14.

Broccoli, A. J. 2000: Tropical cooling at the Last Glacial Maximum:an atmosphere-mixed layer ocean model simulation. J Clim 13:951–976.

Broecker, W.S. 1995: The glacial world according to Wally. Eldigio Press, New York, USA, pp 318.

Burnett, W. H., V. M. Kamenkovich, A. L. Gordon and G. L. Mellor, 2003: The Pacific/Indian Ocean pressure difference and its influence on the Indonesian Seas circulation: Part I - The study with specified total transports. *Journal of Marine Research*, 61(5): 577-611.

Cane, M.A., and P. Molnar, 2001: Closing of the Indonesian seaway as a precursor to east African aridification around 3-4 million years ago, *Nature, 411*, 157-162.

Chong, J. C., J. Sprintall, S. Hautala, W. L. Morawitz, N. A. Bray, and W. Pandoe, 2000: Shallow throughflow variability in the outflow straits of Indonesia, *Geophys. Res. Lett., 27,* 125-128.

Clarke, A.J. and X. Liu, 1993: Observations and dynamics of semiannual and annual sea levels near the eastern equatorial Indian Ocean boundary. *J. Phys. Oceanog.* Vol. 23. p. 386-399.

CLIMAP Project Members, 1981: Seasonal reconstructions of the earth's surface at the Last Glacial Maximum Geological Society of America Map and Chart Series, MC-36, New York.

Conkright, M., S. Levitus, T. O'Brien, T. Boyer, J. Antonov, and C. Stephens, 1998: World Ocean Atlas 1998 CD-ROM Data Set Documentation. Tech. Rep. 15, NODC Internal Report, Silver Spring, MD, 16pp.

Cresswell, G., A. Frische, J. Peterson and Quadfasel, D.R, 1993: Circulation in the Timor Sea. *J. Geophys. Res.* Vol. 98 (C8). p. 7742-7748.

Da Silva, A., A. C. Young, and S. Levitus, 1994: *Atlas of Surface Marine Data 1994*, *Volume 1: Algorithms and Procedures.* NOAA Atlas NESDIS 6, U.S. Department of Commerce, Washington, D.C.

Dannemann, S., B. K. Linsley, D. W. Oppo, Y. Rosenthal, and L. Beaufort, 2003: East Asian monsoon forcing of suborbital variability in the Sulu Sea during Marine Isotope Stage 3: Link to Northern Hemisphere climate, *Geochem. Geophys. Geosyst.*, *4*(1), 1001.

De Deckker, P., N. J. Tapper, and S. Van der Kaars, 2002: The status of the Indo-Pacific Warm Pool and adjacent land at the Last Glacial Maximum, *Global and Planetary Change, 35*, 25-35.

Ewen, T.L.; Weaver, A.J.; and Schmittner, A. 2004: Modelling carbon cycle feedbacks during abrupt climate change. Quaternary Science Reviews 23(3-4):431-448.

Ffield, A., A. Gordon, 1992: Vertical mixing in the Indonesian thermocline. *Journ. of Phys. Oceanog.* Vol.22. pp. 184-195.

Fieux, M., C. André, P. Delecluse, A.G. Ilahude, A. Kartavtseff, F. Mantisi, R. Molcard and J.C. Swallow, 1994 : Measurements within the Pacific-Indian oceans throughflow region. *Deep Sea Res.* Vol. 41. No. 7, p. 1091-1130.

Fine R. A., 1985: Direct evidence using tritium data for the Throughflow from the Pacific into the Indian Ocean, *Nature 315*, 478–480.

Fofonoff, N. P., Millard, J. R., 1983: Algorithms for commutation of fundamental properties of seawater. UNESCO technical papers in marine science 44.

Ganachaud, A., and C. Wunsch, 2003: Large-scale ocean heat and freshwater transports during the World Ocean Circulation Experiment, J. Clim., 16, 696– 705.

Ganachaud, A., Wunsch, C., Marotzke, J., Toole, J., 2000: The meridional overturning and large-scale circulation of the Indian Ocean. *Journal of Geophysical Research*, 105(C11), 26117-26134.

Geyh, M.A., Kudrass, H.-R., Streif, H., 1979: Sea-level changes during the late Pleistocene and Holocene in the Strait of Malacca. *Nature* 278, 441-443.

Gingele, F. X., P. De Deckker, and C.-D. Hillenbrand, 2001: Clay mineral distribution in surface sediments between Indonesia and NW Australia - source and transport by ocean currents, *Mar. Geol., 179,* 135-146.

Gingele, F. X., P. De Deckker, and C.-D. Hillenbrand, 2001: Late Quaternary fluctuations in the Leeuwin Current and palaeoclimates on the adjacent land masses: clay mineral evidence, *Australian J. Earth Sci., 48*, 867-874.

Godfrey, J.S. T.J. Golding, 1981: The Sverdrup Relation in the Indian Ocean, and effect of Pacific-Indian Ocean throughflow on Indian Ocean circulation and on the East Australian Current. *J. Phys. Oceanog.* Vol. 11, p. 771-779.

Godfrey, J.S., 1989: A Sverdrup model of the depth-integrated flow for the world ocean, allowing for island circulations. Geophys. Astrophys. Fluid Dyn, 45, 89-112.

Godfrey, J.S., 1996: The effect of the Indonesian throughflow on ocean circulation and heat exchange with the atmosphere: A review. *J. Geophys. Res.* 101(C5): 12,217-12,238.

Gordon, A. L. and R. D. Susanto, 2001: Banda Sea Surface Layer Divergence, Ocean Dynamics, 52, (1), 2-10.

Gordon, A. L., 2001: Interocean Exchange. In: "Ocean Circulation and Climate", G. Siedler, J.Church and J. Gould (eds.), Academic Press.

Gordon, A. L., Susanto, R. D., & Vranes, K., 2003: Cool Indonesian throughflow as a consequence of restricted surface layer flow. Nature, 425, 824-828.

Gordon, A.L. and R. Fine, 1996: Pathways of water between the Pacific and Indian oceans in the Indonesian seas. *Nature* 379(6561): 146-149.

Gordon, A.L., 1986: Interocean exchange of thermocline water. *J. Geophys. Res.*, 91, 5037-5046.

Gordon, A.L., McClean, J.L., 1999: Thermohaline stratification of the Indonesian Sea: model and observations. *Journal of Physical Oceanography*, 29(2), 198-216.

Gordon, A.L., 1995: When is "Appearance" Reality? Indonesian Throughflow is in fact primarily derived from North Pacific Water Masses. *Journal of Physical Oceanography*, 25(6), 1560-1567.

Gordon, A.L.., Susanto, R.D., Ffield, A., 1999: Throughflow within Makassar Strait. *Geophysical Research Letters*, 26(21), 3325-3328.

Gordon, Arnold L., Claudia F. Giulivi, and A. Gani Ilahude, 2003: Deep topographic barriers within the Indonesian seas. Deep Sea Res. II, 50 (12/13), 2205-2228.

Hanebuth, T., K. Stattegger, and P.M. Grootes, 2000: Rapid flooding of the Sunda Shelf - a late glacial sea-level record, *Science, 288*, 1033-1035.

Hanebuth, T.J.J., Stattegger, K., Schimanski, A., Lüdmann, T., Wong, H.K., 2003: Late Pleistocene forced regressive deposits on the Sunda Shelf (SE Asia). *Marine Geology* 199, 139-157.

Hatayama, T., T. Awaji, K. Akitomo, 1996: Tidal currents in the Indonesian Seas and their effect on transport and mixing, *J. Geophys. Res., 101* 12353-12373 .

Hautala, S. L., J. Sprintall, J. T. Potemra, A. G. Ilahude, J. C. Chong, W. Pandoe, and N. Bray, 2001: Velocity structure and transport of the Indonesian throughflow in the major straits restricting flow into the Indian Ocean. *J. Geophys. Res.*, submitted.

Hautala, S., J. Reid and N. Bray, 1996: The distribution and mixing of Pacific water masses in the Indonesian Seas. *J. Geophys. Res.* 101(C5):12375-12389.

Hautala, S., J. Reid and N. Bray, 1996: The distribution and mixing of Pacific water masses in the Indonesian Seas. *J. Geophys. Res.* 101(C5):12375-12389.

Herbaut C., J. Sirven and A. Czaja, 2001: An idealized model study of the mass and heat transports between the subpolar and subtropical gyres. *Journal of Physical Oceanography*, vol.31, pp. 2903-2916.

Hesp, P.A., Hung, C.C., Hilton, M., Ming, C.L., Turner, I.M., 1998: A first tentative Holocene Sea-level curve for Singapore. *J. Coast. Res*. 14, 308-314.

Hewitt, C. D., A. J. Broccoli, J. F. B. Mitchell and R. J. Stouffer, 2001: A coupled model study of the last glacial maximum: Was part of the North Atlantic relatively warm? Geophysical Research Letters, 28, 1571-1574.

Hewitt, C. D., R. J. Stouffer, A. J. Broccoli, J. F. B. Mitchell, and P. J. Valdes, 2003: The effect of ocean dynamics in a coupled GCM simulation of the Last Glacial Maximum. Climate Dynamics, 20(2/3), 203-218.

Hirst, A.C. and J.S. Godfrey, 1993: The role of Indonesian throughflow in a global ocean GCM. *J. Phys. Oceanog.* Vol. 23. p. 1057-1086.

Hirst, A.C. and J.S. Godfrey, 1994: The response to a sudden change in Indonesian throughflow in a global ocean GCM. *J. Phys. Oceanog.* Vol. 24. pp. 1895-1910.

Huang, B., and V. M. Mehta, 2004: Response of the Indo-Pacific warm pool to interannual variations in net atmospheric freshwater, *J. Geophys. Res.*, 109.

Huthnance, J. M. 1984**:** Slope currents and 'JEBAR'. *Journal of Physical Oceanography*, 14, 795-810.

Ilahude, A. G., A. L. Gordon, 1996: Themocline stratification within the Indonesian Seas, *J. Geophys. Res.,* 101(C5) 12401-12409.

Kalnay, E. et al., 1996: "The NCEP/NCAR 40-year reanalysis project," Bulletin of the American Meteorological Society.

Kamenkovich, V. M., W. H. Burnett, A. L. Gordon and G. L. Mellor, 2003: The Pacific/Indian Ocean pressure difference and its influence on the Indonesian Seas circulation: Part II - The study with specified sea-surface heights. *Journal of Marine Research*, 61(5): 613-634.

Kim, S. J., G. M. Flato, and G. J. Boer, 2003: Acoupled climate model simulation of the last glacial maximum, part 2: Approach to equilibrium, Clim. Dyn., 20, 635–661.

Kim, S.-J., G. Flato, G. Boer, and N. McFarlane, 2002: A coupled climate model simulation of the Last Glacial Maximum, Part 1: Transient multi-decadal response,Climate Dynamics, 19, 515-537.

Kitoh, A., S. Murakami, and H. Koide, 2001: A simulation of the Last Glacial Maximum with a coupled atmosphere-ocean GCM, Geophys. Res. Lett., pp. 2221–2224.

Koutavas, Athanasios, Lynch-Stieglitz, Jean, Marchitto, Thomas M., Jr., Sachs, Julian P., 2002: El Nino-Like Pattern in Ice Age Tropical Pacific Sea Surface Temperature, *Science* 297: 226-230.

Kucera, M., Rosell-Melè, A., Schneider, R., Waelbroeck, C., Weinelt, M., 2005: Multiproxy approach for the reconstruction of the glacial ocean surface (MARGO). *Quaternary Science Reviews*, 24(7-9): 813-819.

Kuhnt, W., Holbourn, A., Hall, R., Zuvela, M., and Käse, R., 2004: Neogene history of the Indonesian throughflow. In Clift, P.D., Wang, P., Hayes, D., and Kuhnt, W. (Eds.), Continent-Ocean Interactions in the East Asian Marginal Seas. Am. Geophys. Union, Geophys. Monogr., 149.

Lambeck, K., Y. Yokoyama, A. Pucell, and P. Johnston, 2002: Reply to the comment by W.R. Peltier, *Quat. Sci. Rev., 21*, 415-418.

Lea, D. W., D. K. Pak, and H.J. Spero, 2000: Climate Impact of Late Quaternary Equatorial Pacific Sea Surface Temperature Variations, *Science, 289,* 1719-1724.

Liu, Z., S. Shin, B. Otto-Bliesner, J. E. Kutzbach, E. C. Brady, and D. E. Lee, 2002: Tropical cooling at the Last Glacial Maximum and extratropical ocean ventilation. *Geophys. Res. Lett.*, 29(10), 1409.

Liu, Z., S. Shin, P. Behling, W. Prell, M. Trend-Staid, S.P. Harrison, and J.E. Kutzbach, 2000: Dynamical and observational constraints on tropical Pacific sea surface temperatures at the last glacial maximum, Geophysical Research Letters, 27, 105-108.

Lohmann, G., and Lorenz, S., 2000: On the hydrological cycle under paleoclimatic conditions as derived from AGCM simulations. Journal of Geophysical Research, 105, no. D13, 17,417-436.

Lukas, R., E. Firing, P. Hacker, P. L. Richardson, C. A. Collins, R. A. Fine, R. Gammon, 1991: Observations of the Mindanao Current during the Western Equatorial Pacific Ocean Circulation Study, *J. Geophys. Res.,* 96, 7089-7104.

Maier-Reimer, E., U. Mikolajewicz, K. Hasselmann, 1993: Mean Circulation of the Hamburg LSG OGCM and Its Sensitivity to the Thermohaline Surface Forcing*, Journal of Physical Oceanography* 23, 731-757.

Manabe S, Broccoli AJ, 1985: The influence of continental ice sheets on the climate of an ice age. J Geophys Res 90: 2167–2190.

Marshall, J., A. Adcroft, C. Hill, L. Perelman, and C. Heisey, 1997a: A finite volume, incompressible Navier Stokes model for studies of the ocean on parallel computers, *J. Geophys. Res.*, 102, 5753-5766.

Marshall, J., C. Hill, L. Perelman, and A. Adcroft, 1997b: Hydrostatic, quasi-hydrostatic and nonhydrostatic ocean modeling, *J. Geophys. Res.*, 102, 5733-5752.

Martinez, J. I., P. De Deckker, and A. R. Chivas, 1997: New estimates for salinity changes in the Western Pacific Warm Pool during the Last Glacial Maximum: oxygen isotope evidence, *Mar. Micropaleontol., 32*, 311-340.

Martinez, J. I., P. De Deckker, and T. T. Barrows, 1999: Palaeoceanography of the last glacial maximum in the eastern Indian Ocean: planktonic foraminiferal evidence, *Palaeogeogr., Palaeoclimatol., Palaeoecol., 147,* 73-99.

Martinez, J. I., P. De Deckker, and T. T. Barrows, 2002: Palaeoceanography of the Western Pacific Warm Pool during the Last Glacial Maximum: Long-term climatic monitoring of the Maritime Continent*, in Bridging Wallace's Line* edited by P. Kershaw, B. David, N. Tapper, D. Penny, and J. Brown. Advances in Geoecology 34, Catena-Verlag, Reiskirchen, Germany, 147-172.

Menemenlis, D., C. Hill, A. Adcroft, J. Campin, B. Cheng, B. Ciotti, I. Fukumori, P. Heimbach, C. Henze, A. Koehl, T. Lee, D. Stammer, J. Taft, J. Zhang, 2004: Towards eddy permitting estimates of the global-ocean and sea-ice circulations. *Eos Trans*. AGU, in press.

Menemenlis, D., I. Fukumori, A. K□ohl, T. Lee, and D. Stammer, 2004: The impact of ECCO surface forcing fields on the results of a global 1/4-deg model, *The ECCO Report Series 30*, Scripps Instituttion of Oceanography, 2004a.

Meyers, G., 1996: Variation of the Indonesian throughflow and the El Nińo-Southern Oscillation. *J. Geophys. Res.* Vol. 101. No. C5, p. 12 255-12 263.

Meyers, G., R.J. Bailey and A.P. Worby, 1995: Geostrophic transport of Indonesian throughflow. *Deep Sea Res.* Vol. 42. No. 7, p. 1163-1174.

Michida, Y, and H. Yoritaka, 1996: Surface currents in the area of the Indo-Pacific throughflow and in the tropical Indian Ocean observed with surface drifters. *J. Geophys. Res.* 101(5): 12 475-12 482.

Miyama, T., Awaji, T., Akitomo, K., Imasato, N., 1995: Study of seasonal transport variations in the Indonesian Seas *Journal of Geophysical Research*, 100(C10), 20517-20541.

Miyama, Toru, Toshiyuki Awaji, Kazunori Akitomo, and Norihisa Imasato, 1996: A Lagrangian Approach to the Seasonal Variation of Salinity in the Mixed Layer of the Indonesian Seas. *Journal of Geophysical Research*, 101, 12,265-12,285.

Molcard, R., A.G. Ilahude, M. Fieux, J.C. Swallow, and J. Banjarnahor, 1994: Low frequency variability of the currents in Indonesian Channels (Savu-Roti M1 and Roti-Ashmore Reef M2). Deep Sea Res., 41, 1643-1662.

Molcard, R., M. Fieux, and A.G. Ilahude, 1996: The Indo-Pacific throughflow in the Timor Passage, *J. Geophys. Res., 101* (C5), 12411-12420.

Molcard, R., M. Fieux, and F. Syamsudin, 2000: The throughflow within Ombai Strait, *Deep-Sea Res., I 48*, 1237-1253.

Molcard, R., M. Fieux, and F. Syamsudin, 2001: The Throughflow within Ombai Strait, Deep-sea Res., I, 48, 1237-1253.

Molcard, R., M. Fieux, J. C. Swallow, A. G. Ilahude, and J. Banjarnahor, 1994: Low frequency variability of the currents in Indonesian Channels, *Deep-Sea Res., 41*, 1643-1661.

Müller, A., and B. N. Opdyke, 2000: Glacial-interglacial changes in nutrient utilization and paleoproductivity in the Indonesian Throughflow sensitive Timor Trough, easternmost Indian Ocean, *Paleoceanography, 15*, 85-94.

Murray, S. P., and D. Arief, 1988: Throughflow into the Indian Ocean through the Lombok Strait. January 1985-January 1986, *Nature, 333*, 444-447.

Murray, S.P., D. Arief, J.C. Kindle, and H.E. Hurlburt, 1989: Characteristics of circulation in an Indonesian Archipelago Strait from hydrography, current measurements and modeling results. NATO Advanced Research Workshop on the Physical Oceanography of Sea Straits, Les Arcs, Kluwer Academic Publishers.

Murtugudde, R., A.J. Busalacchi and J. Beauchamp, 1998: Seasonal to interannual effects of the Indonesian throughflow on the tropical Indo-Pacific basin. *J. Geophys. Res.*, Vol.103., C10, p.21 425-21 441.

NOAA, 1998: Data Announcement 88-MGG-02, Digital relief of the Surface of the Earth. National Geophysical Data Center, Boulder, Colorado.

Oppo, D. W., B. K. Linsley, Y. Rosenthal, S. Dannemann and L. Beaufort, 2003: Orbital and suborbital climate variability in the Sulu Sea, western tropical Pacific, *Geochem. Geophys. Geosystems (G3), 4*(1).

Otto-Bliesner, B. L., E. C. Brady, S. Shin, Z. Liu, and C. Shields, Modeling El Nino and its tropical teleconnections during the last glacial-interglacial cycle, *Geophys. Res. Lett.*, 30 (23), 2198, 2003.

Paul, A. and C. Schäfer-Neth, 2003: Modeling the water masses of the Atlantic Ocean at the Last Glacial Maximum, *Paleoceanography, 18*, 1058.

Peltier, W.R . 1994: Ice age paleotopography. Science 265: 195–201.

Peltier, W.R., 2002: Comments on the paper of Yokoyama et al. (2000), entitled "Timing of the Last Glacial Maximum from observed sea level minima", *Quat. Sci. Rev., 21*, 409-414.

Pinot S, Ramstein G, Harrison SP, Prentice IC, Guiot J, Stute M, Joussaume S, 1999: Tropical paleoclimates at the Last Glacial Maximum: comparison of paleoclimate modeling intercomparison project (PMIP) simulations and paleodata. Clim Dyn 15: 857–874.

Potemra, J.T., R. Lukas and G.T. Mitchum, 1997: Large-scale estimation of transport from the Pacific to the Indian Ocean. *Journ. Geophys. Res.* Vol. 102. No. C13, p.27 795-27 812.

Potemra, James T., Susan L. Hautala, and Janet Sprintall, 2003: Vertical structure of Indonesian throughflow in a large-scale model. Deep Sea Res. II, 50 (12/13), 2143-2161.

Press, W. H., Teukolsky, S. A., Vetterling, W.T., and Flannery, B. P., 2002: Numerical Recipes in C, 2nd ed., *Cambridge University Press*, Cambridge, MA.

Qiu, B., M. Mao, and Y. Kashino, 1999: Intraseasonal variability in the Indo-Pacific Throughflow and the regions surrounding the Indonesian Seas. *J. Phys. Oceanogr.*, 29, 1599--1618.

Quadfasel, D.R. and G. Cresswell, 1992: A note on the seasonal variability of the South Java Current. *J. Geophys. Res.,* 97, 3685 - 3688.

Reimer, P.J., Baillie, M.G.L., Bard, E., Bayliss, A., Beck, J.W., Bertrand, C.J.H., Blackwell, P.G., Buck, C.E., Burr, G.S., Cutler, K.B., Damon, P.E., Edwards, R.L., Fairbanks, R.G., Friedrich, M., Guilderson, T.P., Hogg, A.G., Hughen, K.A., Kromer, B., McCormac, F.G., Manning, S.W., Ramsey, C.B., Reimer, R.W., Remmele, S., Southon, J.R., Stuiver, M., Talamo, S., Taylor, F.W., van der Plicht, J., and Weyhenmeyer, C.E. 2004. IntCal04 Terrestrial radiocarbon age calibration, 26 - 0 ka BP. Radiocarbon 46, 1029-1058.

Ribbe, J., M. Tomczak, 1997: Effect of the Missing Indonesian Throughflow in the Fine Resolution Antarctic Model. *Journal of Physical Oceanography*: Vol. 27, No. 3, pp. 445–455.

Rosenthal, Y., D. W. Oppo, and B. K. Linsley, 2003: The amplitude and phasing of climate change during the last deglaciation in the Sulu Sea, western equatorial Pacific, *Geophys. Res. Lett., 30*, 1428, doi:10.1029/2002GL016612), 11-1 to 11-4.

Schäfer-Neth C., Paul A., 2003: The Atlantic Ocean at the last glacial maximum: 1. Objective mapping of the GLAMAP sea-surface conditions. In: Wefer G., Mulitza S., and Ratmeyer V. (eds) The South Atlantic in the Late Quaternary: Material Budget and Current Systems, Springer, Berlin, 531-548

Schiller, A., 2004 : Effects of explicit tidal forcing in an OGCM on the water mass structure and circulation in the Indonesian Throughflow region, *Ocean Modeling*, 6, 31-49.

Schiller, A., J. S. Godfrey, P. C. McIntosh, G. Meyers, S. E. Wijffels, 1998: Seasonal Near-Surface Dynamics and Thermodynamics of the Indian Ocean and Indonesian Throughflow in a Global Ocean General Circulation Model. *Journal of Physical Oceanography*: Vol. 28, No. 11, pp. 2288-2312.

Schiller, A., S. Godfrey, P. McIntosh, G. Meyers, 1996: A Global Ocean General Circulation Model for climate variability studies. *CSIRO Division of Marine Research Report.* pp56.

Schneider, N. and T.P. Barnett, 1997: Indonesian Throughflow in a coupled general circulation model. *J. Geophys. Res.* Vol.102, No.C6, p.12341-12358.

Schneider, N., 1998: The Indonesian Throughflow and the global climate system. *Journ. of Climate.* Vol.11, p.676-689.

Shin, S., Z. Liu, B. L. Otto-Bliesner, E. C. Brady, J. E. Kutzbach, and S. P. Harrison, 2003: A simulation of the Last Glacial Maximum climate using the NCAR-CCSM. *Clim. Dyn.*, 20, 127-151.

Siedler, G., Church, J., Gould, J.W., 2001: Ocean Circulation and Climate - Observing and Modeling the Global Ocean . San Diego, USA; London, UK : Academic Press, 715 pp.

Song, Q., and A. L. Gordon, 2004: Significance of the vertical profile of the Indonesian Throughflow transport to the Indian Ocean, *Geophys. Res. Lett.*, *31*, L16307.

Song, Q., Gordon, A. L., Visbeck, M., 2004: Spreading of the Indonesian Throughflow in the Indian Ocean, *Journal of Physical Oceanography*, 34, 772-792.

Sprintall, J., A. L. Gordon, R. Murtugudde and R. D. Susanto, 2000: A semiannual Indian Ocean forced Kelvin wave observed in the Indonesian seas in May 1997. J. Geophys. Res., 105, 17217-17230.

Sprintall, J., J.T. Potemra, S.L. Hautala, N.A Bray and W.W. Pandoe, 2003: Temperature and salinity variability in the exit passages of the Indonesian Throughflow. *Deep-Sea Res. II*, 50, 2183-2204.

Stammer D., C. Wunsch, R. Giering, C. Eckert, P. Heimbach, J. Marotzke, A. Adcroft, C.N. Hill and J. Marshall, 2003: Volume, heat, and freshwater transports of the global ocean circulation 1993-2000, estimated from a general circulation model constrained by World Ocean Circulation Experiment (WOCE) data. *Journal of Geophysical Research-Oceans*, vol.108.

Stammer, D., C. Wunsch, R. Giering, C. Eckert, P. Heimbach, J. Marotzke, A. Adcroft, C.N. Hill and J. Marshall, 2003: Volume, heat and freshwater transports of the global ocean circulation 1993 -2000, estimated from a general circulation model constrained by World Ocean Circulation Experiment (WOCE) data . J. Geophys. Res., 108, C1 3007.

Steinke, S., Kienast, M., Hanebuth, T.J.J., 2003: On the significance of sea-level variations and shelf palaeo-morphology in governing sedimentation in the southern South China Sea during the last deglaciation. *Mar. Geol.*, 201,179-206.

Stewart, R. H., 2002: Introduction to Physical Oceanography, Open Source Textbook.

Stott, L., C. Poulsen, S. Lund, and R. Thunell, 2002: Super ENSO and global climate oscillations at millennial time scales, *Science, 297,* 222-226.

Stuiver, M., Grootes, P.M., Braziunas, T.F., 1995: The GISP2 N18O climate record of the past 16,500 years and the role of the Sun, ocean, and volcanoes. Quat. Res. 44, 341-354.

Susanto, R.D. and A.L.Gordon 2004: Velocity and transport of Indonesian throughflow in Makassar Strait, *J. Geophys. Res.* (In Press)

Susanto, R.D., Gordon, A.L., Sprintall, J., Herunadi, B. 2000: Intraseasonal variability and tides in Makassar Strait. *Geophysical Research Letters*, 27(10), 1499-1502.

Timmermann, A., F. Justino, H. Goosse, and F.-F. Jin, 2004: Surface temperature control in the North and tropical Pacific during the last glacial period, Clim. Dyn., 23, 353–370.

Tomczak, M. and J.S. Godfrey, 1994: Regional Oceanography : An Introduction. *Pergamon.* Pp. 422.

van Aken, H. M, J. Punjanan and S. Saimima, 1988: Physical aspects of the flushing of the East Indonesian basins. *Neth. J. Sea Res.* 22, 315-339.

van der Kaars, S., 2001: Pollen distribution in marine sediments from the south-eastern Indonesian waters. *Palaeogeography, Palaeoclimatology, Palaeoecology,* 171: 341-361.

van der Kaars, S., Wang, X., Kershaw, A.P., Guichard, F. and Setiabudi, D.A., 2000: Late Quaternary palaeoecological record from the Banda Sea, Indonesia: patterns of vegetation, climate and biomass burning in Indonesia and northern Australia. *Palaeogeography, Palaeoclimatology, Palaeoecology,* 155: 135-153.

Visser, K, Thunell, R., and Stott**,** L., 2003: Magnitude and timing of temperature change in the Indo-Pacific warm pool during deglaciation. *Nature*, 421, 152-155.

Visser, K., R. Thunell, and L. Stott, 2003: Magnitude and timimg of temperature change in the Indo-Pacific warm pool during deglaciation, *Nature, 421,* 152-155.

Vranes, K., A.L. Gordon, and A. Ffield., 2002: The heat transport of the Indonesian Throughflow and implications for the Indian Ocean heat budget. *Deep-Sea Res., II, 49*, 1391-1410.

Wajsowicz, R. C., Gordon, A. L., Ffield, A., Susanto D. R., 2003: Estimating transport in Makassar Strait, Deep-Sea Research II, 50, 2163-2181.

Wajsowicz, R. C., Schopf, P. S., 2001: Oceanic Influences on the Seasonal Cycle in Evaporation over the Indian Ocean. *Journal of Climate*: Vol. 14, No. 6, pp. 1199–1226.

Wajsowicz, R.C., 1993: A simple model of the Indonesian throughflow and its composition. *J. Phys. Oceanog.* Vol. 23. No.12, p.2683-2703.

Wajsowicz, R.C., 1993: The Circulation of the depth-integrated flow around an island with application to the Indonesian throughflow. *J. Phys. Oceanog.* Vol. 23. No.7, p.1470-1484.

Wajsowicz, R.C., 1994: A relationship between interannual variations in the South Pacific wind stress curl and the Indonesian throughflow, and the West Pacific warm water pool. *J. Phys. Oceanog.* Vol. 24. No.10, p.2180-2187.

Wajsowicz, R.C., 1995: The response of the Indo-Pacific throughflow to interannual variations in the Pacific wind stress. Part1: Idealized geometry and variations. *J. Phys. Oceanog.* Vol. 25. No.8, p.1805-1826.

Wajsowicz, R.C., and E. K. Schneider, 2001: The Indonesian throughflow's effect on global climate determined from the COLA coupled climate system, *J. of Climate,* 14, 3029-3042.

Wajsowicz, R.C., 1996: The response of the Indo-Pacific Throughflow to interannual variations in the Pacific wind stress. Part II: Realistic geometry and ECMWF wind stress anomalies for 1985-89. *Journal of Physical Oceanography*, 26(12), 2589-2610.

Waworunto, J.M., Garzolli, S.L., Olson, D.B., 2001: Dynamics of Makassar Strait. *Journal of Marine Research*, 59(2), 313-325.

Weaver, A. J., et al., 2001: The UVic Earth system climate model: model description, climatology, and applications to past, present, and future climates, Atmos. Ocean, 39, 361–428.

Wijffels, S. E., N. A. Bray, S. Hautala, G. Meyers, and W.M.L. Morawitz, 1996: The WOCE Indonesian throughflow repeat hydrography sections: I10 and IR6. *International WOCE Newsletter*, No. 24, 25-28.

Wijffels, S. E., R. W. Schmitt, H. Bryden, and A. Stigebrand, 1992: Transport of freshwater by the ocean, *J. Phys. Oceanogr*., 22, 155– 162.

Wijffels, S., 2001: Ocean transport of fresh water, Ocean Circulation and Climate, G. Siedler, J. Church and J. Gould, Eds., Academic Press, 475–488.

Wyrtki, K., 1961: Physical Oceanography of the Southeast Asian Waters, Scripps Institution of Oceanography, NAGA Report, 2, pp. 195.

Wyrtki, K., 1961: Physical oceanography of the southeast Asian waters. Univ. Calif., NAGA Rept., No. 2, 195 pp.

Wyrtki, K., 1987: Indonesian throughflow and the associated pressure gradient, *J Geophys. Res., 92*(C12), 12941-12946.

Yokoyama, Y., K. Lambeck, P. De Deckker, P. Johnston, L.K. Fifield, 2000: Timing of last glacial maximum from observed sea level minima, *Nature 406,* 713-716.

Erklärung

Hiermit erkläre ich, daß diese Arbeit meine eigene Arbeit ist, die ich, abgesehen von den Beiträgen meiner akademischen Lehrer, selbständig und nur unter Verwendung der angegebenen Hilfsmittel verfaßt habe. Sie hat weder ganz noch in Teilen einer Prüfungskommission vorgelegen.

Kiel, den 17. April, 2006

Maja Žuvela

Neogene History of the Indonesian Throughflow

Wolfgang Kuhnt and Ann Holbourn

Institut für Geowissenschaften, Christian-Albrechts-Universität zu Kiel, Germany

Robert Hall

SE Asia Research Group, Department of Geology, Royal Holloway University of London, UK

Maja Zuvela and Rolf Käse

Research Unit Impact of Gateways on Ocean Circulation, Climate and Evolution, Christian-Albrechts-Universität zu Kiel, Germany

The Indonesian Throughflow acts as a major switchboard in the global thermohaline circulation, and its variability is strongly related to tropical climate dynamics on shorter and longer timescales. During the Holocene and Pleistocene, fluctuating sea surface temperature and salinity patterns in the Western Pacific Warm Water Pool and Indonesian Seas and variations in East Asian monsoon strength mainly controlled the intensity and hydrological characteristics of the throughflow. Additionally, glacial/deglacial sea-level change strongly influenced throughflow volume in shallow sections of many passages (i.e. the southern part of the Timor passage on the NW Australian shallow shelf) thus altering the related heat transfer between oceans.

The tectonic history of the Indonesian Gateway ultimately controlled the long-term evolution of the throughflow. During the Pliocene, changes in the position and geometry of the inflow passages (Mindanao Passage to the North and Halmahera Passage to the south) in relation to the tropical Pacific front significantly modified the climatic role of the tropical Indian and Pacific Oceans, resulting in reduced atmospheric heat transport from the tropics to high latitudes. However, the precise timing of major restriction in the surface and thermocline water flow is difficult to ascertain. The early evolution of the Indonesian Gateway was characterized by tectonic restriction of the deep water pathway between the Pacific and Indian Oceans at approximately 25 Ma. By the early Miocene, the Indonesian Gateway was already closed as a deep water pathway between the Pacific and Indian Oceans.

INTRODUCTION

Impact of Indonesian Throughflow and West Pacific Warm Pool on Global Climate and Circulation

Today, the West Pacific Warm Pool (WPWP) plays a key role in regulating the heat budget of the Earth [*Bjerknes*, 1969;

Continent–Ocean Interactions Within East Asian Marginal Seas
Geophysical Monograph Series 149

10.1029/149GM16

Wyrtki, 1981, 1987; *Bastacov*, 1996; *Patrick and Thunell*, 1997; *Webb et al.*, 1997]. The western continuation of the WPWP gives rise to the Indonesian Throughflow (IT), a narrow band of warm, low-salinity water that transports excess heat and freshwater from the Pacific to the Indian Ocean through the Indonesian Gateway [*Yan et al.*, 1992; *You and Tomczak*, 1993; *Gordon and Fine*, 1996]. The present day IT transports on yearly average 10–15 Sv (1 Sv=10^6 m^3 s^{-1}) of warm, low-salinity water from the WPWP and the Indonesian-Malaysian archipelago into the eastern Indian Ocean [*Chong et al.*, 2000; *Ganachaud and Wunsch*, 2000]. The IT is regarded as one of the major switchboards in the global thermohaline circulation, and its variability influences the global climate on short term (ENSO-related) and longterm timescales [e.g., *Schott and McCreary*, 2001; *Gordon et al.*, 2003].

The variability of the IT is closely related to fluctuations in the intensity, geographic extent and position of the WPWP. The development of the WPWP and the related intensity of the IT probably play a significant role, although not yet fully understood, in the early stages of the El Niño-Southern Oscillation (ENSO) [*Yan et al.*, 1992; *Meyers*, 1996]. During ENSO events, western Pacific sea-level is lowered due to strong westerly equatorial winds in the Pacific and the throughflow becomes reduced. During these periods extremely cold sea surface temperatures (SSTs) and a shallow thermocline are observed along the Indian Ocean coasts of Java, Timor and Sumatra [*Meyers*, 1996].

The heat export from the Pacific into the Indian Ocean substantially affects atmosphere-ocean coupling in the tropical Pacific and Indian Oceans and on a global scale. Coupled ocean models [*Schneider*, 1998; *Wajsowicz and Schneider*, 2001] indicate, that during periods of intensified throughflow, the center of the WPWP moves westward. Thus, changes in IT intensity would not only drive changes in global atmospheric circulation and affect mid-latitude wind systems, but would also influence interannual climate anomalies, such as the ENSO and southeast Asian monsoon systems [*Nichols*, 1984; *Webster*, 1998]. Throughflow related SST anomalies in the tropical Indian Ocean are additionally related to wind and precipitation anomalies that may have implications on the longterm variability of the Indian and Australasian monsoons and lead to severe floods in eastern Africa and droughts in Indonesia [*Wajsowicz*, 2002; *Sprintall et al.*, 2003].

Tectonic History of the Indonesian Gateway and Paleoceanographic Implications

The Indonesian gateway represents one of the three critical zonal tropical ocean passages, which strongly influenced global ocean circulation in the late Mesozoic, Paleogene and Neogene. Opening and closure of these gateways were associated with dramatic changes in the global thermohaline circulation [e.g., *Kennett et al.*, 1985; *Bice et al.*, 2000]. The Panama and Tethys Gateways are now closed, but the Indonesian Gateway is still open for surface and intermediate water circulation. Thus, the tectonic and oceanographic history of the SE Asia–Australia collision zone is of considerable importance for understanding regional and global climate change during the Neogene. Specifically, constraining the timing of major tectonic and oceanographic changes within this region is critical for understanding the role of the Indonesian Gateway in long term Cenozoic climate evolution as well as the expansion of the WPWP and the ENSO-system. However, the tectonic history of this gateway did not follow a simple unidirectional path of convergence and closure. Tectonic changes have included collision and mountain building, but also extension and formation of new ocean basins in eastern Indonesia (Figures 1, 2). The critical plates are those of SE Asia, India–Australia and the Philippine Sea, and the crucial region lies between Borneo and the Bird's Head of New Guinea, including the islands of Sulawesi and the Banda arc. The relevant time interval comprises the last 30 million years, when tectonic processes led to significant changes in the distribution of land and sea and in particular in the configuration of deep-water passages to the north of Australia.

The long-term history of the IT and its relation to the temporal and spatial variability of the WPWP and consequent climatic and paleocanographic changes are still poorly understood. It is probable that the WPWP did not exist before the Australia-Asia gap became severely restricted or closed. Once collision between Australia and SE Asia (and the Phillipine Sea Plate) began at approximately 25 Ma, the connection probably became restricted, and the passage of deep water, and large volumes of water, between the two oceans decreased.

Kennett et al. [1985] suggested a closure of the Indonesian Gateway in the middle Miocene which had dramatic repercussion on circulation patterns in the Pacific Ocean, and was a critical trigger for global climate change. *Nishimura* [1992] proposed a paleoceanographic model indicating closure of the Indonesian Seaway at the end of the early Miocene (16–17 Ma), based on tectonic evidence. However, plate tectonic reconstructions of SE Asia for the Cenozoic by *Ali et al.* [1994] and *Hall* [1996, 2002] suggest that the Indonesian Gateway began to close earlier than this, at the beginning of the Miocene. In contrast, a Pliocene closure of the Indonesian seaway as a major passage of warm surface water flow from the Pacific to the Indian Ocean between 5 and 3 Ma was suggested by *Cane and Molnar* [2001]. These authors proposed, that the northward advance of New Guinea since approximately 5 Ma switched the source of the Indonesian Throughflow waters. This change in hydrological characteristics would have had far-reaching consequences, such as a sig-

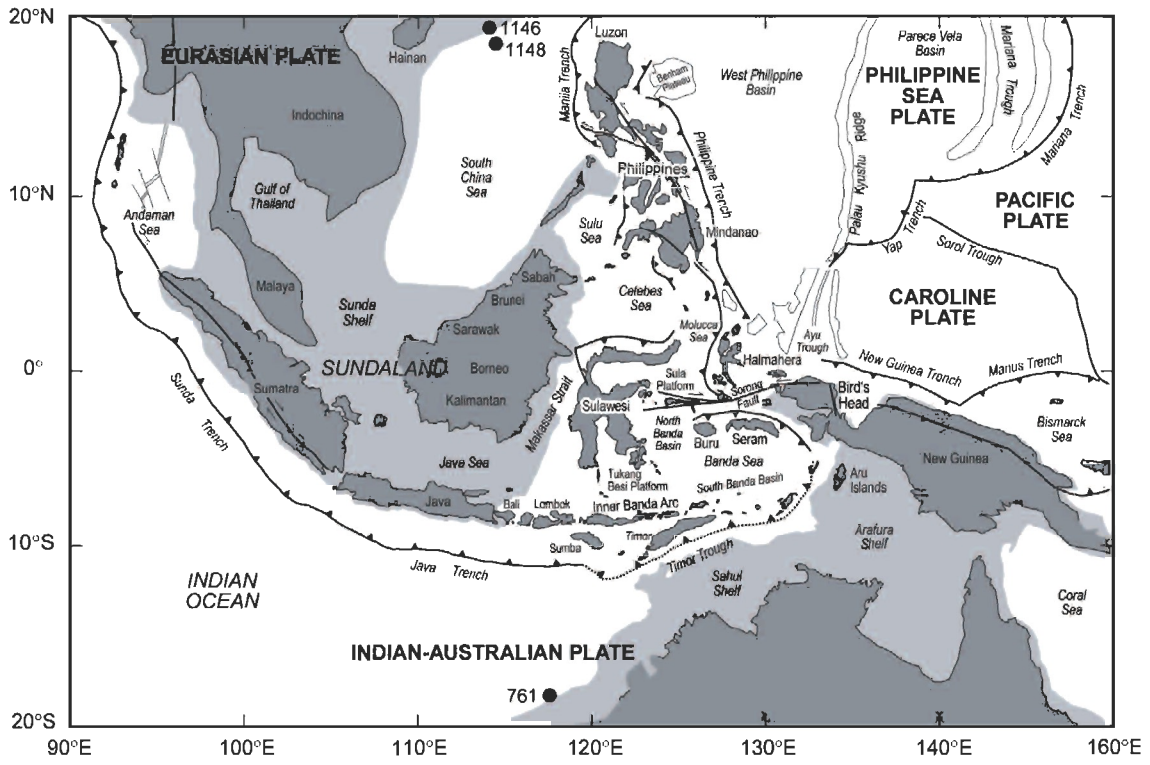

Figure 1. Topography and major plate boundaries of the Indonesian Gateway region. The positions of ODP cores discussed in text are indicated: ODP Site 761 (16°44.23′S, 115°32.10′E, 2189 m water depth), ODP Site 1146 (19°27.40′N, 116°16.37′E, 2092 m water depth), ODP Site 1148 (18°50.17′N, 116°33.94′′E, 3294 m water depth).

nificantly decreased sea surface temperatures in the Indian Ocean, the aridification of East Africa, and reduced atmospheric heat transport from the tropics to high latitudes [*Cane and Molnar*, 2001].

New high resolution proxy records reaching back to the Oligocene/Miocene boundary recently became available from the South China Sea (ODP Leg 184, [*Zhao et al.*, 2001a, b; *Kuhnt et al.*, 2002; *Holbourn et al.*, this volume]) and from the North Australian margin [*Holbourn et al.*, 2004]. In this review we will focus on four key time windows during which major changes in the circulation between the Pacific and Indian Ocean occurred:

1. The Holocene and Late Pleistocene (last 450 ky): Glacial/Interglacial variability and the present day Indonesian Throughflow.
2. The Pliocene–late middle Miocene restriction.
3. The middle Miocene: Sealevel and paleoceanographic perturbations.
4. The early Miocene initial closure.

Our main aims are to provide a review of the tectonic/paleogeographic boundary conditions within the gateway area, and to examine paleoceanographic and modelling evidence for changes in circulation patterns within and on either side of the gateway.

THE HOLOCENE AND LATE PLEISTOCENE (LAST 450 KY): GLACIAL/INTERGLACIAL AND SHORT-TERM VARIABILITY

Topography and Bathymetry of the Indonesian Gateway

The Indonesian Gateway Region includes two major continental plates, Sundaland-Eurasia and Australasia separated by a mosaic of microplates mainly of oceanic character. A comprehensive description of this complex of modern and ancient island arcs, oceanic basins and continental fragments is given in *Hall* [2002] and compiled in Figure 2. The present day IT intensity is controlled by four critical passages, the Makassar, Lombok, Ombai and Timor Straits which have very different transverse profiles, sill depths, and tectonic histories (Figures 3, 4). While the Makassar-Strait represents the major inflow passage through the Indonesian Archipelago, the outflow into the eastern Indian Ocean is distributed between three important gateways: To the west, the Lombok Strait with a sill depth of 250 m is the shallowest passage and only relevant for surface flow. This narrow channel was probably

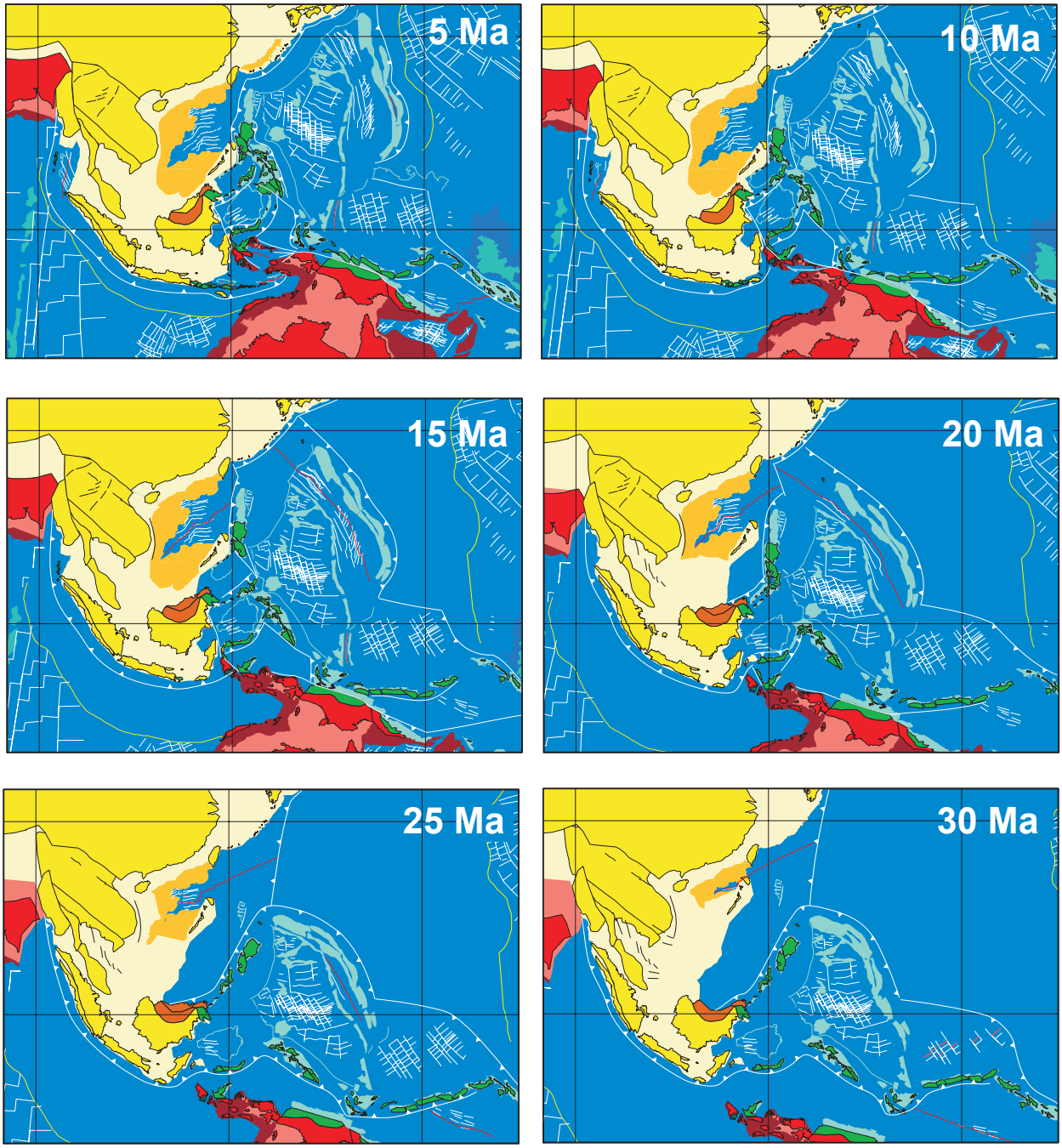

Figure 2. Reconstructions of the Indonesian Gateway from 30 to 5 Ma [*Hall,* 2002]. Areas shaded medium gray represent oceanic crust, submarine arc regions, hot spot volcanics, and oceanic plateaux. Light gray areas within ocean basins represent mainly arc, ophiolitic, and accreted material formed at plate margins during the Cenozoic. White areas represent submerged parts of the Eurasian continental margin. Dark gray colors represent submerged parts of the Australian continental margin. White lines in ocean basins indicate marine magnetic anomalies and strike slip faults, gray lines indicate active spreading centres. White lines with triangles indicate subduction zones.

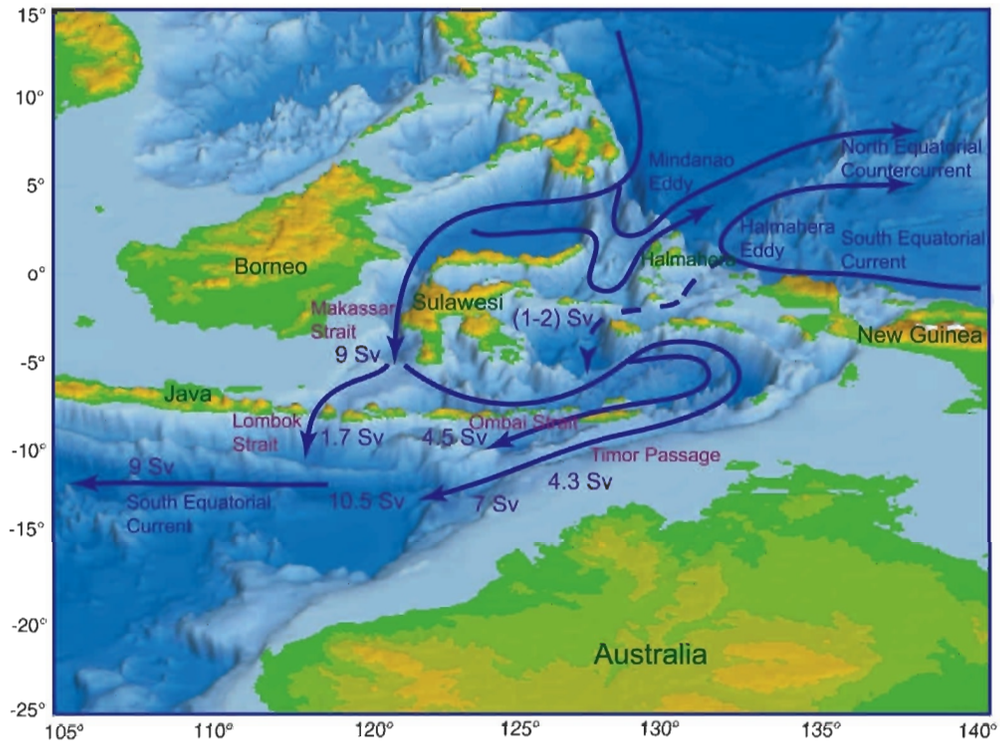

Figure 3. Present day Indonesian Throughflow, modified from *Gordon* [2001] and *Gordon et al.* [2003], and drawn on a topographic basemap derived from the ETOPO-5 bathymetric data set (Data Announcement 88-MGG-02, Digital relief of the Surface of the Earth. NOAA, National Geophysical Data Center, Boulder, Colorado, 1988.)

strongly reduced during glacial sea level lowstands. Further east, the Ombai Strait with a sill depth of 2000 m offers a pathway for surface and intermediate water masses [*Molcard et al.*, 2001]. The flow through the Timor Strait, the most easterly of the three passages with a sill depth of 1500 m, is in the same order of magnitude as the flow through the Ombai Strait. However, it has a strong shallow water component along the NW Australian shelf.

Controls on Indonesian Throughflow Variability

The present day transport through the gateway is complex, as water masses undergo significant modification during a long transit through an intricate array of passages, subjected to the influence of monsoonal climate systems. In turn, transport and temperature profiles of the IT may significantly affect the sea surface temperature and heat budgets of both Pacific and Indian Oceans, and alter patterns of heat and water vapour exchange with the atmosphere. The main inlets of the IT are close to the major tropical Pacific front dividing water masses of North Pacific and South Pacific origin with different temperature, nutrient and salinity properties. Two regional monsoon phases exert major control on the upper ocean salinity and temperature variability in the outflow passages. During the warm wet Northwest Monsoon (November through March) sea surface temperature rises and salinity falls (max. SST around 30°C and sea surface salinity (SSS) as low as 32 psu and below), while during the cooler drier and windier Southeast Monsoon (June to September) upper ocean conditions get cooler (25°C) and saltier (34 psu) [*Sprintall et al.*, 2003]. The maximum throughflow occurs during this boreal summer season as a result of lowered sea level south of Indonesia in response to strong SE trade wind forcing [*Godfrey*, 1996; *McBride*, 1999]. The following annual average throughflow transport values were obtained from mooring measurements:

- Makassar Strait: 9.3 ± 2.5 Sv [Gordon et al., 1998, 1999]
- Lombok Strait: 1.7 Sv [*Murray and Arief*, 1988]
- Ombai Strait: 5.0 ±1 Sv [*Molcard et al.*, 2001]
- Timor Passage: 7.0 Sv [*Cresswell et al.*, 1993]
- Timor Passage 4.5 ±1.5 Sv (for 120–1040 m water depth, *Molcard et al.* [1994])
- Timor Passage 4.3 ±1.0 Sv (for 0–1250 m water depth, *Molcard et al.* [1996])

On the basis of recent current and temperature measurements in the Makassar Strait, estimates of average IT water mass temperature were significantly corrected towards cooler temperatures. Thus, the total heat transport from the WPWP into the Indian Ocean may be less significant than previously inferred [*Gordon et al.*, 2003]. The reason for such a

Table 1. Main characteristics of North and South Pacific inflow waters into the Indonesian passages and their relative importance today and in the past

North Pacific Water (Mindanao Eddy, Western Passage)	South Pacific Water (Halmahera Eddy, Eastern Passage)
Warm but cooling occurs in Makassar Strait	Warm
Low salinity	Normal salinity
Oligotrophic	Mesotrophic
Dominant today	Reduced today
Reduced during El Niño, Glacials, Pre-Pliocene	More important during El Niño, Glacials, Pre-Pliocene

cool IT stems from monsoonal wind patterns, which restrict warm surface flow and favour deep thermohaline flow of cooler water through the Makassar Strait. Since this mechanism requires the presence of a low–salinity surface water mass in the western part of the Java Sea, which would have been absent during the last glacial, the glacial Throughflow may have been comparatively warmer and probably more saline than at present.

Another significant control on the characteristics of the IT water mass, which probably fluctuate on various timescales, is the relative influx of North and South Pacific waters in the IT inflow (Figure 3, Table 1). During periods of intense WPWP development and with the present day topography in the Halmahera area, low–salinity North Pacific thermocline water dominates the inflow (approximately 9 Sv), and saline South Pacific surface water entering from the Halmahera eddy is comparatively small (maximum 1–2 Sv), but a larger South Pacific contribution has been suggested for lower thermocline intermediate water in the Banda Sea [*Hautala et al.*, 1996]. However, the influence of South Pacific water may

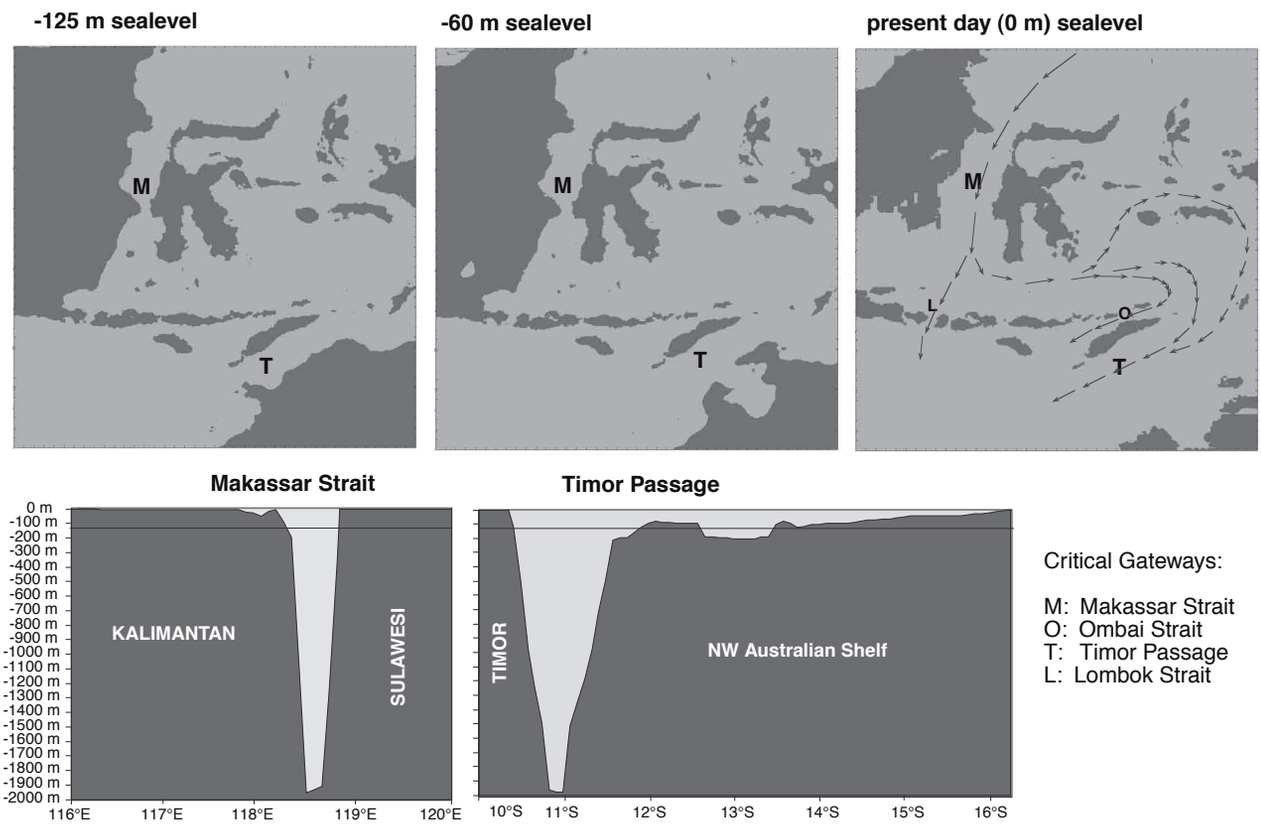

Figure 4. Critical passages for the Indonesian Throughflow and change in cross section geometry with a lowering of sea level by 60 m and 125 m. (Reconstruction using the ETOPO5 bathymetry-data set.)

have been more significant during periods when the WPWP weakened and shifted towards the eastern tropical Pacific (i.e. during El Niño situations and glacials), and in pre-Pliocene times, when the position of Halmahera was not preventing South Pacific waters from entering through the western (Makassar) passage [*Cane and Molnar*, 2001].

The intensity and the pathways of the IT are also significantly influenced by eustatic sealevel fluctuations. A precise reconstruction of sealevel change during the Last Glacial Maximum (LGM) at 22–20 ka is critical for understanding circulation patterns within the Indonesian passages during glacials and glacial terminations. A specifically sensitive feature is the broad and shallow NW Australian Shelf, which today is a major pathway for the shallow water throughflow, but would have been completely exposed at a LGM sealevel below −120 m. High resolution reconstructions of the late post-Pleistocene sea-level rise along transects on the Sunda Shelf [*Hanebuth et al.*, 2000] and the North-Australian Bonaparte Gulf [*Yokoyama et al.*, 2000] have fueled an ongoing controversy regarding sea-level change during the LGM (see discussions of the EPILOG (Environmental Processes of the Ice Age: Land, Ocean Glaciers) working group, *Clark and Mix*, [2002]; *Peltier* [2002]; *Lambeck* [2002]). Evidence for a marginal marine to brackish facies at 121 m below the present day sealevel was provided in the Bonaparte Gulf off NW-Australia by *Yokoyama et al.* [2000]. A sealevel lowstand of approximately 135 m was initially proposed, based on calculations of the geoid and estimates of glacial global ice volume [*Yokoyama et al,.* 2000], but these calculations were partly based on unrealistic modelling assumptions [*Peltier*, 2002; *Lambeck et al.*, 2002]. However, the broadly accepted lowstand of 116–120 m [*Hanebuth et al.*, 2000; *Peltier*, 2002] below present sea level has recently been put into question, and a lowstand of 135 m is once more considered possible [*Peltier*, 2002].

Glacial Circulation Patterns in a General Circulation Model

Experimental setup. A set of sensitivity model experiments was conducted to assess possible changes in the intensity and pathways of the IT during the last glacial period. Experiments were performed with the MIT General Circulation Model [*Marshall et al.*, 1997a, b], a primitive equations model with z-coordinates in the vertical. The model domain covered the Indonesian Seas from 105°E–140°E and 20°S–10°N. In order to capture details of the bathymetry in the main passages, the horizontal resolution of the model was 1/6° in both zonal and meridional direction and it had 25 vertical levels with resolution ranging from 10 m near the surface to 500 m close to 4500 m depth. The model was integrated for at least 3 years with a time step of 600 s. The initial 2 months were excluded from the analysis. Biharmonic viscosity mixing of momentum of $1x10^{11}$ m^4s^{-1} and Laplacian diffusion of $1x10^3$ m^2s^{-1} for mixing of tracers was used in the horizontal. In the vertical, Laplacian coefficients of $1x10^{-3}$ m^2s^{-1} for viscosity and $1x10^{-5}$ m^2s^{-1} for diffusion were used. The model seafloor topography was derived from the ETOPO-5 topography data set [*NOAA*, 1988]. For the glacial simulations, the depth values were reduced by 120 m in order to account for lower glacial sea level.

For present-day conditions the model was forced with monthly wind stress data derived from the Atlas of Surface Marine Data [*da Silva et al.*, 1994] and monthly temperature and salinity fields from the 1998 World Ocean Atlas [*Conkright et al.*, 1998] at the lateral boundaries. Sea surface temperature and salinity were restored on a monthly time scale to climatological values of the same atlas. The velocity field at the lateral boundaries was taken from the global ocean model simulation for present-day conditions [*Paul and Schäfer-Neth*, 2003]. The total volume transport was set to the annual mean value of 12 Sv which is close to the observations [*Gordon*, 2001] and held constant throughout the simulation. In the glacial simulation, the total volume transport was reduced by 1/3 in accordance with global model predictions for the IT transport during the LGM [*Paul and Schäfer-Neth*, 2003]. The glacial boundary conditions for temperature and salinity were adopted from the global ocean model experiment of *Paul and Schäfer-Neth* [2003] for the LGM climate. The glacial wind stress data used in the model are based on the AGCM ECHAM3 experiment as described in *Paul and Schäfer-Neth* [2003].

Three experiments were compared in order to examine the sensitivity of the throughflow to changes in topography and boundary conditions separately:

1. Reference simulation (MOD) with the present-day topography and forcing derived from observed monthly climatology data.
2. Simulation (MOD-LGM) in which the same forcing was applied but sea-level was lowered by 120 m.
3. Glacial simulation (LGM-LGM) with glacial boundary conditions and glacial topography.

A summary of the experimental setup and selection of source data is included in Table 2. The results from the regional model may not be directly compared in detail with observed values since the model forcing was on a monthly timescale and temporal variability of the large scale processes in terms of volume transport was absent. Nevertheless, the model produced mean circulation patterns through the passages in reasonable agreement with observations [*Gordon,* 2001; *Gordon* et al., 2003].

Model results. Our model results show that the bulk of the IT takes the route through the Makassar Strait (Table 3). Some deep water passes through the gateways between

Table 2. Overview of sensitivity experiments with the high-resolution ocean circulation model

Experiment	Bathymetry	Total volume transport (Sv)	Sea Surface Temperature and Salinity	Surface wind stress
MOD	ETOPO 5	12	World Ocean Atlas *Conkright et al.* [1998]	Atlas of Surface Marine Data *da Silva et al.* [1994]
MOD-LGM	ETOPO 5 -120 m	12	World Ocean Atlas *Conkright et al.* [1998]	Atlas of Surface Marine Data *da Silva et al.* [1994]
LGM-LGM	LGM ETOPO 5 -120 m	8	*Paul and Schäfer-Neth* [2003]	*Paul and Schäfer-Neth* [2003]

Sulawesi and New Guinea (North Banda Basin and the Seram Sea). The flow through the Lombok Strait in the model is higher than observed (3.2 Sv compared to 1.7 Sv). In the real world, the Lombok Strait is an 18 km narrow passage, whereas in the model it had to be widened to 36.7 km due to the model resolution. This might be one reason for the overestimated transport. The flow through the Makassar Strait is in approximate geostrophic balance except for the region near the equator.

The experiment with lowered sea level shows that when topography is changed, a higher slope of the sea surface is required to force the flow through the passage as the boundary values remain the same. Approximately, the zonal sea surface gradient in the passage of 2×10^{-7} gives rise to an average meridional velocity in the upper 100 m of 0.2 m s^{-1}. However, the sea surface gradient does only reflect the surface flow and not the total barotropic flow. The slope of the internal density surfaces forces baroclinic shear in the northward direction at intermediate levels and reduces the surface flow.

For the case of lowered sea level under present-day climate conditions, the model-generated circulation through the passages is still in agreement with the observed current system. Model results show net throughflow reduction within the Makassar Strait due to the sea-level lowering (Table 3). A significant effect from sea-level change appears in the Lombok Strait, where the total volume transport is reduced by approximately 50%. When the Lombok and Ombai Straits are blocked, the bulk of the watermass transport takes place along the exit route through the deep northern Timor passage, while the southern shelf region is completely exposed (Figure 5). Experiments with glacial boundary conditions show a decrease in annual mean transport through the main passages in accordance with the total reduction of the throughflow in the large scale model simulations.

Table 3. Mean volume and heat transport through the main Indonesian passages. See Figures 1 and 3 for the location of the passages. Values indicate transport in southward direction and heat gain for the Indian Ocean. The heat transport is defined as temperature transport relative to 3.4°C converted to heat units (PW) [Vranes, 2002].

	Present-day conditions	Present-day conditions with sea level lowered by 120 m	Glacial conditions
Makassar Strait	8.0 ± 1.6 Sv 0.40± 0.12 PW	8.1 ± 2.5 Sv 0.45± 0.17 PW	5.7 ± 2.1 Sv 0.35± 0.20 PW
Seram Sea	3.7 ± 2.5 Sv 0.06± 0.22 PW	4.0 ± 2.5 Sv 0.06± 0.24 PW	2.4 ± 2.1 Sv 0.03± 0.15 PW
Lombok Strait	3.2 ± 0.7 Sv 0.26± 0.06 PW	1.6 ± 0.6 Sv 0.15± 0.06 PW	1.7 ± 0.8 Sv 0.15± 0.07 PW
Ombai Strait	5.9 ± 1.5 Sv 0.20± 0.17 PW	5.5 ± 0.6 Sv 0.19± 0.06 PW	3.4 ± 1.0 Sv 0.11± 0.05 PW
Timor Passage	3.0 ± 1.2 Sv 0.08± 0.09 PW	5.1 ± 0.5 Sv 0.20± 0.05 PW	3.1 ± 0.8 Sv 0.13± 0.06 PW

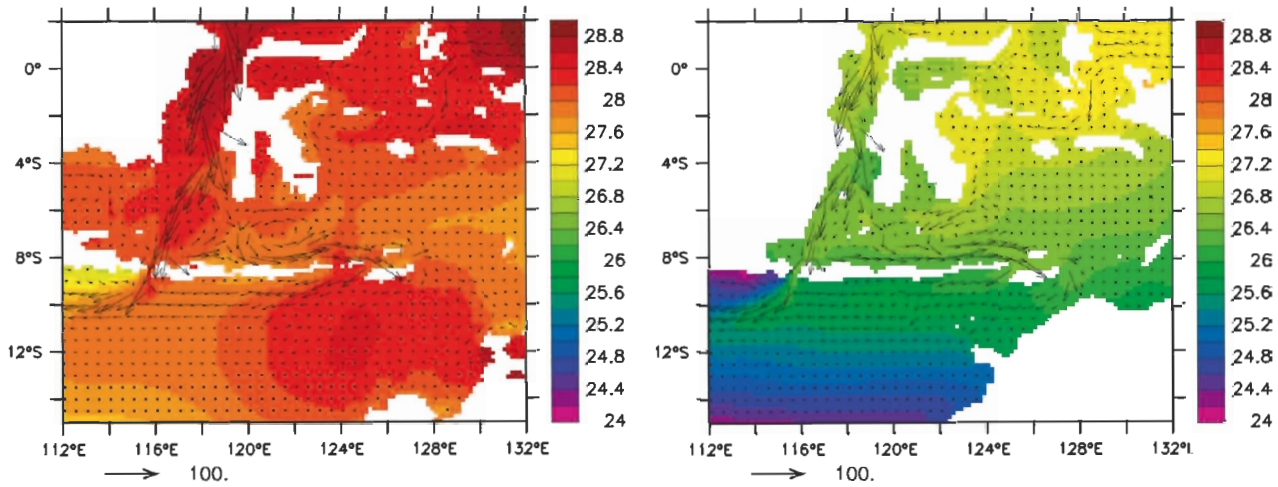

Figure 5. Model generated circulation through the Indonesian passages in the present-day (left) and LGM (right) simulation. The gray scale represents the mean sea surface temperature (°C). Vectors show volume flux ($m^2\ s^{-1}$) above 500 m water depth.

Sea-level lowering has a significant effect on the vertical structure of the throughflow (Figure 6). The present-day simulation shows a subsurface maximum of southward velocities consistent with the current meter measurements from the Makassar Strait [*Wajsowicz et al.*, 2003]. The transport below the sill depth (650 m) in the southern Makassar Strait is actually zero. The experiments with lowered sea level and the glacial simulation show an intensification of the main flow in

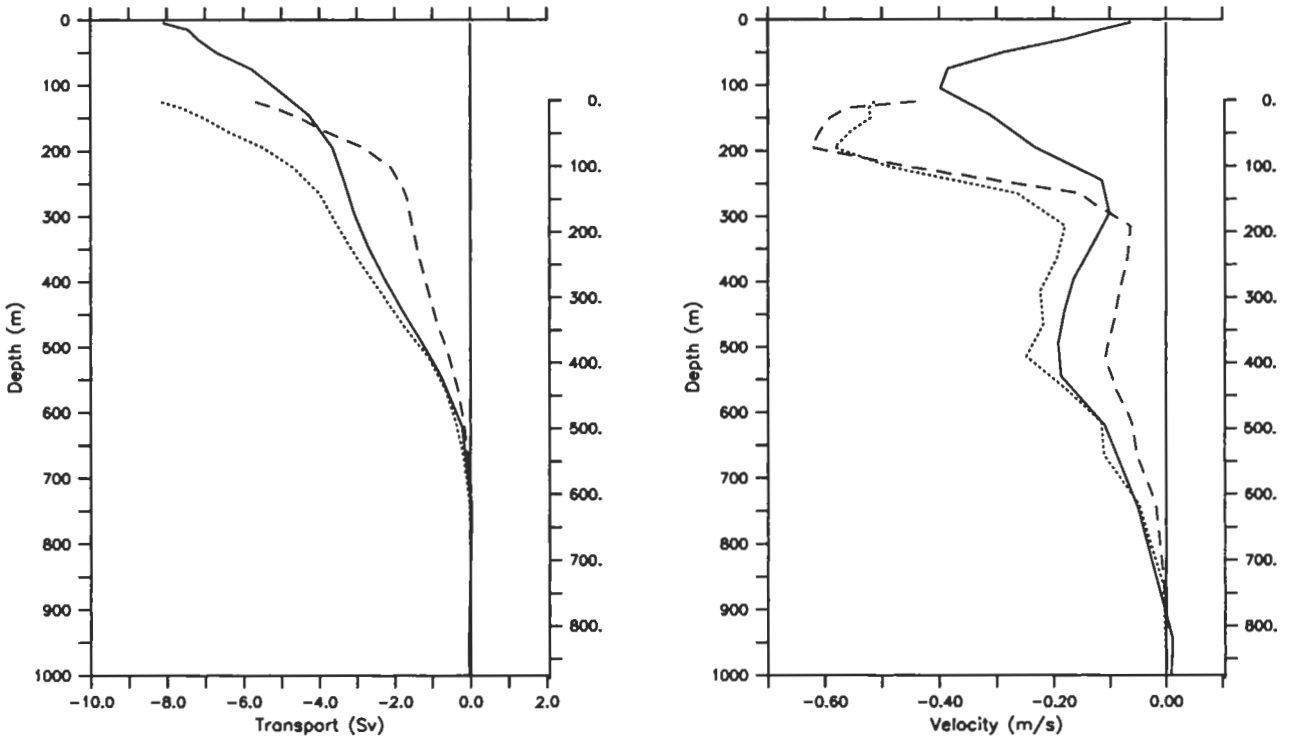

Figure 6. Vertical profile of accumulated transport (left) and meridional velocity (right) within the Makassar Strait at 3°S, 118.5°E for the present-day simulation (solid line), the simulation with present-day boundary conditions and lowered sea level (dotted line) and LGM simulation (dashed line). Negative values indicate flow in southward direction. Depth values of the LGM topography are given on the right vertical axis.

the surface layer (Figure 6) that can be related to the 120 m reduction in the sill depth. Though stronger shallow water transport carries warmer surface layer water into the Indian Ocean, the net heat transport is reduced due to the global lowering of glacial sea surface temperature and reduction in the shelf area (Table 3).

Regarding the heat transport variability associated with the monsoonal wind pattern, *Gordon et al.* [2003] proposed a mechanism on the basis of recent current and temperature measurements in the Makassar Strait. During boreal winter monsoon, low–salinity Java Sea water enters the southern Makassar Strait and inhibits surface warm water transport from the Pacific to the Indian Ocean. This mechanism is reproduced in the present-day simulation (Figure 7 upper left). The glacial simulation shows that the absence of Java Sea water during the Last Glacial Maximum allows unrestricted surface flow through the Makassar Strait during the northwestern monsoon (Figure 7 lower left). Reversal of the wind during present-day northern hemisphere summer (Figure 7 upper right) draws the low-salinity waters from the southern Makassar Strait back into the Java Sea and allows southward surface layer transport. For glacial conditions the southeastern monsoon in the absence of the Java Sea accumulates Banda Sea surface waters in the southern Makassar Strait and inhibits southward flow in the surface layer (Figure 7 lower right). The heat transport during the boreal summer is reduced in the glacial simulation. Thus sea level related changes in topography may lead to a fundamentally different seasonal cycle of surface flow and heat transport in the Makassar Strait.

Pleistocene-Holocene Proxy Records: A Comparison with Results From Model Experiments

A significantly reduced, more salty glacial IT and a reduced heat export from the west Pacific into the Indian Ocean, as indicated by the model experiments should be evident in the SST, SSS, and paleocirculation proxy records from the Indonesian Gateway region.

Sea Surface Temperature (SST) and Sea Surface Salinity (SSS). Oxygen isotope data from the Indonesian Seas including the Sulawesi Sea [*Barmawidjaja et al.*, 1993] and the Banda Sea

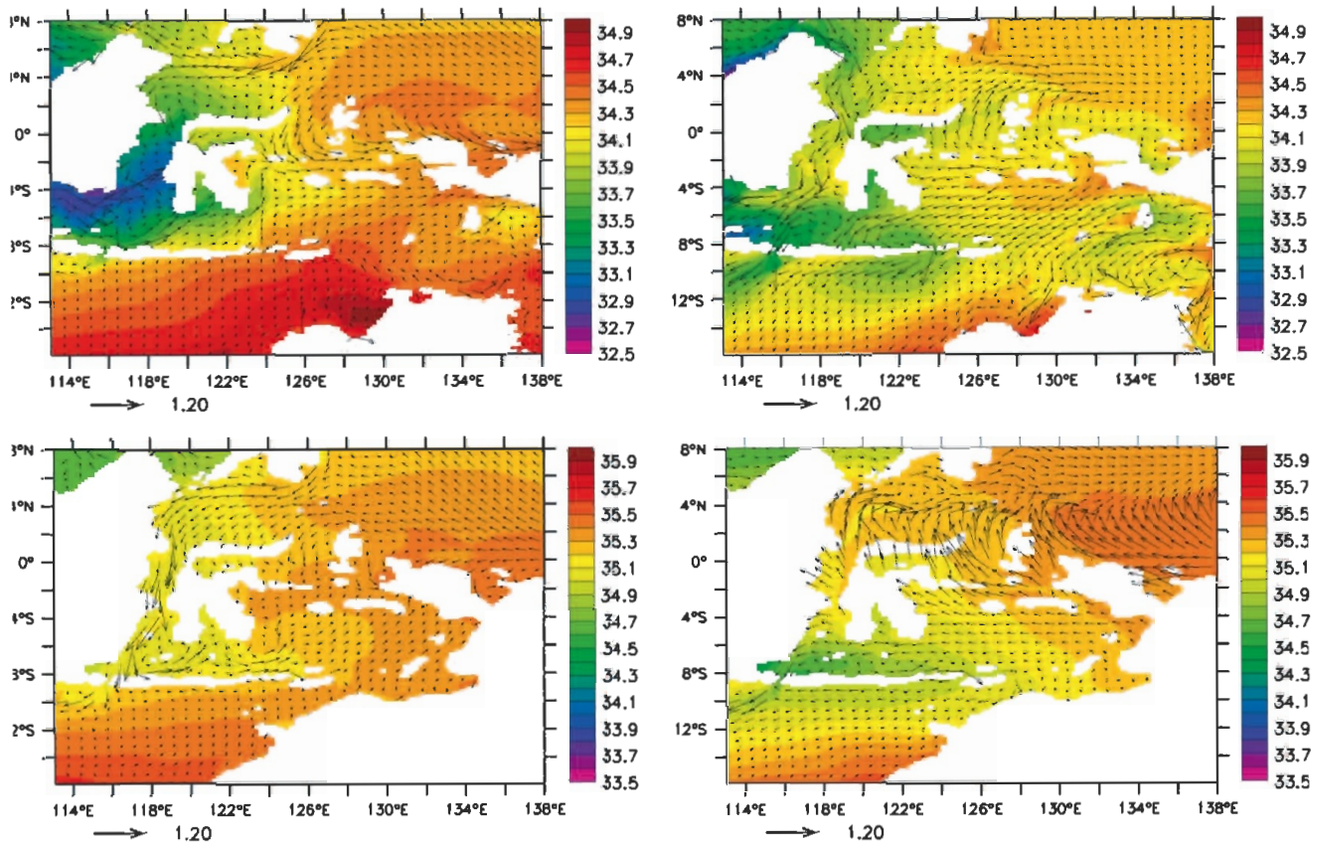

Figure 7. Sea surface salinity (psu) and surface currents (ms^{-1}) for the present-day (upper panels) and LGM conditions (lower panels) during the northwest winter (left) and southeast summer monsoon (right). Note the higher salinity values for the glacial simulation.

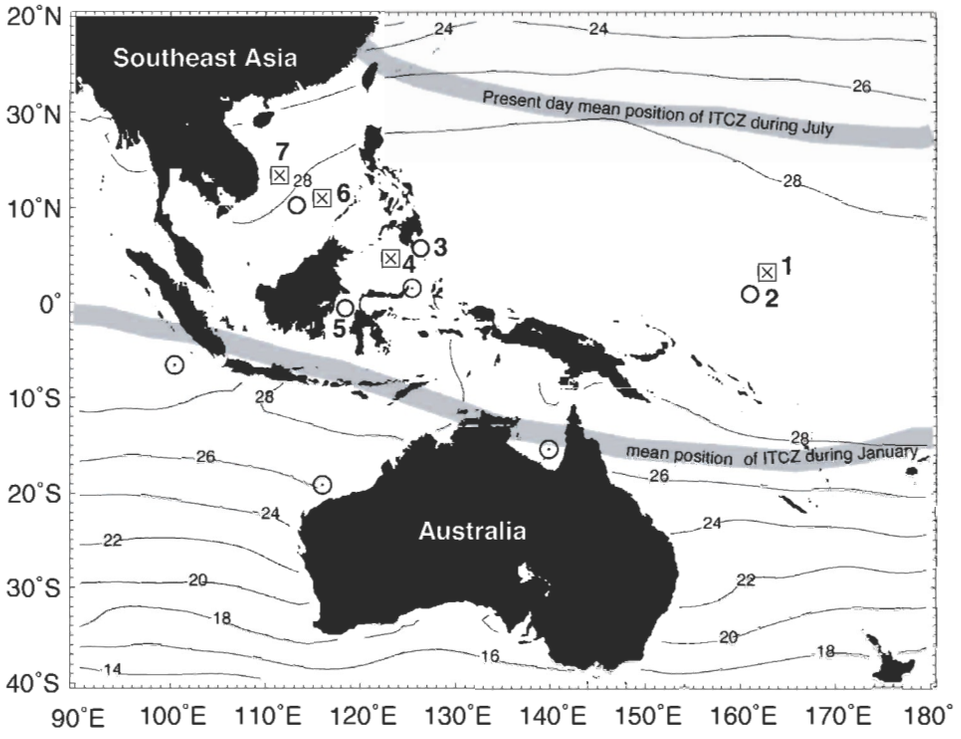

Figure 8. Glacial salinity estimates from $\delta^{18}O$ record and independent paleotemperature reconstructions based on Mg/Ca paleothermometry (1–5) and Uk37 temperatures (6–7). Glacial precipitation estimates from vegetation records are taken from *De Deckker* et al., [2002] (filled circles). Present day mean positions of the ITCZ during January and July are from *Sturman and Tapper* [1996]. Isotope and paleotemperature data are from *Lea et al.* [2000] (1), *Palmer and Pearson* [2003] (2), *Stott et al.* [2002] (3), *Rosenthal et al.* [2003] (4), *Visser et al.* [2003] (5), *Kienast et al.* [2001] (6), and *Wang et al.* [1999] and *Pelejero et al.* [1999] (7). Open circles indicate evidence for conditions similar to the Holocene or drier conditions during the LGM, crosses indicate evidence for wetter conditions during the LGM.

[*Ahmad et al.*, 1995] indicate higher salinities during the LGM than today (see *De Deckker et al.* [2002] for a review). *Martinez et al.* [1997, 1999, 2002] and *De Deckker et al.* [2002] thus suggested more saline glacial conditions throughout the Indo-Pacific Warm Pool. However, the study by *De Deckker et al.* [2002] assumed a minimal or no temperature change from the LGM to the Holocene in this region and generally took the highest $\delta^{18}O$ values as representative for the LGM and not an average over a large number of measurements, which can only be calculated from recent high resolution records [*Rosenthal et al.*, 2003]. Recent studies using high resolution time series of paired Mg/Ca, Uk37 and $\delta^{18}O$ measurements [*Pelejero et al.*, 1999; *Kienast et al.*, 2001; *Stott et al.*, 2002; *Oppo et al.*, 2003, *Rosenthal et al.*, 2003] indicate that the northern part of the WPWP (South China Sea, Sulu Sea and Mindanao Sea) was probably fresher during the last glacial than previously assumed (Figure 8). The Mg/Ca records estimate glacial/interglacial SST differences within the WPWP between 2° and 3°C which results in an approximately 0.3–0.5‰ lower average glacial $\delta^{18}O_{water}$, and consequently lower glacial salinities in the Sulu Sea and South China Sea (Table 4). However, all these records are derived from marginal areas of the WPWP, that may have been significantly influenced by South East Asian monsoon variability. Low glacial salinity is also reported from the Ontong Java Plateau [*Lea et al.*, 2000], although the geographically close *G. sacculifer* record of *Palmer and Pearson* [2003] does not show significant differences between glacial and interglacial $\delta^{18}O_{water}$.

More relevant for glacial temperature and salinity conditions in the IT area is the Makassar Strait record of *Visser et al.* [2003] that not only shows lower modern $\delta^{18}O_{water}$ values than any other records from the WPWP but also glacial values that are significantly higher than today. The low modern SSS may be partly an effect of fresh water from the South China and Java Sea entering the Makassar Strait during winter monsoonal wind conditions [*Gordon et al.*, 2003]. This freshwater lens could not have existed during the LGM, when the sea-level was lower and most of the Sunda Shelf and Java Sea was exposed and formed an effective barrier for freshwater flow from the South China Sea.

Despite the incomplete coverage of glacial salinity reconstructions for the IT area (Figure 8), a pattern arises that the present day monsoonal climatic conditions in the Australasian

Table 4. Present day and glacial SST and $\delta^{18}O_{water}$ as a proxy for SSS of key locations in the WPWP and the Indonesian passages. To calculate $\delta^{18}O_{water}$ we used two paleotemperature equations, that were solved for $\delta^{18}O_{water}$: *Duplessy et al.* [1991]: $\delta^{18}O_{water}$=−21.9+$\delta^{18}O_{calcite}$+5*(12.4244+0.4T)$^{0.5}$ and *Bemis et al.* [1998]: $\delta^{18}O_{water}$ = (T − 16.5 + 4.8+$\delta^{18}O_{calcite}$)/4.8 + 0.27. However, since the slopes of $\delta^{18}O$ change versus temperature are similar (0.20 to 0.23‰ per °C), the choice of paleotemperature equations does not have a large impact on the calculations [*Lea et al.*, 2000]. A reservoir correction of 1.2 ‰ has been applied for LGM $\delta^{18}O_{water}$ values. The estimated uncertainty of the derived $\delta^{18}O_{water}$ values is 0.18‰, calculated from the uncertainty in the paleotemperature equation, the standard error of the Mg/Ca-SST calibration, and the reproducibility of +$\delta^{18}O_{calcite}$ and Mg/Ca in a typical interval [*Lea et al.*, 2000].

	Recent $\delta^{18}O_{calcite}$ (‰ vs. PDB)	Glacial $\delta^{18}O_{calcite}$ (‰ vs. PDB)	Recent SST °C	Glacial SST °C	Recent $\delta^{18}O_{water}$ (‰ vs. SMOW)	Glacial $\delta^{18}O_{water}$ (‰ vs. SMOW)
1. Lea et al. (2000) Ontong Java	-2.4	-1.2	29.2	26.2	0.22	-0.13
2. Palmer and Pearson (2003) ERDC-92	-2.0	-0.3	28.6	26.5	0.94	0.85
3. Stott et al. (2002) Mindanao	-2.8	-1.0	30.0	27.0	0.26	0.28
4. Rosenthal et al. (2003) Sulu Sea	-2.6	-1.4	28.7	26.4	0.22	-0.27
5.Visser et al. (2003) Makassar Strait	-3.2	-1.2	29	25.5	-0.33	-0.25
6a. Kienast et al. (2001) 18287-3 southern SCS	-3.3	-1.5	28.2	25.5	-0.59	-0.55
6b. Kienast et al. (2001) 18252-3 southern SCS	-3.1	-1.5	27.8	25.2	-0.48	-0.62
7. Pelejero et al. (1999) 17961-2 southern SCS	-3.12	-1.72	28.0	25.2	-0.45	-0.84

region were restricted to a narrower zone north of the equator and did not affect the main path of the IT, which apparently was influenced by continental drought and high SSS during the LGM, as numerous land and offshore records from Indonesia and northern Australia demonstrate [*De Deckker et al.*, 2002]. Glacially increased SSS in the IT may thus have been caused by an increase in the proportion of South Pacific high salinity water as proposed by *Martinez et al.* [2002] and enhanced glacial evaporation in the main IT passages as suggested by *De Deckker et al.* [2002].

Circulation and mixing. Müller and Opdyke [2000] suggested that paleoproductivity in the Timor trough is inversely proportional to the strength of the IT, and is inhibited by a cap of warm low-salinity surface water, which moves along the NW Australian shelf and spreads out over the southeastern part of the Indian Ocean (Timor Sea). During the LGM surface waters in the Timor Sea were being depleted of CO_2 and relative nitrate utilization was low [*Müller and Opdyke*, 2000]. This suggests that the thermocline was shallow and that upwelled, nutrient-rich water was present in the Timor Sea region, indicating a strongly reduced low-salinity surface water throughflow.

Clay minerals entrained in the Recent IT have a characteristic assemblage composition and are advected over a considerable distance, reflecting the intensity of the flow through the passages and the propagation and extent of the outflow into the eastern Indian Ocean [*Gingele et al.*, 2001a]. Based on the modern provenance and distribution patterns of the main clay mineral groups, *Gingele et al.* [2001b] concluded that a reduced glacial IT carried significantly lower amounts of kaolinite and chlorite from the Indonesian archipelago into the Timor Passage. While a decrease in precipitation within the archipelago would have a similar effect, a reduction in current speed within the Timor passage is also indicated by the deposition of finer sediment. Clay mineral distribution along the NW Australian margin also indicates a strongly reduced or absent glacial Leeuwin Current, which forms a warm, low–salinity current along the NW and W Australian Margin and is regarded as a continuation of the Timor Sea Outflow [*Gingele et al.*, 2001b].

THE PLIOCENE–LATE MIDDLE MIOCENE RESTRICTION (3–12 MA)

Tectonic Development

For the Holocene and late Pleistocene it is reasonable to assume present topography and bathymetry in most areas around the Indonesian Gateway, and models of the through-

flow can be developed by simply changing sea level and oceanographic boundary conditions. For periods before about 1 Ma this is not possible, as critical regions between Sulawesi and the Bird's Head, and between the southern Philippines and the Banda Sea, changed dramatically in the late Cenozoic (12 Ma to 1 Ma). New land emerged, mountains rose to heights of more than 3 kilometres above sea level, and submarine basins both formed and disappeared (Figure 9). Thus, modelling the throughflow depends on models of paleogeography, which in turn rely upon tectonic reconstructions of the region. The descriptions of tectonic development given here are based on tectonic modelling in *Hall* [2002].

At about 12 Ma Jurassic ocean crust north of Australia began to be subducted as the Sunda Trench propagated east into an oceanic embayment within the Australian margin. The age of the lithosphere north of the NW Shelf was much greater than that being subducted further west (mainly Cenozoic together with some Cretaceous crust) which led to rapid rollback of the subduction hinge as the Jurassic slab fell away into the mantle. The subduction hinge moved southeast, and the rollback induced major extension in the SE Asian upper plate. Extension began by 10 Ma, and led to rapid decompression melting [*Linthout et al.*, 1996, 1997], extension-related metamorphism, initial arc volcanism contaminated by continental crust [*Honthaas et al.*, 1999] and arc splitting. Finally, backarc basin spreading led to the formation of the South Banda Sea from about 6 Ma. The active volcanic arc split, as the South Banda Sea began spreading as a backarc basin. At the same time the subduction hinge was moving towards the Australian continental margin. At about 3 to 4 Ma, the volcanic arc came into collision with the Australian margin in the region of Timor. Spreading ceased in the South Banda Sea and the volcanic arc became coupled to the Australian margin in the Outer Banda Arc region around Timor. After collision, new plate boundaries developed north of the arc in the Flores-Wetar Sea and to the north of the South Banda Sea. On the margins of the Banda Sea, high mountains emerged in Seram and Timor during the Pliocene.

At 12 Ma Halmahera was situated north of New Guinea, but further south and east than at present, with a strike-slip boundary separating the Philippines Sea and Molucca Sea plates from the Australian plate margin in New Guinea. East of Sulawesi, west-directed subduction of the Philippine Sea Plate had been underway since the early Miocene but new east-dipping subduction began at about 12 Ma beneath Halmahera, forming a separate Molucca Sea plate. The subduction on both sides of the Molucca Sea has continued to the present, bringing the two arcs on either side into collision, eliminating the Molucca Sea, and bringing the Halmahera arc to its present position northwest of Bird's Head. Halmahera has thus moved across the equator with New Guinea, and in the last 3 million years the islands of the North Moluccas including Halmahera have emerged from the sea. These tectonic reconstructions suggest that restriction in the throughflow could have occurred between 12 and 3 Ma. By about 10 Ma, the Australia-SE Asian gap appears to have been at its narrowest and areas of land were relatively extensive. The Makassar Strait was still a few hundred kilometers wide but

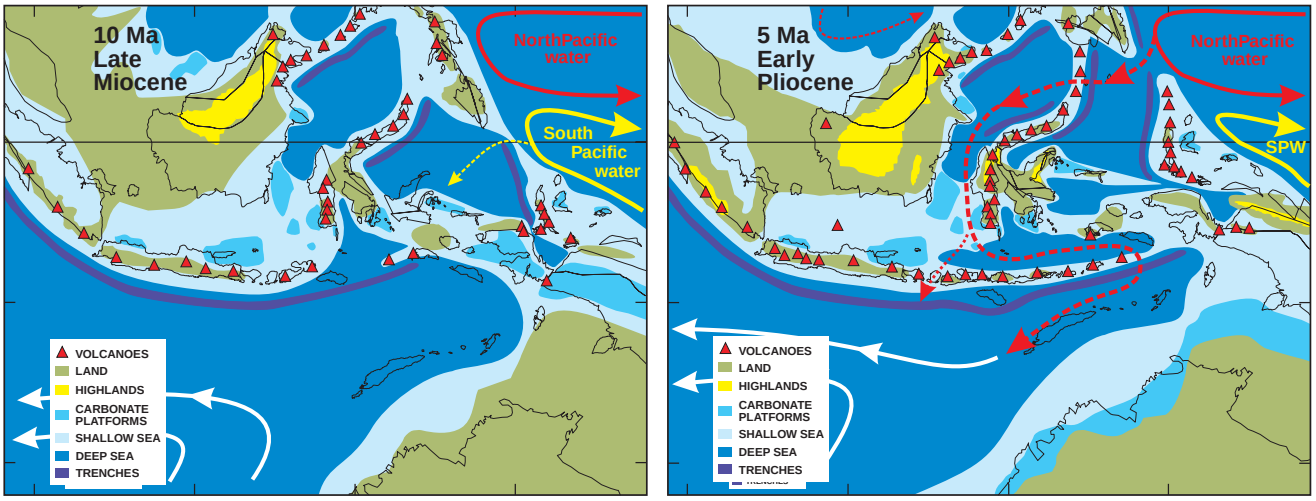

Figure 9. Interpreted distribution of land and sea in the region of the IT from 10 to 5 Ma [modified from *Hall* 1998] showing postulated major ocean currents. North Pacific water is shown in dark gray, South Pacific water in light gray and Indian Ocean currents in white. The positions of the major Pacific flow and return currents are assumed to have remained broadly fixed with respect to the equator as inferred by *Cane and Molnar* [2001]. Flow from the Pacific to the Indian Ocean is therefore dependent on the positions of the small deep basins and channels connecting them, and intervening areas of shallow water and land.

there is evidence for an increase in the area of land in much of Sulawesi. By 5 Ma, there was substantial land in Sulawesi and the very high mountains of west Sulawesi, which are now up to 3 kilometers high, began to rise. Elevation of mountains in New Guinea occurred over a similar period [e.g., *Hill and Raza*, 1999; *Hill and Hall*, 2003] and the even greater height of these mountains, which now reach 5 kilometers, probably induced aridity in northern Australia from the late Miocene, perhaps as early as 10 Ma but certainly by 5 Ma.

Paleoceanographic and Modelling Evidence From the Indian and Pacific Oceans

Srinivasan and Sinha [1998] provided evidence for an early Pliocene restriction (at approximately 5 Ma) of the Indonesian Gateway from a comparison of planktonic foraminiferal species occurrences in north-eastern Indian Ocean and tropical Pacific deep sea cores. These authors concluded that planktonic foraminiferal assemblages were generally similar until the early Pliocene (first appearance of *Globorotalia tumida* at 5.2 Ma), after which the faunal record showed divergence. At that time, the Indonesian Gateway became an effective biogeographic barrier for deep-dwelling planktonic foraminifers such as *Pulleniatina spectabilis*, which is completely absent from all Indian Ocean DSDP and ODP sites. A restriction of IT intensity at approximately 5 Ma can also be inferred from observations that the intermediate water oxygen minimum zone in the central Indian Ocean significantly expanded at this time [*Dickens and Owen*, 1994]. These authors concluded that the expansion of the oxygen minimum zone in the central Indian Ocean was related to regionally increased biological productivity, as the warm oligotrophic IT water mass was strongly reduced.

Cane and Molnar [2001] suggested that the northward movement and emergence of Halmahera had profound effects on ocean circulation and induced African aridity between 5 and 3 million years ago. *Cane and Molnar* [2001] assumed that since the basic form and position of the Asian landmass had changed little since the Miocene, the difference in salinity between western Pacific waters north and south of the equator existed throughout this time. These authors suggested that when New Guinea lay further south, and Halmahera was a smaller island, warm water from the South Pacific would have entered the Indian Ocean, warming sea surface temperatures there and causing a more rainy climate in eastern Africa. According to their model, the northward movement of New Guinea shifted the source of throughflow water further to the north, and the resulting colder throughflow decreased SSTs in the Indian Ocean, thus reducing rainfall over eastern Africa. The ensuing increase in the sea surface temperature gradient, possibly coupled with mountain building in New Guinea, decreased heat transport out of the tropics (end of the Pliocene "permanent El Niño") sufficiently to stimulate global cooling and the eventual growth of ice sheets. This hypothesis strongly depends on the position and history of many small crustal fragments which make up eastern Indonesia. An alternative mechanism would be monsoonal wind related cooling of the throughflow waters during their passage as suggested by *Gordon et al.* [2003]. This mechanism for cooling of the modern IT may have also contributed to a reduction of the warm throughflow during the Pliocene. The timing of the late Pliocene cooling of the IT would be in good agreement with the strengthening of the East Asian monsoon system since approximately 3.6 Ma [*An et al.*, 2001].

MID-MIOCENE EVENTS (17–12 MA): SEALEVEL AND PALEOCEANOGRAPHIC PERTURBATIONS

Tectonic Development

The Indonesian Gateway has been an area of intense tectonic activity since the earliest Miocene. Plate tectonic reconstructions of SE Asia for selected timeslices of the Cenozoic by *Hall* [1996, 2002] indicate that the Molucca Sea, still was a very wide area forming part of the Philippine Sea plate at about 15 Ma (Figure 10). This ocean basin was gradually eliminated by subduction beneath Halmahera only after about 12 Ma, but the

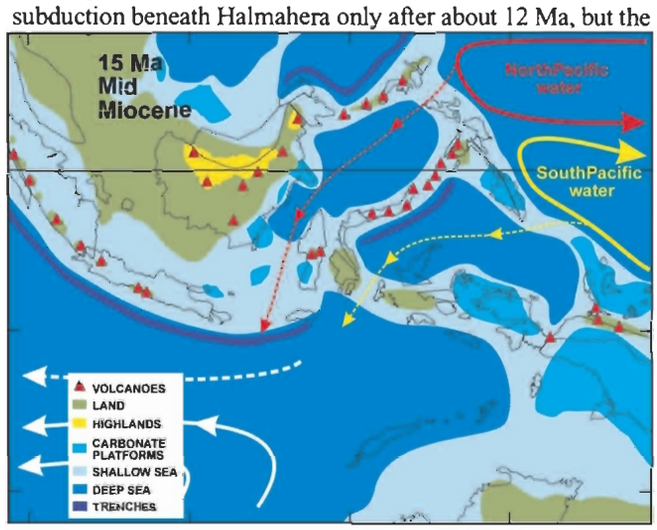

Figure 10. Interpreted distribution of land and sea in the region of the throughflow at 15 Ma [modified from *Hall* 1998] showing postulated major ocean currents. North Pacific water is shown in dark gray, South Pacific water in light gray, and Indian Ocean currents in white. The positions of the major Pacific flow and return currents are assumed to have remained broadly fixed with respect to the equator as inferred by *Cane and Molnar* [2001]. Flow from the Pacific to the Indian Ocean is therefore dependent on the positions of the small deep basins and channels connecting them, and intervening areas of shallow water and land.

deepwater passage between the Indian and Pacific Oceans would have been blocked east of Sulawesi already by 25 Ma. However, the route through the Makassar Strait was always there, probably wider open to the south than today, but would only allow the throughflow of shallow and intermediate water of North Pacific origin as it does today. The region from New Guinea to Sulawesi remained a zone of strike-slip faulting. Very localized transpression and transtension in this zone makes a precise reconstruction of the paleogreography and especially the estimate of sill depths of gateways extremely difficult, but there is no evidence for a major tectonic reorganization of the gateway between the Indian and Pacific Oceans between 17 and 12 Ma.

Sealevel and Paleoceanography

Deep water paleoceanography. Comparison of $\delta^{18}O$ and $\delta^{13}C$ profiles from Site 588 (SW Pacific Ocean, [*Flower and Kennett*, 1993]), Site 761 (E Indian Ocean) and Site 1146 (South China Sea) reveals marked differences in the characteristics of deep water masses at these three sites [*Holbourn et al.*, this volume]. High $\delta^{13}C$ values at the SW Pacific Site 588 indicate relatively well ventilated deep water and close proximity to a southern high latitude source. By contrast, the markedly lower $\delta^{13}C$ values at Site 761, in the E. Indian Ocean and at Site 1146 in the South China Sea Site 1146 point to a different origin for deep/intermediate water masses. However, coherence in the amplitude of $\delta^{13}C$ increases and decreases at the three sites supports a common, global origin for $\delta^{13}C$ changes (carbon burial), and no open low latitude deep-water connection between the Indian and Pacific Oceans is required to explain these synchronous changes. The ranges of $\delta^{18}O$ values are quite comparable at Sites 588 and 1146, but differ markedly at Site 761 (1.1 to 2.4‰), indicating restricted intermediate/deep water exchange between the Pacific Ocean and Indian Ocean through the Indonesian Gateway during the middle Miocene climatic optimum and subsequent global cooling at ~13.9 Ma.

Shallow water throughflow and sealevel history. The eustatic sealevel fall at the end of the Miocene climate optimum, caused by major expansion of the East Antarctic Ice Sheet between about 15 and 13 Ma [*Flower and Kennett*, 1993; *Zachos et al.*, 2001; *Sugden and Denton*, 2003], must have had significant impact on the IT, as the Indonesian passages were fairly shallow at that time (Figure 10). The amount of this sealevel fall may have been in the order of 60–80 m [*Hardenbol et al.*, 1998; *Holbourn et al*, 2004] and probably had as much impact on the IT as the glacial-interglacial sealevel fluctuations of the Pleistocene. A restriction in sealevel would have reduced throughflow intensity over the probably wide and shallow Mid-Miocene barriers more than within the narrow deep passages today. The effect of a significant restriction of surface flow between the Pacific and Indian Ocean on the circulation system of the Pacific Ocean was originally described by *Kennett et al.* [1985], based on paleobiogeographic distribution patterns of planktonic foraminifers. The modern features of the Pacific Ocean circulation system such as the northward and southward deflection of warm equatorial currents to form the Kuroshio and East Australian currents may have first evolved at this time. It is thus quite possible that the major sea-level fall at approximately 13.9 Ma was more significant for the re-organisation of current systems through the Indonesian passages than tectonic constriction. At that time, prevailing strike-slip movements may have caused local transpression but not significant crustal shortening leading to the elimination of passages.

EARLY MIOCENE INITIAL CLOSURE (25–17 MA)

Initial Collision History of Australia and SE Asia

Before Australia and SE Asia began to collide a wide and deep oceanic area existed between them. Thus, before about 25 Ma there would have been largely unimpeded flow of deep and intermediate water from the Pacific to the Indian Ocean, except for possible obstacles such as arcs between West Sulawesi and northern Australia related to northward subduction of the Indian-Australian plate. From the late Eocene (42 Ma), the northward movement of a single Indian-Australian plate was accommodated by subduction of oceanic crust beneath SE Asia at the Sunda Trench. This trench continued east into the Pacific and at 30 Ma, the Indian-Australian plate was being subducted beneath an arc which extended east from west Sulawesi, through the Philippines and Halmahera, into an arc at the southern edge of the Caroline Sea (Figure 11).

During the Paleogene SE Asia was a largely elevated landmass (Sundaland). Sedimentary basins formed around the edges of Sundaland from the Eocene and became marine at different times. The Makassar Strait was one these basins. Extension and subsidence in the Makassar Strait probably began in the early Eocene [*Moss and Chambers*, 1999] and may have led to the formation of oceanic crust in the northern Makassar Strait [*Cloke et al.*, 1999], which was linked to the Celebes Sea and West Philippine Basin [*Hall*, 1996]. By the late Oligocene, there was a deep marine basin to the east of Borneo, which separated Borneo from west Sulawesi, and which may have linked the Celebes Sea to the Indian Ocean, although at the southern edge of SE Asia a volcanic arc may have prevented a complete connection.

At about 25 Ma there was arc-continent collision in New Guinea and in SE Asia (Figure 11). This effectively elimi-

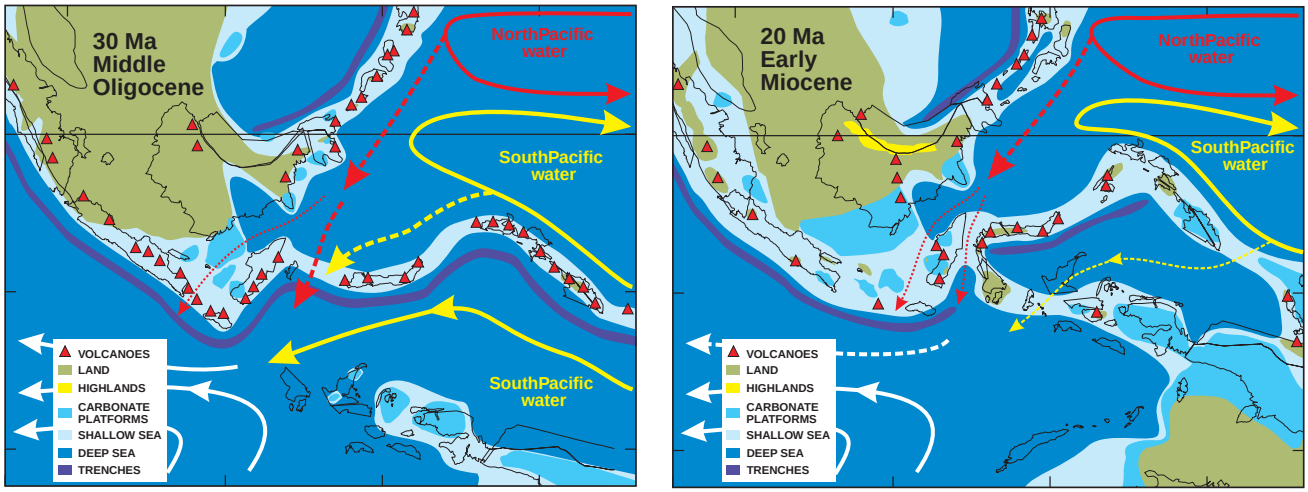

Figure 11. Interpreted distribution of land and sea in the region of the throughflow from 30 Ma to 20 Ma (modified from [*Hall* 1998]) showing postulated major ocean currents. North Pacific water is shown in dark gray, South Pacific water in light gray, and Indian Ocean currents in white. The positions of the major Pacific flow and return currents are assumed to have remained broadly fixed with respect to the equator as inferred by *Cane and Molnar* [2001]. Flow from the Pacific to the Indian Ocean is therefore dependent on the positions of the small deep basins and channels connecting them, and intervening areas of shallow water and land.

nated the wide and deep oceanic gap between Australia and SE Asia but the passage of water between the Pacific and Indian Oceans was probably not completely stopped because the collision did not lead to widespread emergence of land. At this time there was a major reorganisation of plate boundaries. Australia and SE Asia first made contact in east Sulawesi [*Hall and Wilson*, 2000], where sub-ophiolite metamorphic rocks indicate late Oligocene intra-oceanic thrusting and Oligocene to early Miocene subduction [*Parkinson*, 1991, 1998; *Wijbrans et al.*, 1994]. Arc-related volcanic activity ceased in Sulawesi and collision-related deformation dates from the early Miocene. Ophiolites were obducted in SE Sulawesi during the early Miocene and unconformable contacts indicate emergence [*Surono and Sukarna*, 1995]. The ophiolites are interpreted to be thrust over crust of Australian origin throughout east Sulawesi [e.g., *Kündig*, 1956; *Audley-Charles*, 1978; *Villeneuve et al.*, 2000] following the arrival of the Bird's Head microcontinent at the Sulawesi active margin. However, the collisional features are evident only in the eastern parts of Sulawesi. The Makassar Strait remained a deep water region with passive margins to the east and west. In western Sulawesi, there are no significant breaks in marine deposition [*Wilson*, 2000; *Calvert*, 2000], as shown by the lack of regional angular unconformities, and absence of significant orogenic detrital sediment input.

Further east, collision occurred between the Philippines-Halmahera-South Caroline Arc and the New Guinea margin at about 25 Ma [*Dow*, 1977; *Jaques and Robinson*, 1977; *Pigram and Davies*, 1987; *Hill and Raza*, 1999]. There was a change in plate boundaries at the southern edge of the Philippine Sea Plate [*Hall et al.*, 1995]. Northward subduction of the oceanic crust ceased and a major left-lateral strike-slip boundary developed through northern New Guinea. However, there is no evidence of major orogenic deformation in western New Guinea. Most of the Bird's Head remained an area of shallow carbonate deposition until the late Miocene. From 25 Ma until about 12 Ma the clockwise rotation of the Philippine Sea plate caused the region from New Guinea to Sulawesi to remain a zone of strike-slip faulting (Figure 11). Localised transpression and transtension in this zone are likely but cannot yet be reconstructed because of inadequate knowledge of the regional geology. During this period, arc terranes were translated westwards along the margin within the strike-slip system and fragments of continental crust were sliced from the Bird's Head and moved west to arrive in east Sulawesi.

Marine Paleogeography and Paleocirculation Patterns

Translating tectonic reconstruction maps into palaeogeographical maps, which show land and sea, involves significant complexities for Miocene reconstructions. The marine geological record is incomplete because of deformation and erosion; the terrestrial record typically consists of negative evidence such as unconformities and stratigraphic gaps, or comprises sediments with few, often difficult to date fossils. In eastern Indonesia, there was a closure of the marine gap, and collision of the Sula Spur-Bird's Head microcontinental area with the eastern Sunda margin from about 25 Ma onwards. However, despite the continued convergence between the principal plates and the arrival of fragments of

continental crust in Sulawesi, there was at the same time opening of new deep ocean basins. Figure 11 shows the inferred distribution of land and sea on tectonic reconstruction maps for 20 and 30 Ma. However, attempts to differentiate areas of different water depths, and to draw the 500 m isobath are still extremely tentative.

In the west, Borneo remained connected to Sundaland throughout the Cenozoic. Sundaland was mainly emergent, or intermittently transected by very shallow seas. Opening of the South China Sea in the Oligocene [*Briais et al.*, 1993] formed a deep-water seaway to the north of Borneo but this ocean, and its predecessor the proto-South China Sea always terminated to the southwest in the shallow marine or emergent shelf of Sundaland. Thus, there could never have been a significant oceanic connection between the Pacific and Indian Oceans north of Borneo. In contrast, from the Eocene onwards the Celebes Sea and Makassar Strait formed deep water regions to the north and east of Borneo through which an oceanic connection may have existed. Deep trenches must have occurred along the eastern Sundaland margin that extended into the west Pacific.

As collision of Australia and SE Asia began at about 25 Ma, mountains rose in Borneo, possibly as high as those now in New Guinea, considerably expanding the area of land, as large deltas built out rapidly into the surrounding deep basins [*Nichols and Hall*, 2002]. However, the Makassar Strait remained wider than at present, with a very deep water central area and wide marine shelves. From the early Miocene there is good evidence for emergence in SE Sulawesi, but in western Sulawesi emergence and elevation of mountains occurred in the late Miocene or later.

Impact of Initial Closure in Deep Water Isotope Records?

The time of the initial closure of the Indonesian deep water passage between 25 Ma and 22 Ma coincides with major changes in the global deep sea isotope record: first a major shift towards lower oxygen isotope values in the late Oligocene (Late Oligocene Warming, 26–24 Ma), followed by a rapid return towards higher oxygen isotope values (Mi-1 Glaciation, 23 Ma [*Miller et al.*, 1991]) and a significant positive carbon isotope excursion at the base of the Miocene [e.g., *Zachos et al.*, 2001]. The synchroneity of the initial collision between Australia and Eurasia and the significant perturbation of the climate system in the latest Oligocene-early Miocene may not be due to coincidence, as the closure of the Indonesian deepwater pathway would have radically altered global thermohaline circulation patterns.

The compilation of deep water benthic isotope data for the Indian Ocean by *Zachos et al.*, [1992] indicates a change of Indian Ocean ventilation at approximately 23–24 Ma. For a brief interval at around 22.5 Ma, masses of comparatively ^{13}C-enriched waters were present at intermediate and deep water depths. By early Miocene time, the distinct $\delta^{18}O$ gradient which was characteristic of the Oligocene was weakened, as intermediate and deep waters warmed and cool deep-water masses remained restricted to the southern part of the Indian Ocean. In their compilation of Miocene benthic isotope data from the Atlantic, Indian and Pacific Oceans *Woodruff and Savin* [1989] recorded high (>0.5‰) inter–oceanic $\delta^{13}C$ differences at the Equator at 2 km water depth between the Indian and Pacific Oceans in the entire lower to middle Miocene (23–14 Ma), indicating a better ventilated Indian Ocean. These authors proposed a scenario of young, $\delta^{13}C$-rich intermediate waters (1–2.5 km) originating in the northern Indian Ocean, probably from a salty turbulent plume of Tethyan origin, similar to the modern Mediterranean Outflow waters. The southern and eastern Indian Ocean would be mainly influenced by deep water of Antarctic origin, that may have partly originated from cooled salty Tethyan water, that had surfaced at high southern latitudes. The distinct $\delta^{13}C$ differences of Indian Ocean and Pacific tropical intermediate waters would thus contradict a significant zonal exchange of intermediate tropical water via a deep Indonesian Passage at least since the early Miocene (21–23 Ma time slice of *Woodruff and Savin* [1989]).

A comparison of benthic deep water isotope records from ODP Sites on both sides of the gateway for the time period 24 to 11 Ma reveals a significant divergence in deep water $\delta^{18}O$ curves prior to 23.5 Ma (Figure 12). While tropical Pacific records (South China Sea, Site 1148 [*Zhao et al.*, 2001a, 2001b]) indicate warming of deep waters coinciding with the major global carbon isotope excursion at the Oligocene-Miocene boundary, the two Indian Ocean records (ODP Sites 709 and 761, [*Woodruff et al.*, 1990, 1991; *Holbourn et al.*, 2004]) indicate cooling. Cooling occurred later, between 23 and 21 Ma, in the South China Sea, at a time when Indian Ocean deep water already had reached high $\delta^{18}O$ values (Figure 12). Thus, closure of the Indonesian passage as an important deepwater gateway appears to have occurred very early, prior to approximately 23.5 Ma, when a major divergence in the paleoceanographic characteristics of the tropical Indian Ocean and Pacific deep water is already evident.

CONCLUSIONS

The earliest restriction of the Indonesian deep water pathway probably occurred at approximately 25 Ma, when the Australian plate first began to collide with SE Asia. Deep water benthic foraminiferal isotope records from the western Pacific, South China Sea, and eastern Indian Ocean indicate a restricted deep water exchange through the passage by the early to middle Miocene.

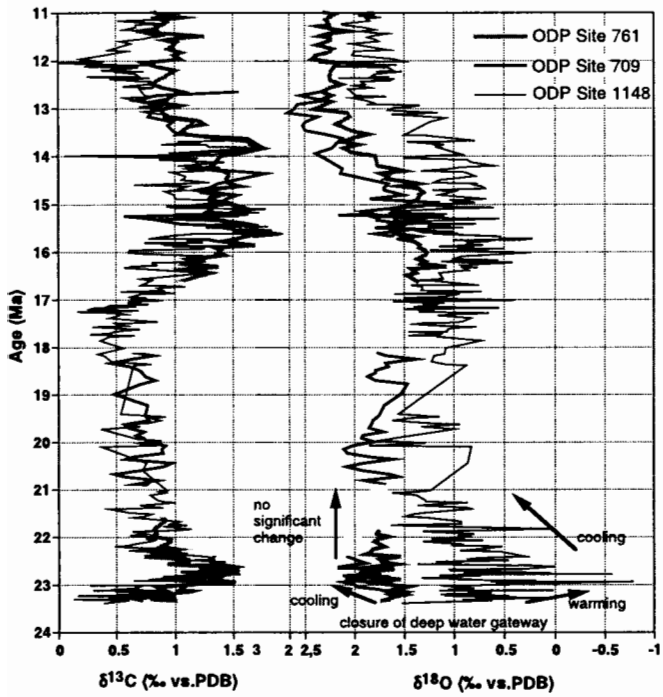

Figure 12. Comparison of benthic isotope records (11–24 Ma) from the tropical western Indian Ocean (ODP Site 709 [*Woodruff et al.*, 1990, 1991]), eastern Indian Ocean (Site 761 [*Holbourn et al.*, 2004]) and South China Sea (Site 1148 [*Zhao et al.*, 2001a, b]). All records were tuned to the age model of Site 761 using the carbon isotope record [*Holbourn et al.*, 2004].

The timing of the restriction for surface and thermocline water flow is more difficult to ascertain, and various restriction events have been proposed for the middle Miocene, late Miocene, Pliocene and late Pleistocene, based on changes in circulation patterns in the equatorial Pacific Ocean and paleoceanographic evidence from the Indian Ocean [e.g., *Kennett et al.*, 1985; *Srinivasan and Sinha*, 1998; *Cane and Molnar*, 2001]. Tectonic evidence for the restriction in surface water flow within the passages is ambiguous, and continuous surface water proxy records are needed on both sides of the passages to test the hypothesis of a stepwise restriction in surface water throughflow intensity.

During the Pleistocene and Holocene, IT fluctuations strongly influenced the paleocenography of the eastern Indian Ocean and western Pacific Ocean. During the last glacial cycles, changes in the intensity of the South Asian monsoon and productivity fluctuations in the easternmost Indian Ocean were closely related to IT strength. Modelling results indicate that glacial climatic boundary conditions (wind-stress in passages and SSS and SST conditions in the WPWP) may have been as important controls of throughflow intensity as topographic changes stemming from sealevel change. The warm surface flow through the Makassar Strait may have been even stronger during the LGM, although the total transport through the Makassar Strait was reduced. Today, the presence of a low SSS water mass in the Java Sea and the prevalence of monsoonal wind patterns drive low-salinity surface water from the South China Sea and Java Sea into the southern part of the Makassar Strait and thus build up an effective barrier for warm surface flow. SSSs probably were overall higher in the Indonesian passages during glacials, although recent paired Mg/Ca, Uk37 and $\delta^{18}O$ records from the South China Sea and Sulu Sea indicate the presence of very low-salinity surface waters and significant continental runoff in the northern part of the WPWP during the LGM. The lowered glacial sealevel would, however, have prevented the interaction of low-salinity water originating from the South China Sea with the IT.

Neither higher frequency glacial and Holocene fluctuations in throughflow intensity on a Dansgaard-Oeschger timescale nor changes related to ENSO-cycles have been documented so far in the paleoceanographic record. There remain open questions about the duration and origin of the ENSO system and its relation to IT fluctuations, about the onset and influence of the SE Asian monsoon system on the Indonesian passages, and the sensitivity of the regional and global climate to land and sea topographic and hydrographic change in the Indonesian passages. To address these questions we urgently need high resolution records of the Holocene and the last glacial cycles specifically from the inflow passages and the southern part of the Australasian archipelago and continuous longterm records on both sides of the passages that reach back into the late Oligocene.

Acknowledgments. We are most grateful to Jason Ali, Peter Clift, Jim Kennett, and an anonymous reviewer for helpful comments. We thank the Deutsche Forschungsgemeinschaft (DFG) for funding our research on the history of the Indonesian Throughflow in the framework of the Research Unit "Impact of Gateways on Ocean Circulation, Climate, and Evolution" (FOR 451/1,2) and individual grants (KU649-13, 14 and 15). This research used samples and/or data provided by the Ocean Drilling Program (ODP). The ODP is sponsored by the U.S. National Science Foundation (NSF) and participating countries under management of Joint Oceanographic Institutions (JOI), Inc.

REFERENCES

Ahmad, S. M., F. Guichard, K. Hardjawidjaksana, M. K. Adisaputra, and L.D. Labeyrie, Late Quaternary paleoceanography of the Banda Sea, *Mar. Geol., 122,* 385–397, 1995.

Ali, J. R., S. J. Roberts, and S. J. Hall, The closure of the Indo-Pacific Gateway: a new plate tectonic perspective, in *Proceedings of the international workshop on Neogene evolution of Pacific Ocean gateways*, edited by F. Hehuwat, E. Utomo, and A. Dharma, pp. 10–20, Nishimura, Kyoto, 1994.

An, Z., J. E. Kutzbach, W. L. Prell, S. C. Porter, Evolution of Asian monsoons and phased uplift of the HimalayaTibetan plateau since Late Miocene times, *Nature, 411,* 62–66, 2001.

Audley-Charles, M. G., Indonesian and Philippine archipelagoes, in *The Phanerozoic Geology of the World II: The Mesozoic*, edited by M. Moullade, and A. E. M. Nairn, pp. 165–207, A. Elsevier, Amsterdam, the Netherlands, 1978.

Bemis, B. E., H. J. Spero, J. Bijma, and D. W. Lea, Reevaluation of the oxygen isotopic composition of planktonic foraminifera: experimental results and revised paleotemperature equations, *Paleoceanography 13,* 150–160, 1998.

Bacastov, R. B., The effect of temperature change of the warm surface waters of the oceans on atmospheric CO2, *Global Biogeochem. Cycles, 10,* 319–333, 1996.

Barmawidjaja, B. M., E. J. Rohling, W. A. Van der Kaars, C. Vergnaud Grazzini, and W. J. Zachariasse, Glacial conditions in the northern Molucca Sea (Indonesia). *Palaeogeogr., Palaeoclimatol., Palaeoecol., 101,* 147–167, 1993.

Bice, K. L., C. R. Scotese, D. Seidov, and E. J. Barron, Quantifying the role of geographic change in Cenozoic ocean heat transport using uncoupled atmosphere and ocean models, *Palaeogeogr., Palaeoclimatol., Palaeoecol., 161*, 295–310, 2000.

Bjerknes, J., Atmospheric teleconnections from the equatorial Pacific, *Mon. Weather Rev., 97,* 163–172, 1969.

Briais, A., Patriat, P., and P. Tapponnier, Updated interpretation of magnetic anomalies and sea floor spreading stages in the South China Sea: implications for the Tertiary tectonics of Southeast Asia, *J. Geophys. Res., 98,* 6299–6328.

Calvert, S. J., The Cenozoic evolution of the Lariang and Karama basins, Sulawesi, *Proc. Indonesian Petroleum Assoc., 27th Annual Convention*, 505–511, 2000.

Cane, M. A., and P. Molnar, Closing of the Indonesian seaway as a precursor to east African aridification around 3–4 million years ago, *Nature, 411*, 157–162, 2001.

Chong, J. C., J. Sprintall, S. Hautala, W. L. Morawitz, N. A. Bray, and W. Pandoe, Shallow throughflow variability in the outflow straits of Indonesia, *Geophys. Res. Lett., 27,* 125–128, 2000.

Clark, P. U., and A. Mix, Ice sheets and sea level of the Last Glacial Maximum, *Quat. Sci. Rev., 21,* 1–7, 2002..

Cloke, I. R., J. Milsom, and D. J. B. Blundell, Implications of gravity data from east Kalimantan and the Makassar Straits: a solution to the origin of the Makassar Straits?, *J. Asian Earth Sci., 17*, 61–78, 1999.

Conkright, M., S. Levitus, T. O'Brien, T. Boyer, J. Antonov, and C. Stephens, *World Ocean Atlas 1998 CD-ROM Data Set Documentation.* Tech. Rep. 15, NODC Intern. Rep., Silver Spring, MD, 1998. 16pp.

Cresswell, G., A. Frische, J. Peterson, and D. Quadfasel, Circulation in the Timor Sea, *J. Geophys. Res., 98*(C8), 14379–14389, 1993.

Da Silva, A., A. C. Young, and S. Levitus, *Atlas of Surface Marine Data 1994, Volume 1: Algorithms and Procedures.* NOAA Atlas NESDIS 6, U.S. Department of Commerce, Washington, D.C., 1994.

De Deckker, P., N. J. Tapper, and S. Van der Kaars, The status of the Indo-Pacific Warm Pool and adjacent land at the Last Glacial Maximum, *Global and Planetary Change, 35*, 25–35, 2002.

Dickens, G. R., and R. M. Owens, Late-Miocene-early Pliocene manganese redirection in the central Indian Ocean: Expansion of the intermediate water oxygen minimum zone. *Paleoceanography, 9*, 169–181, 1994..

Dow, D. B., *A geological synthesis of Papua New Guinea*, BMR Australia, Geol. Geophys. Bull., 201, 41pp, 1977.

Duplessy, J.-C., L. Labeyrie, A. Juillet-Leclerc, F. Maitre, J. Duprat, and M. Sarnthein, Surface salinity reconstruction of the North Atlantic Ocean during the last glacial maximum, *Oceanologica Acta, 14*, 311–324, 1991.

Flower, B. P., and J. P. Kennett, Middle Miocene ocean-climate transition: high resolution oxygen and carbon isotopic records from DSDP Site 588A, southwest Pacific, *Paleoceanography, 8*, 811–843, 1993.

Ganachaud, A., and C. Wunsch, Improved estimates of global ocean circulation, heat transport and mixing from hydrographic data, *Nature, 408*, 453–457, 2000.

Gingele, F. X., P. De Deckker, and C.-D. Hillenbrand, Clay mineral distribution in surface sediments between Indonesia and NW Australia—source and transport by ocean currents, *Mar. Geol., 179,* 135–146, 2001.

Gingele, F. X., P. De Deckker, and C.-D. Hillenbrand, Late Quaternary fluctuations in the Leeuwin Current and palaeoclimates on the adjacent land masses: clay mineral evidence, *Australian J. Earth Sci., 48*, 867–874, 2001.

Godfrey J. S., The effect of the Indonesian throughflow on ocean circulation and heat exchange with the atmosphere: A review, *J. Geophys. Res., 101*(C5), 12217–12237, 1996.

Gordon, A. L., Interocean Exchange, in *Ocean Circulation and Climate*, edited by G. Siedler, J. Church and J. Gould, 303–314, Academic Press, 2001.

Gordon, A. L., and R. A. Fine, Pathways of water between the Pacific and Indian Oceans in the Indonesian Seas, *Nature, 379,* 146–149, 1996.

Gordon, A. L., R. D. Susanto, and K. Vranes, Cool Indonesian throughflow as a consequence of restricted surface layer flow, *Nature, 425,* 824–828, 2003.

Gordon, A. L., R. D. Susanto, A. Ffield, and D. Pillsbury, Makassar Strait transport: preliminary Arlindo results from MAK-1 and MAK-2, *Int. WOCE Newslett., 33*, 30–32, 1998.

Gordon, A. L., R. D. Susanto, and A. Ffield, Throughflow within Makassar Strait, *Geophys. Res. Lett., 26*, 3325–3328, 1999.

Hall, R., Reconstructing Cenozoic SE Asia, In *Tectonic evolution of Southeast Asia*, edited by R. Hall and D. Blundell, Geol. Soc. Spec. Pub., 106, 153–184, 1996.

Hall, R., The plate tectonics of Cenozoic SE Asia and the distribution of land and sea, in *Biogeography and Geological Evolution of SE Asia*, edited by R. Hall, and J.D. Holloway, pp. 99–131, Backhuys Publishers, Leiden, The Netherlands, 1998.

Hall, R., Cenozoic geological and plate tectonic evolution of SE Asia and the SW Pacific: computer-based reconstructions, model and animations, *J. Asian Earth Sci., 20*, 353–434, 2002.

Hall, R., J. R. Ali, and C. D. Anderson, Cenozoic motion of the Philippine Sea Plate—paleomagnetic evidence from eastern Indonesia, *Tectonics, 14*, 1117–1132, 1995.

Hall, R., and M. E. J. Wilson, Neogene sutures in eastern Indonesia, *J. Asian Earth Sci., 18*, 787–814, 2000.

Hanebuth, T., K. Stattegger, and P. M. Grootes, Rapid flooding of the Sunda Shelf—a late glacial sea-level record, *Science, 288*, 1033–1035, 2000.

Hardenbol, J., J. Thierry, M. B. Farley, T. Jacquin, P.-C. De Graciansky, and P. R. Vail, Cenozoic sequence chronostratigraphy. In: *Mesozoic and Cenozoic sequence chronostratigraphic framework of European Basins*, edited by P.-C. De Graciansky, J. Hardenbol, T. Jacquin, and P. R. Vail, SEPM Spec. Pub. 60, 3–13, Charts 1–8, 1998

Hautala, S. L., J. Sprintall, J. Potemra, J. C. C. C. Chong, W. Pandoe, N. Bray, and A. G. Ilahude, Velocity structure and transport of the Indonesian throughflow in the major straits restricting flow into the Indian Ocean, *J. Geophys. Res., 106,* 19527–19546, 2001.

Hautala, S., J. L. Reid, and N. Bray, The distribution and mixing of Pacific water masses in the Indonesian seas, *J. Geophys. Res., 101,* 12375–12389, 1996.

Hill, K. C. and R. Hall, Mesozoic–Cainozoic evolution of Australia's New Guinea margin in a West Pacific context. In: *Defining Australia: The Australian Plate*, edited by Hillis, R. and R. D. Müller, Planet Earth. Geol. Soc. Australia Spec. Pub., 22 and GSA Spec. Paper, *372*, 259–283, 2003.

Hill, K. C., and A. Raza, Arc-continent collision in Papua New Guinea: Constraints from fission track thermochronology, *Tectonics, 18*, 950–966, 1999.

Holbourn, A. E., W. Kuhnt, and M. Schulz, Orbitally paced climate variability during the middle Miocene: High resolution benthic foraminiferal stable-isotope records from the tropical western Pacific, in *Continent-Ocean Interactions in the East Asian Marginal Seas*, AGU Monograph, this volume.

Holbourn, A. E., W. Kuhnt, J. A. Simo, and Q. Li, Middle Miocene isotope stratigraphy and paleoceanographic evolution of the northwest and southwest Australian margins (Wombat Plateau and Great Australian Bight), *Palaeogeogr., Palaeoclimatol., Palaeoecol, 208*, 1–22, 2004.

Honthaas, C., R. C. Maury, B. Priadi, H. Bellon, and J. Cotten, The Plio-Quaternary Ambon arc, eastern Indonesia, *Tectonophysics, 301*, 261–281, 1999.

Jaques, A. L., and G. P. Robinson, The continent/island-arc collision in northern Papua New Guinea, *BMR J. Australian Geol. Geophys., 2*, 289–303, 1977.

Kennett, J. P., G. Keller, and M. S. Srinivasan, Miocene planktonic foraminiferal biogeography and paleogeographic development of the Indo-Pacific region, in *The Miocene Ocean: Paleoceanography and Biogeography*, edited by J. P. Kennett, pp. 197–236, 1985.

Kienast, M., S. Steinke, K. Stattegger, and S. Calvert, Synchronous tropical South China Sea SST change and Greenland warming during deglaciation, *Science, 291*, 2132–2134, 2001.

Kündig, E., Geology and ophiolite problems of East Celebes, *Verhandelingen Koninklijk Nederlands Geologisch en Mijnbouwkundig Genootschap, Geologische Serie, 16*, 210–235, 1956.

Kuhnt, W., Holbourn, A., and Q. Zhao, The early history of the South China Sea: Evolution of Oligocene-Miocene deep water environments, *Rev. de Micropaléontologie, 45*, 99–159, 2002.

Lambeck, K., Y. Yokoyama, A. Pucell, and P. Johnston, Reply to the comment by W.R. Peltier, *Quat. Sci. Rev., 21*, 415–418, 2002.

Lea, D. W., D. K. Pak, and H. J. Spero, Climate Impact of Late Quaternary Equatorial Pacific Sea Surface Temperature Variations, *Science, 289,* 1719–1724, 2000.

Linthout, K., H. Helmers, and J. Sopaheluwakan, Late Miocene obduction and microplate migration around the southern Banda Sea and the closure of the Indonesian Seaway, *Tectonophysics, 281*, 17–30, 1997.

Linthout, K., H. Helmers, J. R. Wijbrans, and J. D. A. M. van Wees, $^{40}Ar/^{39}Ar$ constraints on obduction of the Seram Ultramafic Complex: consequences for the evolution of the southern Banda Sea, in *Tectonic Evolution of SE Asia,* edited by R. Hall, and D. J. Blundell, pp. 455–464, Geol. Soc. Spec. Pub., 106, 1996.

Macdonald, A. M., and C. Wunsch, An estimate of global ocean and heat fluxes, *Nature, 382,* 436–439, 1996.

Marshall, J., A. Adcroft, C. Hill, L. Perelman, and C. Heisey, A finite volume, incompressible Navier Stokes model for studies of the ocean on parallel computers, *J. Geophys. Res.*, 102, 5753–5766, 1997a.

Marshall, J., C. Hill, L. Perelman, and A. Adcroft, Hydrostatic, quasi-hydrostatic and nonhydrostatic ocean modeling, *J. Geophys. Res.*, 102, 5733–5752, 1997b.

Martinez, J. I., P. De Deckker, and T. T. Barrows, Palaeoceanography of the last glacial maximum in the eastern Indian Ocean: planktonic foraminiferal evidence, *Palaeogeogr., Palaeoclimatol., Palaeoecol., 147,* 73–99, 1999.

Martinez, J. I., P. De Deckker, and T. T. Barrows, Palaeoceanography of the Western Pacific Warm Pool during the Last Glacial Maximum: Long-term climatic monitoring of the Maritime Continent, *in Bridging Wallace's Line* edited by P. Kershaw, B. David, N. Tapper, D. Penny, and J. Brown. Advances in Geoecology 34, Catena-Verlag, Reiskirchen, Germany, 147–172, 2002.

Martinez, J. I., P. De Deckker, and A. R. Chivas, New estimates for salinity changes in the Western Pacific Warm Pool during the Last Glacial Maximum: oxygen isotope evidence, *Mar. Micropaleontol., 32*, 311–340, 1997.

McBride, J., Indonesia, Papua New Guinea and Tropical Australia: the southern Hemsiphere Monsoon, *in Meteorology of the Southern Hemisphere*, edited by Vincent, D., and D. Karoly, Am. Meterological Soc., Boston, 89–99, 1999.

Meyers, G., Variations of Indonesian throughflow and El Nino-Southern Oscillation, *J. Geophys. Res., 101*(C5), 12255–12263, 1996.

Miller, K. G., J. M. Wright, and R. G. Fairbanks. Unlocking the Ice House: Oligocene-Miocene oxygen isotopes, eustasy, and margin erosion, *J. Geophys. Res., 96,* B4, 6829–6848, 1991.

Molcard, R., M. Fieux, and F. Syamsudin, The throughflow within Ombai Strait, *Deep-Sea Res., 1 48*, 1237–1253, 2001.

Molcard, R., M. Fieux, and A.G. Ilahude, The Indo-Pacific throughflow in the Timor Passage, *J. Geophys. Res., 101* (C5), 12411–12420, 1996.

Molcard, R., M. Fieux, J. C. Swallow, A. G. Ilahude, and J. Banjarnahor, Low frequency variability of the currents in Indonesian Channels, *Deep-Sea Res., 41*, 1643–1661, 1994.

Moss, S. J., and J. L. C. Chambers, Tertiary facies architecture in the Kutai Basin, Kalimantan, Indonesia, *J. Asian Earth Sci., 17* (1–2), 157–181, 1999.

Müller, A., and B. N. Opdyke, Glacial-interglacial changes in nutrient utilization and paleoproductivity in the Indonesian Throughflow sensitive Timor Trough, easternmost Indian Ocean, *Paleoceanography, 15*, 85–94, 2000.

Murray, S. P., and D. Arief, Throughflow into the Indian Ocean through the Lombok Strait. January 1985–January 1986, *Nature, 333*, 444–447, 1988.

Nichols, N., The Southern Oscillation and Indonesian Sea surface temperature, *Mon. Weather Rev., 112*, 424–432, 1984.

Nichols, G. J., and R. Hall, History of the Celebes Sea Basin based on its stratigraphic and sedimentological record. *J. Asian Earth Sci., 17*, 47–59, 1999.

Nishimura, S., Tectonic approach to changes in surface water circulation between the tropical Pacific and Indian Oceans, *in Pacific Neogene: Environment, Evolution and Events*, edited by R. Tsuchi, and J.C. Ingle, pp. 1570–1167, University of Tokyo Press, Tokyo, 1992.

Oppo, D. W., B. K. Linsley, Y. Rosenthal, S. Dannenmann and L. Beaufort, Orbital and suborbital climate variability in the Sulu Sea, western tropical Pacific, *Geochem. Geophys. Geosystems (G3), 4*(1), doi:10.1029/2001GC000260, 2003.

Palmer, M. R., and P. N. Pearson, A 23,000-Year Record of Surface Water pH and PCO2 in the Western Equatorial Pacific Ocean, *Science, 300*, 480–482, 2003.

Parkinson, C. D., *The petrology, structure and geologic history of the metamorphic rocks of central Sulawesi, Indonesia*, Ph.D. Thesis, University of London, 337 pp., 1991.

Parkinson, C. D., Emplacement of the East Sulawesi ophiolite: evidence from subophiolite metamorphic rocks, *J. Asian Earth Sci., 16*, 13–28, 1998.

Patrick, A. and R. C. Thunell, Tropical Pacific sea surface temperatures and upper water column thermal structure during the last glacial maximum, *Paleoceanography, 12*, 649–657, 1997.

Paul, A. and C. Schäfer-Neth, Modeling the water masses of the Atlantic Ocean at the Last Glacial Maximum, *Paleoceanography, 18*, 1058, 2003.

Pelejero, C., J. O. Grimalt, M. Sarnthein, L. Wang, and J.-A. Flores, Molecular biomarker record of sea surface temperature and climatic change in the South China Sea during the last 140,000 years, *Mar. Geol., 156*, 109–121, 1999.

Peltier, W. R., Comments on the paper of Yokoyama et al. (2000), entitled "Timing of the Last Glacial Maximum from observed sea level minima", *Quat. Sci. Rev., 21*, 409–414, 2002.

Pigram, C. J., and H. L. Davies, Terranes and the accretion history of the New Guinea orogen, *BMR J. Australian Geol. Geophys., 10*, 193–212, 1987.

Potemra, J. T., S. L. Hautala, and J. Sprintall, Interaction between the Indonesian seas and the Indian Ocean in observations and numerical models, *J. Phys. Oceanogr., 32*, 1838–1854, 2002.

Rosenthal, Y., D. W. Oppo, and B. K. Linsley, The amplitude and phasing of climate change during the last deglaciation in the Sulu Sea, western equatorial Pacific, *Geophys. Res. Lett., 30*, 1428, doi:10.1029/2002GL016612), 2003.

Schneider, N., The Indonesian Throughflow and the global climate system, *J. Climate, 11*, 676–689, 1998.

Schott, F. A, and J. P. McCreary, The monsoon circulation of the Indian Ocean, *Progress Oceanogr., 51*, 1–123, 2001.

Sprintall, J., Potemra, J. T., Hautala, S. L., Bray, N. A., and W. W. Pandoe. Temperature and salinity variability in the exit passages of the Indonesian Throughflow. *Deep Sea Res. II, 50*, 2183–2204, 2003.

Srinivasan, M. S., and D. K. Sinha, Early Pliocene closure of the Indonesian Seaway: evidence from north-east Indian Ocean and Tropical Pacific deep sea cores, *J. Asian Earth Sci., 1*, 29–44, 1998.

Stott, L., C. Poulsen, S. Lund, and R. Thunell, Super ENSO and global climate oscillations at millennial time scales, *Science, 297*, 222–226, 2002.

Sturman, A.P., and N. Tapper, *The Weather and Climate of Australia and New Zealand*, 476 pp., Oxford University Press, Melbourne, 1996.

Sugden, D., and G. Denton, Evolution of the Antarctic climate system: a synthesis of land and offshore records from southern Victoria Land, *Eos Trans., AGU, 84*(46), Fall Meeting Supplement, Abstract PP32D-04, 2003.

Surono and Sukarna, Sedimentology of the Tolitoli Conglomerate Member of the Langkowala Formation, Southeast Sulawesi, Indonesia, *J. Geol. Mineral Resources, GRDC Bandung, Indonesia*, 5, 1–7, 1995.

Tapper, N., Climate, climatic variability and atmospheric circulation patterns in the Maritime Continent region, in *Bridging Wallace's Line* edited by P. Kershaw, B. David, N. Tapper, D. Penny, and J. Brown, pp. 12–30, Advances in GeoEcology, 34, Catena Verlag, 35447 Reiskirchen, 2002.

Villeneuve, M., J. J. Cornee, W. Gunawan, M. C. Janin, J. Butterlin, P. Saint-Marc, and H. Samodra, Continental block collision in the eastern arm of Sulawesi (Indonesia). Structure and geodynamic interpretation, *C. R. Acad. Sci.*, Paris, 330, 371–378, 2000.

Visser, K., R. Thunell, and L. Stott, Magnitude and timimg of temperature change in the Indo-Pacific warm pool during deglaciation, *Nature, 421*, 152–155, 2003.

Vranes, K., A. L. Gordon, and A. Ffield., The heat transport of the Indonesian Throughflow and implications for the Indian Ocean heat budget. *Deep-Sea Res., II, 49*, 1391–1410, 2002.

Wajsowicz, R. C., Air-sea interaction over the Indian Ocean due to variations in the Indonesian Throughflow. *Climate Dynamics, 18*, 437–453, 2002.

Wajsowicz, R. C., and E. K. Schneider, The Indonesian throughflow's effect on global climate determined from the COLA coupled climate system, *J. Climate, 14*, 3029–3042, 2001.

Wajsowicz, R. C., A. L. Gordon, A. Ffield, D. R. Susanto, Estimating transport in Makassar Strait, *Deep-Sea Res. II, 50*, 2163–2181, 2003.

Wang, L., M. Sarnthein, H. Erlenkeuser, J. GrimaltJ., P. Grootes, S. Heilig, E. Ivanova, M. Kienast, C. Pelejero, and U. Pflaumann, East Asian monsoon climate during the Late Pleistocene: high resolution sediment records from the South China Sea, *Mar. Geol., 156*, 245–284, 1999.

Webb, R. S., D. H. Rind, S. J. Lehmann, R. J. Healy, and D. Siegmann, Influence of ocean heat transport on the climate of the Last Glacial Maximum, *Nature, 385,* 695–699, 1997.

Webster, P. J., Monsoons: processes, predictibility and the prospects of prediction, *J. Geophys. Res., 103,* 14451–14510, 1998.

Wijbrans, J. R., H. Helmers, and J. Sopaheluwakan, The age and thermal evolution of blueschists from South-East Sulawesi, Indonesia: the case of slowly cooled phengites, *Mineralogical Mag.*, 58A (L-Z), 975–976, 1994.

Wilson, M. E. J., 2000. Tectonic and volcanic influences on the development and diachronous termination of a Tertiary tropical carbonate platform, *J Sedimentary Res., 70,* 310–324, 2000.

Woodruff, F., and S.M. Savin, Miocene deepwater oceanography. *Paleoceanography, 4,* 87–140, 1989.

Woodruff, F., S. M. Savin, and L. Abel, Miocene benthic foraminifer oxygen and carbon isotopes, Site 709, Indian Ocean, in Proceedings of the Ocean Drilling Program, Scientific Results edited by R. A. Duncan, J. Backman, & L. C. Peterson, pp. 519–528. College Station, Texas: Ocean Drilling Program, 1990.

Woodruff, F., and S. M. Savin, Mid-Miocene isotope stratigraphy in the deep-sea: high resolution correlations, plaeoclimatic cycles, and sediment preservation, *Paleoceanography, 6,* 755–806, 1991.

Wyrtki, K., An estimate of equatorial upwelling in the Pacific, *J. Phys. Oceanogr., 11,* 1205 – 1214, 1981.

Wyrtki, K., Indonesian throughflow and the associated pressure gradient, *J Geophys. Res., 92*(C12), 12941–12946, 1987.

Yan, X.-H., C.-R. Ho, Q. Zheng, and V.Klemas, Temperature and size variabilities of the Western Pacific Warm Pool, *Science, 258,* 1643–1645, 1992.

Yokoyama, Y., K. Lambeck, P. De Deckker, P. Johnston, L. K. Fifield, Timing of last glacial maximum from observed sea level minima, *Nature 406,* 713–716, 2000.

You, Y. and M. Tomczak, Thermocline circulation and ventilation in the Indian Ocean derived from water mass analysis, *Deep-Sea Res. I, 40,* 13–56, 1993.

Zachos, J. C., D. K. Rea, K. Seto, R. Nomura, and N. Niitsuma, Paleogene and Early Neogene Deep Water Paleoceanography of the Indian Ocean as Determined from Benthic Foraminifer Stable Carbon and Oxygen Isotope Records. *Geophys. Monogr., 70,* 351–385, 1992.

Zachos, J., Pagani, M., Sloan, L., Thomas, E., and Billups, K., Trends, rhythms, and aberrations in global climate 65 Ma to present, *Science, 292,* 686–693, 2001.

Zhao, Q., P. Wang, X. Cheng, J. Wang, B. Huang, J. Xu, Z. Zhou, and Z. Jian, A record of Miocene carbon excurison in the South China Sea, *Sci. China (Series D), 44,* 943–951, 2001a.

Zhao, Q., Z., J., Wang, J., Cheng, X., Huang, B., Xu, J., Zhou, Z., Fang, D., & Wang, P., Neogene oxygen isotopic stratigraphy, ODP Site 1148, northern South China Sea, *Sci. China (Series D), 44,* 934–942, 2001b.

Robert Hall, SE Asia Research Group, Department of Geology, Royal Holloway University of London, Surrey TW20 0EX, UK.

Ann Holbourn and Wolfgang Kuhnt, Institut für Geowissenschaften, Christian-Albrechts-Universität zu Kiel, Olshausenstr. 40, D-24118 Kiel, Germany. (wk@gpi.uni-kiel.de; ah@gpi.uni-kiel.de)

Rolf Käse, and Maja Zuvela, Research Unit Impact of Gateways on Ocean Circulation, Climate and Evolution, Institut für Meereskunde, Christian-Albrechts-Universität zu Kiel, Olshausenstr. 40, D-24118 Kiel, Germany.